Modification of the Molten Carbonate in Dual-Phase Membranes for Improved Carbon Dioxide Separation

By Liam McNeil

Doctor of Philosophy

Newcastle University
School of Engineering
March 2020

Acknowledgements

I would first like to thank my family, Alison, Ian and James McNeil. Their encouragement pushed me to pursue a PhD and their continued love and support throughout my 3 years helped me stay focused and their understanding provided me with freedom to work hard and accomplished my goals. I would also like to thank Samantha Arathimou, she has been my true motivator throughout my PhD. She inspired me to be ambitious within my research and without her I could not have performed to the level I achieved.

I would like to thank Prof. Ian Metcalfe for providing me with this opportunity and I'm extremely grateful to have had this invaluable experience over the past 3 years, where I have learnt so much about both science and myself. Your high standards pushed me to perform to the best of my abilities and revealed my true potential, which I will carry with me throughout the rest of my career. I would also like to express my gratitude towards my secondary supervisory team. Thank you, Dr. Greg Mutch for your exceptional patience, guidance and supervision. Your role in helping me from the moment you joined the group was extremely appreciated and I cannot thank you enough. Thank you to Dr. Evangelos Papaioannou and Dr. Guangru Zhang for your support, especially in my first year, where you helped me to settle into my PhD role. Your expertise in dual-phase membranes was essential in providing me with a foundation to build upon throughout my PhD. Thank you also to Dr. Wenting Hu, Georgios Triantafyllou and Dr. Dragos Neagu for your time and guidance.

Throughout my PhD I made many friends in the office and without them my PhD experience would not have been the same. I would like to thank Stephen Johnson, Maria Kazakli, Chris De Leeuwe and Leonidas Bekris for your friendship.

During my PhD I was lucky enough to be given the opportunity to collaborate with multiple universities and meet and share ideas with many brilliant scientists along the way. I would like to thank all members of the SynFabFun collaboration from Manchester, Bath, Edinburgh and Imperial universities. I would also like to thank our collaborators from UCL, the sample analysis you performed on our behalf has played a vital role in our paper and my thesis.

I would like to thank the Newcastle University EPSRC DTP for providing the funding for my project.

To everyone else, you know who you are, no matter how small or large, your contribution towards helping me throughout my PhD has not gone unnoticed and I am truly grateful.

i

Abstract

Solid metal and metal oxide supports for high-temperature dual-phase molten salt membranes often contain high-cost metals such as samarium, cobalt or silver. These metals are used due to their oxide and/or electron-conductive properties, which assist in carbon dioxide transport by enhancing the rate of carbonate ion formation at the feed-side surface. A cheaper alternative approach would be to use a low-cost, abundant high-temperature stable ceramic support, such as alumina, and improve membrane performance by using small quantities of metals to modify or add functionality to the membrane.

First, CO_2 release from the permeate-side surface was found to be slower than the uptake of CO_2 on the feed-side surface. Therefore, two different doping methods were explored to improve the rate of CO_2 release from the permeate side. However, due to difficulties with solubility and precipitation, both approaches proved unsuccessful. To navigate around these issues, an effective dopant would need to still provide functionality after precipitation, one such material is silver, as it maintains its electron conductivity after precipitation from molten carbonate. Therefore, by using silver as the dopant, precipitation was used advantageously to coat the walls of the support to produce self-forming pathways that contributes to the support's functionality. The molten carbonate was used as a carrier to redistribute silver that was doped into the membrane using multiple controlled techniques. Due to the concentration gradient across the dual-phase membrane, the silver was redistributed to form electron-conducting pathways that span the cross-section of the membrane. This process was performed *in-situ* during permeation and transformed a low-flux alumina supported membrane (Al_2O_3-MC) into a high-flux, low-silver content alumina/silver supported membrane (Ag/Al_2O_3-MC).

The self-forming Ag/Al_2O_3-MC membrane presented in this thesis provided a CO_2 flux of 1.25 mL min^{-1} cm^{-2} at 650°C. This flux is higher than any oxide or electron-conducting supported membrane at the same temperature while using a CO_2 and O_2 feed or CO_2 alone. Furthermore, when normalising the flux to account for gas feed partial pressure, membrane thickness and amount of silver used (mol m^{-1} s^{-1} Pa^{-1} mol Ag^{-1}), the Ag/Al_2O_3-MC membrane had a permeability per mol of silver one order of magnitude higher than silver-supported membranes in the literature. The membrane also demonstrated stability at temperatures exceeding 650°C, where silver-supported membranes have been known to suffer as a result of carbonate retention issues. Computed tomography investigations indicated that could be due to silver not coating the entire pore wall. The Ag/Al_2O_3-MC membrane reached a permeance and permeability in the range reported as required for economically competitive carbon capture.

Table of Contents

Table of Figures

Chapter 3

Table of Tables

Experiment Acknowledgments

X-ray diffraction

Experiments were performed by Dr. Maggie White from Newcastle University and data was interpreted by Liam McNeil.

Raman Spectroscopy

Experiments were performed by Dr. Greg Mutch from Newcastle University and data was interpreted by Liam McNeil.

Mercury Intrusion Porosimetry

Experiments were performed by Dr. Ji Jing from the University of Bath and data was interpreted by Liam McNeil.

Two-point DC Measurements

Experiments were performed by Dr. Evangelos Papaioannou and Dr Gaurav Gupta from Newcastle University and data was interpreted by Liam McNeil.

Computed Tomography

Experiments were performed by Dr. Francesco Iacoviello from UCL, images were constructed by Dr. Josh Bailey from UCL and data was interpreted by Liam McNeil.

Chapter 1. General Introduction

This chapter provides a general introduction to carbon capture and the dual-phase membrane field followed by review of the literature on the modifications made to dual-phase membranes, including: modification of support material; modification of the support geometry; and modification of the molten salt.

1.1 The Dual-Phase Membrane

Carbon dioxide (CO_2) and other greenhouse gas emissions are of great concern due to their contribution towards climate change. CO_2 atmospheric concentrations have increased dramatically since the beginning of the industrial era, from approximately 277 parts per million (ppm) in 1750 [1], to 409 ppm in 2019 [2]. Global CO_2 emissions from fossil fuel combustion in 2018 was 37.1 ± 1.8 Gt and is expected to rise by ~2.7% each year [3]. Due to its cost efficiency when compared to other carbon abatement techniques [4], [5], carbon capture, utilization and storage (CCUS) is well recognized as playing a fundamental role in the mitigation of CO_2 to meet climate change recommendations and targets set by the Intergovernmental Panel on Climate Change (IPCC) and the Conference of Parties (COP21) [6]–[8]. CCUS is divided into 4 sectors, starting with the capture of CO_2 which acts as the initiating role for the subsequent 3 sectors; transport, storage and utilization of CO_2. Current carbon capture technologies are typically targeted at two different processes: pre-combustion and post-combustion. Pre-combustion carbon capture is most suitable for integrated gasification combined cycle (IGCC) power plants where CO_2 is separated from a gas stream containing CO_2 and hydrogen (H_2) (syngas) (Fig. 1. 1a) [9]. Whereas, post-combustion carbon capture is most effective when used for pulverized coal-fired (PC) and natural gas combined cycle (NGCC) power plants where CO_2 is separated from a gas stream containing predominantly nitrogen (N_2), oxygen (O_2) and CO_2 (flue gas) (Fig. 1. 1b) [9].

2
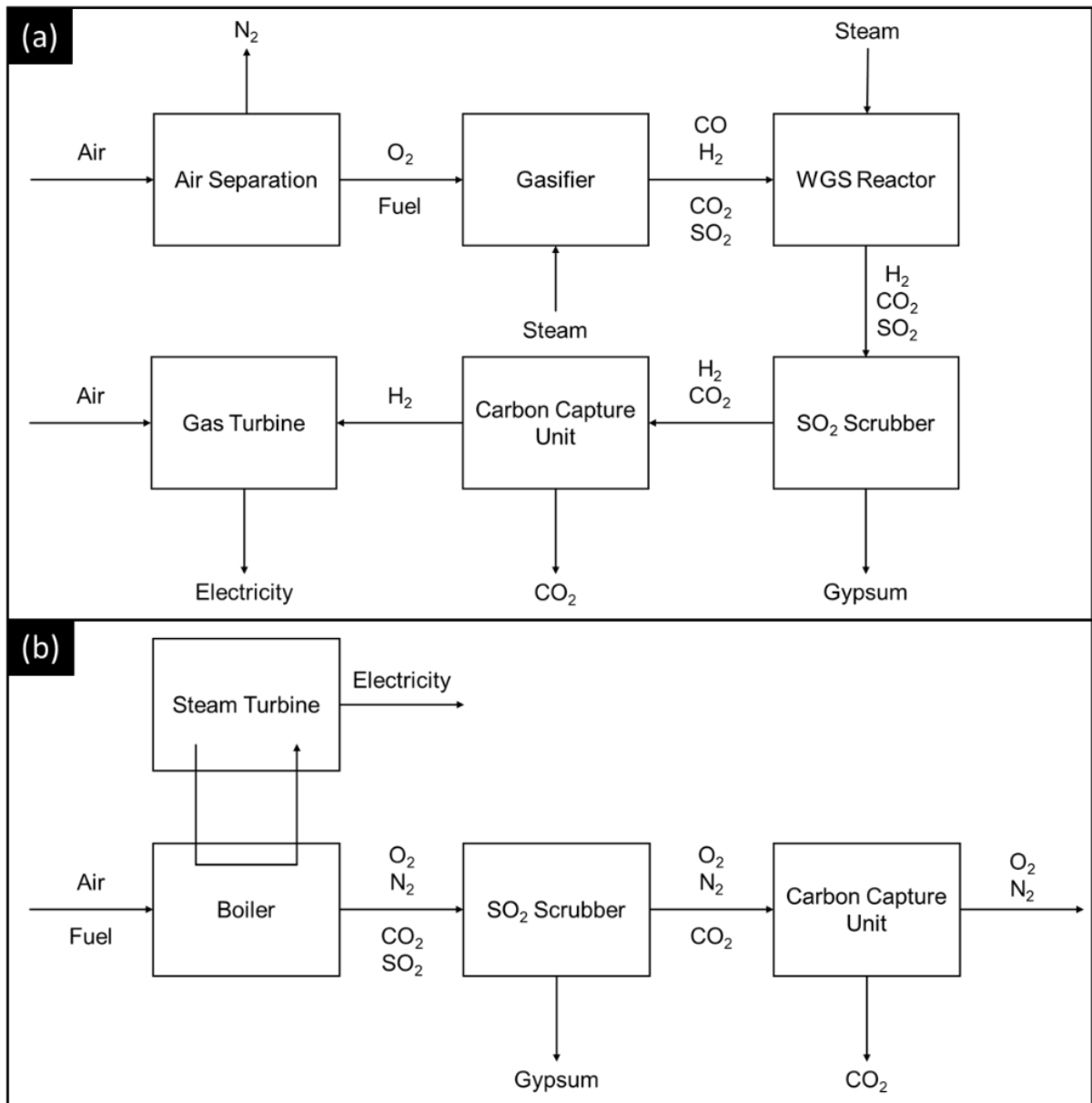
Fig. 1. 1 Process flow diagrams for (a) pre-combustion and (b) post-combustion carbon capture processes.

Chemical absorption using liquid solvents is presently the upscaled technology available for carbon capture with two commercial scale post-combustion capture facilities in operation at PC power plants in the U.S. and Canada [7], [10]. However, reducing the carbon footprint of a power plant comes at the expense of reduced power generation. The major challenge for chemical absorption technologies relate to the steam and energy requirement (parasitic load) for solvent regeneration. Its predicted that a PC power plant using chemical absorption for carbon capture will incur a 20-30% loss in power generation [11]. Therefore, researchers continue to explore methods to make carbon capture more cost and energy efficient.

Membranes offer a cheaper alternative as they operate on a continuous basis *via* the formation of a CO_2 concentration gradient across the membrane which requires no additional electricity

input *i.e.* a pressurized CO_2 containing flue gas or syngas is fed to the feed side of the membrane, while CO_2 is enriched in the permeate side. Membranes for carbon capture can largely be divided into two classes: organic and inorganic. Organic, also referred to as polymeric membranes offer a system with no chemical or steam load and have shown to possess permeabilities that exceed the level required for cost-effective CO_2 separation [12]–[20]. However, these membranes are unable to operate with a high temperature process stream (> 200°C) which causes them to lose selectivity (selective separation of one gas from a mixed gas stream) and consequently lowers product purity. Use of porous inorganic materials has produced membranes with greater chemical and thermal stability at higher temperatures than their organic counterparts, yet due to their porosity they still suffer similar selectivity issues to polymeric membranes, especially at temperatures exceeding 500°C [21]–[26]. In general, polymeric and inorganic membranes function *via* a selectivity/ permeability trade-off and they are defined by the Robeson upper bound plot [27], [28] *i.e.* a porous membrane is either highly selective or highly permeable. To achieve a theoretically infinitely selective membrane while sustaining a high permeability, a dense and functional membrane is required. This has previously been shown for O_2 [29]–[31] and H_2 [32]–[34] separation *via* dense electrochemically active single-phase inorganic membranes. Unlike solution and diffusion gas transport mechanisms used in porous organic and inorganic membranes, dense ionic membranes only allow electrochemically active species to transport through the membrane under an electrochemical gradient. Such membranes are fabricated from mixed ionic and electronic conducting materials (MIEC) which have been shown to exclusively separate O_2 (or H_2) from a mixed gas stream by carrying oxygen ions (or hydrogen protons) across the across the membrane while electrons move in the opposite (or same) direction to maintain electron neutrality. For a dense membrane to separate CO_2, the membrane must transport carbonate ions. To date, there has been no report of a single-phase dense solid carbonate ion transport membrane, however the same feat has been achieved using a molten salt-supported dual-phase membrane. This membrane consists of two key components; an inorganic solid phase and a molten salt liquid phase. The solid phase acts as a porous framework that supports the liquid phase by capillary forces, creating a dense membrane, which is theoretically infinitely selective towards CO_2. Gases are selectively transported through the membrane *via* mechanisms dependent upon the solid and liquid phases used. Three classes of membrane support have been presented in the literature and their proposed respective mechanisms for CO_2 transport are displayed in Fig. 1. 2 [35], [36].

Non-conducting support

$$CO_{2\,(g)} + O^{2-}_{(l)} \leftrightarrow CO^{2-}_{3\,(l)}$$

Oxide-conducting support

$$CO_{2\,(g)} + O^{2-}_{(s)} \leftrightarrow CO^{2-}_{3\,(l)}$$

Electron-conducting support

$$CO_{2\,(g)} + \frac{1}{2}O_{2\,(g)} + 2e^-_{(s)} \leftrightarrow CO^{2-}_{3\,(l)}$$

$$CO^{2-}_{3\,(l)} \leftrightarrow CO_{2\,(g)} + O^{2-}_{(l)}$$

$$CO^{2-}_{3\,(l)} \leftrightarrow CO_{2\,(g)} + O^{2-}_{(s)}$$

$$CO^{2-}_{3\,(l)} \leftrightarrow CO_{2\,(g)} + \frac{1}{2}O_{2\,(g)} + 2e^-_{(s)}$$
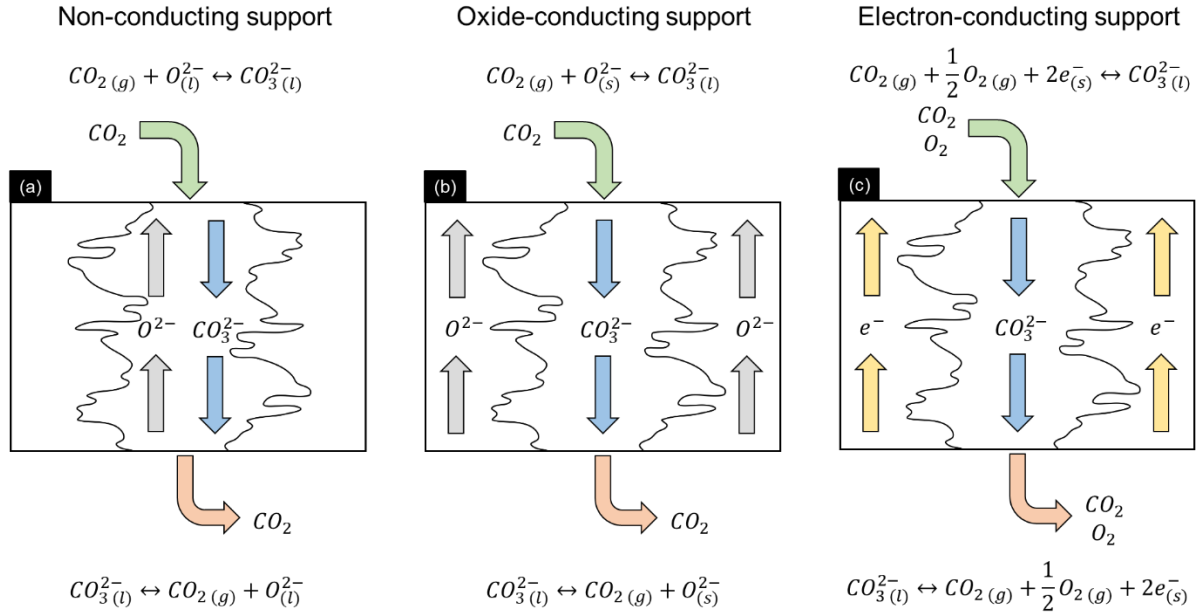
Fig. 1. 2 Schematic illustration of the CO_2 transport mechanism for (a) non-conductive supported membrane (b) oxide-conductive supported membranes and (c) electron-conductive supported membranes.

The non-conducting support is the simplest class of membrane support, where gas transport is solely dependent upon the solubilities of the gas components in the molten salt liquid phase. Thus, for CO_2 separation, molten carbonate is used as the liquid phase. This liquid phase consists of a collection of dissolved carbonate ions (CO_3^{2-}) and oxide ions (O^{2-}). CO_2 transport through molten carbonate forms a carbonate ion synthesis and decomposition cycle (see Fig. 1. 2a) from the two-phase (salt-gas) boundaries on the feed-side surface to the permeate-side surface *via* the forward and reverse of reaction (1.1), respectively. Molten oxide ions within the melt move in a counter-current direction to the carbonate ions (permeate-side to feed-side, as shown in Fig. 1. 2a) to maintain the carbonate ion synthesis and decomposition cycle. Therefore, the overall net reaction is zero if the same pressure of CO_2 is on both sides of the membrane. However, a change in CO_2 partial pressure on either side of the membrane will affect driving force, causing the counter-current mechanism described here.

$$CO_{2\,(g)} + O^{2-}_{(l)} \leftrightarrow CO^{2-}_{3\,(l)} \tag{1.1}$$

However, while this class of membrane can be cheap due to the option to use an inert and highly abundant support material, such as Al_2O_3, the associated CO_2 flux with this membrane class is comparatively low to other support materials. This is because the oxide ion concentration within the melt is low which limits carbonate ion diffusion. Rough calculation estimates that the concentration of carbonate ions in the melt is 1.9×10^{-2} mol cm^{-3} compared to 7.2×10^{-12} mol cm^{-3} for oxide ions in the melt.

Therefore, to increase carbonate ion transport and consequently increase CO_2 flux the transport mechanism can be changed by adding an oxide-conducting support to create a mixed oxide-ion carbonate-ion conducting membrane (MOCC) [37]–[53]. The same synthesis and decomposition cycle is formed, however the reactions on each side of the membrane occur at the triple-phase (salt-gas-solid) boundaries and oxide ions transport through the solid phase, as shown in Fig. 1. 2b and reaction (1.2). It should be noted that oxide ions likely still transport through the melt (as shown in Fig. 1. 2a and reaction (1.1)), however the addition of the oxide-conducting pathway through the support provides an additional route for ion transport:

$$CO_{2\ (g)} + O^{2-}_{(s)} \leftrightarrow CO^{2-}_{3\ (l)} \tag{1.2}$$

Alternatively, reaction (1.1) can be modified by implementing an electron-conducting support to create a mixed electron carbonate-ion conducting membrane (MECC) [54]–[64]. Again, a carbonate ion synthesis and decomposition cycle is formed, however this support requires the co-transport of O_2 with CO_2 to complete the cycle, as shown in Fig. 1. 2c and reaction (1.3):

$$CO_{2\ (g)} + \frac{1}{2}O_{2\ (g)} + 2e^-_{(s)} \leftrightarrow CO^{2-}_{3\ (l)} \tag{1.3}$$
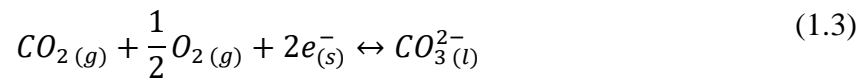
The theory behind dual-phase membranes that utilise reaction (1.3) to achieve selective CO_2 and O_2 separation is similar to the working principles of a molten carbonate fuel cell (MCFC). MCFC's typically operate at 650°C and are composed of three layers, with an electrolyte, namely molten carbonate, sandwiched between an anode and a cathode. CO_2 and O_2 are fed to the cathode causing reaction (1.3) to take place at the triple-phase boundary, resulting in carbonate ion migration towards the anode. Meanwhile, the anode is fed with H_2, which reacts with the migrated carbonate ions producing steam, CO_2 and an electrical current as described by reaction (1.4), meaning there is a net transfer of CO_2 from the cathode, to the anode, through the electrolyte. The electrical current flows through an external electrical circuit back towards the cathode to maintain electron neutrality and to allow the continuous occurrence of reaction (1.3) at the cathode. The reversible standard cell potential (E^0) of the electrochemical reactions (1.3) and (1.4) is 1.229 V [65]. A schematic illustration of the operating principles of a MCFC is displayed in Fig. 1. 3.

$$H_{2\ (g)} + CO^{2-}_{3\ (aq)} \leftrightarrow CO_{2\ (g)} + H_2O_{(g)} + 2e^- \tag{1.4}$$
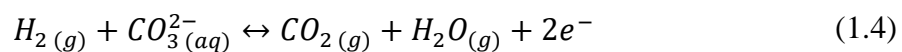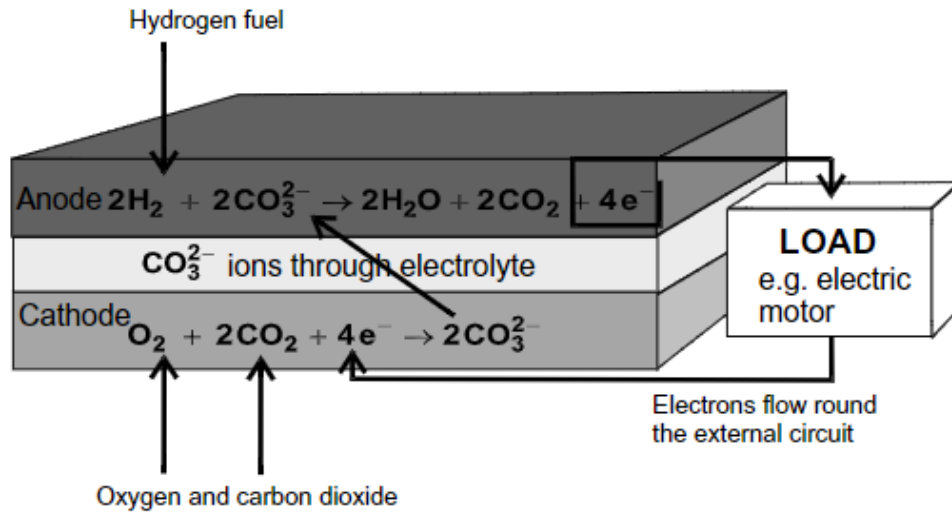
Fig. 1. 3 Operating principle of the molten carbonate fuel cell, showing the anode and cathode reactions when hydrogen is used as fuel [66].

While MCFC's continue to provide a promising prospect for electricity generation, the theory can also be used for CO_2 separation. However, an external circuit is not required to maintain electron neutrality and subsequently achieve net CO_2 transfer. Instead, the molten carbonate is suspended in a porous electron-conducting support allowing carbonate ions to migrate through the melt from the feed- to the permeate-side surface, while electrons move in the opposing direction through the solid support phase as described in Fig. 1. 2c.

While reaction (1.3) is widely reported in the dual-phase membrane literature as the most accepted mechanism for CO_2 transport in the presence of an oxidising feed gas, it is likely an oversimplification. There are other reactions between the oxidising gas, the molten carbonate and the electron conducting support that could occur, for example, reaction (1.3) only describes a process using one of a possible three oxygen reduction reactions (ORR). In reaction (1.3) the following reaction (1.5) between oxygen (on a one molar basis) and the electron conducting support takes place:

$$O_{2\,(g)} + 4e^-_{(s)} \leftrightarrow 2O^{2-}_{(s)} \tag{1.5}$$

Where the O^{2-} then reacts further with CO_2 from the feed gas to form CO_3^{2-} in a similar way to that described in reaction (1.2) and by balancing the two equations reaction (1.3) is achieved. However, a similar reaction can take place in the presence of two or one electrons to form peroxide (1.6) and superoxide (1.7), respectively.

$$O_{2\,(g)} + 2e^-_{(s)} \leftrightarrow O^{2-}_{2\,(l)} \tag{1.6}$$

$$O_{2\,(g)} + e^-_{(s)} \leftrightarrow O^-_{2\,(l)} \tag{1.7}$$
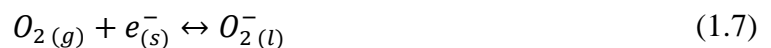
However, the subsequent reaction with CO_2 for each of these resulting oxide species does not form the same CO_3^{2-} species presented in Fig. 1. 2. Instead, for the former a peroxymonocarbonate (CO_4^{2-}) is well reported as a stable species in molten carbonate [67] upon interaction with CO_2 (1.8).

$$CO_{2\,(g)} + O_{2\,(s)}^{2-} \leftrightarrow CO_{4\,(l)}^{2-} \tag{1.8}$$

Based on the reaction mechanisms described in Fig. 1. 2, it is evident that MOCC membranes are more suitable to reducing streams (*i.e.* syngas) found in a pre-combustion power plant. Whereas, the requirement for the co-transport of O_2 for MECC membranes restricts their use for only oxidizing streams (*i.e.* flue gas) found in a post-combustion power plant. There are however some materials, similar to those used for O_2 transport membranes, that can be considered both oxide conducting and electron conducting, or MIEC, which could theoretically be used for both processes [39]–[41]. Furthermore, recently there have been reports where separate oxide-conducting and electron-conducting materials have been combined to achieve the same effect as MIEC membranes [68], [69].

Due to the variety of supports and mechanisms for CO_2 transport available, there have been multiple reports that suggest different ways that the dual-phase membrane can be effective for carbon capture. For MECC membranes (or MIEC membranes used in a post-combustion process), the co-permeated O_2 must be removed to achieve product purity. It has been suggested that the product stream could be recycled with the addition of steam for oxy-fuel combustion (See Fig. 1. 4) [9]. Alternatively, Fang *et al.* [58] demonstrated that the co-permeated O_2 can be converted to steam by adding H_2 into the permeate-side inlet gas, the idea being that this could then be condensed to achieve a pure CO_2 product. Fang *et al.* [58] also suggested that a similar CO_2 and steam mixture could be achieved by combusting the permeate in syngas. In addition, Rui *et al.* [70] modelled how the product from a dual-phase membrane (with or without O_2 co-permeation) could be used for dry-methane reforming to produce H_2 [69], [71], [72]. Lastly, Dong *et al.* demonstrated how the feed for the water gas shift reaction could simultaneously separate CO_2 and produce a H_2 rich stream [73].
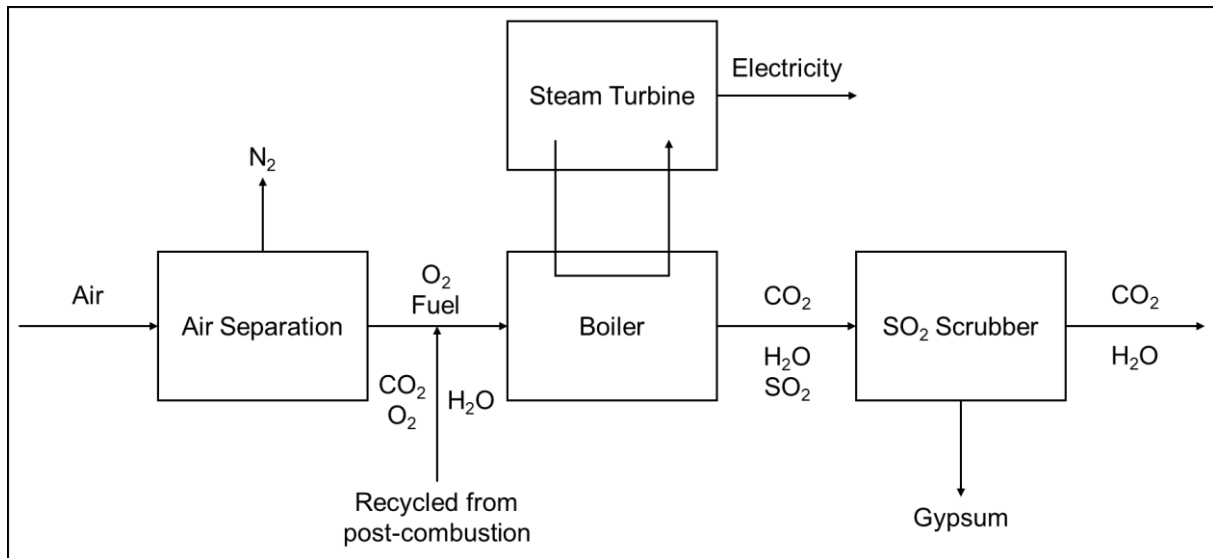
Fig. 1. 4 Process flow diagram for oxy-fuel combustion with recycled post-combustion product stream

Currently, it is common practice in the dual-phase membrane literature to use a predominantly inert gas as the permeate-side inlet gas to create a driving force for gas separation, which is then continuously remove (vented) to allow continuous gas separation. It should be noted that this is not a true representation of what a membrane would function like in an industrial application. This is because the permeated gas is simply diluting an inert gas stream, which would then need to be separated further as the presence of the inert gas would occupy too much volume for carbon storage or reuse, which would be wasteful. Therefore, for membrane upscale the permeate-side gas would likely consist of a vacuum or steam. For the latter the steam could be condensed, leaving behind the pure permeated gas.

While dual-phase membranes are still in the early stages of research, with a technology readiness level (TRL) of 3 [7], researchers are already beginning to realise their potential for carbon capture [23], [74]. A study by Anantharaman *et al.* [9] discussed a model stating the use of dual-phase membranes for power plant carbon capture could be more energy efficient than conventional chemical absorption technologies used for IGCC, PC and integrated reforming combined cycle (IRCC). Furthermore, the authors reported that dual-phase membranes could also be competitive for NGCC power plants if exhaust gas recirculation is implemented [75].

As well as the support material, the support geometry is essential in dictating the permeation performance of the dual-phase membrane. This has led researchers to modify the membrane support thickness, pore structure, porosity and surface area in order to achieve a highly permeable membrane. While modifications of the support material and geometry are well documented, modifications of the molten salt phase remain largely unexplored.

1.2 Modifications of the Dual-Phase Membrane

1.2.1 Support material modification

Dual-phase membrane support materials are typically categorized into three groups; MOCC, MECC or MIEC. There is also a fourth non-conducting material category, such as alumina (Al_2O_3), however their contribution towards gas transport is limited on their own. Multiple different oxide-conducting support materials have been presented in the literature for use in dual-phase membranes and their fluxes (mL min^{-1} cm^{-2}) as a function of temperature are displayed in Fig. 1. 5b [40], [41], [46], [47], [53]. As is the case across all membrane literature, there are many inconsistencies in permeation experiment parameters, which makes comparing the fluxes of different membranes challenging. Therefore, since flux only accounts for gas flow rate and active surface area, permeability (mol m^{-1} s^{-1} Pa^{-1}) was also used for membrane comparison (Fig. 1. 5a) as this unit normalises the following parameters:

- Gas flow rate
- Gas component partial pressure
- Membrane thickness
- Active surface area

However, these units do not account for differences in membrane porosity or pore structure. For the most comparable survey, the supports reported in Fig. 1. 5 used a random pore packing fabrication technique (uniaxial pressing or tape casting), while the effects of changing the bulk structure of the membrane will be discussed in section 1.2.2.
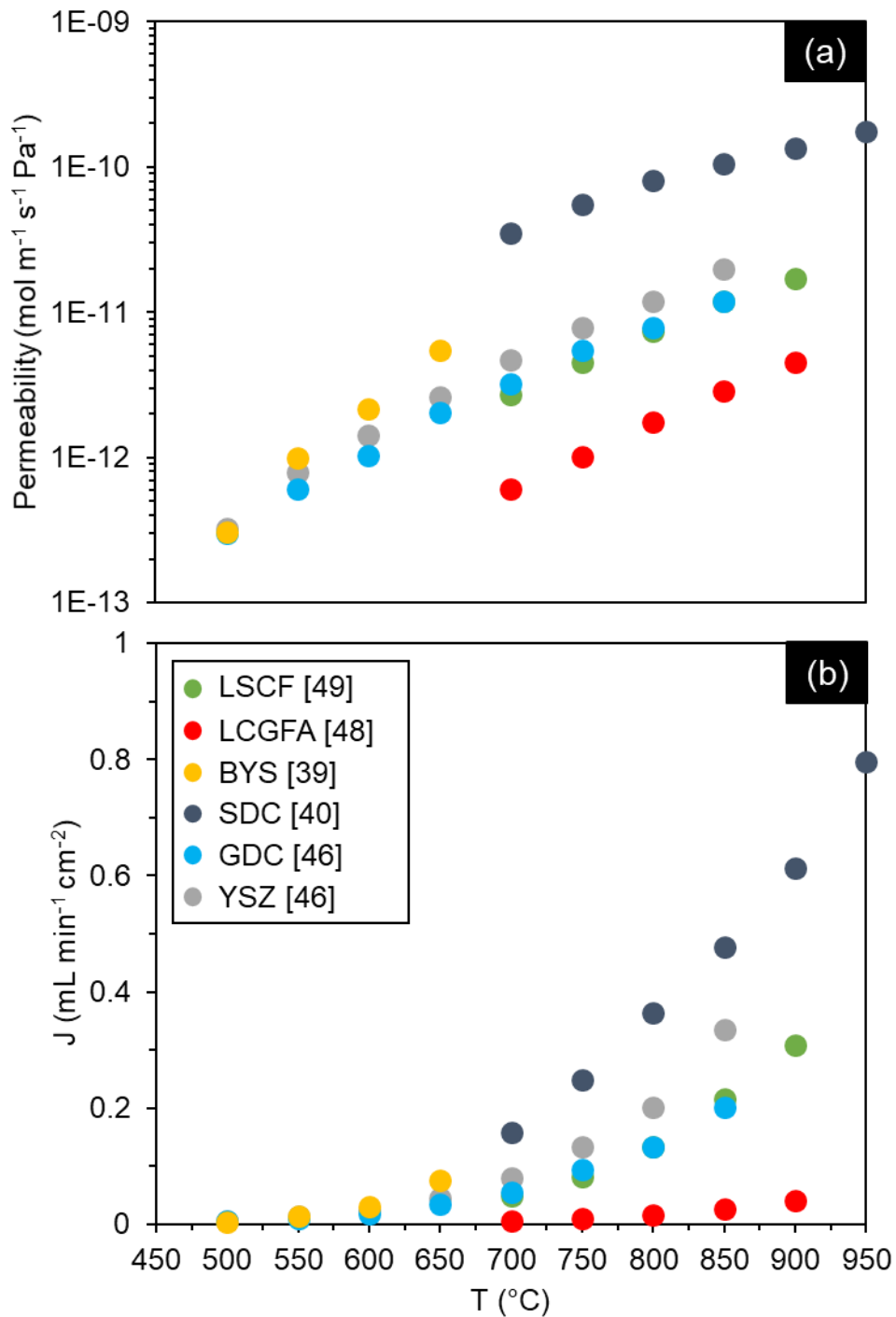
Fig. 1. 5 Comparison of (a) CO_2 permeability and (b) CO_2 flux as a function of temperature for oxide-conducting supported dual-phase membranes.

From the collection of data presented in Fig. 1. 5 it is apparent that flux increases with temperature and that these ceramic membranes are most effective at temperatures exceeding 650°C. This is shown by the fluxes below this temperature being nearly two orders of magnitude lower than the target flux for commercial use (1.0 mL min^{-1} cm^{-2}) [51]. Alternatively, all membranes are within the required permeability range for economically competitive CO_2 capture (10^{-13}-10^{-12} mol m^{-1} s^{-1} Pa^{-1}) [76].

The first dual-phase membrane to selectively separate CO_2 from a non-oxidising stream was fabricated from a ceramic perovskite-type material; $La_{0.6}Sr_{0.4}CO_{0.8}Fe_{0.2}O_{3-\delta}$ (LSCF – see Fig. 1. 5) [41]. The membrane, fabricated using uniaxial pressing, achieved a flux of 0.3 mL min^{-1} cm^{-2} (1.7×10^{-11} mol m^{-1} s^{-1} Pa^{-1}) at 900°C with a 375 µm thick membrane. However, the membrane experienced stability issues at temperatures between 800-900°C, which caused the flux to decrease considerably before reaching stable flux after 65 hrs. These instability issues were related to reactions between the support phase and the molten carbonate, which resulted in the formation of an insulating strontium carbonate layer at the interface between the CO_2 gas and the oxide ions. This led researchers to find a material that is stable in molten carbonate under a non-oxidizing CO_2 atmosphere. One such material that was able to operate stably for more than 275 hrs at 900°C was $La_{0.85}Ce_{0.1}Ga_{0.3}Fe_{0.65}Al_{0.05}O_{3-\delta}$ (LCGFA – see Fig. 1. 5) [40]. However, the increased stability came at the cost of low flux (0.04 mL min^{-1} cm^{-2} at 900°C). Fluorite-type membranes supported with yttria-stabilized-zirconia (YSZ – see Fig. 1. 5) and gadolinium-doped-ceria (GDC – see Fig. 1. 5) were reported by Wade *et al.* [53] using a tape casting technique and a samarium-doped yttria-bismuth oxide (BYS – see Fig. 1. 5) membrane was reported by Rui *et al.* [46]. Each membrane achieved fluxes lower than the LSCF membrane and did not report any experiment that lasted longer than 65 hrs each.

Since their first reporting by Zhang *et al.* [51] samarium-doped-ceria (SDC) has become widely recognized as one of the best supports for dual-phase membranes based on the high fluxes they have produced. Using the same uniaxially pressed pellet fabrication technique described for the LSCF, LCGFA and BYS membrane supports, a flux of 0.8 mL min^{-1} cm^{-2} at 950°C was achieved. Furthermore, due to the thickness of the membrane (1.5 mm) the permeability was an order of magnitude higher than its competitors (1.8×10^{-10} mol m^{-1} s^{-1} Pa^{-1}). In addition, the authors reported that the membrane was able to operate 35 days with a simulated syngas feed (35 mol% CO_2, 50 mol% CO, 10 mol% H_2 and 5 mol% N_2) and achieved fluxes ranging between 0.35 and 0.26 mL min^{-1} cm^{-2}. They did however report the formation of samarium oxide (SmO_3) on the feed side, which the authors state was due to decomposition of the fluorite structure due to H_2 exposure. However, this was limited to the feed-side surface and the rest of the membrane maintained its original structure, allowing selective CO_2 transport.

The benefits of using a support made from a ceramic oxide-conducting material for a pre-combustion application is emphasised by a study from Tong *et al.* [57]. The authors showed how an electron-conducting support material made from silver (Ag) achieved a low flux of 0.02 mL min^{-1} cm^{-2} with a CO_2 and N_2 gas feed mixture. However, some studies have also shown the benefits of using an oxide-conducting support for use in a post-combustion process, or more

12

accurately the use of an oxide and electron-conducting support material (MIEC). LSCF is known to be both electron conducting and oxide conducting, therefore when O_2 was added to the feed gas, a new CO_2 transport mechanism was activated, allowing the initiation of reaction (1.3). The addition of 25 mol% O_2 increased the CO_2 flux by an order of magnitude between 850-950°C (1.7 – 4.0 mL min^{-1} cm^{-2}) [39]. The ratio between permeated CO_2 and O_2 was 2:1 which agrees with the stoichiometry of reaction (1.3). Furthermore, the use of O_2 in the feed gas inhibited the reaction between CO_2 and the support described previously, which allowed the membrane to operate for 600 hrs. An alternative way to increase the stability of perovskite materials compared to using the low flux LCGFA membrane or adding O_2 into the feed gas was described by Ovalle-Encinia *et al.* [43]. The authors reported a mixed fluorite/perovskite-supported membrane ($Ce_{0.85}Sm_{0.15}O_{2-\delta}$ and $Sm_{0.6}Sr_{0.4}Al_{0.3}Fe_{0.7}O_{3-\delta}$ – SDC/SSAF) which achieved a flux of 0.23 mL min^{-1} cm^{-2} at 900°C with a 15 mol% CO_2 in N_2 feed gas. The authors reported that the membrane produced no secondary phases linked to reactions between the perovskite support and the molten carbonate, however the authors did not report how long the membranes were operated for, thus the membranes long-term stability is currently unclear. In addition, due to the electron conductivity of the perovskite component in the mixed support, when 6 mol% O_2 was added to the feed gas the CO_2 flux increased to 0.29 mL min^{-1} cm^{-2} at 900°C [43]. The membrane co-permeated O_2 at a flux of 0.12 mL min^{-1} cm^{-2} creating a 2.5:1 CO_2: O_2 flux ratio, which indicates that both reaction (1.2) and (1.3) occurred during permeation. Furthermore, a later development on this study by the same authors deposited metallic gold-palladium (Au-Pd) particles on the SDC-SSAF membrane feed-side surface to concentrate electrons at the feed-side surface to improve carbonate ion formation, resulting in a CO_2 flux of 0.35 mL min^{-1} cm^{-2} at 900°C with a 15 mol% CO_2 and 6 mol% O_2 feed gas [68]. Through permeation experiments, the authors found three separate transport pathways:

1. CO_2 and O_2 permeation through the melt due to the addition of the metallic particles on the feed-side surface or through reaction with electron conductive perovskite phase, which promotes reaction (1.3).
2. CO_2 permeation through the membrane due to reactions between the melt and the oxide-conducting support, which promotes reaction (1.2).
3. O_2 permeation as a result of oxygen ion transport through the support from the mixed conducting perovskite material, similar to how O_2 transport membranes operate.

However, the increase in CO_2 flux for the modified membrane was only ~20%, which is low considering the expense of depositing Au-Pd particles. A possible reason or the limited increase is that while the particles increase the formation of carbonate ions on the feed side, the cross-

section and permeate-side is not electron conductive, therefore the gas flux will be limited by the rate at which gas is released on the non-electron conducting permeate side. Therefore, for a membranes' modification to increase gas flux significantly, *i.e.* greater than 20%, the membrane must provide a continuous and consistent route of conduction throughout the membrane for the forward and backwards of reaction (1.2) and/or (1.3) to occur at equal rates on each side of the membrane.

In addition, while the single fluorite membrane supports discussed in Fig. 1. 5 are considered to be solely oxide-conducting materials, materials such as SDC and YSZ are known to have electron conductivity, albeit lower than their oxide conductivities [77], [78]. Therefore, when an SDC supported membrane (with no perovskite or metallic particle doping) was subjected to and oxidizing feed, O_2 was found to co-permeate with CO_2 in a 5:1 CO_2: O_2 ratio [49]. As the O_2 partial pressure was increased in the feed gas (and CO_2 was kept constant), CO_2 permeation also increased which indicated a coupled transport mechanism between the CO_2 and O_2, likely *via* reaction (1.3). The difference in permeation stoichiometry suggests that the primary mechanism of CO_2 transport is likely still reaction (1.2), however the authors calculated that roughly one third of the CO_2 transported *via* reaction (1.3). This coupled transport mechanism disagrees with a model presented by Rui *et al.* [35] which suggested that O_2 permeation through MOCC membranes was independent of flux. Either way, the co-transport of O_2 through MIEC and MOCC membranes indicates that their use for post-combustion would require O_2 separation, similar to a MECC membrane reactor. As a result, their use compared to MECC membranes are not advantageous in achieving CO_2 product purity for such application. The only difference between the membrane systems is that O_2 can be removed prior to an MIEC or MOCC membrane instead of afterwards, which is required for MECC membranes. Therefore, a broader flux comparison including MECC membranes with oxidising feed streams can be made to determine which supports are better for a post-combustion carbon capture process.

The first MECC membrane to be reported was supported by a stainless-steel framework [61]. A feed gas containing 2:1 mixture of CO_2 and O_2 supplied a CO_2 flux of 0.23 mL min^{-1} cm^{-2} at 650°C and CO_2 and O_2 permeated in a 2:1 ratio, agreeing with the LSCF membrane and reaction (1.3). However, at temperatures exceeding 650°C, it was found that the stainless-steel support became oxidized, forming an insulating $LiFeO_2$ layer at the liquid-solid phase boundary. $LiFeO_2$ is known to have a low electronic conductivity [79] which resulted in a reduction in the supports electronic conductivity, causing an order of magnitude decrease in CO_2 flux at 750°C compared to 650°C. This result indicates that an electron conducting support is required that does not oxidise in molten carbonate.

N. Xu *et al.* [60] reported for the first time, an Ag-supported dual-phase membrane. It was found that this membrane had the ability to maintain its electronic conductivity at high temperatures and a peak CO_2 flux of 0.8 mL min^{-1} cm^{-2} at 650°C was achieved with a 2:1 CO_2: O_2 ratio. However, similar to the stainless-steel support, the Ag support suffered stability issues of its own. It was found that the membrane was unable to retain carbonates within the pores of the Ag support for long periods of time. This instability was attributed to two reasons: (1) wettability issues between Ag and molten carbonate [80], and (2) sintering of the support. This meant that during the first 20 hours of operation the CO_2 flux increased gradually as molten carbonate was pushed out of the pores, thus making the membrane thinner and hence the diffusion path length shorter. After 20 hours, the membranes pores began to open from carbonate loss, which causes gas to break through the open pores of the membrane resulting in non-selective permeation. After correcting for gas leakage, the CO_2 flux decreased over the following 55 hrs by 22% until the experiment was stopped. This flux reduction is thought to be due to a reduction in molten carbonate available for gas transport. Furthermore, when a separate membrane was heated to 700°C the peak flux decreased by 25% compared to at 650°C. A likely reason for this decrease is due to the loss of carbonates happening at a faster rate, which meant the membrane was unable to retain the carbonates for long enough to achieve a flux higher than at 650°C. The findings presented in this study outlined the need to improve the carbonate retention within the Ag support. Attempts have been made to improve the wettability between the molten carbonate and the Ag and reduce Ag sintering by coating the melt-solid interface with Al_2O_3 [54], [55], [57], [59] or zirconia (ZrO_2) [62] nanolayer coatings. The effects of these coatings on the flux (and permeability) were compiled in Fig. 1. 6. For fair comparison, only membrane supports prepared using uniaxial pressing were described here. Modification of the pore structure is discussed in section 1.2.2.
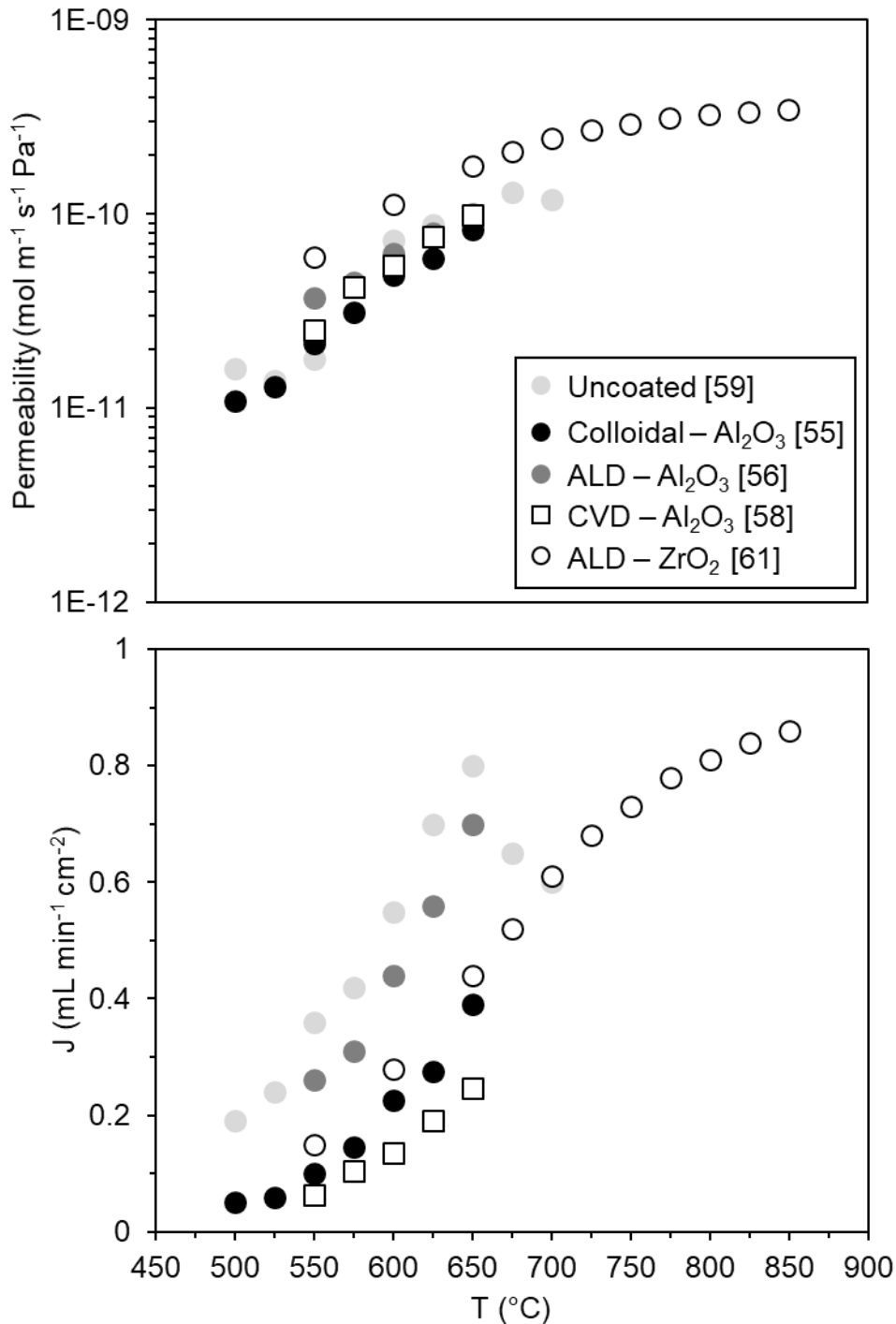
Fig. 1. 6 Comparison of (a) CO$_2$ permeability and (b) CO$_2$ flux as a function of temperature for Ag-supported dual-phase membranes with different surface coatings.

The data presented in Fig. 1. 6 shows that the permeabilities across all temperatures are tightly grouped for all Ag membranes compared to the ceramic membranes (see Fig. 1. 5a), which is expected since all the supports are made from the same material here. Any variations in flux can mainly be attributed to differences in driving force. This indicates that in general, the surface coatings had little effect on the flux of the Ag membrane. Which is reasonable as the

purpose of the coatings are not to increase the flux, they are added to increase the stability of the membrane and in response increase the flux for long-term use.

The first reported uncoated Ag-supported membrane by Xu *et al.* [60] has a higher flux than any of the coated membranes shown in Fig. 1. 6b. However, reported flux data for different uncoated Ag membranes in the literature is inconsistent. Zhang *et al.* [54] reported a CO_2 flux of 0.45 mL min^{-1} cm^{-2} for an uncoated membrane. Both Xu and Zhang's uncoated membranes were prepared using the same method and each had a feed gas containing 42 mol% CO_2, 42 mol% O_2 in N_2. The differences in flux is counter-intuitive since the membrane presented by Zhang was 0.53 mm thinner (1.67 mm compared to 1.14 mm). Furthermore, two identically prepared uncoated membranes (0.82 mm thick, 40% porosity) fed with 15 mol% CO_2, 10 mol% O_2 in N_2 produced different fluxes again. The uncoated membrane reported by Tong *et al.* [57] was ~0.12 mL min^{-1} cm^{-2} while the same membrane reported by Zhang *et al.* [62] was ~0.45 mL min^{-1} cm^{-2}. While the authors from the four different papers never explain their differences in flux, the results serve as a reference for the magnitude of flux variation between experiments, likely caused by wettability and sintering issues. A further reason for the disparity between the fluxes for uncoated membranes can be explained by the transient behaviour for all uncoated Ag membrane experiments. Since all uncoated Ag membranes are unstable and succumb to wettability and sintering issues, a logical data point to describe the membranes flux is difficult. Different authors will likely report their fluxes after different lengths of operation, which can have a major impact when comparing values across separate studies. For example, one author could report their flux after 20 hrs and receive a flux of 0.8 mL min^{-1} cm^{-2} when the diffusional path length is at its shortest and before pores start to open. Whereas, another author may report their flux after 50 hrs when multiple pores are open and the amount of carbonate available for gas transport is much lower and thus, the flux is much lower. Therefore, it is important to achieve an Ag membrane that does not experience this degradation in flux to fully understand the capabilities of the support.

The variations between the fluxes of different uncoated membranes makes it difficult to determine if a surface coating has positively influenced flux for long-term operation as it is unclear how long each membrane had been operated for. The only coated membrane to outperform Xu's uncoated membrane's permeability was the ZrO_2-coated membrane (Fig. 1. 6a) [62], all other coatings produced lower or equal fluxes and permeabilities. However, when comparing the coated membranes to uncoated membranes in their own respective studies, all coatings improved or achieved the same flux as the reference uncoated membranes at 650°C. The biggest improvement was reported by Fang *et al.* [57] where they coated the membrane

with a layer of Al_2O_3 using atomic layer deposition (ALD) and achieve a flux improvement of a factor of six or higher throughout the entire experiment. This consistent improvement is never explained, as one would expect the uncoated membrane to have a higher flux at the start of the experiment as the path length becomes shorter due to molten carbonate expulsion from the pores. One argument that could substantiate their findings is that the addition of the highly wettable nano-Al_2O_3 layer improved the contact between the support and the molten carbonate. This would result in an increased density of triple-phase boundaries available for electron transport, which would increase the rate of reaction (1.3) and hence, cause an increase in flux. Furthermore, Fang discussed that the activation energy of CO_2 transport for their membrane was higher than CO_3^{2-} diffusion and suggested that the process was limited by surface exchange reactions. Therefore, the improvement in flux is likely attributed to better contact between the molten carbonate and the porous support at each surface, resulting in a faster catalytic process initiated by Ag. Interestingly, despite the already high CO_2 flux, the flux ratio in this study was 1:1.5 in favour of O_2. Fang *et al.* later explained that the "remarkable" O_2 flux was due to a second O_2 transport pathway that takes place at the two-phase (gas-liquid) boundary *via* reaction (1.9) and forms a new peroxymonocarbonate species (CO_4^{2-}) [63], [64]:

$$\frac{1}{2}O_{2\ (g)} + CO_{3\ (aq)}^{2-} \leftrightarrow CO_{4\ (aq)}^{2-} \tag{1.9}$$
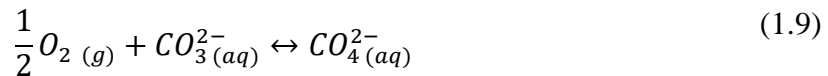
This species transports through the melt and dissociates on the permeate side, similar to the mechanism described by reaction (1.3). This dilutes the 2:1 ratio routinely found with electron-conducting dual-phase membranes. The authors explain that the two-phase boundaries form as a result of molten carbonate "flooding" the permeate-side surface which reduces the number of triple-phase boundaries, thus promoting reaction (1.9) [64]. This would contradict the explanation for the increased CO_2 flux compared to the uncoated membrane. Fang *et al.* [57] also suggested that the increased O_2 flux could be due to the increased basicity in the melt as a result of the Al_2O_3 surface coating which increases the rate of O_2 dissolution at the triple-phase boundaries for the formation of CO_4^{2-} and promotion of the reaction (1.10):

$$CO_{2\ (g)} + \frac{3}{2}O_{2\ (g)} + CO_{3\ (aq)}^{2-} + 2e^- \leftrightarrow 2CO_{4\ (aq)}^{2-} \tag{1.10}$$
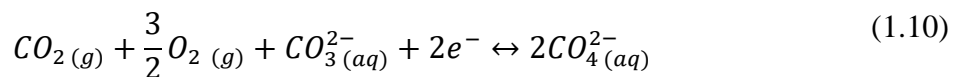
P. Zhang *et al.* [62] demonstrated that by coating the Ag support with ZrO_2 using ALD the membranes were able to retain carbonates within the porous Ag network long enough to achieve a continuous increase in flux across temperatures ranging from $650 - 850°C$. This improvement was attributed to reducing the grain growth *i.e.* sintering of the Ag support and produced a flux of 0.86 mL min^{-1} cm^{-2} at 850°C, which is higher in operation temperature and flux than any other Ag-supported membrane in the literature.

While each surface coating improved the flux of CO_2 in their own respective studies, there was still carbonate loss resulting in flux decline (after an initial increase due to shortening of the diffusional path length) during long-term operation for the coated membranes, albeit reduced compared to uncoated membranes. Only the membrane using chemical vapour deposition (CVD) for Al_2O_3 coating was able to maintain a stable flux for 100 hours without seeing any decline in flux (or increase at the start) [59], however this membrane achieved the lowest flux out of all coating methods. While the authors do not explain why the flux is lower than an Al_2O_3 or ZrO_2 coated membrane using ALD, a possible reason could be because the Al_2O_3 layer was thicker than other coating methods which increased the carbonate retention but decreased the electron conductivity of the Ag support. The Al_2O_3 layer produced using CVD was ~1 µm while the layers produced using ALD were ~20 nm. This indicates that there seems to be a stability/flux trade-off for Ag-supported membranes that should be addressed in the future to achieve a stable, high-flux membrane.

The membranes presented in Fig. 1. 6 and Fig. 1. 5 illustrate a striking difference between the operation of Ag and ceramic membranes at 650°C or lower. The CO_2 permeabilities for the ceramic membranes operated at 650°C were all of the order ~10^{-12} mol m^{-1} s^{-1} Pa^{-1} compared to ~10^{-11} mol m^{-1} s^{-1} Pa^{-1} for Ag-supported membranes.

In addition, when comparing fluxes at 650°C the highest flux for a single fluorite or perovskite supported membrane was no higher than 0.1 mL min^{-1} cm^{-1} [46], [53], while the Ag-supported membranes reached fluxes around 0.8 mL min^{-1} cm^{-2} [60]. When including ceramic membranes fed with O_2 at the same temperature, the Ag-supported membranes still produced higher fluxes, indicating that Ag is the best support for a post-combustion process based on flux alone. In terms of stability, the uniaxially pressed Ag membranes require improvement. Issues with the support resulting in a degradation in flux seems to be a common theme for all membrane supports discussed in this section. Even the SDC and LSCF supports which were operated for 35 and 25 days, respectively saw fluctuations from their peak flux value by ~20% due to reactions with the support. These results demonstrate the need for a membrane where the flux does not depend on the properties of the support and instead can achieve high and stable flux from another source *i.e.* the molten carbonate.

1.2.2 *Support geometry and pore structure modification*

While the membranes discussed in the previous section were all fabricated into similar disk-shaped geometries, there are other factors that must be considered when comparing fluxes to identify which supports materials are most effective. The previously discussed membranes (Section 1.2.1) all had different support thicknesses, porosities, pore sizes and had different

fabrication techniques: LSCF, LCGFA, SDC and BYS supports were fabricated using uniaxial pressing technique while the YSZ and GDC supports were fabricated using tape casting technique. These differences have led researchers to try to understand the relationship between the bulk structure of the support and the membranes flux.

While the uniaxial pressed pellet fabrication technique uses minimal amounts of resources and time, the simplistic nature of the procedure creates a framework with randomly packed pores and a highly tortuous network, which limits bulk diffusion through the membrane. Therefore, to improve the flux further regardless of support material, control of the bulk porous framework is needed, which was shown by Ortiz-Landeros *et al.* [81]. In their study, they sintered 4 uniaxially pressed powder pellets of LSCF at different temperatures (900, 1000, 1050 and 1100°C) and characterised the sintering temperatures effect on porosity and electrical conductivity using helium permeation and electrical conductivity measurements. As expected, the results showed that the membrane sintered at the highest temperature, 1100°C, was the least porous, with an open porosity of 23% compared to 53% from a membrane sintered at 900°C. In contrast, the least porous membrane offered an order of magnitude higher electrical conductivity at 900°C (1434 S cm^{-1} compared to 199 S cm^{-1}) due to the higher solid fraction in the support provided by increased sintering. When the partially sintered supports were infiltrated with molten carbonates and used for permeation experiments, comparison of the fluxes showed that a balance must be made between porosity and support conductivity for the LSCF support. The membranes with the most and least sintered supports provided the lowest CO_2 flux across all operation temperatures between 750-900°C. The highest flux was produced by a membrane sintered at 1000°C, which had a porosity of 46%. This membrane had a CO_2 flux 2-3 times higher across all operation temperatures compared to the 900°C sintered membrane, which highlights the effect a 7% difference in porosity can make on a membranes flux capability. The membrane support sintered at 1000°C also had an electrical conductivity more than a factor of two higher than the 900°C sintered membrane support (451 S cm^{-1}) which could also have contributed to the increase in flux. The increased support electrical conductivity is due to the lower porosity of the membrane caused by increased sintering which results in a less tortuous network for an electrical current to flow. Therefore, the support conductivity can be increased further by forming straight, parallel pores that span the entire cross-section, where the framework for the pores consists of a dense conductive material, such as those discussed in Fig. 1. 5 and Fig. 1. 6.

A similar study of the effect of porosity on gas flux was carried out by Zhang *et al.* [51]. However, in their study they controlled the porosity using a combined "co-precipitation" and

"sacrificial-template" method instead of sintering, described previously. This was achieved by controlling the volume ratio between the sacrificial phase (nickel oxide – NiO) and the final support phase (SDC). The volume of the sacrificial phase constituted the final open porosity once the NiO had been removed. Volume ratios for NiO:SDC between 30:70 and 50:50 were tested *i.e.* open porosity of 30-50%. The result of this study showed that the membrane with a 50% open porosity achieved the highest flux across all operation temperatures (550-700°C) and had a flux 2-3 times higher than a membrane with 40% open porosity. This flux enhancement is similar to that shown by Ortiz-Landeros *et al.* [81] described previously, where an increase in porosity from roughly 40% to 50% resulted in a 2-3 times flux improvement. Furthermore, the SDC membrane in the work of Zhang *et al.* achieved a flux an order of magnitude higher than the uniaxially pressed pellet SDC membrane reported in T.T. Norton's study while operating at the same temperature (700°C) [47]. The uniaxially pressed pellet SDC membrane had an open porosity of 36%, which could explain the discrepancy in flux. In addition, the sacrificial-template SDC membrane was fed with 4.8 mol% H_2 in the feed gas to lower the partial pressure of O_2 in the feed gas, resulting in an increase in oxide and carbonate ion transport and consequently an increase in CO_2 flux. The authors did not explain how adding H_2 would lower the partial pressure of O_2 since O_2 was not fed to either side of the membrane, however it is likely that they reduced the partial pressure of O_2 from air leaks and gas impurities in the feed-side inlet.

As well as improvements to gas flux, modification of support pore structure has also shown benefits for membrane stability for Ag-supported membranes. A study by Fang *et al.* [58] demonstrated that carbonate retention for Ag-supported membranes could be improved by reducing the pore size. The routinely observed ~10 µm pores from the uniaxial pressing technique previously described were reduced to <1 µm using a dealloying fabrication technique. By reducing the pore size, the capillary forces inside each pore was increased which increased the carbonate retention, allowing the membrane to operate for 900 hrs. Furthermore, the membrane achieved a flux of 1.3 mL min^{-1} cm^{-2} at 700°C, which is higher than any other Ag-supported membrane, regardless of temperature used. The authors attributed the increase in flux to the increase in density of triple-phase boundaries as a result of pore size reduction *i.e.* the number of contact points between the melt and the electronically conductive surface was increased. Another reason for the increased flux can be explained by the presence of 10 mol% H_2 in the permeate-side inlet gas. Similar to the SDC membrane with H_2 in the feed-side inlet, the H_2 here reduced the partial pressure of co-permeated O_2 on the permeate side, *via* the formation of steam through reaction (1.11):

$$H_{2\,(g)} + O_{2\,(g)} \leftrightarrow H_2O_{(g)} \qquad\qquad (1.11)$$

Since O_2 and CO_2 transport is linked through reaction (1.3), a decrease in O_2 content in the permeate side chamber increases the driving force for CO_2 separation, while also achieving a condensable CO_2 and steam product as described by the MCFC anodic reaction discussed previously (1.4).

The authors demonstrated that by removing H_2 from the permeate-side inlet gas, the flux decreased by a factor of two at 600°C. However, the membrane still achieved a permeability higher than all other Ag membranes at the same temperature (2.3×10^{-10} mol m^{-1} s^{-1} Pa^{-1}, see Fig. 1. 6a), which outlines the improvements in flux made by the pore structure modification technique. Reaction (1.11) and (1.4) clearly illustrates a disruption in the mechanism and driving forces for CO_2 transport when compared to membranes fed with an inert gas in the permeate-side inlet. For this reason, it would be unreliable to compare these membranes directly. Instead, future studies in this area should only compare membranes where the same driving forces are applied across the membrane to isolate the impact of the support used and to not confuse flux improvement from the materials and gases used.

Aside from pore structure modification, another method of support modification, which has improved the flux and stability of dual-phase membranes is the fabrication of asymmetric membranes. The idea of these membranes is to take favourable properties from two different materials and combine them to make a more effective membrane. The most commonly used asymmetric dual-phase membrane used in the literature uses a combination of SDC and BYS [38], [82], [83]. SDC was used as the support phase as porous SDC supports filled with molten carbonate have been regularly reported to achieve the highest CO_2 flux of all oxide-conducting materials used due to the supports high O^{2-} ion conductivity which consequently lowers ionic resistivity for both CO_3^{2-} and O^{2-} [51]. However, it is known to have carbonate retention issues beyond 10-15 hours of operation [51]. Therefore, a second porous SDC/BYS support is sintered to the underside of the SDC support and due to the non-wettability of BYS with molten carbonate, the molten carbonate is "repelled" from infiltrating into the lower BYS support, thus improving carbonate retention in the upper SDC support. SDC is mixed into the lower BYS base support in a 40:60 ratio to ensure the sintering temperatures match between the upper and lower layers. In addition, the use of the non-wettable lower support means that the upper SDC support can be reduced in thickness while maintaining its mechanical strength from the SDC/BYS base. The effects of reducing support thickness on gas flux is well documented. The first ceramic membrane reported by Anderson and Lin [41], demonstrated that by decreasing the thickness of an LSCF support by an order of magnitude they were able to increase the flux

by an order of magnitude. Therefore, a study by Lu and Lin presented an asymmetric SDC-SDC/BYS membrane with a 150 μm upper SDC layer and a 2 mm non-wettable SDC/BYS layer [82]. The resulting membrane achieved a flux of 0.88 mL min^{-1} cm^{-2} at 700°C, which is only lower than a sacrificial-template SDC membrane, however the asymmetric membrane was shown to operate for more than ten times longer (160 hrs). In place of SDC, a ~10 μm YSZ layer has been used to form an asymmetric membrane with a 2 mm thick BYS base [84]. For this asymmetric support, no additions were needed for the BYS base as the sintering temperatures for BYS and YSZ aligned. The YSZ-BYS membrane achieved a flux of 0.52 mL min^{-1} cm^{-2} at 650°C. The high fluxes and stability exhibited by asymmetric membranes has led researchers to consider the required geometry for industrial upscale. The support materials discussed thus far have all been of "flat disk" geometry. While useful for research scale due to their ease of fabrication, flat disk membranes have limited surface area and do not represent a realistic packing for industrial upscale. Dong *et al.* [83] demonstrated the use of a tubular geometry for an asymmetric SDC-SDC/BYS membrane which achieved a flux of 2.05 mL min^{-1} cm^{-2} which is currently the highest flux of any dual-phase membrane with a non-oxidising feed gas stream. The use of asymmetric membranes for both flat-disk and tubular geometry clearly display that supports can be manipulated to improve flux, wettability and stability.

While the modifications discussed here indicate the best approach to fabricating an ideal dual-phase membrane support (< 500 μm thick, ~50% porosity, < 1 μm pores, straight non-tortuous pores, highly wettable material with molten carbonates) there are however, other factors which influence flux and are harder to define. A study by Patrício *et al.* [44] possibly contradicts the aforementioned relationship between porosity, thickness and flux. In their study, they fabricated a GDC support with a porosity of 27% and achieve a CO$_2$ flux of 0.6 mL min^{-1} cm^{-2} at 850°C. This flux is a factor of 3 higher than the GDC support prepared by Wade *et al.* [53] at the same temperature, which had a porosity of 36%. Furthermore, Patrício's support was 2-3 times thicker than Wade's, thus making the diffusion path length greater, which disagrees with Anderson and Lin's work. While Patrício *et al.* did not elucidate on why their flux is higher, there are however, other factors that may have contributed to the difference in flux. For example, the supports were prepared using different techniques (uniaxial pressing *vs.* tape casting) which could modify the contact between the support and the molten carbonate. Furthermore, Patrício *et al.* did not report their average pore size distribution but studies have shown that pore size can affect the flux of a membrane (and its stability) [58]. In addition, the authors also did not discuss the tortuosity of the pore network, which is known to have an effect of the conductivity of the support [81]. The results of this paper indicate that reliable

comparisons between membrane supports and geometry modifications must be made internally where all parameters can be controlled, or that different studies need to adopt common principles to allow comparison between them. There are too many unaddressed factors that may contribute to the flux of a membrane that the current state of the dual-phase membrane literature has not yet attempted to understand.

An important consideration to make when analysing and comparing the CO_2 flux of dual-phase membranes, is leakages. Thus far, leakages have been discussed in the context of carbonate retention issues within the porous network, however nearly all dual-phase membrane papers acknowledge that gas leaks can occur as a result of breaks in the sealant. While, sealant breaks are an issue limited to research scale, as industrial upscale will likely use membranes with no hot sealing region, the requirement to maintain a good seal when demonstrating a new membrane is critical to report reliable gas fluxes. In the literature, it is common practice to subtract leaks from the final calculated flux. This is done by monitoring a "leak gas", say N_2, and if N_2 is detected by the permeate side gas analysis instruments, then depending on the ratio of the N_2 and CO_2 in the feed gas, the equivalent amount of CO_2 is subtracted from the calculated flux. However, this method of leak subtraction does not account for the reduction in driving force for CO_2 across the membrane as gas prefers to move through the least restricting route. It also does not account for any air leaks in the permeate-side chamber. As N_2 is the most abundant gas in the atmosphere, an air leak into permeate side of the reactor would lower the driving force for N_2 leak across the membrane but would not inhibit the amount of CO_2 transmembrane leakage. Therefore, when the CO_2 is subtracted based on the N_2 leak, it could be underestimated. To ensure that transmembrane sealant leaks do not misrepresent the gas flux, membranes should be fabricated in a way to remove leaks. One approach that could reduce leaks is to fabricate membranes with no hot sealing region.

1.2.3   *Molten carbonate modification*

The target for previously discussed support modifications is often to improve the CO_2 flux in terms of rate, while feasibility of upscale is often ignored. The composition of a dual-phase membrane is roughly 50:50 in vol% for the solid support phase and the molten carbonate phase, however the cost of the support phase is far higher. The support materials that have shown to produce the most CO_2 permeable membranes in the literature all include materials such as samarium (Sm), lanthanum (La), cobalt (Co) and Ag (Ag), all of which come at a high cost:

- Sm and other rare-earth metals are expensive due to China dominating the market and regulating the export of such minerals from their country [85]. In addition, rare earth

ores often include radioactive elements that must be removed which also increases their cost [85], [86].

- The price of Co has increase by 450% over the past 2 years due its demand in electric cars [87]. In addition, more than half of the worlds production of Co comes from the Democratic Republic of Congo which have had issues with corruption in their Co mines and are well understood to use child labour and poor infrastructure [87], all of which is reflected in the price of Co on the London Metal Exchange.

- Ag is also expensive due to the high demand for the precious metal in jewellery.

Therefore, the cost of these materials makes scaling up the membrane for industrial use expensive, which indicates that efforts must be made to use cheaper materials. One method would be to exploit the molten carbonate to achieve high flux as the components that form the carbon eutectic are cheaper and instead a low-cost support material could be used. Furthermore, modification to the support does not change the flux much as shown by the variations in flux all being within the same order of magnitude (see Fig. 1. 5), thus modifying the molten carbonate may be more beneficial to increase gas flux. However, it is often believed that oxide ion conductivity in the support phase limits carbonate ion transport [33], [38], [39], [44], [45], [51], thus any modifications to the melt would have diminishing returns, which could explain why much focus for dual-phase membranes centres around modification of the support. However, a study by Xing et $al.$ [88] proved otherwise. In their study, using an oxide conducting CeO_2 support they identified that dissolved oxide conductivity in the melt limits carbonate ion transport between 550-650°C. This conclusion was drawn by performing the same porosity modification experiment, previously described (see section 1.2.2). Similar to work by Ortiz-Landeros et $al.$ [81] and Zhang et $al.$ [51] they found that the flux increased by a factor of 2-3 when the porosity of the ceria oxide (CeO_2) support was increased from 38% to 50%. If oxide ion conductivity in the support was rate limiting, then increasing the porosity would decrease the oxide ion conductivity of the support, which would result in a reduction in CO_2 flux. Therefore, since oxide ion conduction in the melt was found to be rate limiting the authors doped the carbonate melt with metal oxides (cesium vanadate, $CsVO_3$ and molybdenum oxide, MoO_3) resulting in a factor of two CO_2 flux increase when compared to an undoped molten carbonate membrane. While the flux reported by the doped membrane was higher than the undoped membrane, the flux was still lower than all reported oxide-conducting supported membranes in Fig. 1. 5. Therefore, different metal oxides should be explored to understand the relationship between flux and the addition of foreign oxides. Furthermore, only one temperature was used in this study for the doped membrane (550°C) and the authors mention that increased

flux from oxide doping may only occur at low temperatures ($< 550°C$). They explain that at increased temperature the ionic conductivity of the support and the melt would increase which could shift the rate-limiting step, however they provide no evidence to support this claim. Therefore, it would be useful to research the effect of temperature on the flux of a doped molten carbonate dual-phase membrane.

While one study explored the addition of different metal oxides and cations into the melt, there have also been some studies that have explored the addition of different anions in the melt and the effects they pose on gas flux. These anion additions occur *via* reactions between different feed gases and the melt, which can introduce different anions into the melt and the consequence of this can affect the membranes CO_2 flux. A study by Chen *et al.* [89] found that by adding 2500 ppm sulphur dioxide (SO_2) into the feed gas, the membrane experienced an 85% decline in flux compared to when CO_2 was fed alone. The authors explained that the decrease was due to sulphate ion fouling of the molten carbonate caused by SO_2 exposure. Post-experiment analysis identified that 66% of the molten carbonate had converted to molten sulphate after 30 minutes of SO_2 exposure. They also reported that the carbonate ion conductivity was reduced to a value lower than the oxide ion conductivity of the SDC support, which was believed to be rate limiting. This indicated that carbonate ion transport in the melt was now rate limiting in the sulphated carbonates, resulting in an increase in activation energy for the transport process. In addition, a further study by Chen *et al.* [90] identified a similar poisoning effect when hydrogen sulphide (H_2S) was added to the feed gas. However, this time the authors attributed the reduction in flux to a reaction between the H_2S and both the carbonate and the SDC support, forming a Ce-O-S compound, likely to be Ce_2O_2S [91]. While the authors did not analyse the permeate-side outlet, it is likely the sulphate ion contamination in the melt would have allowed SO_2 co-permeation with CO_2. This can be explained by work from Zhang *et al.* [92] where nitrogen dioxide (NO_2) and nitric oxide (NO) were found to permeate through a dual-phase membrane with a wholly molten nitrate melt. Furthermore, chlorine gas and SO_2 have been separated from mixed gas streams using a molten salt membrane governed by a applied voltage gradient. For chlorine separation the molten salt used was a binary molten chloride eutectic [93] and for the SO_2 separation, a ternary molten sulphate eutectic [94] or a potassium pyrosulphate has been used ($K_2S_2O_7$) [95].

While the addition of sulphate ions into the carbonate melt inhibited CO_2 transport, addition of other ions have been shown to improve CO_2 flux. A study by Xing *et al.* [96] demonstrated how the addition of 2.5 mol% of steam into the permeate-side inlet resulted in the addition of hydroxide ions into the carbonate melt, leading to a 250-300% increase in gas flux across all

operation temperatures explored (550-650°C). 50 mol% CO_2 in N_2 was used as the feed gas for this study. The authors explained that the increase in flux when steam was added to the permeate-side inlet was due to a counter-current mechanism formed by the opposing CO_2 and steam chemical gradients across the membrane controlled by the following equilibrium (1.12):

$$OH_{(aq)}^- + CO_{2\,(g)} \leftrightarrow H_2O_{(g)} + CO_{3\,(aq)}^{2-} \tag{1.12}$$
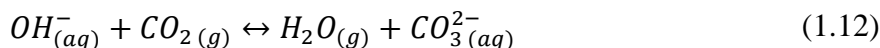
Where the forward reaction occurs on the feed side of the membrane, replacing the forward of reaction (1.2) when a dry permeate side gas is used and the reverse reaction occurs on the permeate side resulting in counter-current steam permeation. The authors explained that the electrochemical hydroxide gradient in the melt created by the presence of steam in the permeate-side inlet enhanced the electrochemical gradient of carbonate ions moving in the opposing direction, thus resulting in an increase in CO_2 flux. This is likely because hydroxide ions have a higher mobility in molten carbonate than carbonate ions.

The effects of adding sulphate and hydroxide ions to the carbonate melt clearly illustrates the melts sensitivity to different gaseous atmospheres and driving forces. The results have shown positive and negative influences on gas flux and this should be explored further with different gaseous driving forces to understand how the molten carbonate anions can be manipulated to elicit a change in gas flux.

Alternative methods for utilizing the molten carbonate to achieve a high flux membrane have been explored. One paper exploited the molten carbonates highly oxidizing nature at high temperatures. Support materials such as stainless-steel and LSCF have reported flux degradation as a result of reactions between the support and the molten carbonate, and Zhang *et al.* [56] used this knowledge to their advantage. They demonstrated that by using a cheap porous NiO support they were able to use the molten carbonate as a fabricating tool by allowing the salt to react with the NiO support to form an electronically conductive lithiated nickel oxide ($Li_{0.4}Ni_{1.6}O_2$ – LNO) layer *in-situ* at the melt-solid interface. This fabricating technique forms a thin electron-conducting layer which means no excess materials are required, which keep costs low and the membrane gets its mechanical strength from the unreacted NiO framework below the thin reacted LNO surface. Furthermore, while the LNO membrane is much cheaper than Ag, the membrane was able to produce a flux of ~1.0 mL min^{-1} cm^{-2} at 850°C which is only lower than the dealloyed Ag membrane discussed previously [58], albeit at 700°C. Furthermore, the LNO membrane had better wettability between the support and the molten carbonate, which allowed the membrane to operate for 150 hrs at 850°C. While the authors report that the LNO layer remains after cooling the membrane to 25°C, to date, no permeation

experiments have been performed with this membrane below 750°C, therefore its ability to achieve high flux below this temperature remains to be seen. The results of the LNO membrane indicates that sufficient electron conduction to achieve high CO_2 flux is possible with a thin conductive layer at the melt-solid interface, which means that the whole solid framework does not need to be made from an expensive, conductive material. This identifies an economically effect method for membrane fabrication. The same concept could be applied with different metals such as Ag, taking advantage of the fact it is the most electronically conductive metal.

In summary, dual-phase membrane research over the past 20 years has almost solely focussed on modification of the support phase's geometry and material to enhance the flux of the membrane, meanwhile the molten carbonate has remained largely unexplored. In light of this, conclusions can be made to critically assess the current state of the dual-phase membrane literature to identify alternate methods of producing a high-flux membrane. The following conclusions have been made throughout this literature review, which form the basis for the thesis research objectives (see section 1.3):

- The feed- and permeate-side inlet gases can be manipulated to improve CO_2 flux as shown with H_2 and H_2O.
- The molten carbonate component of a dual-phase membrane can be doped with an oxide, resulting in an increase in gas flux.
- A functional support material should not oxidise in molten carbonate to form a non-conductive oxide layer at the melt-solid interface resulting in a reduction in conductivity.
- Similarly, a membrane support should not be deformed through sintering or have wettability issues with the molten carbonate, each resulting in carbonate retention issues leading to a decline in flux.
- The conductivity of the support can be improved by modifying its porosity, resulting in a less tortuous network for conduction.
- For a support using an electron conductive material (or deposit), electron conductivity should be connected across the membrane bulk (from feed-side surface to permeate-side surface) and not limited to one side of the membrane.
- The support materials which have produced the highest fluxes contain expensive cations such as Sm, La, Co and Ag.
- Sufficient electron conduction to achieve a high-flux membrane can be achieved from a thin layer at the melt-solid interface instead of fabricating the entire support from a costly conductive material.

- Asymmetric membranes demonstrate that different support materials can be combined to improve flux, wettability and stability.
- Fair comparisons of membrane performance can only be made by directly comparing membranes from the same study or by standardising a method for membrane fabrication and permeation testing.
- Disk shaped membranes for lab-scale use are known to have sealing issues during permeation testing, which should be addressed.

1.3 Research Aims & Objectives

The aim of this thesis is to improve the stability and separation performance of dual-phase membranes by modifying the molten carbonate phase to increase oxide concentration within the melt or add functionality to an inert support phase. To do so, the following objectives were pursued:

- Use a well-defined membrane support geometry as a model system for understanding the impact of e.g. tortuosity, thickness, and sealants.

- Use non-doped, non-conducting-supported, dual-phase membranes as a reference system to understand the subsequent effect of gas feeds, operating temperature, dopant loadings, dopant addition techniques.

- Understand which reactions and/or transport phenomena for gas permeation through the molten carbonate component alone are slower, by using a non-conducting support that does not contribute to permeation and has a variable feed and permeate-side surface area.

- Modify the oxide concentration within the melt through doping non-conducting-supported molten carbonate with metal oxides or manipulation of the feed/permeate gas phase.
    - Manipulate gas phase on feed and permeate sides to stimulate alternative gas-liquid reactions that lead to uptake of more oxide ions into the carbonate melt and the subsequent release of CO_2.
    - Dope molten carbonate with a soluble metal oxide to manipulate the oxide concentration within the molten carbonate that leads to increased release of CO_2.

- Dope molten carbonate with a sparingly-soluble conductive metal and utilize the molten carbonate as a carrier to add functionality to the non-conducting-supported dual-phase membrane.

- Perform high-resolution, time-resolved characterisation studies to determine transport mechanisms and to precisely quantify membrane geometrical properties, which impact permeation.

Chapter 2. Materials & Methods

This Chapter provides an overview of the methodologies that are common across multiple chapters in the thesis. More detailed technical descriptions specific to each chapter are given in the experimental sections of their respective results chapters.

2.1   Permeation Experiments

2.1.1   Dual-phase membrane support preparation

Two types of dual-phase membrane support geometries were used for the permeation experiments conducted in this thesis: (1) uniaxially pressed pellet (henceforth known as pressed pellet) and (2) parallel pore supports.

For the pressed-pellet support, Al_2O_3 powder (Alpha Aesar, ACS, 99.5% min) was mixed with home-made 10 wt% PVA binder. Approximately, 1 mL of PVA was used per 1.5 g of Al_2O_3 powder and 1 g of the subsequent mixture was pressed into a ~1.75 mm thick, 20 mm Ø pellet at 3 tonnes (Atlas Power T25 hydraulic press). Pressed pellets were sintered at 1200°C for 5 hours at a ramp rate of 2°C per minute.

Following the preparation of the pressed-pellet Al_2O_3 support, Ag was introduced onto the supports surface using two different techniques. The two techniques used were electroless plating and dry impregnation and their respective methods for preparation are discussed in their own results chapter experimental sections (section 4.2.1 and 5.2.2 respectively).

For the parallel pore membrane support (Fig. 2. 1), a closed-end Al_2O_3 tube (20 cm length, 20 mm OD, 15 mm ID), was purchased from Precision Ceramics. The closed-end was manufactured to have a thickness of ~500 µm. The tube was then sent to Laser Micromachining Ltd. for laser drilling, where the central 15 mm diameter of the closed-end was drilled with 2000 pores. The pores were conically shaped (due to the inherent Gaussian shape of the laser beam), with a permeate-side diameter of 75 µm and a feed-side diameter of 150 µm. Images of the parallel pore membrane are shown in Fig. 2. 1.
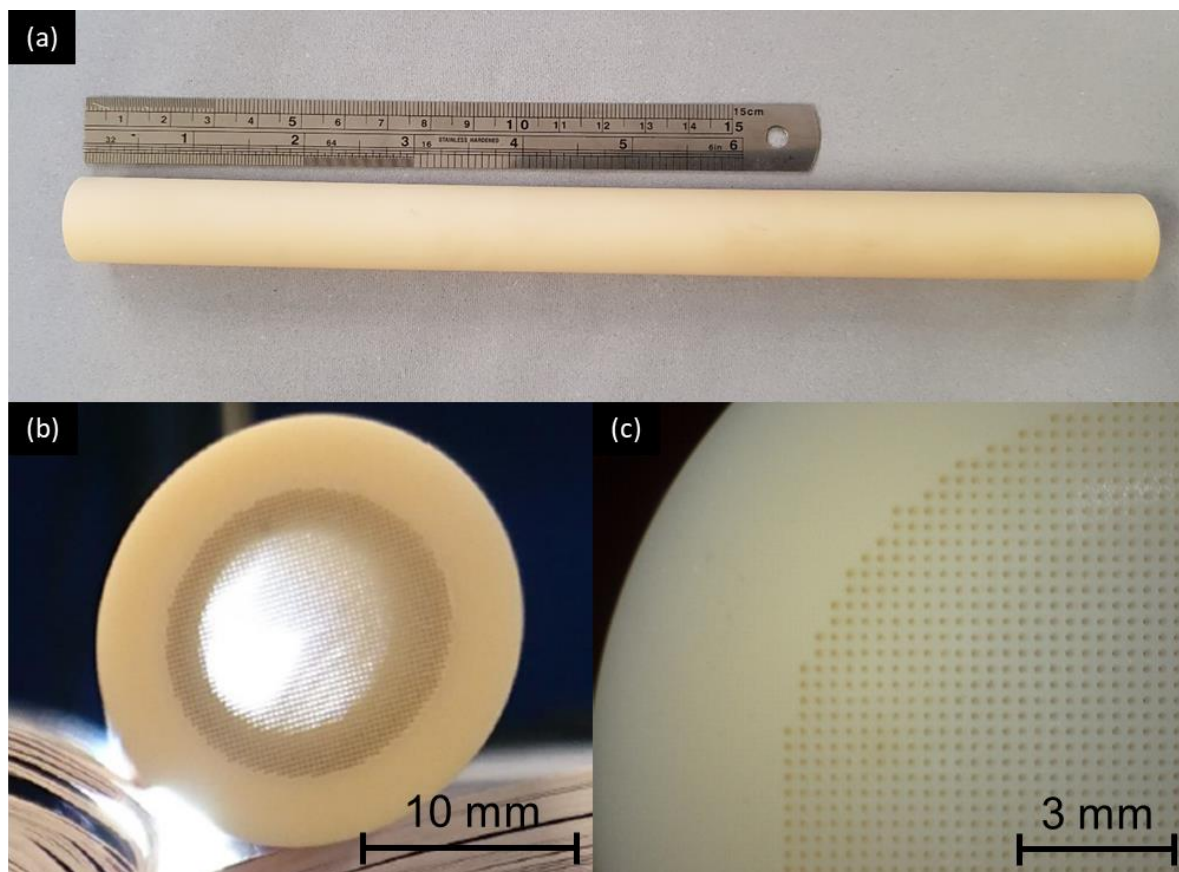
Fig. 2. 1 (a) Plan view of closed-end Al_2O_3 tube, (b) end-on view of laser-drilled closed-end and, (c) microscope image of the laser-drilled parallel pores.

2.1.2 Molten carbonate preparation

Three different carbonate mixtures were used in this thesis, the first being an undoped ternary alkali carbonate eutectic, which also served as the basis for the subsequent two mixtures. The latter two mixtures were doped with a set amount of either Ag powder or La_2O_3 powder. The method of doping is explained in their respective results chapters.

For the undoped ternary carbonate eutectic, lithium (Li), sodium (Na) and potassium (K) carbonates (($Li/Na/K)_2CO_3$) were dried separately at 300°C for 24 hours in air (Alpha Aesar, ACS, 99.5% min) to ensure all bicarbonate has been decomposed prior to mixing. Dried carbonates were mixed in a 43.5/31.5/25 mol% ratio, creating a ternary carbonate eutectic.

2.1.3 Membrane reactors, infiltration and permeation testing

For all the studies conducted in this thesis, two membrane reactors were used which were dependent upon the membrane geometry used from the two types discussed in section *2.1.1*. For pressed-pellet membranes, the reactor shown in Fig. 2. 2 was used. For the parallel pore membranes, the reactor shown in Fig. 2. 3 was used. To complete the preparation of the dual-phase membrane, molten carbonates must be infiltrated into the support's pores. This process is completed *in-situ* with the permeation testing.

Before infiltration and permeation testing for the pellet membranes, an extra step is required to seal the support to the reactor. This is not required for a parallel pore membrane due to the seamless geometry. The pellet support was sealed to an Al_2O_3 tube (inner diameter: 9 mm; outer diameter: 12 mm) using Au ink (Fuelcellmaterials, 70 wt%), unless otherwise stated and inserted into the membrane reactor. The gold sealant was dried at 850°C at a rate of 1°C min^{-1} in air. It is important to note that the active permeate-side diameter was ~7 mm, as permeated gases were always collected from the inside of the Al_2O_3 tube. Of the 9 mm inner diameter of the Al_2O_3 tube a further 2mm was lost due to Au sealant spreading. After holding the support at 850°C for 1 hour, the reactor was cooled at a rate of 1°C min^{-1} to room temperature.

After the reactor was cooled, the dual-phase membrane support could be infiltrated. Herein, the pellet and parallel pore membranes preparation and permeation operation is the same, except from the amount of carbonate powder used for each system. For each membrane, the carbonate powder described in section 2.1.2 (either doped or undoped depending on the experiment) was pressed into a pellet and placed on the surface of the membrane support in the cooled reactor. The amount of carbonates powder used for each membrane support was calculated to entirely occupy the pore structure. 0.6 g and 0.06 g of carbonate powder was used for the pellet and parallel pore membranes, respectively. The size of the carbonate powder pellet was dependent upon the size of region where the support was porous. 20 mm and 15 mm diameter pellets were made for the pellet and parallel pore membranes, respectively. To complete the formation of the dense dual-phase membrane, the reactor with the membrane support and carbonate pellet were enclosed using a quartz tube (35 mm outside diameter). The reactor was heated to 450°C, this being above the melting point of the carbonate mixture, at 1°C min^{-1} [97]. To avoid carbonate decomposition during heating, the same gas to be used during permeation was fed to both sides of the membrane, unless otherwise stated. Gases were fed at a rate of 30 mL min^{-1} for all experiments. Gas flow rates were controlled using Brooks Smart II mass flow controllers.

After holding at 450°C for 1 hour, to allow sufficient time for carbonate infiltration, the reactor was then heated further to a temperature between 600-750°C, depending on the experiment. A ramp rate of 1°C min^{-1} was used whilst maintaining the same gas feed on each side of the membrane used for infiltration. Upon reaching the target temperature, the permeate- and feed-side inlet gases were changed to match the experiments specifications. The feed gas always contained N_2, which was used for leak detection. All experiments were allowed to reach stable flux, which is defined as a region where the flux range is unchanging over a 4-hour period.

Due to difficulties in sealing the dual-phase membranes at high temperature, the permeation experiments were only performed once due to time constraints. However, one experiment was

repeated twice to demonstrate the reliability of the results. For these two experiments, all experimental parameters were kept constant (membrane composition, operation temperature, feed-side inlet gas, permeate-side inlet gas, gas flow rate, gas analysis equipment) and their fluxes were compared. Details of the experiments can be found in the appendix (A.1). The results showed that there was a 5% difference in flux between the experiments, which indicates that the preparation and operation of the membranes showed good consistency and repeatability.
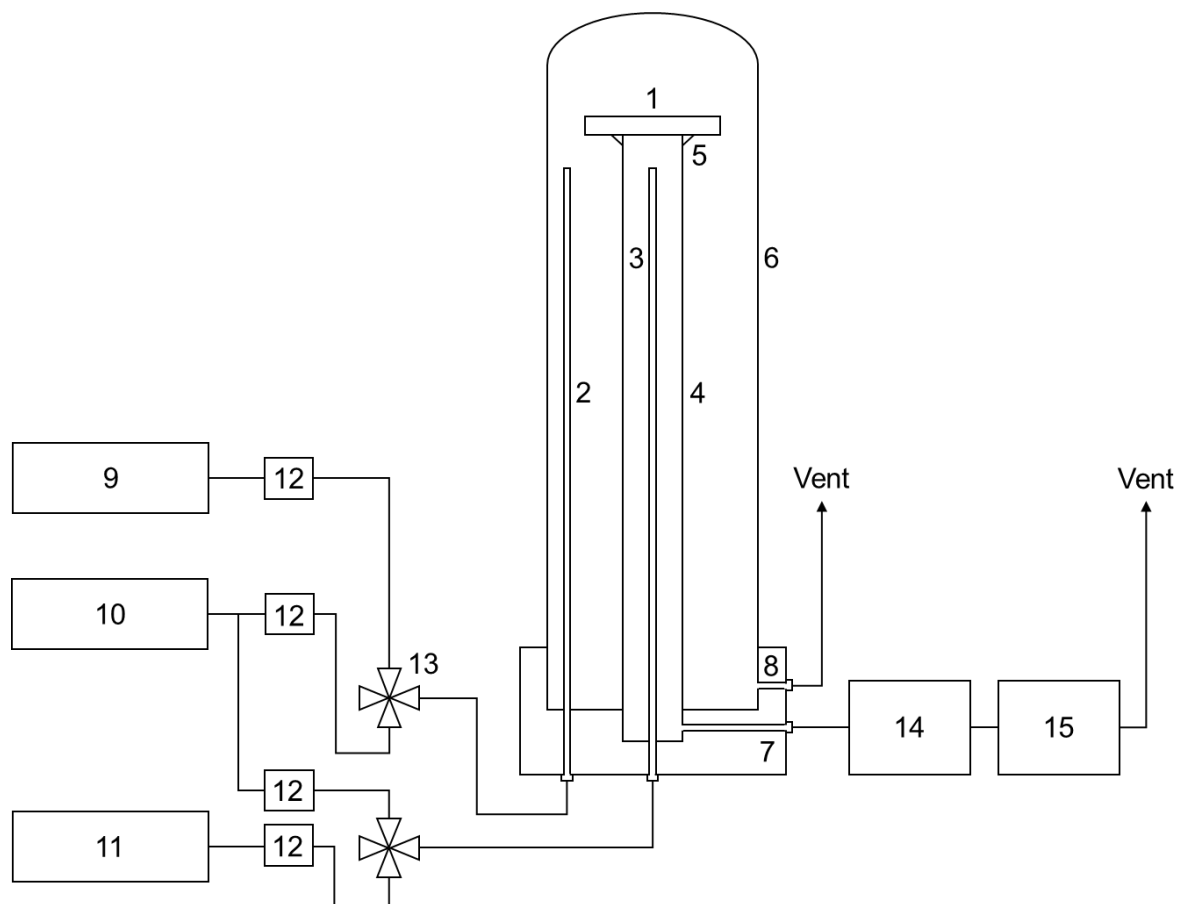
Fig. 2. 2 Schematic of the high temperature pellet membrane gas permeation reactor. (1) Pellet dual-phase membrane, (2) Feed-side inlet, (3) Permeate-side inlet, (4) Inner tube, (5) Au ink sealant, (6) Outer tube, (7) Permeate-side outlet, (8) Feed-side outlet, (9) 50 mol% CO_2, 25 mol% O_2 in N_2 gas cylinder, (10) 50 mol% CO_2 in N_2 gas cylinder, (11) Ar gas cylinder, (12) Mass flow controller, (13) 4-way valve, (14) FT-IR, (15) Mass spectrometer.
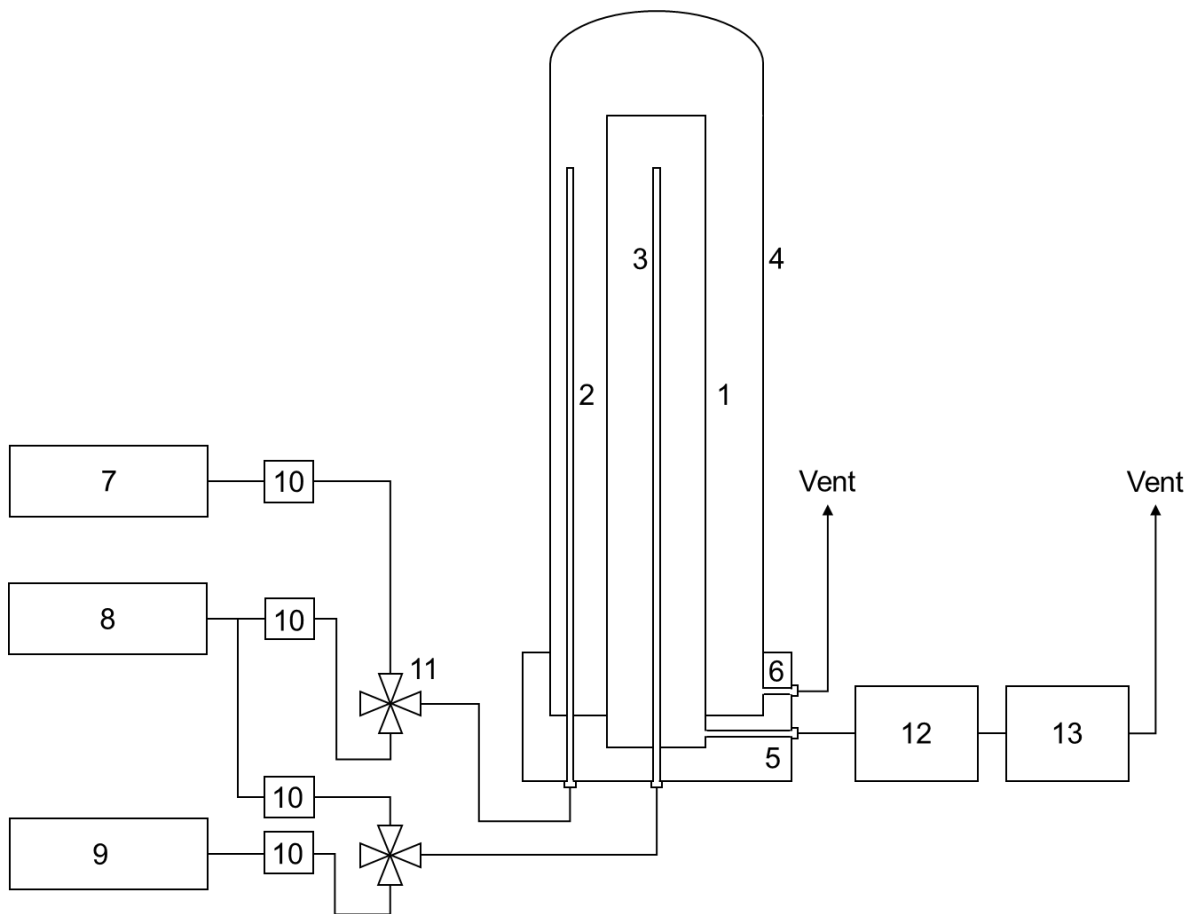
Fig. 2. 3 Schematic of the high temperature parallel pore membrane gas permeation reactor. (1) Parallel pore dual-phase membrane, (2) Feed-side inlet, (3) Permeate-side inlet, (4) Outer tube, (5) Permeate-side outlet, (6) Feed-side outlet, (7) 50 mol% CO_2, 25 mol% O_2 in N_2 gas cylinder, (8) 50 mol% CO_2 in N_2 gas cylinder, (9) Ar gas cylinder, (10) Mass flow controller, (11) 4-way valve, (12) FT-IR, (13) Mass spectrometer.

2.1.4   Sealant challenges

This biggest challenge encountered throughout the course of this study was the difficulty in achieving a gas tight seal for long periods of time at temperatures around 650°C. This prompted multiple changes in the sealant curing process until an effective sealing methodology was found. The following successful sealing procedure was employed for all studies in this thesis, regardless of sealing material used:

1) The inner tube was clamped in place vertically and the rim of the top side was coated with gold or silver ink using a stainless-steel needle.

2) The clamped tube was rotated 180° until the coated end was facing downwards.

3) The porous membrane support was placed directly below the inner tube and the coated end was lowered onto its surface until the see the ink started to flatten and then the inner tube was re-clamped in place.

4) Using the same stainless-steel needle, extra ink was coated around the periphery where the inner tube meets the porous support.

5) The inner tube was held in place for 1 hour to set.

6) The inner tube was carefully released from the clamp and lifted upwards in one motion, ensuring not to knock the porous support.

7) Vacuum grease was applied to outside of the non-sealed end of the inner tube and inserted into the membrane reactor.

8) The gold sealant was dried at 850°C for 1 hour at a ramp rate and cooling rate of 1°C min^{-1} in air.

9) The infiltration procedure described in section 2.1.3 was followed to finish the sealing process and start the permeation experiment.

Steps 1-4 are illustrated in Fig. 2. 4 for clarity.
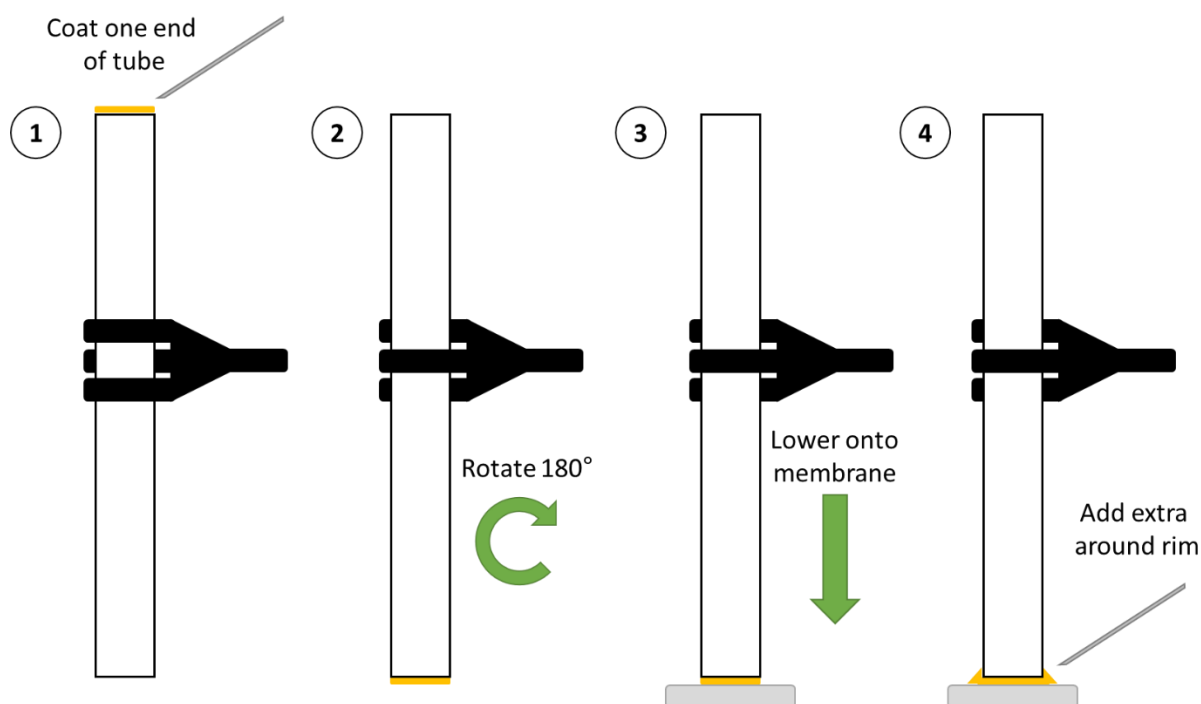
Fig. 2. 4 Schematic illustration of the pre-drying membrane sealing procedure used in these studies.

2.1.5 Gas analysis

During permeation, the permeate-side outlet gas was monitored using two different instruments shown in Fig. 2. 2 and Fig. 2. 3. The mole fraction of CO_2 on the permeate side was recorded using an FTIR analyser (MKS MultiGas Analyzer - 2030). This instrument was used because of its high accuracy (±1 ppm), precision (±1 ppm) and detection limit (1 ppm) for CO_2 analysis. O_2 flux and leak detection, $i.e.$ N_2 detection, was performed using a mass spectrometer (Hiden analytical QGA). Experiments were stopped if the N_2 signal (m/z-ratio = 28) exceeded 12% of

the CO_2 signal (m/z ratio = 44) after the background had been subtracted. Experiments were repeated with variations of experiment duration, temperature and Ag loading in the system.

Due to difficulties with maintaining a seal at high temperatures, further transmembrane leak tests were performed during operation where a feed gas containing 50 mol% CO_2, 25 mol% O_2 and 25 mol% N_2 was switched with a 50 mol% CO_2 and 50 mol% N_2 mixture. If a leak was present, the N_2 signal from the mass spectrometer (m/z ratio = 28) would increase due to the increased driving force for N_2 across the membrane and the experiment would be stopped.

Before and after each permeation experiment, the mass spectrometer and FT-IR were calibrated. Calibration was carried out by flowing gases of known concentrations (as close to the expected permeation value during the experiment as possible) through the reactor, FT-IR and mass spectrometer in the same sequence shown in Fig. 2. 2 and Fig. 2. 3. This was to ensure that any possible air leaks into the 4 units during permeation testing were accounted for upon data analysis. The gases calibrated were Ar, CO_2, O_2, and N_2. Ar was always calibrated first and was used to get a background reading for all instruments and subtract this from subsequent readings. CO_2 was calibrated separately from O_2 and N_2 to ensure there was no overlap of 28 m/z ratio in the mass spectrometer.

The mole fraction readings for CO_2 and O_2 taken from the FT-IR and the mass spectrometer were converted to flux, permeability and permeance using equations (2.1), (2.2) and (2.3), respectively. Equations for the conversion of O_2 ion current readings from the mass spectrometer into mol fractions are displayed in the appendix (A.1) and (A.2):

Flux (mL min^{-1} cm^{-2}):

$$J_i = \frac{y_i \times Q_G}{100} \times \frac{1}{A} \tag{2.1}$$

Permeability (mol m^{-1} s^{-1} Pa^{-1}):

$$Permeability = \frac{y_i \times Q_G}{100 \times 22400} \times \frac{1}{A \times 10^{-4}} \times \frac{1}{60} \times \frac{1}{Pa''_i - Pa'_i} \times \emptyset \tag{2.2}$$

Permeance (mol m^{-2} s^{-1} Pa^{-1}):

$$Permeance = \frac{y_i \times Q_G}{100 \times 22400} \times \frac{1}{A \times 10^{-4}} \times \frac{1}{60} \times \frac{1}{Pa''_i - Pa'_i} \tag{2.3}$$

Where y_i represents the mole fraction of i in the gas phase (here $i = CO_2$ or O_2), Q_G is the volumetric flow rate of the permeate-side gas (mL min^{-1}), A is the active permeate-side area (cm^2) and $Pa''x$ and $Pa'x$ are the partial pressures of CO_2 or O_2 on the feed side and permeate side, respectively (Pa) and $\emptyset$ is the membrane thickness (m). Conversion of permeability to Ba can be applied by the follow: 1 Ba = 3.35×10^{-16} mol m^{-1} s^{-1} Pa^{-1}.

2.2   Membrane Characterisation for Pre and Post-Experimentation

Multiple techniques were used throughout this thesis to characterise the dual-phase membranes before and after use. A background of each technique and their working principles are listed here, while details for their specific uses and experimental procedures are described in more detail in their respective results chapters. For post-experiment membrane analysis, the membranes were quenched at the end of the permeation experiment by rapid cooling under permeating conditions.

2.2.1   Scanning electron microscopy

Scanning electron microscopy (SEM) provides visual information about the surface topography of a sample. It does this by firing a focused electron beam at the sample, which is controlled by a series of electromagnetic coils. The electrons are reflected off the surface of the sample (known as secondary electrons) and directed to a detector where an image of the sample surface is generated onto a computer screen. In the case of dual-phase membranes, an SEM can be used to obtain microstructural information of the feed- and permeate-side surfaces, as well as cross-sectional analysis, provided the membrane is cut open to expose the bulk structure. The instrument used for SEM in this thesis was a Tescan Vega 3LMU.

2.2.2   X-ray diffraction

X-ray diffraction (XRD) is used to obtain crystal structure information for a sample. It does this by firing x-ray beams at a crystalline sample, which causes the x-rays to diffract into a detector. The angles produced by diffraction from the sample correspond to different crystal structures. The detector not only measures the diffraction angles but also the corresponding intensity of the diffracted beam. The diffraction angles and the beam intensities dictate the crystal structure of a sample. For dual-phase membranes, x-ray diffraction can be used to understand the crystal structure of the solid support phase. The instrument used for XRD in this thesis was a PANalytical X'Pert Pro MPD, with CuKα radiation.

2.2.3   Raman spectroscopy

Raman spectroscopy is used to provide information on molecular interactions and chemical structure for a given solid or liquid sample. It does this by firing an incident laser (light source) at a sample, which is then scattered. Most of the scattered light is of the same wavelength which provides no useable information (Rayleigh scatter), however a small portion is scattered at different wavelengths which is called Raman scatter. This scattered light is collected and separated into its component wavelengths by a holographic grating. The separated light is then focused onto a CCD array detector where the intensity of each wavelength is then measured and converted into a readable signal, or fingerprint for the sample and displayed on a computer.

In the case of dual-phase membranes, Raman spectroscopy can be used to identify chemical species in the carbonate melt and the chemical structure of the solid support phase. The instrument used for this thesis was a Horiba LabRam HR Evolution with Linkam TS1500 heated stage and a Laser Quantum 532 nm Nd:YAG laser.

2.2.4 *Mercury intrusion porosimetry*

Mercury intrusion porosimetry (MIP) is used to provide information on the porosity and pore size distribution for a porous sample. It does this by applying a controlled pressure to a sample immersed in mercury. Due to the high non-wettability of mercury, external pressure is required to infiltrate the mercury into the sample pores. The pressure required to infiltrate the sample is inversely proportional to pore size *i.e.* large pores require less pressure for infiltration. From the pressure *vs.* intrusion data, the instrument generates volumes and pore size distributions using the Washburn equation. In the case of dual-phase membranes, MIP can be used to understand the porosity of the porous solid framework prior to infiltration with molten carbonate. In this thesis, the MIP instrument used was a Pascal 440 Porosimeter.

2.2.5 *Energy dispersive X-ray spectroscopy*

Energy dispersive x-ray spectroscopy (EDX) is used to provide elemental analysis of a sample. EDX is often integrated into an SEM sample chamber, the Tescan Vega 3LMU SEM in this case. When an electron beam is fired at a sample in SEM the connection of the beam and the sample produces a variety of emissions, including x-rays. An EDX detector in the sample chamber is used to separate the x-rays, which are characteristic of different elements into a spectrum. In the case of dual-phase membranes, EDX can be used to understand which elements are present in a given location of the surface of a dual-phase membrane. In this thesis, a Bruker EDX instrument was used in combination with the aforementioned SEM.

2.2.6 *Micro computed tomography*

Computed tomography (CT) is used to generate multiple cross-sectional images or "slices" of a samples, which can then be merged together to create a 3D reconstruction of the sample. It does this by used a motorised x-ray source that rotates around the sample. As the x-rays pass through the sample, they are detected by a digital x-ray detector and transmitted to a computer. After each rotation of the sample the computer uses mathematics to construct a 2D image of the slice. Upon completion of the scan, all the individual slices can be merged together to form a 3D image. Depending upon the grayscale from the slices, different compounds from each 2D slice can be separated into separate images or coloured to highlight the presence of different materials. In the case of dual-phase membranes, micro CT can be used to create 3D reconstructions of the bulk of the membrane to understand how different materials are

distributed within the cross-section of a membrane. For this thesis, micro CT was performed using a Zeiss Xradia 520 Versa (Carl Zeiss X-ray Microscopy, Pleasanton, USA) and a Nikon XT H 225 (Nikon Metrology UK Ltd, Tring, UK).

2.2.7   Two-point DC resistance measurements

Two-point DC can be used to understand the electrical conductivity of a sample. This is done by coating each side of the membrane with Ag ink and covered with carbon tape. The membrane was then placed between two electrode plates and a voltage was then applied and the current is measured, which can then be used to determine the resistance and resistivity of the sample. Due to the nature of the sample, two-point DC could not be used which meant that the contact resistance incurred from the Ag ink, carbon tape and electrodes could not be removed from the calculated resistance of the membrane. However, this technique was sufficient for comparative studies, where samples were prepared in the same way, but it is likely that any calculated resistance is an over estimation. In the case of dual-phase membranes, two-point DC resistance measurements can be performed to understand the electron conductivity of the porous solid support phase.

Chapter 3. Modification of the Molten Carbonate Ion Composition to Improve Flux

This Chapter presents two methods of modifying the ion composition in the melt of a dual-phase membrane: doping the melt with a foreign cation and introduction of oxidising permeate-side inlet gas. The effects these modifications had on the membranes flux and stability were explored.

3.1 Introduction

To understand how molten carbonate can be modified to improve the flux across the membrane while using a cheap inert support, the gas transport process in a membrane must be understood. Transport of CO_2 across an inert-supported dual-phase membrane is divided into at least 5 chronological processes:

1. Mass transfer of CO_2 (and O_2) from the high pCO_2 chamber to the feed side of the membrane surface.
2. Absorption of gas into the molten carbonate at the feed-side membrane surface and association of CO_2 molecules and oxide ions into carbonate ions.
3. Transport of carbonate ions through the molten carbonate within the membrane.
4. Dissociation of carbonate ions into oxide ions and CO_2 molecules and desorption of CO_2 from the molten carbonate at the permeate-side membrane surface.
5. Mass transfer of gaseous CO_2 (and O_2) from the permeate side of the membrane surface to the low pCO_2 chamber.

Stages 1 and 5 are restricted if the flow rates are too low or there is a fixed quantity of feed or permeate-side inlet gas available *i.e.* no flow rate. These problems can be avoided by increasing the flow rate or changing to a continuous process in place of fixed quantity. Stage 3 can be improved by decreasing the thickness of the membrane support, regardless of the support material. Studies by Anderson and Lin [41] using an LSCF support, Zhang *et al.* [54] using a Ag support and Dong *et al.* [83] using an SDC support have all shown increases in flux when the thickness of the membrane support is reduced. While no study has been conducted to monitor the effect of membrane thickness on gas flux for a non-conducting support such as Al_2O_3, it can be assumed having a thin membrane support to decrease ion diffusion through the melt would be preferable.

While methods to improve gas transport by modifying the membrane thickness and gas flow rates are well understood, the modification of absorption and association, or the dissociation and desorption of CO_2 is more complex. It should also be noted that when an oxide- or electron-conducting support is used, the CO_2 is adsorbed onto the surface before associating with oxide ions, unlike the absorption process described here for inert-supported membranes. To understand how the adsorption and association, or the dissociation and desorption of CO_2 contribute to gas transport, the reactions on each side of the membrane must first be identified. When an inert support, such as Al_2O_3 is used, the feed and permeate-side reactions are limited to between the gas and the molten salt and are shown in Fig. 1. 2a and can be described by the formation and decomposition reaction for molten carbonate, respectively (3.1):

$$CO_{2\,(g)} + O^{2-}_{(l)} \leftrightarrow CO^{2-}_{3\,(l)} \tag{3.1}$$

The forward reaction in (3.1) represents the feed-side adsorption and association reaction (formation of molten carbonate), while the reverse describes the dissociation and desorption reaction (decomposition of molten carbonate). By understanding the operating principles of a dual-phase membrane used for CO_2 separation it is possible to understand which of the two processes should be targeted to improve gas transport.

Using reaction (3.1) as a guide, when CO_2 is not present the equilibrium shifts to the right to produce CO_2, thus causing carbonate decomposition. Alternatively, when a high concentration of CO_2 is present, the equilibrium will shift in the opposing direction to maintain the molten carbonate composition. This is why CO_2 is able to transport across the membrane because a concentration gradient is formed due to the aforementioned scenarios happening simultaneously on opposing sides of the membrane, as described by the following:

1. Due to the presence of a high concentration of CO_2 in the feed-side gas feed, CO_2 is absorbed into the melt where it associates with oxide ions to produce carbonate ions.
2. Due to the lack of CO_2 in the permeate-side gas feed, the carbonate ions dissociate into CO_2 and oxide ions and CO_2 desorbs from the permeate-side surface.

To improve the rate of CO_2 transport, the slowest process should be targeted. To date, no study has identified whether adsorption and association, or the dissociation and desorption of CO_2 is slower in a dual-phase membrane system. However, literature studies can be used to identify which processes commonly limit gas transport. A study by Xing *et al.* [88] stated that the oxide conductivity inside the molten carbonate limited gas transport. In their study, they showed that by reducing the porosity of their oxide-conducting CeO_2 support the CO_2 flux decreased. The authors explain that had oxide conductivity of the support been rate limiting, then reducing the porosity would have increased flux. Alternatively, as explained in section 1.2.2 a study from Ortiz-Landeros *et al.* [81] showed that there is likely a trade-off between support conductivity and porosity. However, in the case where a non-conducting support such as Al_2O_3 is used, it is acceptable to assume that oxide conductivity in the molten carbonate would be rate limiting as gas transport is solely dependent upon the molten carbonate.

The reason for the limitation with oxide conductivity in the melt can be explained by looking at the ion composition of the molten carbonate. Using Gibbs free energy and the rate constant equation as a guide, the density of oxide ions in the melt can be estimated. Using equation (3.2), (3.3) and (3.4) the concentration of oxide ions in the melt is found to be approximately 7.2 ×

10^{-12} mol cm^{-3}, which is ten orders of magnitude lower than the concentration of carbonate ions in the melt (1.9×10^{-2} mol cm^{-3}).

$$\Delta G = -RT \ln K \tag{3.2}$$

$$K = \left(\frac{[CO_3^{2-}]}{P_{CO_2}[O^{2-}]} \right) \tag{3.3}$$

$$\Delta G = \sum \Delta G_{f\ (products)} - \sum \Delta G_{f\ (reactants)} \tag{3.4}$$

For this calculation the Gibbs free energy data was supplied by Ren *et al.* [98] and enthalpy and entropy data was supplied by Licht and Wu [99]. The difference in ion concentrations support the claim that oxide conductivity in the molten carbonate is rate limiting, provided the membrane is sufficiently thin and there is a continuous removal of gas supplied to the membrane. Therefore, methods to increase the concentration of oxide ions in the melt, while using the same non-conducting Al$_2$O$_3$ support should be explored.

One method to increase the concentration of oxide ions in the melt could be to incorporate an additional reaction on the permeate-side surface along with the current carbonate decomposition reaction (reverse of reaction (3.1)) that introduces oxide ions into the melt.

To understand how the permeate-side reactions can be modified, the composition of the cations and anions in the carbonate melt must be understood. The cations used in dual-phase membranes for CO$_2$ capture consist of binary or ternary mixtures of Li$^+$, Na$^+$ and K$^+$, while there is a more complex mixture of anions depending on the conditions the membrane is exposed to. The most commonly referenced are CO$_3^{2-}$ and O^{2-} used in reaction (3.1). However, using DFT, Robert Carper *et al.* [100] found numerous anions that are theoretically stable in molten carbonate, such as CO$_4^{2-}$, C$_2$O$_6^{2-}$, CO$_5^{2-}$, O$_2^{2-}$ and O$_2^-$. Accessing some of these different anions in the melt require different conditions, for example, oxide species such as peroxide (O$_2^{2-}$) and superoxide (O$_2^-$) are only stable under an O$_2$ containing atmosphere *via* the following reaction (3.5):

$$\frac{1}{2}O_2 + CO_3^{2-} \leftrightarrow O_2^{2-} + CO_2 \tag{3.5}$$
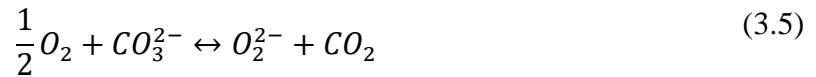
In this case, the addition of peroxide ions into the molten carbonate may initiate the formation of an additional counter-current mechanism within the carbonate melt that could occur alongside the mechanism described in Fig. 1. 2a. The addition of peroxide ions at the permeate-side surface would form a concentration gradient forcing them to the feed-side surface where

they can react with CO_2. Peroxide ions are known to react with CO_2 to form a peroxymonocarbonate (CO_4^{2-}) *via* reaction (3.6) [67]:

$$CO_2 + O_2^{2-} \leftrightarrow CO_4^{2-} \tag{3.6}$$

The effect of increasing the density of oxides in the melt has been explored elsewhere. Instead of modifying the permeate-side gas feed, Xing *et al.* [88] demonstrated how oxide concentration in the melt could be increased by doping the melt with foreign oxides, namely $CsVO_3$ and MoO_3, which resulted in an increase in CO_2 flux by a factor of 2.

Aside from $CsVO_3$ and MoO_3, other oxides are known to form stable complexes in molten carbonate. The aim when choosing a foreign oxide dopant, is to find an oxide that will form an equilibrium, similar to that shown in reaction (3.1), however the resulting carbonate dopant should more readily release CO_2 than Li^+, Na^+ and K^+ *i.e.* the equilibrium is shifted further towards the left in this case.

Using Gibbs free energy as a guide, since the decomposition of molten carbonate is an unfavourable reaction, a carbonate can be selected which has a ΔG of reaction closer to zero *i.e.* decomposition is more thermodynamically favourable than alkali carbonates. Lanthanum oxide (La_2O_3) is known to form a stable lanthanum dioxycarbonate ($La_2O_2CO_3$) in molten alkali carbonate and has a ΔG of $+42$ kJ mol^{-1} (compared to $+80$, $+180$ and $+250$ kJ mol^{-1} for Li_2, Na_2 and K_2CO_3) for its decomposition at 650°C [101], [102]. The decomposition reaction is displayed in reaction (3.7):

$$La_2O_2CO_3 \leftrightarrow CO_2 + La_2O_3 \tag{3.7}$$

While reaction (3.7) is unfavourable (forward reaction ($+42$ kJ mol^{-1})), it is more favourable than its alkali counterparts. Thus, based on Gibbs free energies, a La_2O_3-doped (herein denoted as La-doped) carbonate melt may decompose (or release CO_2) on the permeate side at an enhanced rate, thermodynamically speaking. Of course, thermodynamics does not dictate the rate of a reaction, kinetics does. However, thermodynamic data provides information on what materials could provide more favourable reactions, which forms a hypothesis for investigation and kinetic (permeation) experiments can be performed to prove or disprove the hypotheses.

Furthermore, $La_2O_2CO_3$ doping in the melt has been known to improve O_2 solubility for work with MCFC's [67], [103], [104], therefore this doping method could be combined with adding O_2 into the permeate-side inlet to increase the concentration of oxide species in the melt, resulting in increased CO_2 release.

In this chapter, molten carbonate was modified using three different techniques to manipulate the oxide concentration within the molten carbonate in order to increase CO_2 flux across the membrane by doping the melt with:

1. Oxide species using O_2 in the permeate-side inlet.
2. La_2O_3.
3. La_2O_3 and oxide species.

For all experiments in this study, a non-conducting Al_2O_3 support was used to ensure any route of flux enhancement was related to molten carbonate modification. Each of the three doping techniques were compared to an undoped molten carbonate dual-phase membrane to determine its effect on CO_2 flux. The membranes were characterised using Raman spectroscopy to identify ionic species in the carbonate melt, SEM-EDX was used to visualise the membranes surfaces after operation and XRD was used to identify the phases present in the support phase upon membrane quenching.

3.2 Experimental

3.2.1 Dual-phase membrane support preparation

Two membrane supports were used for the study; pressed-pellet and parallel pore. The preparation procedures for each support are described in section 2.1.1.

For Raman spectroscopy experiments an Al_2O_3 single crystal with dimensions $5 \times 5 \times 1$ mm was used to simulate the conditions of a permeate-side pore. The single crystal was laser drilled with 8 closed pores by Laser Micromachining Ltd. (Fig. 3. 1). The pore dimensions are divided below:

- 4 pores had a diameter of 250 µm and a length of 500 µm
- 4 pores had a diameter of 100 µm and a length of 450 µm
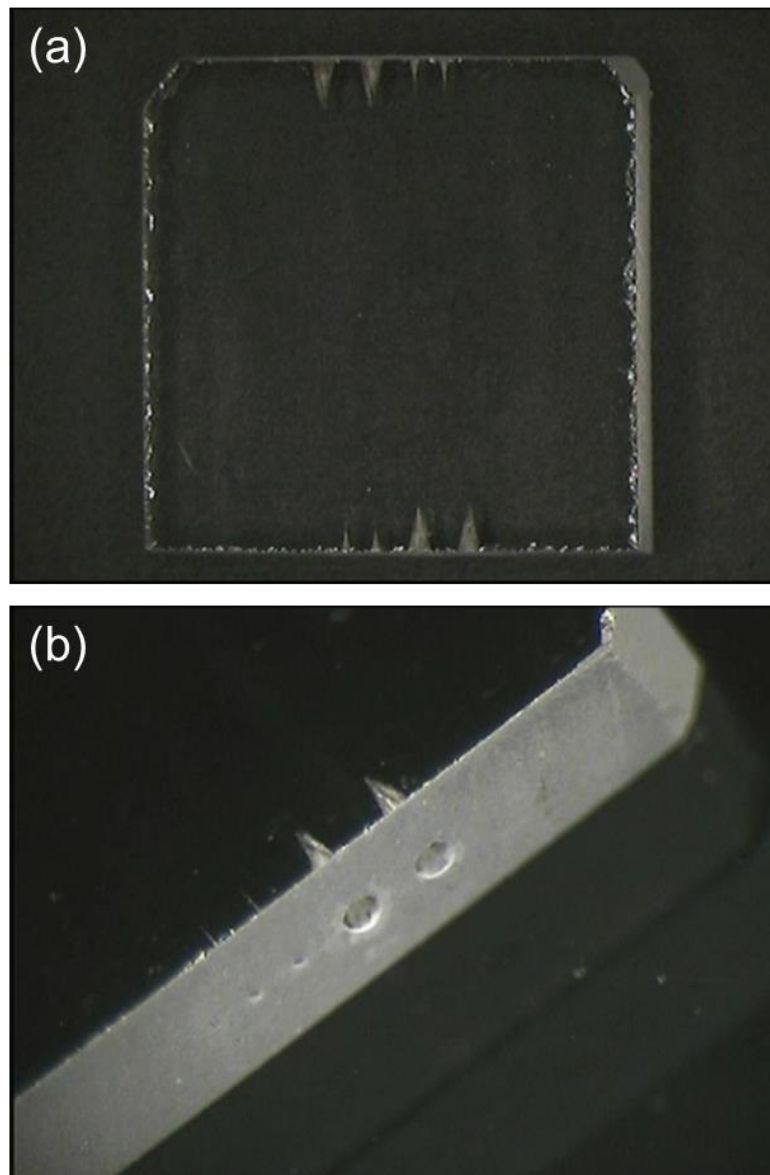
Fig. 3. 1 (a) plan view digital image of Al_2O_3 single crystal, (b) side view digital image of the laser drilled closed pores.

3.2.2 Molten carbonate preparation

Three carbonate powders were used for the permeation experiments in this chapter:

1. Undoped Li/Na/K ternary carbonate eutectic described in section 2.1.2.

2. Undoped Na/K binary carbonate eutectic in a 56/44 mol% ratio.

3. A La-doped carbonate mixture was prepared by drying La_2O_3 at 400°C to ensure all lanthanum hydroxide $(La(OH)_3)$ was decomposed prior to mixing. After drying, 0.5 mol% of La_2O_3 was added into the pre-prepared ternary carbonate eutectic.

3.2.3 Permeation measurements

For permeation tests the parallel pore membrane reactor (Fig. 2. 3) and the pressed pellet membrane reactor (Fig. 2. 2) were used for their respective supports. One feed-side inlet gas was used in this study:

1. 50 mol% CO_2 in N_2.

Two permeate-side inlet gases were used in this study:

1. 100 mol% Ar
2. 25 mol% O_2 in Ar depending on the experiment.

Reactor temperatures used in this study range between 600-750°C depending on the experiment. For experiment repeats with the parallel pore membrane, the tube was removed from the reactor and placed in a flask of DI water and sonicated in a water bath for 30 minutes to remove the carbonates.

3.2.4 Dual-phase membrane characterisation

Microstructural and elemental surface analysis of pellet membranes after operation was performed using scanning electron microscopy and energy dispersive X-ray spectroscopy (model details in section 2.2). The SEM scans were performed by Au coating the pellet and mounting the sample on a stainless-steel stage separated by carbon tape. Scans were made using an accelerator voltage of 15 kV with a working distance of 8 mm.

Two experiments were performed using Raman Spectroscopy[1]:

- For peroxide species identification, one closed pore of the Al_2O_3 single crystal (with a diameter of 250 µm and a length of 500 µm) was loaded with ternary carbonate powder

---

[1] Experiments were performed by Dr. Greg Mutch from Newcastle University and data was interpreted by Liam McNeil.

was inserted (loaded pore facing upwards) into the Raman spectrometer and fed with 50 mol% CO_2 in N_2 during heat-up to 650°C. Upon reaching temperature, the gas was switched to 25 mol% O_2 in Ar and held for 2 hours while spectral readings were collected in 30-minute intervals.

- For interfacial product identification, ternary carbonate powder was placed on the surface of a porous Al_2O_3 pellet and heated to 650°C under a 50 mol% CO_2 in N_2 gas feed and held for one hour. The gas feed was then switched to Ar and spectral readings were acquired at 10-minute intervals until 1 hour. The gas feed was then switched back 50 mol% in N_2 and spectral readings were acquired at 15-minute intervals until 1 hour.

For the Raman experiments a 20X objective was used, with the laser aperture set at 200 microns. 10 accumulations of 10 scans were taken, with a centre position of 1050 cm^{-1}. A 2400 groove grating was used, at ~100% of the laser power (the high power was needed to see the dilute species).

Phase identification was completed using X-ray diffraction (model details in section 2.2) [2]. Prior to analysis, pellet samples were mounted onto obliquely-cut zero-background silicon wafers and inserted into stainless steel sample holders, then levelled using a glass slide. Mounted samples were placed in the diffractometer and data sets were collected over the range of 10-100° 2θ with a step size of 0.0334° 2θ. A nominal time per step of 150 seconds was used with the scanning X'Celerator detector together with incident beam fixed divergence and anti-scatter slits of 1/16° and 1/8°, respectively, a beam mask of 10mm and soller slits of 0.04 radians. Total scan time for the sample was 55 minutes. Phase identification was carried out by means of the X'Pert accompanying software program PANalytical High Score Plus in conjunction with the ICDD Powder Diffraction File 2 Database (2004), ICDD Powder Diffraction File 4 - Minerals (2018) and the Crystallography Open Database (July 2016; www.crystallography.net).

---

[2] Experiments were performed by Dr. Maggie White from Newcastle University and data was interpreted by Liam McNeil.

3.3 Results & Discussion

3.3.1 *Rate determining step for CO_2 separation using dual-phase membranes*

To verify which process is slower between the adsorption and association (uptake of CO_2), or the dissociation and desorption (release of CO_2) processes, a novel dual-phase membrane support was fabricated. This novel membrane support, henceforth known as a 'parallel pore membrane', consisted of a seamless hollow tube with one closed end. The tube was fabricated from dense Al_2O_3 and the closed end was laser drilled with 2000 pores. Each pore was conical in shape (due to the inherent Gaussian shape of the laser beam) with the outer side having a ~ 150 µm diameter while the inner side was ~ 75 µm (Fig. 3. 2).
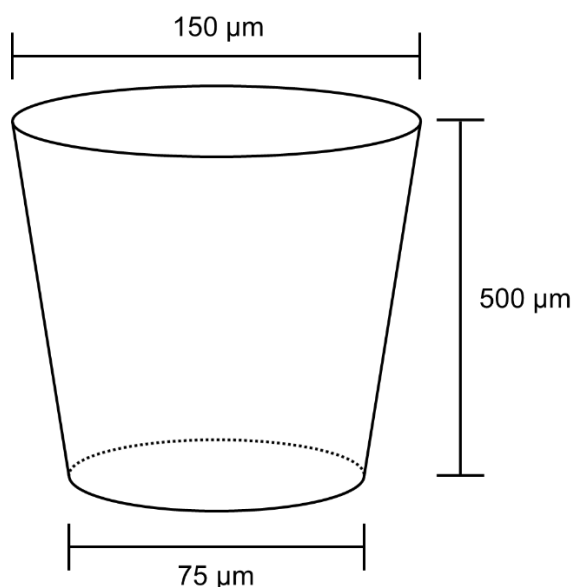
Fig. 3. 2 Schematic illustration of the conical shaped pores in the parallel pore membrane.

The conical shape of the pores was ideal for this study as the shape creates a different permeate-side surface area depending on the direction CO_2 is fed. One side of the membrane has a permeate-side surface area of 8.75×10^{-2} cm^2 while the other is double this (1.75×10^{-2} cm^2). The closed end tube was designed to be 500 µm thick, which is the same order of magnitude as the only other study to use an Al_2O_3 support [53]. Lastly, the membranes seamless geometry meant there was no hot-sealing region, thus transmembrane leaks could not arise as a result of sealant failure which would distort the flux data.

To understand whether CO_2 uptake or release from the membrane was slower, a permeation experiment was performed using an undoped molten carbonate and the parallel pore membrane (Fig. 3. 3).
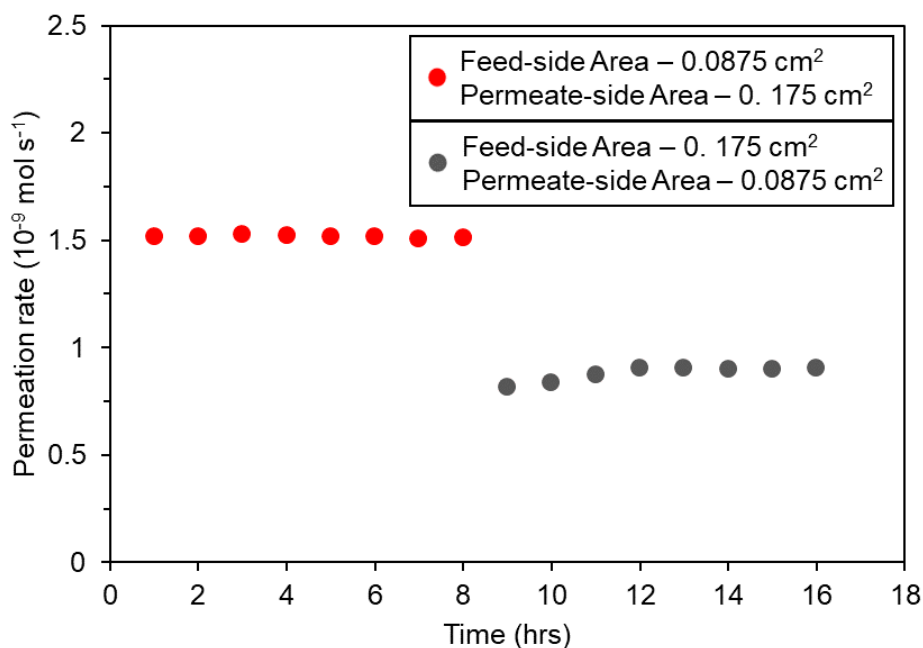
Fig. 3. 3 CO_2 permeation rate through the large and small permeate-side surface area of a parallel pore membrane with truncated-conical pores with ternary carbonate eutectic at 650°C.

For the first section of the experiment (< 8 hrs), 50 mol% CO_2 in N_2 was fed to the low surface area side and pure Ar was fed to the high surface area side and a stable CO_2 permeation rate of 1.5×10^{-9} mol s^{-1} was recorded over an 8-hour period[3]. For the second section of the experiment (> 8 hrs), the gases were switched so that CO_2 permeated in the opposite direction which increased the feed-side surface area and lowered the permeate-side surface area. This resulted in a decrease in permeation rate (0.7×10^{-9} mol s^{-1}) and remained stable over an 8-hour period. This result illustrates that the permeation rate was independent of feed-side surface area, indicating that the dissociation and desorption of carbonate ions into CO_2 molecules and oxide ions is slower. This finding agrees with the hypothesis and indicates that rate of CO_2 release from the permeate-side surface should be targeted as an approach to increase CO_2 flux.

3.3.2 *Introduction of oxide species into the melt to increase CO_2 flux*
The rate of release of CO_2 from the permeate-side surface could be accelerated by increasing the formation of dissolved metal oxide species at the permeate-side surface *via* the introduction of O_2 into the permeate-side inlet gas (see reaction (3.5)). As a result, this will cause more oxides to move down their concentration gradient to the feed-side surface, thus increasing the

---

[3] Permeation rate (mol s^{-1}) was used as a measure of CO_2 permeation for these experiments because flux, permeance and permeability are all normalised by membrane area. Therefore, the latter 3 units see no difference in CO_2 permeation.

driving force for carbonate ion formation at the feed-side surface. To test this, two parallel pore membranes were infiltrated with undoped ternary carbonates and fed with 50 mol% CO_2 in N_2 between 600-750°C. For the permeate-side inlet, one membrane was fed with 25 mol% O_2 in Ar, while the other was fed with pure Ar. Their CO_2 fluxes were recorded at the permeate-side outlet and compared to elucidate the effect of adding O_2 into the permeate-side inlet gas (Fig. 3. 4).
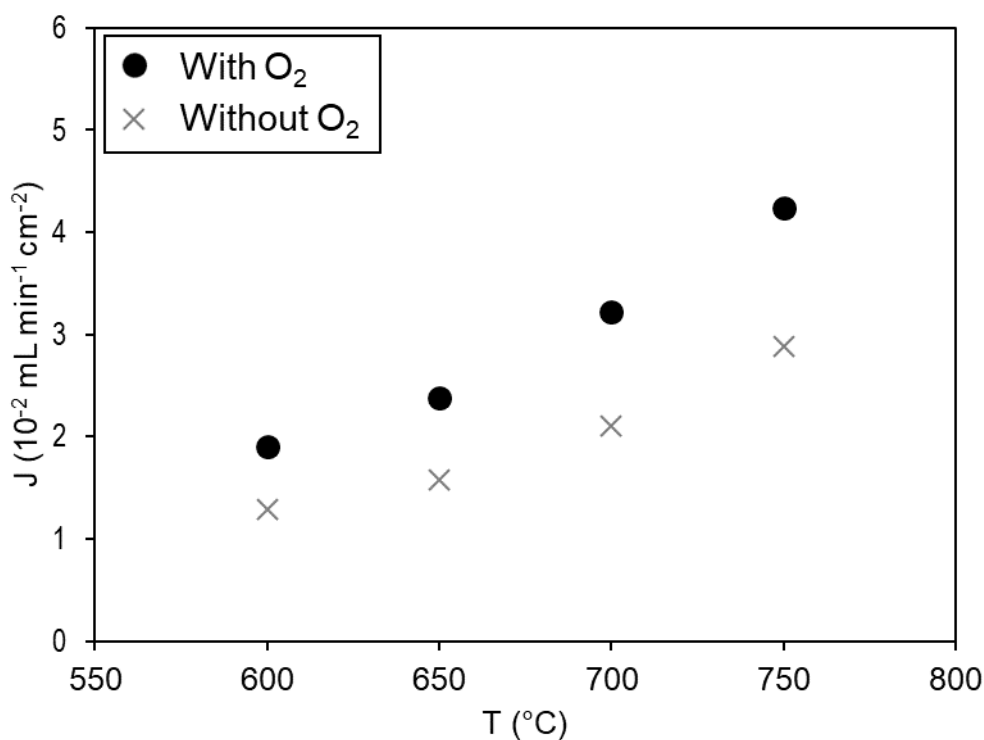
Fig. 3. 4 CO_2 flux as a function of temperature and permeate-side inlet for two parallel pore membranes with undoped ternary carbonate eutectics. Feed-side inlet: 50 mol% CO_2 in N_2. Permeate-side inlet: 25 mol% O_2 in Ar (With O_2) *vs.* pure Ar (Without O_2).

Fig. 3. 4 shows that when O_2 is added to the permeate-side inlet a ~ 50 % increase in CO_2 flux across all temperatures is observed. This increase in flux is in-line with the hypothesis, indicating that the CO_2 flux can be increased by adding O_2 into the permeate-side gas phase to accelerate the formation of oxide ions (see reaction (3.5)) resulting in enhanced CO_2 release. However, the flux with of the membrane with O_2 in the permeate-side inlet was still over an order of magnitude lower than the highest flux dual-phase membranes reported in the literature. The flux was likely limited by the low solubility of O_2 in molten carbonate. Scaccia *et al.* [67] reported that 0.13×10^{-6} mol cm^{-3} of O_2 was soluble in an unmodified binary (Li/Na) molten carbonate eutectic at 650°C when a 50:50 mixture of CO_2 and O_2 was fed to the melt. This value is nearly three orders of magnitude lower than the solubility of CO_2 in molten carbonate (9.95×10^{-4} mol cm^{-3}) reported by Peeters *et al.* [105]. Thus, to increase the flux further using

this modification technique a permeate-side inlet gas is required that is more soluble in molten carbonate than O_2, causing a heavier disruption of the ion concentration in the melt. One gas that has been shown to produce a similar effect is steam. A report by Xing *et al.* [96] showed that by adding steam into the permeate-side inlet, the CO_2 flux increased by 300% at 650°C. Although, in the paper they make no connection to oxide concentration in the melt, the work presented in this chapter serves as an indication that the methods of flux enhancement may be similar, albeit with different reactions. In the steam study, Xing explains that the increase in flux was a result of a second equilibrium that establishes and results in the formation of a counter-current mechanism involving hydroxide ions (OH^-) moving in the opposing direction to carbonate ions (CO_3^{2-}). Where the forward of reaction (3.8) occurs on the feed-side surface and the reverse of (3.8) occurs at the permeate-side surface. They explain that the electrochemical gradient created by the steam from the permeate side to the feed side caused an enhancement to the chemical gradient of CO_2 in the opposing direction, resulting in an increase in flux.

$$OH^-_{(aq)} + CO_{2\,(g)} \leftrightarrow H_2O_{(g)} + CO_3^{2-}{}_{(aq)} \tag{3.8}$$
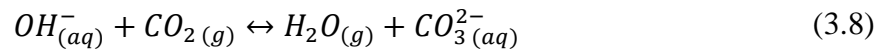
To test whether this counter-current mechanism occurred with the O_2 containing permeate gas, a further experiment was performed. An undoped ternary carbonate eutectic was infiltrated into the parallel pore membrane and fed with 50 mol% CO_2 in N_2 in the feed-side inlet and pure Ar in the permeate-side inlet at 650°C. However, the gas analysis instruments connected to the outlet of the membrane reactor (see label 14 and 15 from Fig. 2. 3) were rerouted so that the feed-side outlet was monitored instead. After allowing the membrane 25 hours to stabilize, the permeate-side inlet gas was switched to 25% O_2 in Ar and the change in m/z 32 signal from the mass spectrometer was recorded from the feed-side outlet (Fig. 3. 5).
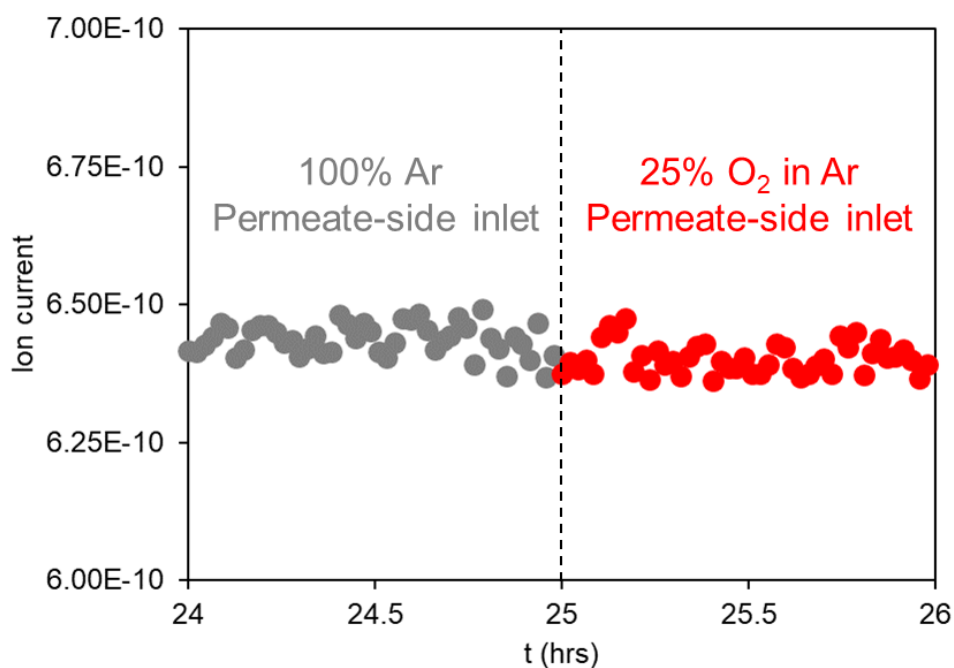
Fig. 3. 5 Evidence of no O_2 counter-permeation mechanism by monitoring the m/z 32 signal from the feed-side outlet with two different gas feeds into the permeate-side inlet at 650°C. Membrane: undoped ternary carbonate eutectic membrane. Feed-side inlet: 50 mol% CO_2 in N_2. Permeate-side inlet: 100% Ar ($<$ 25 hrs), 25 mol% O_2 in Ar ($>$ 25 hrs).

Fig. 3. 5 shows that when O_2 was introduced into the permeate-side inlet after 25 hours of operation, there was no detectable increase in O_2 signal on the feed side *i.e.* O_2 was not found to permeate in the opposing direction to CO_2. This means O_2 does not form a counter-current permeation system, similar to the steam system. However, due to the low CO_2 flux on the permeate side and the stoichiometry of reaction (3.5), it is possible that O_2 permeation on the feed side was below the measurable limit of the mass spectrometer (~10 ppm).

To understand how the O_2 in the permeate-side inlet reacted with the melt, an Al_2O_3 single crystal crucible filled with molten carbonate was fed with 25 mol% O_2 in Ar at 650°C and the species in the melt were analysed using Raman spectroscopy (Fig. 3. 6).

The chart shows the reaction $O_2 + CO_3^{2-} = 2O_2^{2-} + 2CO_2$
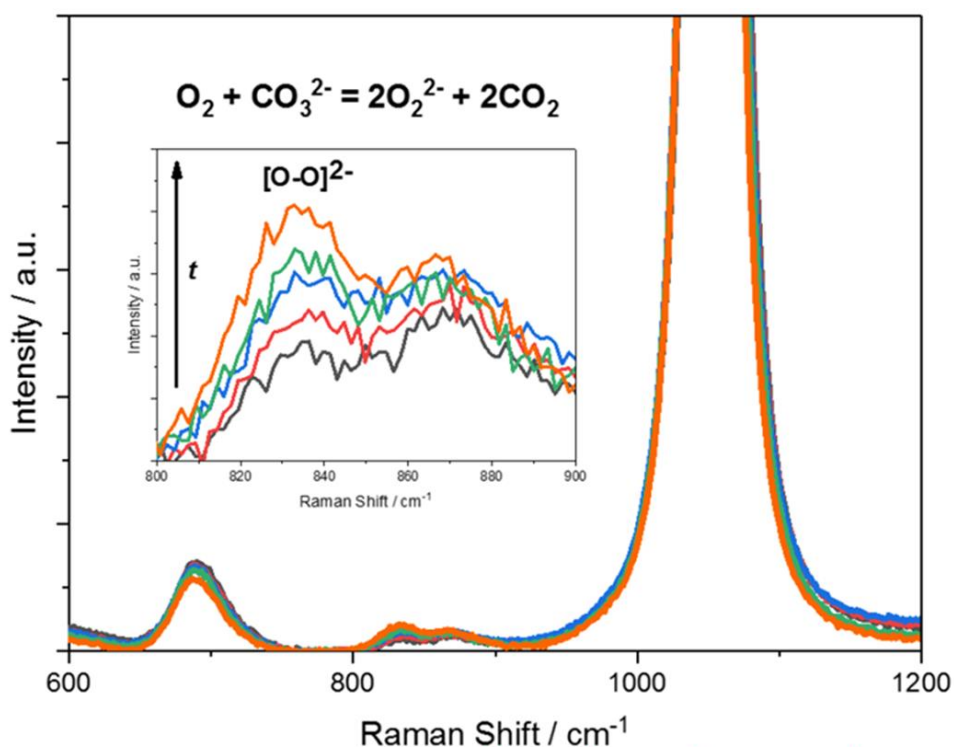
Fig. 3. 6 Raman spectra of the growing peroxide peak with time in undoped molten ternary carbonate eutectic at 650°C. Feed gas: 25 mol% O_2 in Ar.

Fig. 3. 6 shows that a peak at 830 cm^{-1} formed with time under an O_2 containing atmosphere. This peak aligns with the presence of peroxide (O_2^{2-}) in the melt reported by Chen *et al.* [106]. Thus, confirming that reaction (3.5) occurs on the permeate side of the membrane when subjected to a gas mixture containing O_2 in an inert balance gas. However, when this soluble oxide species moves down its concentration gradient to the feed-side surface, its reaction with CO_2 may result in the formation of CO_4^{2-} (see reaction (3.6)) and this could explain why no O_2 counter-permeation is seen at the feed-side outlet.

In summary, the addition of an oxidising gas resulted in an increase in CO_2 flux, which can be attributed to the increase in concentration oxides species formed at the permeate-side surface (see reaction (3.5)), which results in an increased driving force for carbonate ion formation at the feed-side surface. The use of O_2 in the permeate-side inlet means O_2 must be removed downstream to achieve a pure CO_2 product, which would incur an extra energy penalty if used in a pre-combustion process. Alternatively, these results present a possible option for air capture. A stream of air could be fed to each side of the membrane where one side has O_2 removed upstream of the membrane. While the membrane will have no chemical driving force for CO_2 separation (~400 ppm on each side of the membrane), the removal of O_2 on one side provides a driving force for CO_2 separation in the direction of the O_2 containing side. Using O_2 to pull CO_2 against its concentration gradient has previously been shown by E.I. Papaioannou

et al. [45], albeit with an electron-conducting support. They were able to carry CO_2 from the feed side with a CO_2 concentration of 0.5 mol% to the permeate side with a CO_2 concentration of 1.0 mol% with the aid of 20 mol% O_2 in the feed side. To achieve the same flux enhancement by manipulating the oxide concentration within the melt without the need to add O_2, oxide species must be doped into the melt directly prior to operation.

3.3.3 Introduction of a foreign cation into the melt to increase CO_2 flux

To gain an understanding of how the composition of cations in molten carbonate affects gas flux, two reference experiments were carried out. For the first experiment, the parallel pore was infiltrated with an undoped ternary carbonate eutectic and fed with 50 mol% CO_2 in N_2 in the feed-side inlet and pure Ar in the permeate-side inlet and operated at 725°C. For the second experiment, the same operation temperature and gases were used, while a binary Na/K eutectic was used for the molten carbonate. The permeation experiments were operated at 725°C because the melting point of the Na/K eutectic is 710°C (Fig. 3. 7) [97].
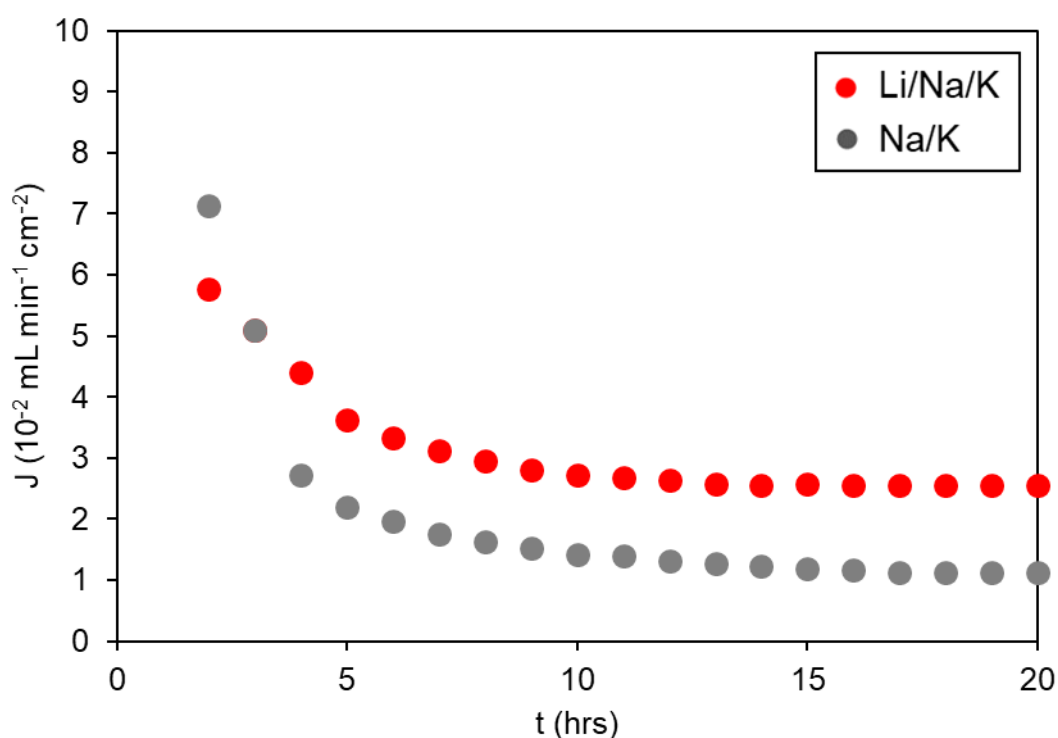
Fig. 3. 7 CO_2 flux evolution with time for two parallel pore membranes with differing carbonate eutectics at 725°C; ternary (Li/Na/K) and binary (Na/K) carbonate eutectic. Feed-side inlet: 50 mol% CO_2 in N_2. Permeate-side inlet: Ar.

Fig. 3. 7 shows that when the binary Na/K eutectic is used instead of the ternary carbonate eutectic, the flux decreases from 2.6 to 1.1×10^{-2} mL min cm^{-2} at 725°C. For the binary eutectic,

using the same thermodynamic data library previously used, an average ΔG of reaction for molten carbonate decomposition is $+210 \, kJ \, mol^{-1}$ based on the wt% of the individual carbonates in the eutectic at 725°C. Whereas, for the ternary eutectic the ΔG of reaction is $+165 \, kJ \, mol^{-1}$ at the same temperature. The decrease in flux exhibited by the Na/K carbonate membrane is in-line with the hypothesis that the ΔG of reaction for molten carbonate decomposition, *i.e.* release of CO_2, is linked to the membranes flux when the release of CO_2 is rate limiting.

The difference between these two ΔG's and their subsequent gas fluxes demonstrates the importance of the use of Li_2CO_3 in an alkali carbonate eutectic. A reason for the flux difference is likely due to its stability in a molten carbonate, as Li_2CO_3 is the least stable alkali carbonate, as shown by having a ΔG of reaction for its decomposition closer to zero than any other alkali carbonate [98]. Therefore, the flux could be increased further by doping the melt with a material that is stable in molten carbonate, yet less stable than Li_2CO_3. A further explanation for the higher flux with Li_2CO_3 containing melt can be found from a study by Nafe [107]. Nafe showed that the electrical conductivity and mobility of the ions in the melt decreases as the ionic radius of the alkali ion increases, *i.e.* Li_2CO_3 has a smaller ionic radius than Na_2CO_3 and K_2CO_3 and thus, has greater mobility and conductivity. Therefore, it is unsurprising to see that the melt containing Li_2CO_3 had a higher flux as the ions in the melt are more mobile which can allow faster CO_2 transport.

To test the former, La_2O_3 was selected as the dopant due to the thermodynamics of carbonate decomposition being more favourable than the alkali carbonates already present (see reaction (3.7)) and its known stability in molten carbonate. Scaccia *et al.* [67] reported that 0.5 mol% La_2O_3 is stable in molten carbonate under a CO_2 atmosphere in its $La_2O_2CO_3$ form. Therefore, permeation experiments were performed with a 0.5 mol% La-doped dual-phase membrane at temperatures between 600-750°C. The membrane was fed with 50 mol% CO_2 in N_2 in the feed-side inlet and pure Ar in the permeate-side inlet. The results were compared to a membrane with an undoped ternary carbonate mixture to examine the dopants effect on CO_2 flux (Fig. 3. 8).
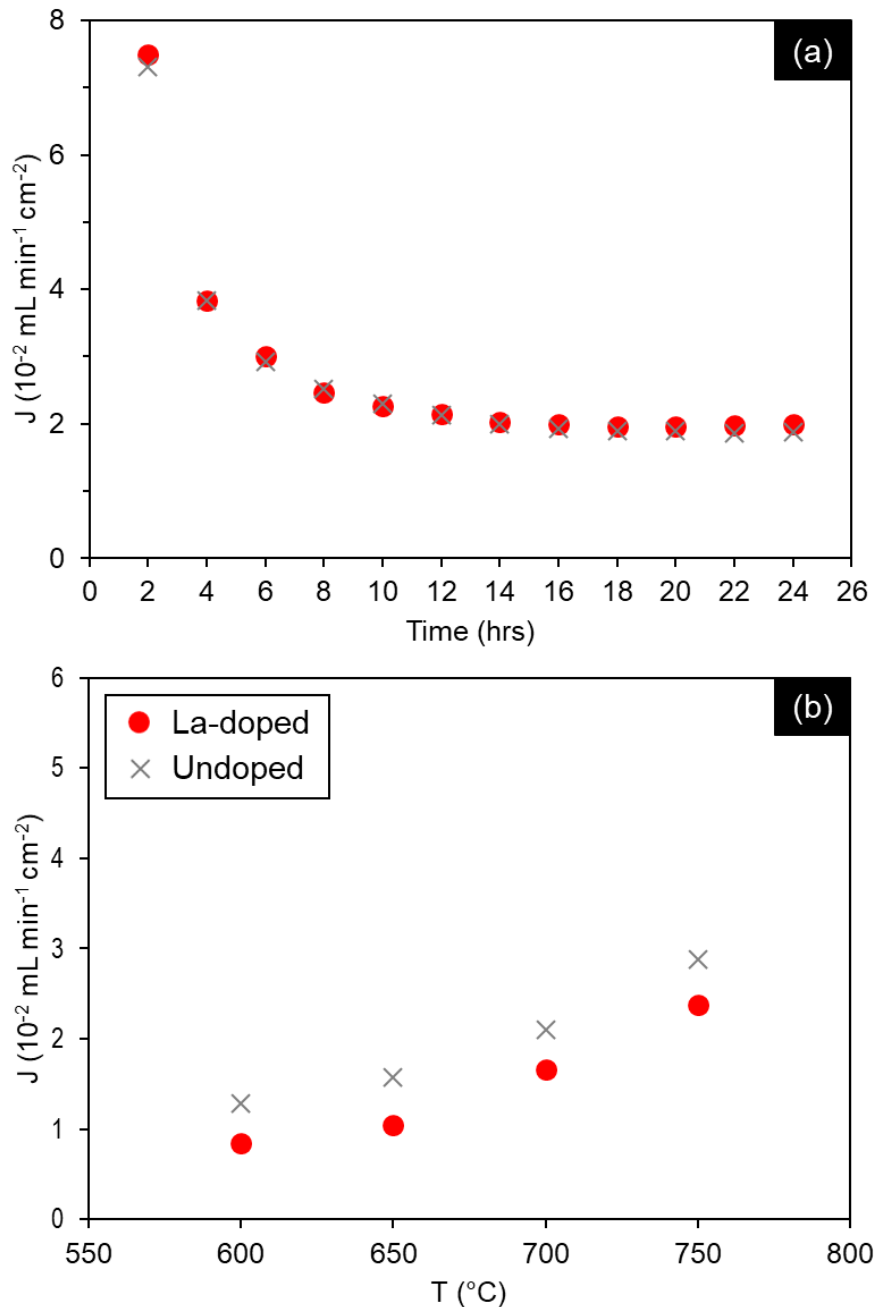
Fig. 3. 8 (a) CO_2 flux as a function of time for two unused parallel pore membranes at 650°C. (b) CO_2 flux as a function of temperature for two used parallel pore membranes. The two membranes in each study were infiltrated with differing carbonate eutectics; "Undoped" ternary eutectic and "La-doped" ternary eutectic with 0.5 mol% La_2O_3. Gas feeds for each study were identical; Feed-side inlet: 50 mol% CO_2 in N_2. Permeate-side inlet: Ar.

Fig. 3. 8a shows the flux evolution with time at 650°C for two parallel pore membranes during their first use with their respective carbonate mixtures. It was found that the La-doped membrane achieved a flux of 2.0×10^{-2} mL min^{-1} cm^{-2} after 24 hours of operation, while the undoped membrane achieved a flux of 1.9×10^{-2} mL min^{-1} cm^{-2} after the same length of time. The experiments were repeated using the same parallel pore membrane (see section 3.2.3). After the second run, the CO_2 flux for the La-doped membrane decreased by 45% to 1.2×10^{-2} mL

min^{-1} cm^{-2} and was still decreasing by 5.63×10^{-4} mL min^{-1} cm^{-2} each hour. The undoped membrane also produced a 6% decline in flux to 1.8×10^{-2} mL min^{-1} cm^{-2}. Fig. 3. 8b shows the fluxes of each membrane after their second permeation experiments. The undoped ternary carbonate membrane produced fluxes ranging from 1.3 to 3.0×10^{-2} mL min cm^{-2} for 600 to 750°C, respectively. The addition of 0.5 mol% La_2O_3 caused a decrease in CO_2 flux across all temperatures with a flux range of 0.8 to 2.4×10^{-2} mL min^{-1} cm^{-2}.

The flux for the La-doped membrane was higher for the parallel pore membranes first use because of a reaction between $La_2O_2CO_3$ and the Al_2O_3 support on the permeate side of the membrane *via* reaction (3.9), which creates lanthanum aluminate ($LaAlO_3$) and releases of CO_2:

$$La_2O_2CO_3 + Al_2O_3 \leftrightarrow 2LaAlO_3 + CO_2 \tag{3.9}$$
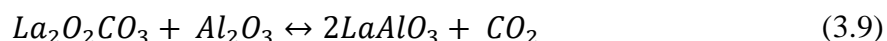
The formation of $LaAlO_3$ is evidenced in Fig. 3. 9, which displays the XRD data from a fragment of the parallel pore membrane permeate-side surface which has been subjected to multiple La-doped permeation experiments. The data shows that the samples strongest signal is $LaAlO_3$, which is confirmed by reference data. The remaining peaks represent the unreacted Al_2O_3 support.
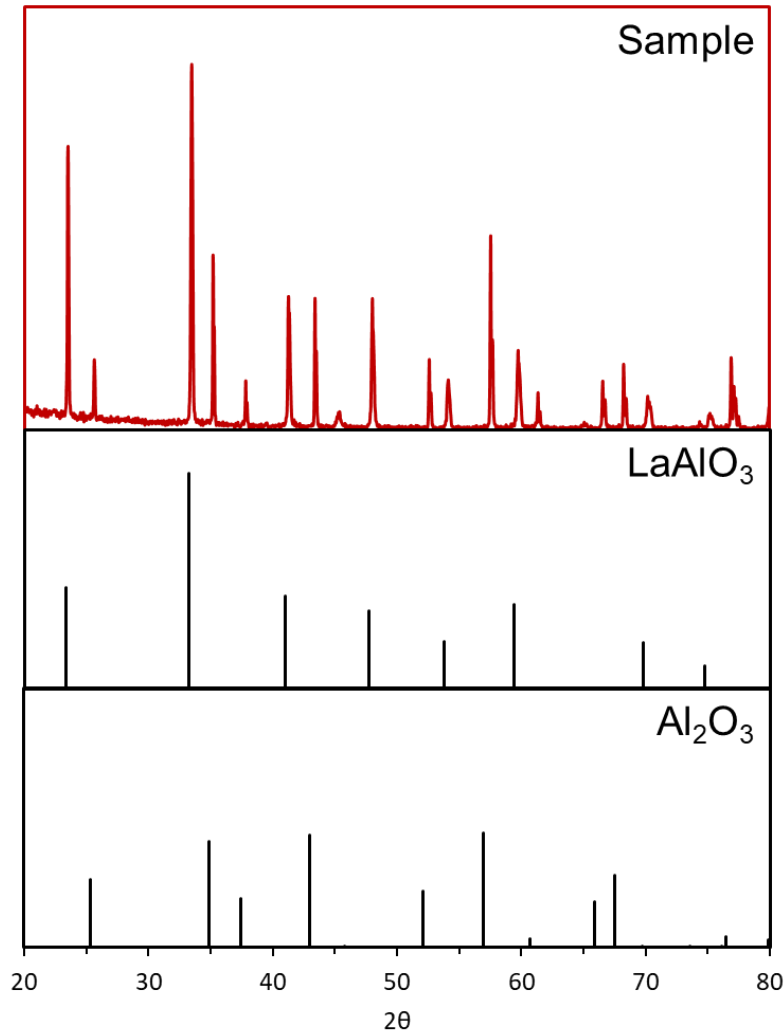
Fig. 3. 9 XRD analysis of a fragment of the permeation-side surface of a tested parallel pore membrane which has been subjected to La-doped carbonate during permeation experiments.

Therefore, the flux for the first experiment is a "false flux", or a combined flux and reaction by-product mechanism, as the extra CO_2 release comes from a reaction between $La_2O_2CO_3$ and Al_2O_3, which is not sustainable. Thus, due to the reuse of the parallel pore membrane (see section 3.2.3), the subsequent experiments provided less Al_2O_3 to react with the $La_2O_2CO_3$, causing a reduction in the rate of reaction (3.9), which results in less CO_2 release and hence a reduced "false flux". The 6% reduction produced by the undoped membrane is likely from a similar reaction where Li_2CO_3 reacts with Al_2O_3 to form lithium aluminate ($LiAlO_2$) and CO_2 shown by reaction (3.10):

$$Li_2CO_3 + Al_2O_3 \leftrightarrow 2LiAlO_2 + CO_2 \tag{3.10}$$
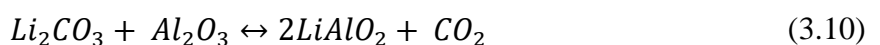
To help explain reaction (3.10) and consequently reaction (3.9), an experiment using Raman spectroscopy was conducted (Fig. 3. 10). Ternary carbonate eutectic powder was placed on top

of a porous Al_2O_3 pellet and heated to 650°C under a 50 mol% CO_2 in N_2 atmosphere and held under these conditions for 1 hour before switching to pure Ar. Fig. 3. 10a shows that when the high pCO_2 containing gas is removed from the system there is no CO_2 available to stop the formation of $LiAlO_2$ (forward reaction (3.10)), a peak at 487 cm^{-1} was formed with time which corresponds to the strongest peak with $LiAlO_2$ (Fig. 3. 10c). When 50 mol% CO_2 was restored after 1 hour of feeding pure Ar, the peak at 487 cm^{-1} remained which indicates the forward reaction for (3.10) is irreversible (Fig. 3. 10b). This can help to explain why subsequent permeation experiments see a decline in "false flux" because the amount of CO_2 released by reaction (3.10) declines as more of the Al_2O_3 support is permanently converted to Li or $LaAlO_3$. This reaction (as well as reaction (3.9)) will continue to decrease until all Al_2O_3 sites have been converted, at which point the membranes "true flux" will be revealed.
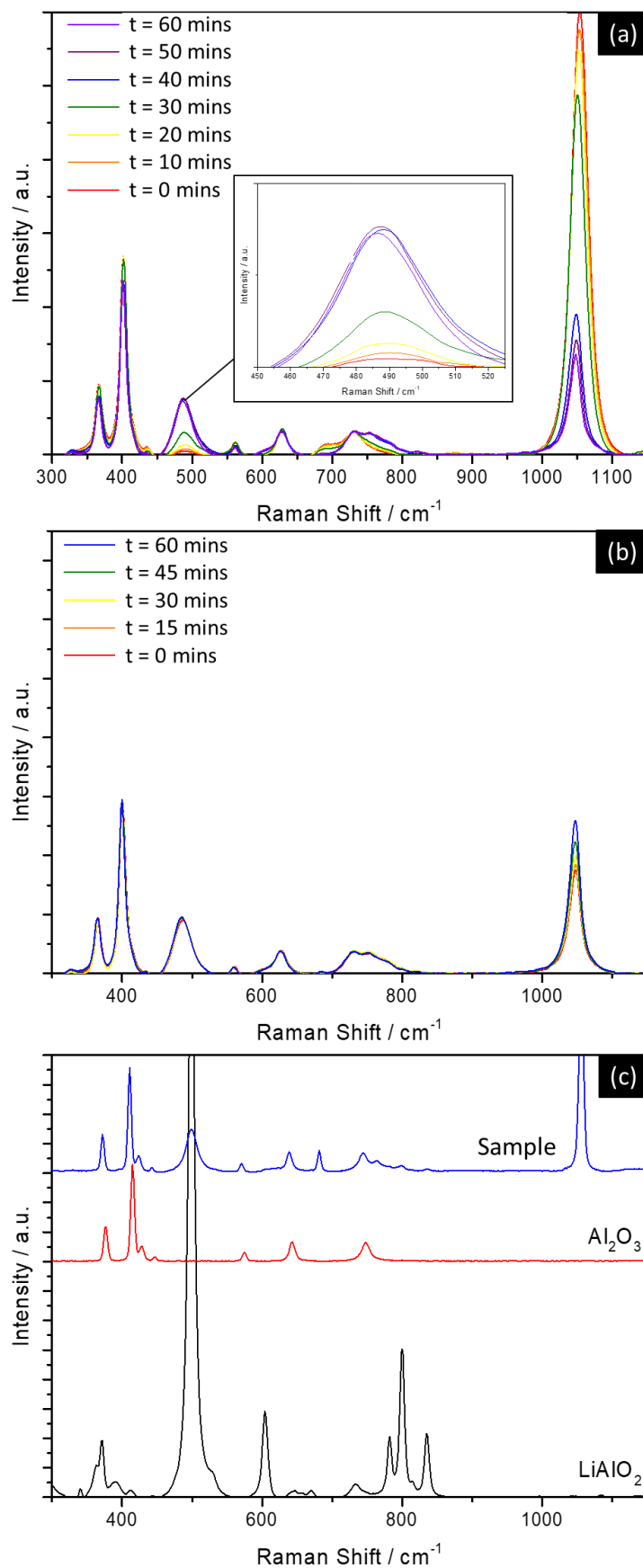
Fig. 3. 10 (a) Development of LiAlO$_2$ after removal of CO$_2$ containing feed gas. Feed gas a t = 0 is 50 mol% CO$_2$ in N$_2$. Feed gas a t > 0 is Ar. (b) Stability of LiAlO$_2$ with restoration of CO$_2$ containing feed gas. Feed gas a t = 0 is Ar. Feed gas a t > 0 is 50 mol% CO$_2$ in N$_2$. (c) Raman spectra comparison of tested sample to LiAlO$_2$ and Al$_2$O$_3$ reference data.

To understand why the flux of the La-doped membrane was lower than the undoped membrane after the parallel pores first use, two permeation experiments were performed using pellet membranes. One membrane was infiltrated with La-doped carbonates while the other was infiltrated with undoped carbonates. After operation, both pellets were removed from their reactors and their permeate sides were analysed using SEM-EDX (Fig. 3. 11).
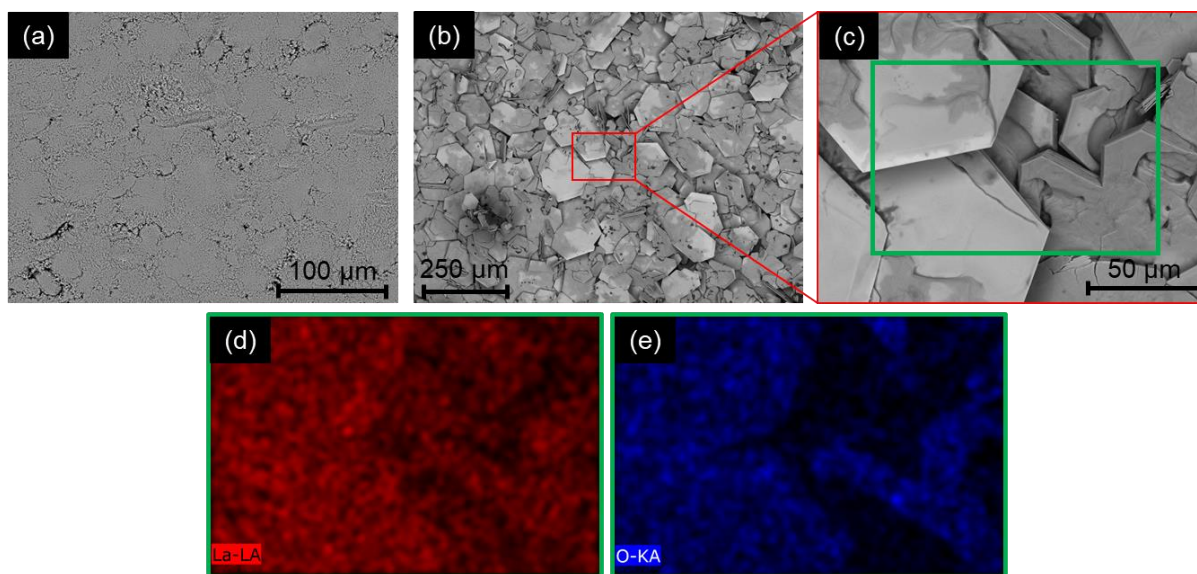
Fig. 3. 11 (a) SEM image of the permeate side of a tested undoped Al_2O_3-MC pellet membrane (b and c) SEM images of the permeate side of a tested Al_2O_3-MC pellet membrane doped with 0.5 mol% La_2O_3 in the carbonate; (c and d) EDX mapping of La and O from inside the green box shown in (b). Both pellet membranes were subjected the following conditions during permeation: Operation temperature: 650°C. Feed-side inlet: 50% CO_2 in N_2. Permeate-side inlet: Ar.

When comparing the two membranes, it was clear that the permeate side of the La-doped membrane was covered by a La-containing compound, with particle sizes of ~50-100 µm (Fig. 3. 11a-c). Based on the unit cell shapes reported by Hirsch *et al.* [108] and elemental analysis (Fig. 3. 11d-e) it can be deduced that the hexagonal crystal structures were likely that of $La_2O_2CO_3$.

A reason for the $La_2O_2CO_3$ precipitation can be described from the work by Matsuzawa *et al.* [109]. The authors showed that solubility of $La_2O_2CO_3$ in a ternary molten alkali carbonate eutectic is a function of pCO_2. In their study, they state that under high pCO_2 (> 50 mol%) and 650°C, 0.5 mol% is soluble in molten carbonate. However, under low pCO_2 (< 5 mol%) the solubility is over an order of magnitude less. Therefore, based on the non-equilibrium conditions of a dual-phase membrane, the $La_2O_2CO_3$ dissolves on the feed side, due to the high pCO_2 and $La_2O_2^{2+}$ and CO_3^{2-} ions move down their concentration gradient before precipitating on the permeate side due to their exposure to the pure Ar *i.e.* low pCO_2. This indicates that the

La precipitates during permeation and not upon cooling which can explain why the flux is much lower than an undoped carbonate due to blockage of the permeate-side surface. Therefore, to understand if La_2O_3 could increase CO_2 flux in a dual-phase membrane, a method for keeping $La_2O_2CO_3$ in the melt at the permeate side must be achieved. However, this would likely require pressurising the system, which would not be energy efficient for a carbon capture process.

This precipitation could also add an extra explanation for why the "false flux" was higher for the parallel pore membranes first use. During the membranes first use, the $La_2O_2CO_3$ was consumed to form $LaAlO_3$, meaning that extra CO_2 was released as a by-product (see reaction (3.9)), but as a result less $La_2O_2CO_3$ was now available to block the permeate-side surface, therefore a reduction in flux is not seen. However, for subsequent experiments, once all the sites for $LaAlO_3$ formation have been used (see reaction (3.9)) the $La_2O_2CO_3$ precipitates and blocks the surface.

Since it is well documented that La_2O_3 increases the solubility of O_2 in molten carbonate [67], [103], the two separate modification techniques described in this chapter were combined. Permeation experiments using the 0.5 mol% La_2O_3 ternary carbonate eutectic were performed with 50 mol% CO_2 in N_2 in the feed-side inlet and 25 mol% O_2 in Ar in the permeate-side inlet at 650°C. The flux data was compared to an undoped carbonate membrane operated under the same gas feeds and operating temperature to determine if La_2O_3 increased the solubility of O_2 on the permeate side and thus, increased the rate of CO_2 release (Fig. 3. 12).
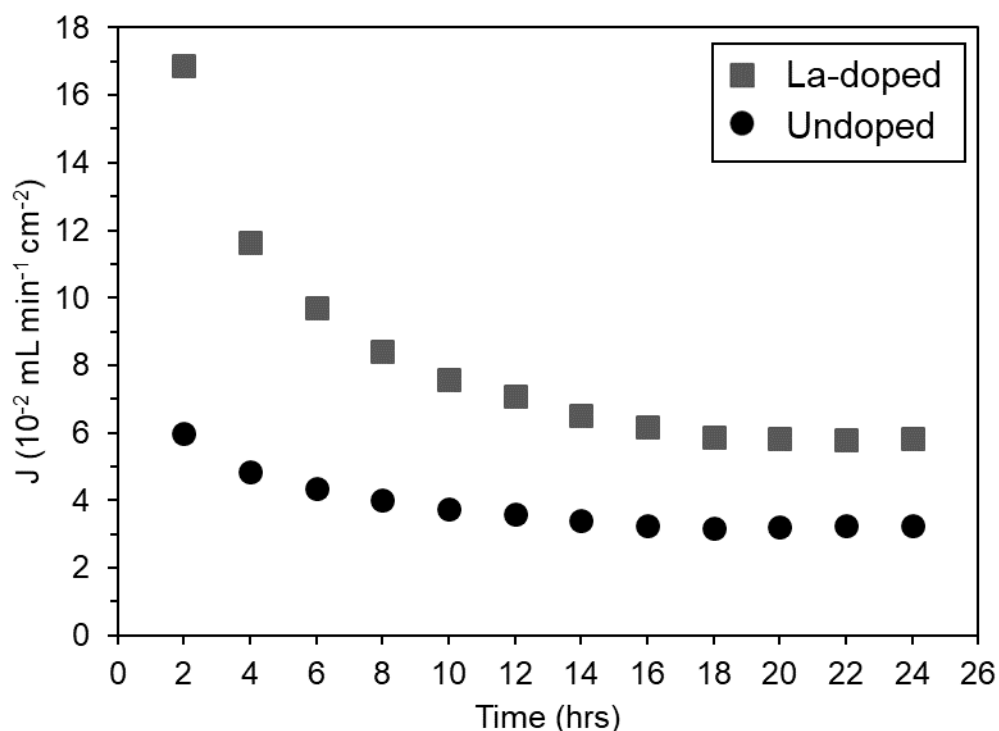
Fig. 3. 12 Comparison of CO_2 fluxes for a 0.5 mol% La-doped ternary carbonate and undoped ternary carbonate membrane for each parallel pore membranes first use at 650°C. Feed-side inlet: 50 mol% CO_2 in N_2, permeate-side inlet: 25 mol% O_2 in Ar.

Fig. 3. 12 shows CO_2 flux data of two fresh parallel pore membranes first 25 hours of operation. The "false flux" of the La-doped membrane was 5.8×10^{-2} mL min^{-1} cm^{-2}, which was 78% higher than the undoped membrane (3.3×10^{-2} mL min^{-1} cm^{-2}). However, after the experiment was repeated the La-doped membranes "false flux" decreased by 45%, due to the reduction in Al_2O_3 available to form $LaAlO_3$ (see reaction (3.9)). The final reported flux was 2.9×10^{-2} mL min^{-1} cm^{-2}, thus falling below the undoped membranes flux. In a similar fashion to without O_2 in the permeate-side inlet, once reaction (3.9) was exhausted, the decrease in flux compared to the undoped membrane was due to blockage of the permeate-side surface from precipitated $La_2O_2CO_3$. Furthermore, by performing a quick calculation, integration of the area under each curve from Fig. 3. 12 reveals that 1.8×10^{-4} and 8.9×10^{-5} moles of CO_2 were released from the La-doped and undoped membranes first uses, respectively. By subtracting the latter from the former to isolate the La contribution, a CO_2 mol difference of 9.5×10^{-5} is obtained. This is of the same order of magnitude as the amount of $La_2O_2CO_3$ produced after La_2O_3 addition (3.0×10^{-5} mol), which again supports the presence of reaction (3.9).

In summary, the addition of La into the carbonate melt did not result in an increase in flux, likely due to its precipitation on the permeate-side surface as a result of its low solubility in a low pCO_2 atmosphere. Therefore, for a dopant to have a positive effect on gas flux the material must be highly soluble in molten carbonate, such as the dopants used in the study by Xing *et*

al. [88] where an order of magnitude more dopant was added to the carbonate mixture. Alternatively, precipitation could be used to add functionality to a non-conductive support phase. For this to work, the precipitated material must be conductive, and precipitation must be controlled in a way to provide a connected pathway that spans the entire cross-section of the dual-phase membrane to promote either of the transport mechanisms described in Fig. 1. 2b or c. The non-equilibrium conditions of a permeating dual-phase membrane could be one way to control precipitation. However, $La_2O_2CO_3$ is neither electron or oxide conducting, therefore precipitation adds no functionality to the Al_2O_3-melt interface. In addition, base metals such as copper or aluminium which are well known electron conductors would also likely not be suitable for these studies because the materials are easily oxidised. While these metals undergo passivation to maintain their electron conduction beneath the non-conducting oxide layer, the interface between the melt and the metal would be non-conductive which would reduce electron conduction between the phases. Therefore, the material must not oxidise under high temperatures or in the presence of molten carbonate *i.e.* a noble metal must be used. However, platinum (Pt) and Au have been reported as highly resistant to corrosion in molten carbonate, with the latter reporting no detectable weight change in multiple studies [80], [110]. If the material is highly resistant to corrosion, then precipitation to add functionality to the support will be negligible. Therefore, Ag provides an alternative option due to its appreciable solubility in molten carbonate and the ability to maintain its metallic form after precipitation from molten carbonate [110].

3.4   Conclusion

This chapter confirmed the dissociation of carbonate ions into oxide ions and CO_2 molecules and desorption is a slower process than the absorption and association of CO_2 molecules and oxide ions into carbonate ions. The results that followed presented initial research and testing of attempts to modify molten carbonate in a dual-phase membrane to enhance the rate of CO_2 release from the permeate-side surface. Three methods were explored and the following conclusions were made:

1. Introduction of oxide species (O_2^{2-}) into the melt.
   - The introduction of O_2 into the permeate-side inlet provided a 50% flux increase when compared to a membrane using pure Ar. Thus, confirming the hypothesis that the permeate side decomposition reaction can be replaced with a reaction to introduce oxides into the carbonate melt resulting in an increase in the rate of CO_2 released at the permeate-side surface.
   - The flux improvement was limited to 50% improvement, likely due to the low solubility of O_2 gas in molten carbonate.
2. Introduction of a foreign cation into the carbonate melt.
   - The addition of La_2O_3 caused a decline in flux across all temperatures ranging from $600 – 750°C$ when compared to an undoped membrane.
   - The decrease in flux was caused by the low solubility limit of $La_2O_2CO_3$ in molten carbonate under low pCO_2. This led to precipitation of a $La_2O_2CO_3$ layer on the permeate-side surface, which blocked the membrane resulting in a decline in flux.
3. Introduction of a foreign cation and oxide species into the carbonate melt.
   - When combining the two modification methods, the results were inconclusive. The results showed that during the membranes first use the combined modifications showed a 78% CO_2 flux increase, when compared to an undoped membrane with O_2 in the permeate-side inlet.
   - However, after further use using the same parallel pore membrane, the CO_2 flux decreased to below the undoped membranes flux due to precipitation of $La_2O_2CO_3$ on the permeate-side surface.
   - A reason for the higher CO_2 flux during the parallel pore membranes first use is likely due to $La_2O_2CO_3$ reacting with the Al_2O_3 support, resulting in a release of CO_2 and permanent transformation of Al_2O_3 to $LaAlO_3$. This reaction also

reduces the amount of $La_2O_2CO_3$ available to block the surface during the first run.

Chapter 4. Using the molten carbonate to control dopant precipitation to create a self-forming electronically conductive membrane

This chapter presents the results of the development of the first Ag/Al_2O_3-MC membrane ever made. Multiple membrane CO_2 fluxes are compared under different chemical driving forces, with and without the addition of Ag and each membrane is characterised to understand the interactions between the Ag and the dual-phase membrane. Much of work presented here is used in the publication accepted by *Energy & Environmental Science* titled "Dendritic Ag self-assembly in molten-carbonate membranes for efficient CO_2 capture".

4.1 Introduction

Chapter 3 suggested that dopant solubility in molten carbonate was a determining factor when trying to improve the flux of a dual-phase membrane *via* modification of the molten carbonate. Therefore, for molten carbonate modification to have a lasting effect on flux enhancement, the dopant should still offer performance enhancement if the material precipitates. A novel approach would be to use the molten carbonate as a carrier to coat the melt-solid interface of an inert support with a high-cost, functional dopant once it drops out of solution, thus providing functionality to a low-cost, inert support at reduced expense.

It is often the case, that the materials used for oxide and electron-conducting supported membranes are expensive. A few examples include Ag, LSCF and SDC-supported dual-phase membranes. Ag is known to be expensive due to being a precious metal, while reasons for the elevated costs of LSCF and SDC are linked to the availability and accessibility of the individual cations (as discussed in Section 1.2.3). Membranes that use these materials for their supports produce some of the highest CO_2 fluxes for dual-phase membranes used in post and pre-combustion carbon capture, however their use incurs a high cost (£365 kg^{-1} for Ag [111] *vs.* £9 kg^{-1} for nickel [112], as listed on the London Metal Exchange) that is a concern for future scale-up. Furthermore, the amount of material used is likely in excess. It is currently unclear how much of a given support contributes to the gas flux and how much is simply there for mechanical strength. By using molten carbonate as a carrier to coat the melt-solid interface with an oxide or electron-conducting layer, the same conducting properties could be achieved, but with lower cost.

A related idea has been shown by Zheng *et al.* [56], [69] where molten carbonate was used to transform a cheap nickel oxide (NiO) support into a high flux electron-conducting membrane. This was achieved by lithiation of the NiO support to form a thin lithiated NiO layer ($Li_{0.4}Ni_{1.6}O_2$) on the surface of the pores. The electron-conduction provided by the thin $Li_{0.4}Ni_{1.6}O_2$ layer enabled higher fluxes than any other electron-conducting supported dual-phase membranes. At 850°C, the lithiated NiO membrane achieved a CO_2 and O_2 flux of ~1.0 and 0.5 mL min^{-1} cm^{-2} respectively, matching the 2:1 CO_2:O_2 flux ratio seen with other electron-conducting membranes *via* reaction mechanism (4.1):

$$CO_2 + \frac{1}{2}O_2 + 2e^- \leftrightarrow CO_3^{2-} \tag{4.1}$$

This self-forming, electron-conducting layer meant that no excess material was used for conduction and the lithiated NiO gained mechanical strength from the NiO framework. However, while this lithiated NiO membrane offers a lower fabrication cost compared to other

71

electron-conducting membranes, Ag is the most electronically conductive metal available. Therefore, optimisation of the Ag dual-phase membrane is desirable.

Ag-supported dual-phase membranes were initially researched [60] as an alternative to the first stainless steel dual-phase membrane. Ag was considered as a better alternative as it does not form an insulating layer at high temperatures which reduces electron conductivity (as discussed in Section 1.2.1). With the ability to avoid the formation of an insulating layer, seen with stainless steel [61] and LSCF [41] supports, came CO_2 fluxes that reached up to ~0.8 mL min^{-1} cm^{-2} at 650°C. This shows an improvement of more than 450% when compared to a stainless steel supported dual-phase membranes, which achieved a CO_2 flux of ~0.17 mL min^{-1} cm^{-2} with a CO_2 and O_2 feed gas at 650°C. Both supports have shown a 2:1 permeation ratio for CO_2 and O_2, agreeing with (4.1).

The CO_2 and O_2 co-permeation is enabled *via* a two-step reaction on the feed-side surface. Firstly, the O_2 from the feed gas reacts with the solid Ag support to form solid Ag_2O as shown by reactions (4.2) and (4.3):

$$2Ag_{(s)}^0 \leftrightarrow 2Ag_{(s)}^+ + 2e_{(s)}^- \tag{4.2}$$

$$\frac{1}{2}O_{2\,(g)} + 2e_{(s)}^- \leftrightarrow O_{(s)}^{2-} \tag{4.3}$$

The standard cell potential (E^0) for reaction (4.2) is -0.8 V, regardless of the number of moles of Ag and electrons as voltage is an intensive property [113]. The CO_2 from the same feed gas then reacts with the newly formed Ag_2O resulting in dissolution of Ag into the molten carbonate *via* reaction (4.4):

$$CO_{2\,(g)} + O_{(s)}^{2-} \leftrightarrow CO_{3\,(l)}^{2-} \tag{4.4}$$

Reactions (4.3) and (4.4) can be simplified to (4.1). Due to the CO_2 and O_2 concentration gradient created across the membrane as a result of the inert permeate-side inlet gas, the carbonate ions and Ag cations move towards the permeate-side surface. This then causes a chain reaction of electron donation and recombination across the membrane cross-section until the Ag cation reaches the permeate-side surface. Due to the negligible CO_2 content in the permeate-side chamber and the continuous removal of the permeate-side chamber the reverse of reaction (4.4) *i.e.* the carbonate ion releases CO_2 and the Ag cation recombines with the oxide ion to form Ag_2O. Similarly, due to the negligible amount of O_2 in the permeate-side chamber, combined with the fact that Ag_2O thermally decomposes above 200°C [114] in the absence of O_2, the reverse of reactions (4.2) and (4.3) proceed *i.e.* O_2 is released from the Ag_2O and metallic Ag is reformed.

For the Ag membrane to allow CO_2 permeation the Ag must dissolve into the molten carbonate. However, while it has long since been known that Ag dissolution occurs in molten carbonate under the conditions described for the Ag-supported membrane [110], [115], no authors for the Ag-supported membranes have discussed what effect this could have on the functionality of the membrane. In addition, no author has discussed how this phenomenon can be exploited to prepare a cheap, low-Ag content, electronically conductive membrane using a similar method to that described for the lithiated NiO membrane.

This is possible, due to Ag migration under the non-equilibrium conditions of permeation, as proposed in (Fig. 4. 1). If Ag is added to an inert ceramic-supported dual-phase membrane, in contact with molten carbonate and exposed to a CO_2 and O_2 gradient across the membrane the same reaction scheme described by reactions (4.2), (4.3) and (4.4) will proceed. However, while the Ag-supported membrane had a continuous electron conductive path to allow a chain reaction of electron donation and recombination the inert support cannot provide this. Instead, the Ag cations formed from the two-step reaction at the feed-side will migrate to the permeate-side surface, due to the CO_2 and O_2 concentration gradient, where the reverse of the aforementioned reactions will occur *i.e.* CO_2 and O_2 will be released (permeated) from the permeate-side membrane surface and the Ag cations will recombine with the released electrons to form metallic Ag.
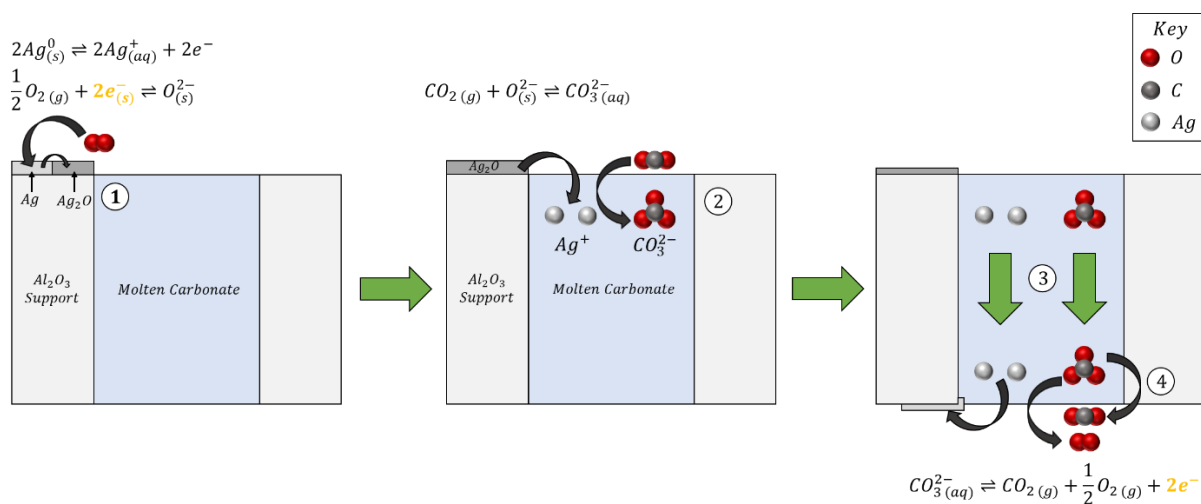
Fig. 4. 1 Schematic illustration of a single Al_2O_3-MC pore with Ag doped onto the surface. The process follows; (1) Ag oxidation to Ag_2O *via* reaction with O_2 (2) Ag_2O dissolution and simultaneous carbonate ion formation, (3) Ag cation and carbonate ion migration and (4) the reverse of (1) and (2) resulting in CO_2 and O_2 release with simultaneous Ag precipitation.

Fig. 4. 1 shows the proposed hypothesis which outlines three stages showing dissolution and migration of Ag due to gas transport and subsequently precipitation on the permeate side. However, while the first three stages are reasonable to suggest, given the known dissolution of

Ag in molten carbonate and the non-equilibrium conditions associated with permeation, a fourth "growth" stage is required. For Ag dissolution to have a lasting effect on enhanced gas flux, the precipitated Ag must extend back towards the feed side of the membrane, to create a self-forming electron-conducting pathway, that functions in a similar way to that of an Ag-supported membrane. It is this electron-conducting pathway that could conceivably provide a flux improvement, which could explain the lack of flux enhancement with $La_2O_2CO_3$ in Chapter 3, because the material is non-oxide or -electron conducting. The alternative is that Ag does not extend back towards the feed side and instead, continues to migrate to the permeate side and subsequently precipitate until all the permeate side is blocked-off by precipitated Ag, which would likely result in a drop in flux. The extent to which Ag migration could be used as an *operando* preparation method to self-assemble a continuous Ag structure throughout such a membrane and to ultimately produce an electronically conductive support with a reduced quantity of Ag, remains to be explored.

In this chapter, the molten carbonate phase was used as a carrier to transport Ag throughout the membrane to create a self-assembling, electron-conducting support:

- Ag was plated onto a non-conducting, porous, Al_2O_3 support and infiltrated with molten carbonate to create an Ag/Al_2O_3-MC membrane.
- Permeation experiments with Ag/Al_2O_3-MC membranes were performed using different gas feeds and compared with Al_2O_3-MC membranes to determine the effect of Ag addition on gas flux.
- Tested membranes were characterised using SEM-EDX and micro-CT to probe the four hypothesized Ag dissolution, migration, precipitation and growth stages for the self-assembly of electron-conducting pathways.

4.2 Experimental

4.2.1 Dual-phase membrane support preparation

Porous pressed-pellet Al_2O_3 supports were used for all permeation experiments in this chapter and were prepared using the method described section *2.1.1*.

4.2.2 Method of Ag introduction

The porous Al_2O_3 pressed pellet was modified using electroless plating to introduce Ag onto the pellet surface, similar to methods described by Paglieri and Way [116] and Mardilovich *et al*. [117]. First, the Al_2O_3 supports were covered on one side with PTFE tape. The exposed side was then activated with Pd nuclei *via* sensitisation in an acidic $SnCl_2$ solution, followed by activation in an acidic $PdCl_2$ solution. The activation process was carried out by immersing the half-covered Al_2O_3 support in five 30 mL chemical baths sequentially (Fig. 4. 2): $SnCl_2$ solution for 5 minutes, deionised water for 5 minutes, $PdCl_2$ solution for 5 minutes, 0.01 M HCl solution for 2 minutes, deionised water for 3 minutes. All chemical baths were homogenously mixed by air bubbling and the sensitisation/activation process was repeated for six cycles. The bath compositions are outlined in Table 4. 1.
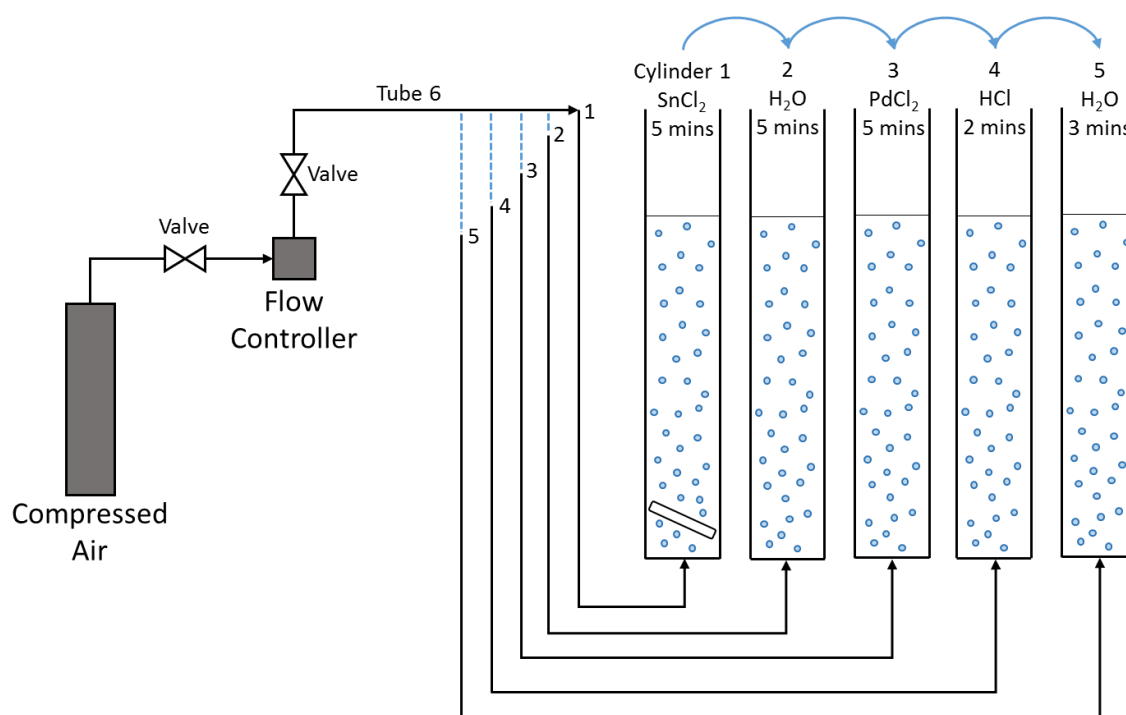
Fig. 4. 2 Schematic representation of the sequential baths for the sensitisation/activation process.

Table 4. 1 Composition of sensitisation/activation and plating bath solutions.

Step	Composition	Concentration (M)
Sensitisation	$SnCl_2.2H_2O$	4.43×10^{-3}
	HCl (37 %)	3.29×10^{-2}
Activation	$PdCl_2$	5.64×10^{-4}
	HCl (37 %)	3.29×10^{-2}
Rinsing	HCl	1.00×10^{-2}
Electroless plating	$AgNO_3$	3.06×10^{-3}
	Na_2EDTA	1.19×10^{-1}
	NH_4OH	4.97
	N_2H_4	1.75×10^{-1}

Activated Al_2O_3 supports were submerged in the plating solution described in Table 1 and maintained at 60°C, creating a metallic Ag layer in place of the Pd seeds. The experimental set-up is shown in Fig. 4. 3. To ensure full submersion of the support, 18 mL of plating solution was used. The solution was homogenously mixed by air bubbling and the supports were held in solution for 60 minutes before washing and re-submerging in a fresh plating solution. The plating process was repeated for six cycles.
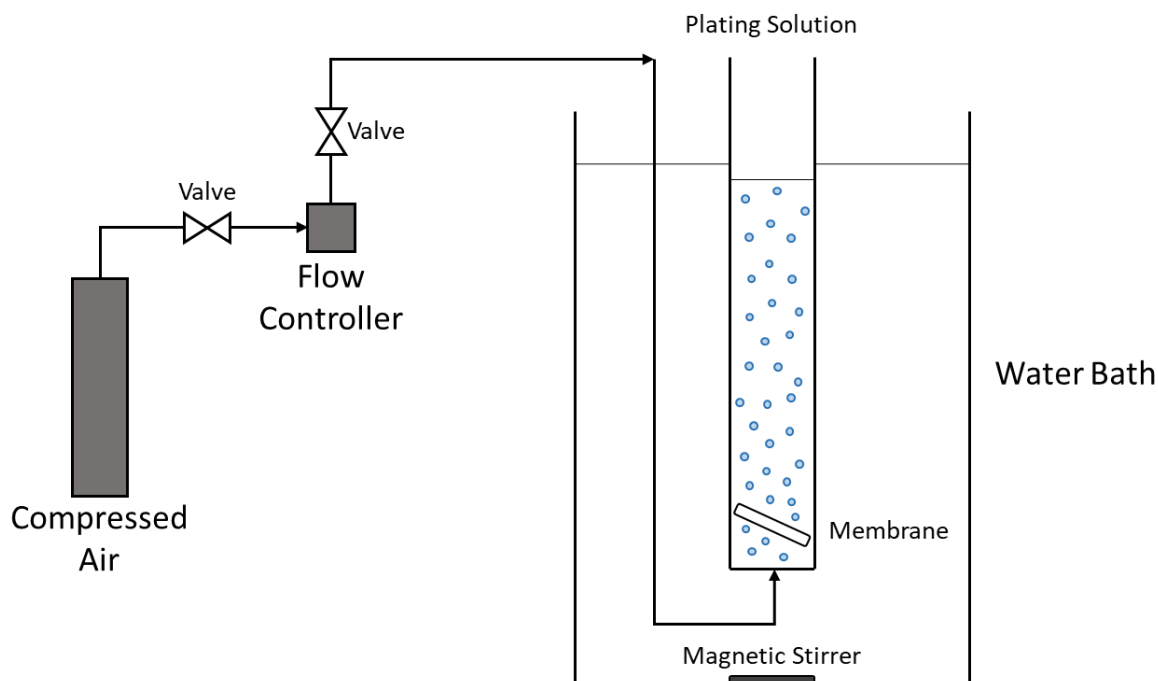
Fig. 4. 3 Schematic representation of the electroless plating process.

4.2.3 Molten carbonate preparation

The ternary carbonate eutectic described in section 2.1.2 was used for all experiments in this chapter.

4.2.4 Permeation measurements

For permeation tests, the pressed pellet membrane reactor (Fig. 2. 2) were used. Three feed-side inlet gases were used in this study:

1. 50 mol% CO_2 in N_2
2. 25 mol% O_2 in N_2
3. 50 mol% CO_2, 25 mol% O_2 in N_2

One permeate-side inlet gas was used in this study:

1. 100 mol% Ar

For the experiment where 25 mol% O_2 in N_2 was used as the feed-side inlet gas, 50 mol% CO_2 in N_2 was used for each side of the membrane during reactor heat-up to prevent carbonate decomposition. A temperature of 650°C was for all experiments in this study.

4.2.5 Dual-phase membrane characterisation

Microstructural and elemental surface analysis of pellet membranes before and after operation was performed using scanning electron microscopy and energy dispersive X-ray spectroscopy (model details in section 2.2). These tests included cross-section analysis where the membrane was secured in a resin and cut through the cross-section (to form two semi-circles) using a diamond cutter. The SEM scans were performed using the method described in section 3.2.4.

Phase identification was completed using X-ray diffraction (model details in section 2.2)[4]. The same procedure as described in section 3.2.4 was carried out, however the following parameters were varied:

- The nominal time per step was 500 seconds.
- The incident beam fixed divergence and anti-scatter slits were 1/4° and 1/4°, respectively.
- The scans were carried out in 'continuous mode'.

---

[4] Experiments were performed by Dr. Maggie White from Newcastle University and data was interpreted by Liam McNeil.

The pellets' pore size distribution, the median pore size and overall pellet porosity was characterized using mercury intrusion porosimetry (MIP)[5] over a pressure range of 0.01 – 1000 MPa (indicating a pore-size cut-off of ~5 nm) and with a set stabilisation time of 10 s (model details in section 2.2).

Micro-computed tomography was used to observe the Ag distribution throughout the internals of the dual-phase membrane using a Nikon XT H 225 (Nikon Metrology UK Ltd, Tring, UK) [6]. The series of scans were all conducted at a voxel dimension of 10.5 µm, at voltage and current of 160 kV and 50 µA, respectively. The exposure time used for each scan was 1 s and the number of projections for each scan was 3176, as per manufacturer default settings.

Two-point DC technique was used to measure the electrical conductivity of membranes[7]. For each measurement a thin Ag electrode was deposited on both the feed side and permeate side of the membranes, to serve as current collectors. The measured voltage was adjusted in the range of 50 – 500 mV and the corresponding current was measured and recorded across the probes connected to the Ag electrodes.

---

[5] Experiments were performed by Ji Jing from University of Bath and data was interpreted by Liam McNeil.

[6] Experiments were performed by Dr. Francesco Iacoviello from UCL, images were constructed by Dr. Josh Bailey from UCL and data was interpreted by Liam McNeil.

[7] Experiments were performed by Dr. Evangelos Papaioannou & Dr Gaurav Gupta Newcastle University and data was interpreted by Liam McNeil.

4.3 Results & Discussion

4.3.1 Morphological characteristics of the Al₂O₃ and Ag/Al₂O₃ support

Phase identification using XRD showed that the prepared supports were α-Al$_2$O$_3$ phase as identified by the peak comparison with the α-Al$_2$O$_3$ reference data (Al$_2$O$_3$ #04-007-1400) in Fig. 4. 4c. This phase is expected given the sintering temperature and the slow ramp rate used during support fabrication [118]. SEM identified the support as porous (Fig. 4. 4a) which is expected as the densification temperature required for Al$_2$O$_3$ is 1500°C [119]. Using MIP, it was found that the sintered supports had an average pore diameter of 200 nm (Fig. 4. 4b). This average pore size is of the same order of magnitude seen for the highest flux membranes in the literature, albeit with a different material [41], [51], [58], [83]. The majority of pore sizes found in the literature are 200-600 nm, meaning that our pore size is below the average, but this is reasonable considering no pore former was used during fabrication.
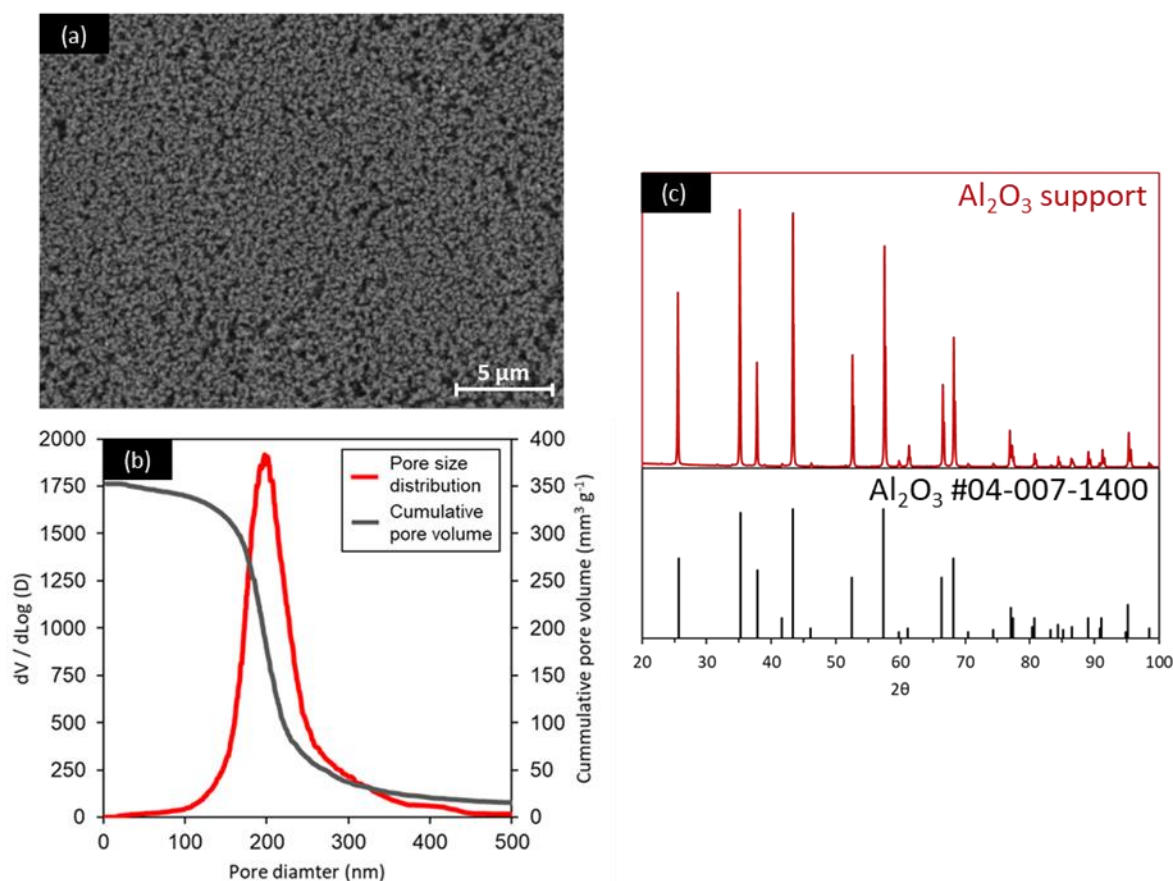
Fig. 4. 4 (a) SEM image of the surface of the Al$_2$O$_3$ support; (b) Al$_2$O$_3$ support pore size distribution obtained by mercury intrusion; (c) Al$_2$O$_3$ phase obtained by XRD.

The overall porosity of the supports was calculated to be ~55%, which is higher than average for dual-phase membranes. A study by Ortiz-Landeros [81] showed that they were able to increase the membranes flux by 200% by decreasing the porosity from 52.8 to 46.1%. This was

achieved by increasing the sintering temperature by 100°C, albeit with a different support. Therefore, it is suggested that increasing the sintering temperature may be beneficial for future studies. However, in their study an LSCF support was used, therefore a balance needed to be made between the volume of molten carbonate available for CO_2 transport and the ionic conductivity available for carbonate ion formation, as discussed in section 1.2.2. In this study, an Al_2O_3 support is used which provides no conductivity to assist in carbonate ion formation and CO_2 transport, therefore only molten carbonate is responsible for CO_2 flux and thus, its volume should be maximised. In summary, a porosity of ~55% is reasonable for the given support in order to achieve a high volume of molten carbonate for CO_2 transport. It should also be noted that this porosity was measured using MIP, which includes "dead-end pores" *i.e.* pores that do not span the entire cross-section, therefore the 55% porosity presented here is likely an overestimation, however, given that other dual-phase membranes have used the same method for porosity measurement [41], [51], [55], [72], [83], [120] this value can be used comparatively.

While the pore size is small, and the porosity is high, the geometry is suitable for the purpose of this proof of concept study as flux comparisons will be made internally. However, Chapter 5 will discuss the effects modifying the geometry has on the flux of the membrane. The overall porosity ($P\%$) for the support used in this study was found using the equation below:

$$P\% = \rho_d V_i \times 100 \tag{4.5}$$

Where ρ_d is the sample bulk density (g/cm^3) and V_i is the sample intruded volume (cm^3/g).

After fabricating the porous Al_2O_3 support, Ag was introduced onto the feed-side surface of the *via* electroless plating. After plating, the membrane had gained a porous (Fig. 4. 5a) ~10 µm thick layer of Ag (Fig. 4. 5b). The layer only appeared on the surface of the porous Al_2O_3 support, as expected when using electroless plating. This is due to the autocatalytic nature of the process once the initial surface is coated. Although, using Rutherford backscattering, Witjens *et al.* [121] found that the plated metal can penetrate up to 1.4 µm into the porous Al_2O_3 support. The plating area had a diameter of 14 mm providing an estimated total Ag mass of 17 mg (in agreement with gravimetric analysis ± 0.3 mg). This was calculated by assuming the plated area was cylindrical and using (4.6):

$$V_s = \frac{\pi d^2}{4} h \tag{4.6}$$

where V_s, d and h are the volume (cm³), diameter (cm) and thickness (cm) of the plated Ag layer, respectively. The mass of the Ag-plated layer (m_s) was calculated from the volume and the density of Ag (ρ_s):

$$m_s = V_s \times \rho_s \qquad (4.7)$$

The permeate side (Fig. 4. 5c) of the plated membrane did not show any evidence of Ag deposition. XRD (Fig. 4. 5d) confirmed that the deposited layer on the feed side was metallic Ag.
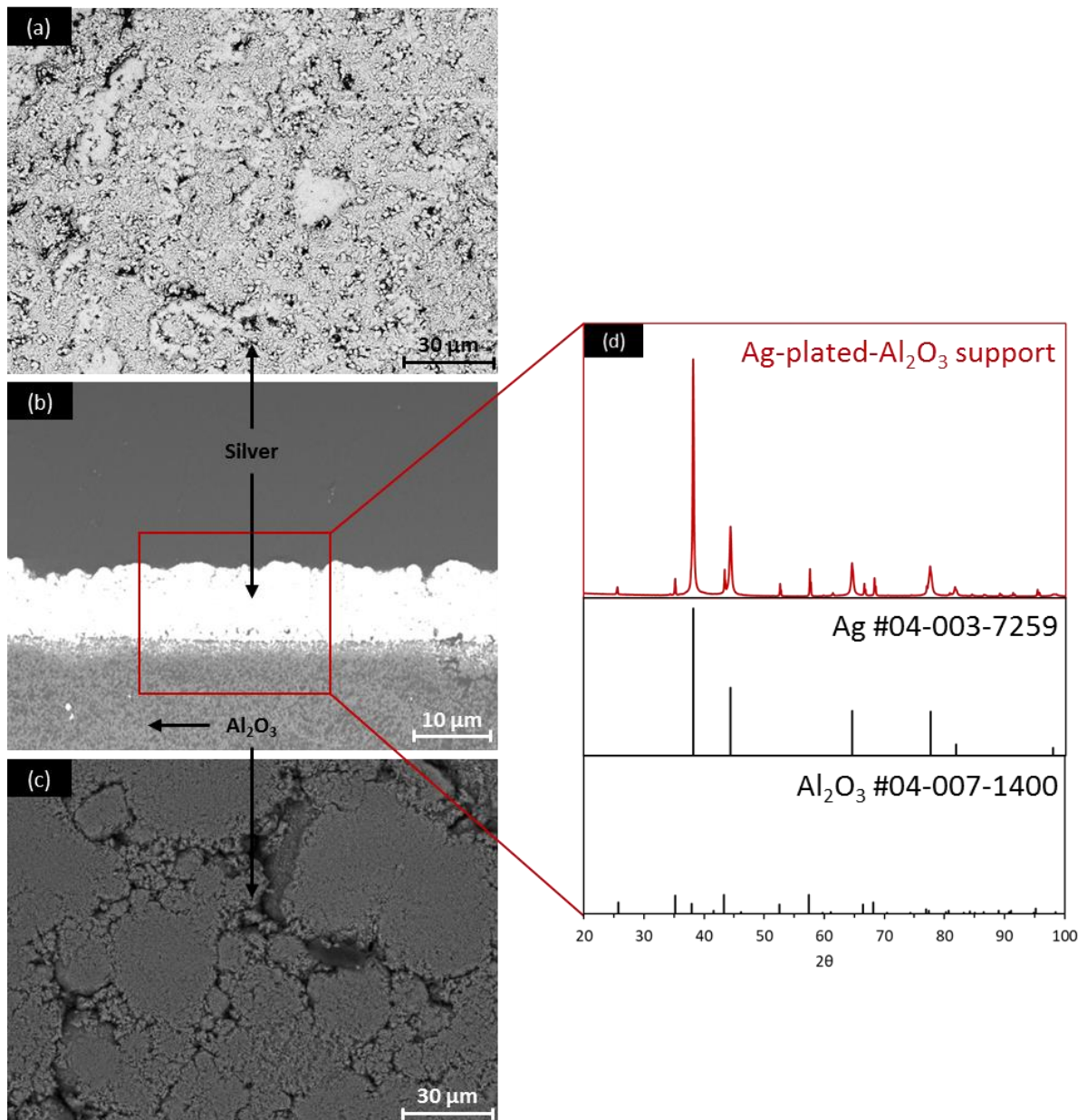
Fig. 4. 5 (a, b and c) SEM images of the feed side, Ag-plated surface cross-section and permeate side of an Ag electroless plated Al₂O₃ support respectively; (d) Crystalline structure of the Ag layer obtained by XRD.

4.3.2 The effect on electron-conducting pathway growth without a CO_2 and O_2 chemical driving force

As described by the hypothesis, it is expected that the Ag electron-conducting pathways will only form with a CO_2 and O_2 chemical driving force across the membrane. To see that this is the case, two control experiments were carried out where the membranes were fed with either 50 mol% CO_2 in N_2 or 25 mol% O_2 in N_2 in the feed-side inlet and pure Ar in the permeate-side inlet and operated at 650°C. After permeation, the membranes feed- and permeate-side surfaces were analysed using SEM-EDX to visualise any changes to each side of the membrane. The membranes cross-sections were analysed using a digital microscope to see if any electron-conducting pathways had been formed.

For the first control experiment, 50 mol% CO_2 in N_2 was used as the feed-side inlet, a common gas mixture used in the literature for testing dual-phase membranes for pre-combustion carbon capture. For the permeate-side inlet, pure Ar was used, creating a chemical driving force for CO_2 separation. Given the materials used for the Ag/Al_2O_3-MC membrane it is expected that without O_2 the Ag addition will pose minimal, if any, improvement to flux. To test this the Ag-plated membrane flux was compared with a non-Ag-plated Al_2O_3-MC membrane using the same chemical driving force (Fig. 4. 6).
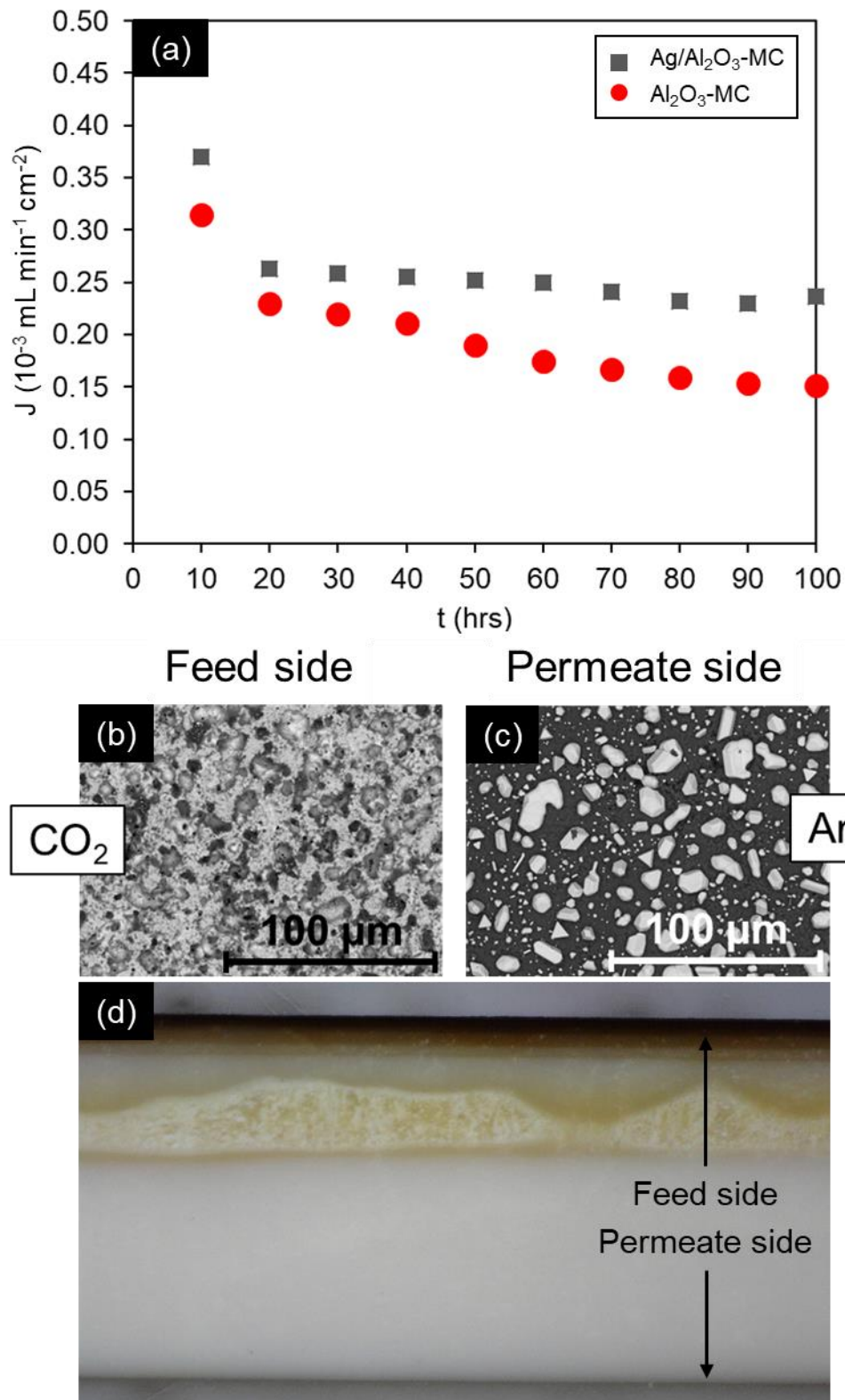
Fig. 4. 6 (a) CO_2 flux evolution with time at 650°C for an Ag/Al_2O_3-MC membrane compared to a non-Ag-plated Al_2O_3-MC membrane. SEM images of the (b) feed side and (c) permeate side and (d) digital images of the cross-section of the tested Ag/Al_2O_3-MC membrane. Feed-side inlet: 50 mol% CO_2 in N_2. Permeate-side inlet: Ar.

Fig. 4. 6a confirms that the Ag addition in the Ag/Al_2O_3-MC membranes does not offer significant flux improvement for use in pre-combustion when compared to an inert support.

This was shown by the small flux improvement from 0.15 to 0.25×10^{-3} mL min^{-1} cm^{-2} for the Al$_2$O$_3$-MC and Ag/Al$_2$O$_3$-MC respectively. While this improvement shows a 66% increase from the non-Ag-plated membrane, the flux alone is still two order of magnitude lower than other oxide-conducting dual-phase membranes in the pre-combustion field [47], [51], [82], [84].

Furthermore, post-experiment SEM analysis showed that only two of the four hypothesized stages for electron-conducting pathway growth occurred. The feed side still remained heavily occupied by the Ag-plated layer (Fig. 4. 6b) showing that without O$_2$ present with CO$_2$ in the feed-side inlet, Ag dissolution was restricted. This is expected because Ag will not dissolve without the presence of O$_2$ to allow the initiation of reaction (4.3) which is also described in section 1.1:

Therefore, CO$_2$ alone cannot dissolve Ag. This restriction of Ag dissolution is a possible contributor for why no electron-conducting pathways are seen throughout the membranes cross-section (Fig. 4. 6d). However, SEM images confirm that Ag migration to the permeate side (Fig. 4. 6c) occurred. A reason for this is likely due to the restricted, yet apparent Ag dissolution. While Ag is only known to corrode in an oxidising atmosphere, it has been mentioned elsewhere that rigorous exclusion of trace amounts of air from molten salt is difficult [110]. It is possible that some O$_2$ (air) was trapped in the carbonate powder before it melted, or it is also possible a small air leak into the feed-side chamber could have fed O$_2$ to the Ag-plated surface, allowing reactions (4.2) and (4.3) to occur simultaneously resulting in some Ag$_2$O formation at the triple phase boundary. Therefore, subsequent reaction of Ag$_2$O and CO$_2$ *via* reaction (4.4) will result in the presence of Ag cations in the melt.

The Ag cations have their own concentration gradient in the carbonate melt, which forces them to migrate towards the permeate side where the cations precipitate back to form metallic Ag, as already established by the work with La$_2$O$_2$CO$_3$. Each of these two explanations for how Ag migration occurred could explain why we see a small increase in CO$_2$ gas flux (Fig. 4. 6a). However, if the former is true then the increase in flux will be short-lived as the trapped O$_2$ in the carbonate powder is not sustainable and will eventually run out. This could possible explain why the flux doesn't appear to fully stabilize after 100 hrs of operation.

For the second control experiment, O$_2$ was fed to the membrane alone. Based on the findings in Chapter 3, it was expected that the O$_2$ flux was going to be low due to the low solubility of O$_2$ in molten carbonates (as discussed in Chapter 3) and Fig. 4. 7 reaffirms this.
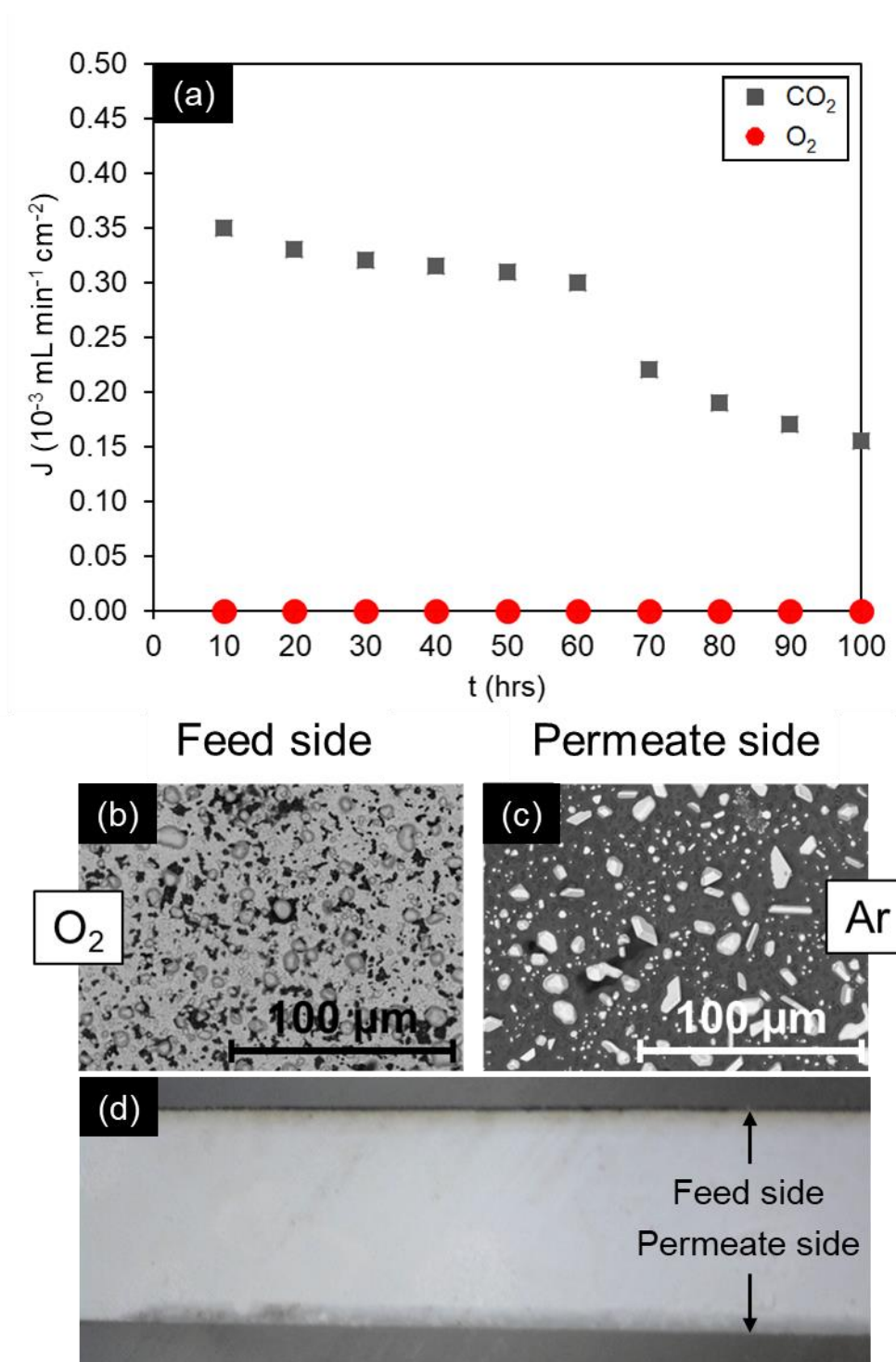
Fig. 4. 7 (a) CO_2 and O_2 flux evolution with time at 650°C for an Ag/Al_2O_3-MC membrane. SEM images of the (b) feed side and (c) permeate side and (d) digital images of the cross-section of the tested Ag/Al_2O_3-MC membrane. Feed-side inlet: 25 mol% O_2 in N_2. Permeate-side inlet: Ar.

Fig. 4. 7a shows that without CO_2, O_2 permeates below the gas analysis equipment's minimum measurable limit (~10 ppm). Furthermore, the absence of CO_2 destabilizes the membrane. Without CO_2 in the feed-side inlet, there is nothing to stop molten carbonate from decomposing on both sides of the membrane *via* the reverse of the following reaction (4.8):

$$CO_{2\,(g)} + O^{2-}_{(l)} \leftrightarrow CO^{2-}_{3\,(l)} \tag{4.8}$$

The presence of reaction (4.8) explains why a low CO_2 "flux" is still measured. However, this "flux", or better described as decomposition, is unstable and not suitable for long-term operation, because carbonate ions are not being replenished on the feed side due to the absence of CO_2. Therefore, the CO_2 release is finite and eventually all molten carbonate will decompose. A similar scenario was displayed in Chapter 3 where a finite amount of CO_2 was released *via* the formation $LiAlO_2$ and $LaAlO_3$ on the permeate-side surface. The instability in the membranes flux here is characterised by the lack of ability to reach stable flux after 100 hours. Based on the quantity of molten carbonate infiltrated into the membrane support (0.6 g), it is estimated that the membrane will have completely decomposed all of its carbonates after approximately 3700 hours of operation.

$$t = J_{CO_2} \times CO_{2_{carbonates}} \times A \tag{4.9}$$

where t is the time taken to decompose all the carbonates, J_{CO_2} is the average flux of CO_2, $CO_{2_{carbonates}}$ is the weight of CO_2 in the carbonates and A is the active permeation area.

Furthermore, without CO_2 in the feed gas together with the O_2, the dissolution of the Ag on the feed-side surface (Fig. 4. 7b) is similar to that of CO_2 alone (Fig. 4. 6b), resulting in no Ag pathways forming across the cross-section (Fig. 4. 7d). While Ag is known to react with O_2 *via* reactions (4.2) and (4.3), the absence of CO_2 does not allow Ag dissolution into the molten carbonate, instead Ag_2O is formed at the interface. Without, CO_2 the newly formed Ag_2O layer will stay at the feed-side surface. However, the Ag observed on the permeate side (Fig. 4. 7c) has likely migrated there *via* reaction with the CO_2 which is released from the feed side as a result of molten carbonate decomposition due to the reasons previously described.

Fig. 4. 6 and Fig. 4. 7 confirmed that feeding CO_2 or O_2 alone did not promote the reaction mechanism required to transport Ag throughout the membrane and create electron-conducting pathways, based on the hypothesis shown in Fig. 4. 1. Therefore, to test that a CO_2 and O_2 chemical driving force is required together, a further permeation experiment should be performed.

4.3.3 *Ag dissolution, migration and precipitation and its effect on gas flux for the Ag/Al₂O₃-MC membrane*

The same permeation experiment procedure was followed as for the aforementioned control experiments, albeit with 50 mol% CO_2, 25 mol% O_2 in N_2 in the feed-side inlet. Fig. 4. 8 shows that in the presence of an Ag-plated layer on the feed side of the membrane at the start of the experiment, a CO_2 and O_2 flux of 5.0 and 2.5×10^{-2} mL min^{-1} cm^{-2} is achieved (Fig. 4. 8a)

which is over an order of magnitude higher than the CO_2 flux for the membranes fed with CO_2 or O_2 alone. The 2:1 CO_2:O_2 ratio conforms with wholly Ag-supported dual-phase membranes reported in the literature and more generally with the stoichiometry of reaction (4.1). The fluxes from the Ag-plated membrane showed a factor of five improvement when compared to a non-Ag-plated Al_2O_3-MC membrane (1.0 and 0.5×10^{-2} mL min^{-1} cm^{-2} for CO_2 and O_2 respectively) (Fig. 4. 8b).
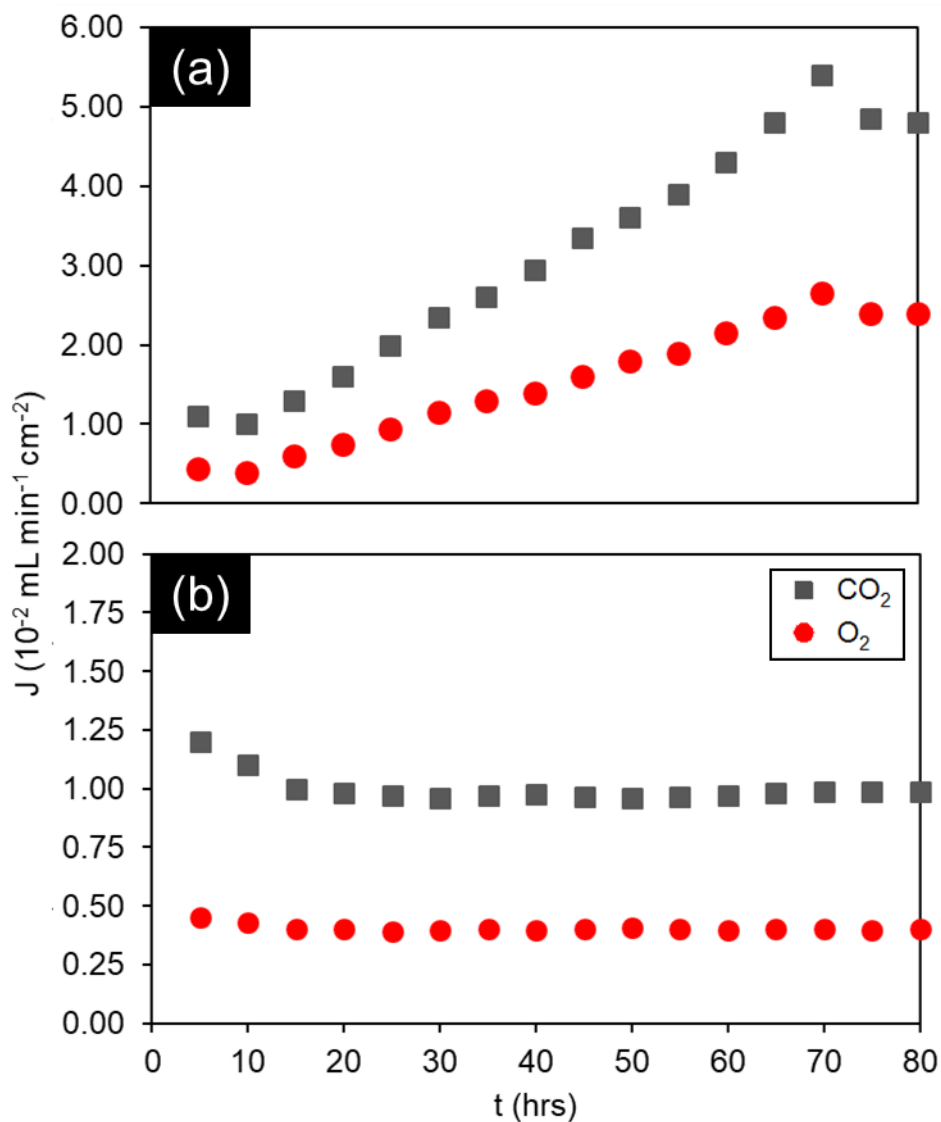
Fig. 4. 8 CO_2 and O_2 flux evolution with time at 650°C for (a) Ag/Al_2O_3-MC membrane and (b) Al_2O_3-MC membrane. Feed-side inlet: 50 mol% CO_2, 25 mol% O_2 in N_2. Permeate-side inlet: Ar.

Fig. 4. 8b shows that the non-Ag-plated Al_2O_3-MC membrane had a flux an order of magnitude higher than the same membranes fed with either CO_2 or O_2 alone and also had a 2:1 CO_2:O_2 ratio, similar to that of an electron-conducting support. This O_2 co-permeation does not agree with the mechanisms described in Fig. 1.2a as an inert support material cannot donate an

electron to promote reaction (4.1). Since there was no measurable leak during the experiment (< 10 ppm), the results indicate that either the interaction between the melt and a feed gas containing CO_2 and O_2 together is not understood, or another component of the dual-phase membrane is contributing to gas flux. This will be discussed in detail in Chapter 5 (section 5.3.4). Furthermore, aside from the notable flux improvement Ag addition offers compared to the non-Ag-plated Al_2O_3-MC membrane, the transient flux regions were also notably different. The Ag/Al_2O_3-MC membrane took 75 hours to reach stable flux compared to the 20 hours required for the Al_2O_3-MC membrane. This disparity in the transient behaviour is likely linked to Ag dissolution on the feed side and redistribution throughout the membrane, investigated in detail in Chapter 5.

After 80 hours of operation, the permeation experiment was stopped by rapidly cooling the membrane to room temperature under permeating conditions (Feed-side inlet: 50 mol% CO_2, 25 mol% O_2 in N_2. Permeate-side inlet: Ar). Upon post-experiment characterisation of the used Ag/Al_2O_3-MC membrane, it was clear that the plated Ag layer on the feed side had been dissolved to a significant extent (compare Fig. 4. 9a and Fig. 4. 9c), with Ag appearing to have migrated to the permeate side (compare Fig. 4. 9b and Fig. 4. 9d), confirmed by EDX (Fig. 4. 9e, f). Thus, confirming the first three stages of the proposed mechanism for electron-conducting pathway growth; Ag dissolution, migration and precipitation.
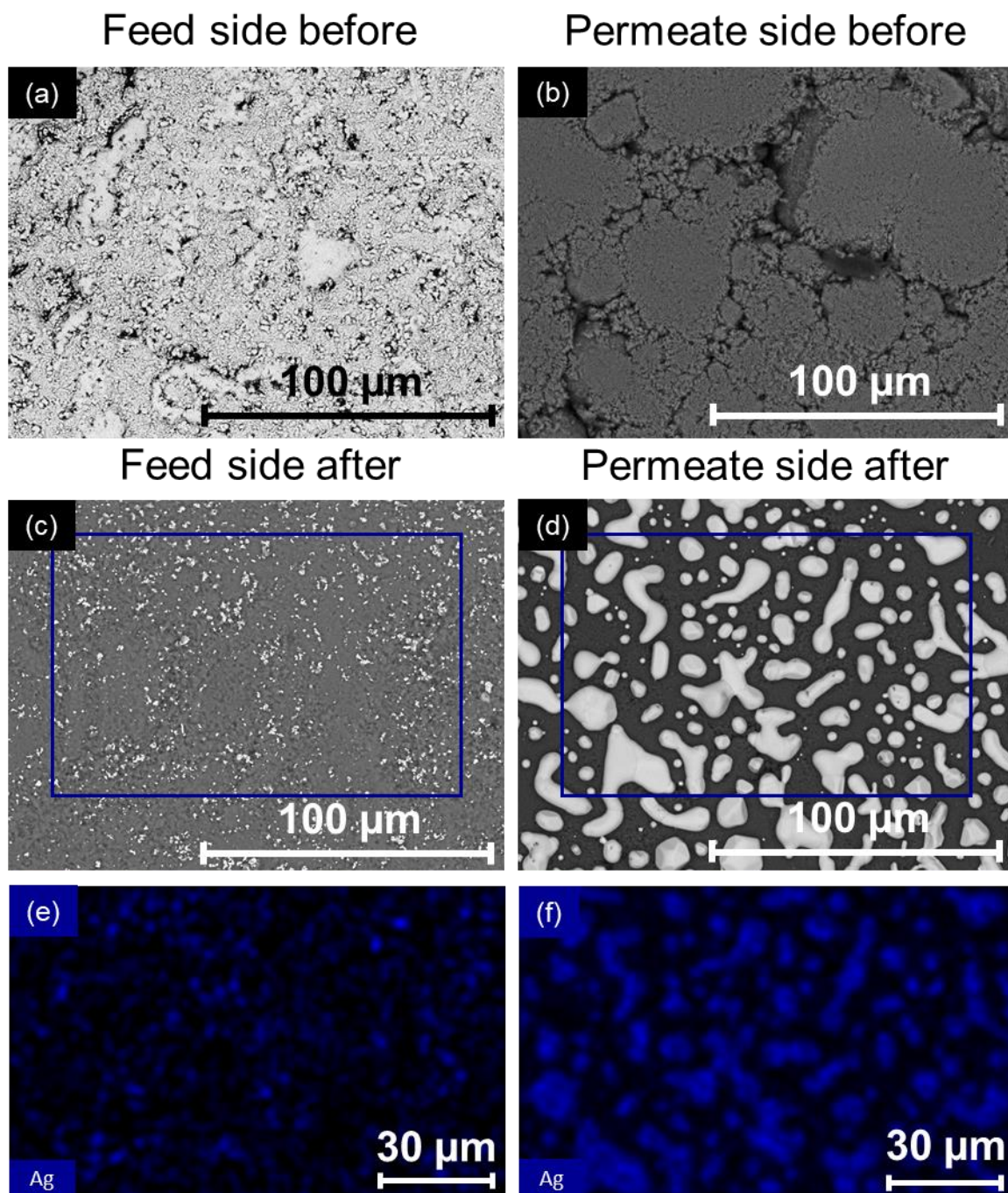
Fig. 4. 9 (a and b) SEM images of the feed and permeate side of an Ag/Al$_2$O$_3$-MC membrane support prior to permeation testing (c and d) SEM images of the feed and permeate side of a tested Ag/Al$_2$O$_3$-MC membrane fed with 50 mol% CO$_2$ and 25 mol% O$_2$ at 650°C; (e and f) EDX mapping of Ag from inside the blue box shown in (c and d).

To ensure that the migrated Ag found on the permeate side (Fig. 4. 9d) was linked to CO$_2$ and O$_2$ transport, a further permeation experiment was conducted where the CO$_2$ and O$_2$ driving force for gas separation was nullified. This was achieved by removing the pure Ar from the permeate-side inlet and introducing the same gas as the feed-side inlet. This created a symmetrical gaseous atmosphere across the membrane, *i.e.* no driving force for permeation.

The tested membrane was then analysed using SEM to understand the Ag dissolution and migration processes (Fig. 4. 10a-b).
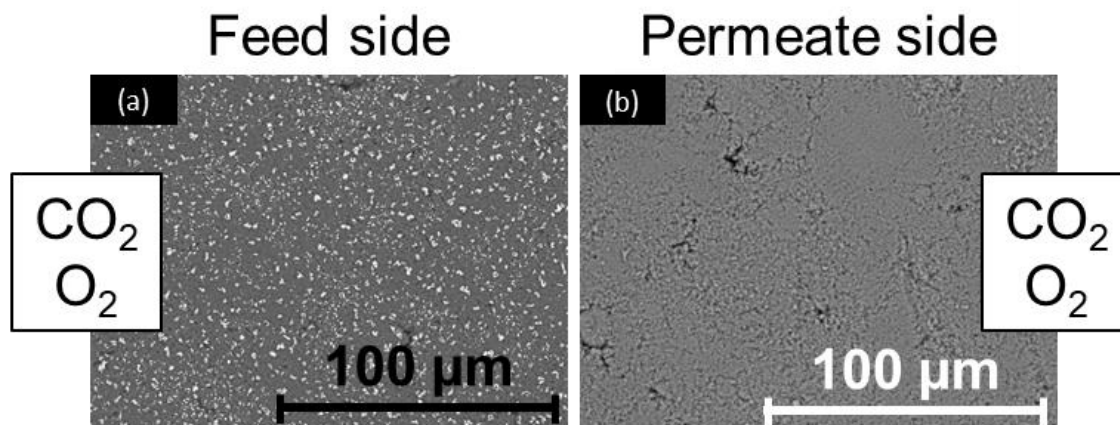
Fig. 4. 10 SEM images of the (a) feed side and (b) permeate side of tested Ag/Al$_2$O$_3$-MC membranes exposed to a symmetrical feed and permeate-side inlet gas regime at 650°C. Feed- and permeate-side inlet: 50 mol% CO$_2$, 25 mol% O$_2$ in N$_2$.

It was found that without a chemical potential gradient for CO$_2$ and O$_2$ separation, Ag was not detected on the permeate side using SEM. This indicated that a chemical gradient was required for Ag migration and was not simply a result of physical migration as a result of *e.g.* gravity or capillarity. Interestingly, the Ag on the feed side still dissolved. This Ag dissolution was due to reaction (4.1) occurring at the triple-phase boundary between the Ag-plated surface, molten carbonate and the CO$_2$ and O$_2$ gas and appeared to be independent of chemical gradient across the membrane. If, like Fig. 4. 6 and Fig. 4. 7, the feed-side inlet gas is modified to remove either CO$_2$ or O$_2$ or both, the rate of Ag dissolution would be greatly reduced.

While the Ag/Al$_2$O$_3$-MC membrane presented a 550% improvement when compared to an non-Ag-plated Al$_2$O$_3$-MC membrane, the flux was still an order of magnitude lower than Ag-supported membranes in the literature [57], [58], [60], [62]. A possible reason that could explain the low flux may be due to the membrane thickness and the tortuosity of the pore network. For the former, the thickness used in this study is thicker than any other Ag support reported in the literature (1.75 mm). The effects of membrane thickness on gas flux is well understood. Anderson and Lin reported that they were able to increase the gas flux of an LSCF dual-phase membrane by over 200% by decreasing the thickness from 3 mm to 0.75 mm [41]. Furthermore, the simplistic pressed-pellet fabrication method used here results in randomly packed pores which creates a highly tortuous gas transport pathway, which is known to hinder flux [81]. Therefore, Chapter 5 will look at the affect these parameters have on the gas flux for this membrane system.

4.3.4 *Evidence of Ag dendritic pathway growth in the Ag/Al₂O₃-MC membrane*

The experiments conducted so far have shown that CO_2 and O_2 are required together to achieve higher fluxes and to dissolve a significant amount of the Ag-plated layer to efficiently redistribute the Ag. However, while the Ag dissolution, migration and precipitation stages of the electron-conducting pathway growth mechanism have been demonstrated, the ability to form a connected electron-conducting pathway has not. However, the existence of the electron-conducting pathways are implied by the results shown in Fig. 4. 8 and Fig. 4. 9. For example, if the proposed mechanism was incorrect and instead all the plated Ag dissolved and migrated with no growth, then the flux improvement would not be sustainable. Without the growth stage the membrane would eventually block due to a build-up from Ag continuously migrating to the permeate side of the membrane until no Ag is left on the feed side, at which point a drop in CO_2 flux would occur. The growth stage is vital to provide connected electron-conducting pathways across the membrane for high and stable flux, observed in Fig. 4. 8a. Furthermore, post-experimental analysis using Fig. 4. 9d revealed that only ~3% of the 17mg of Ag initially deposited on the feed side had migrated to the permeate side. This calculation was achieved using (4.6) where V_s was calculated *via* surface area mapping of the Ag particles on the permeate side using ImageJ, combined with permeate-side surface cross-section SEM analysis to determine average Ag particle thickness (Fig. 4. 11).
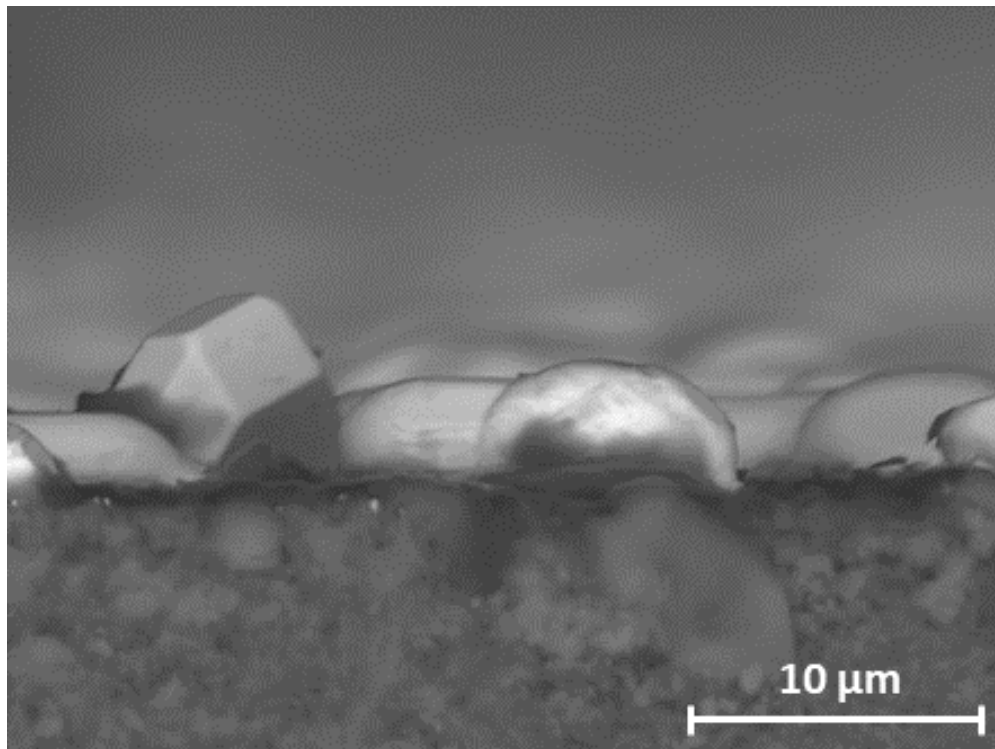
Fig. 4. 11 SEM image with a cross-sectional view of the permeate-side surface of a tested Ag/Al₂O₃-MC membrane fed with 50 mol% CO_2 and 25 mol% O_2 at 650°C.

To investigate where the remaining 97% of Ag resides and to test the hypothesis of the growth of Ag electron-conducting pathways, cross-section analysis was performed. To look inside the tested Ag/Al_2O_3-MC membranes, the resin technique described in section 4.2.5 was used. The cross-sections were then analysed using a digital microscope and SEM (Fig. 4. 12). The digital microscope image of the cross-section shown in Fig. 4. 12a revealed multiple branched Ag structures stemming from the permeate side, appearing to take the form of dendrites. Under greater magnification using a digital microscope (Fig. 4. 12b-c) the Ag structures, while easily visible to the naked eye, appeared distorted and faded under a higher magnification. This is due to a large portion of the Ag dendrite residing below the surface from which the cross-section cut was made. This is reasonable to assume given the random tortuous nature of the pores, which is attributed to the support fabrication process. Therefore, when the same cross-section was analysed using SEM-EDX, only a series of disjointed fragments could be detected (Fig. 4. 12d-e) due to SEM having a penetration depth of ~1 µm [122]. Elemental analysis of one of the "fragments" confirmed them to be Ag (Fig. 4. 13).
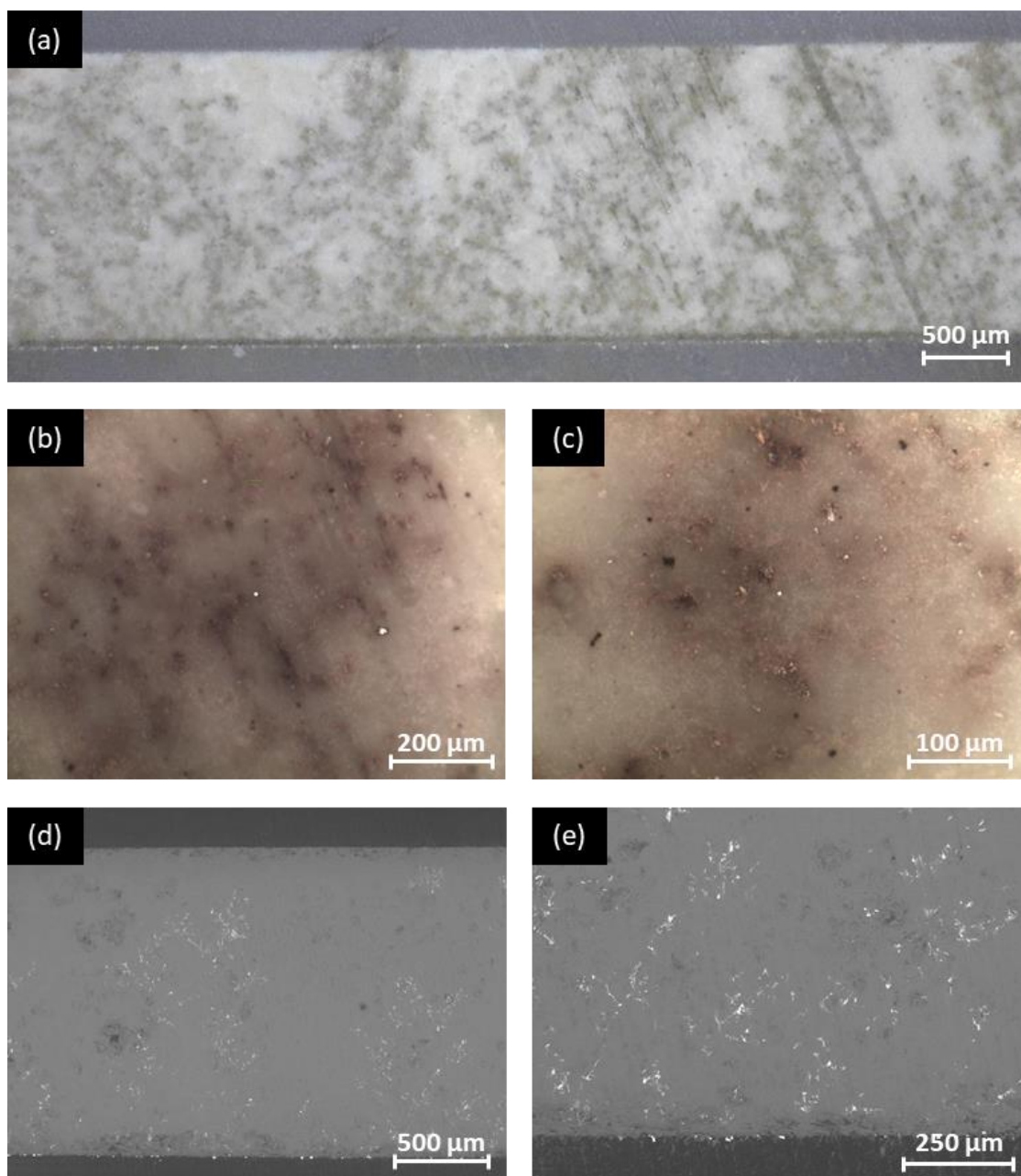
Fig. 4. 12 Optical microscope (a-c), and SEM (d-e), images of the cross-section of a tested Ag/Al$_2$O$_3$-MC membrane fed with 50 mol% CO$_2$ and 25 mol% O$_2$ at 650°C. Orientation of images: Feed side is top, permeate side is bottom.
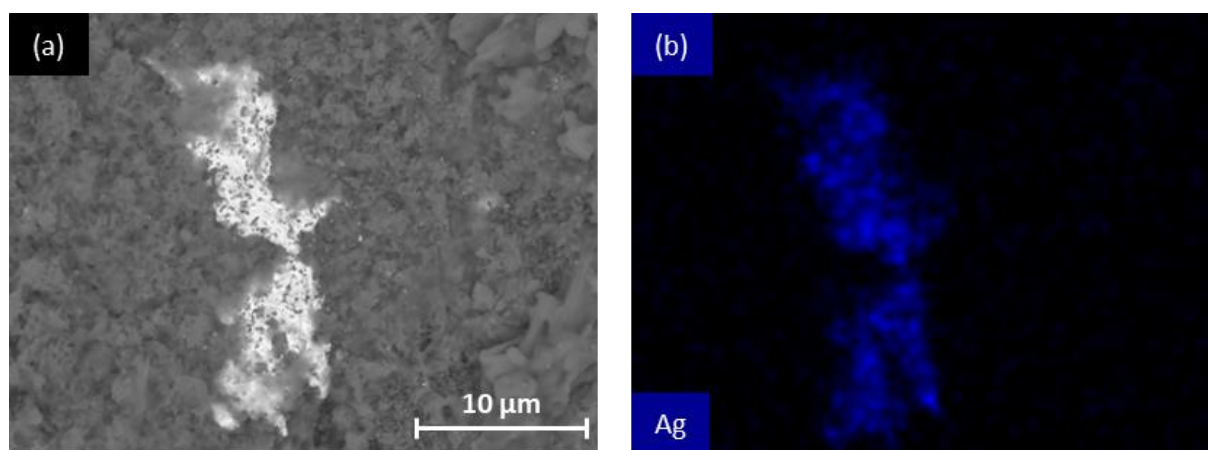
Fig. 4. 13 SEM (a) and EDX (b) images of a fragment of an Ag dendrite in a tested Ag/Al$_2$O$_3$-MC membrane fed with 50 mol% CO$_2$ and 25 mol% O$_2$ at 650°C.

While the branch-like Ag structures were visible to the naked eye and appeared to have a structure similar to Ag dendrites found in the literature, the digital microscope and SEM images were unable to reliably confirm that these pathways were connected. To test this, two further characterisation techniques were performed; (1) micro-CT and (2) two-point DC resistance measurements. For the former, micro CT was used to create a 3D reconstruction of the internal structure of the Ag/Al$_2$O$_3$-MC membrane after 80 hours of operation (Fig. 4. 14). The 3D reconstructions showed that following permeation, the Ag layer had dissolved and migrated to the permeate side, in agreement with SEM (Fig. 4. 9c-d) and had formed Ag pathways from the feed side to the permeate side of the membrane. The CT data from the tested membrane also showed that Ag pathways were only present within the central ~7 mm diameter of the permeate side of the membrane. Although molten carbonate will be present throughout the entire 20mm diameter Al$_2$O$_3$ pellet, the active permeate-side area was ~7mm in diameter, indicating that the migration of Ag was driven by gas permeation. However, while micro-CT helped to confirm the presence and location of the Ag pathways within the dual-phase membrane, due to the resolution of the instrument (> 10.5 µm), it could not be confirmed that the Ag had formed a connected conductive pathway. To achieve this, the same membrane was tested using two-point DC resistance measuring. It was found that the visible pathways endowed electronic conductivity to the insulating Al$_2$O$_3$ support (Fig. 4. 15). The conductivity of the self-forming Ag pathways is elaborated upon in Chapter 5 (see section 5.3.2).
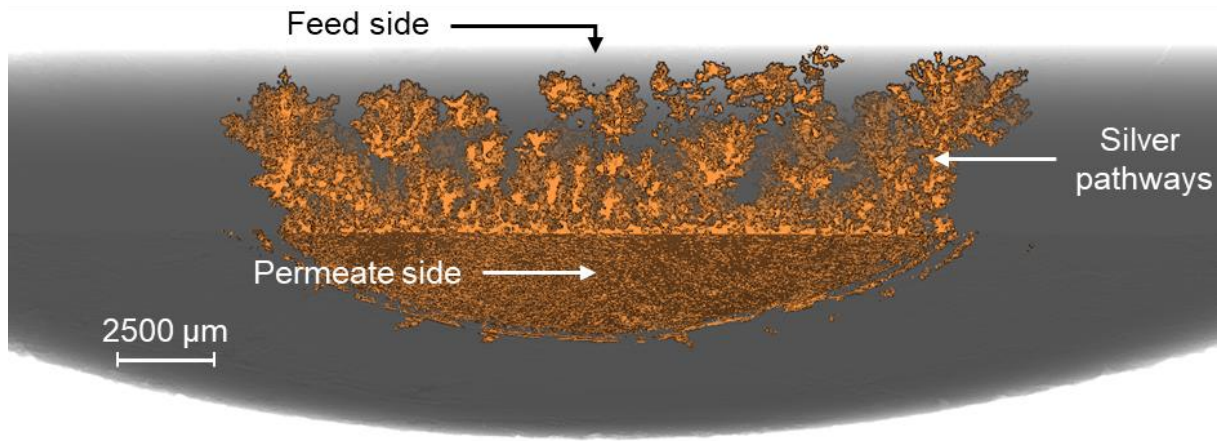
Fig. 4. 14 Micro-CT 3D reconstruction of the cross-section and permeate side of the Ag dendritic pathways in a tested Ag/Al_2O_3-MC membrane fed with CO_2 and O_2 at 650°C.
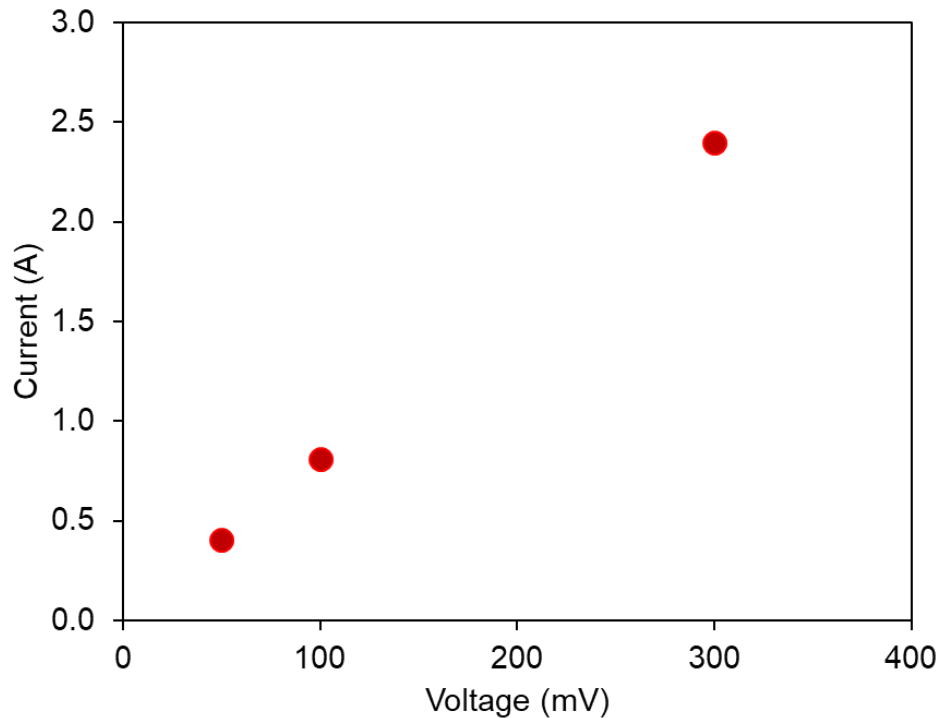
Fig. 4. 15 Current from two-point DC resistance measurements for a tested Ag/Al_2O_3-MC dual-phase membrane from seed-side to permeate side. The membrane was fed with 50 mol% CO_2 and 25 mol% O_2 at 650°C.

The results from micro-CT and two-point DC confirmed the remaining "growth" stage from the hypothesis for electron-conducting pathway growth. However, the order in which each stage occurs is unclear. It would be reasonable to assume Ag dissolution comes first, as without this the Ag cannot redistribute throughout the membrane. The next stage is not clear from the experiments conducted in this study. Based on the results it can be deduced that the stage following Ag dissolution can follow one of two paths. Either the dissolved Ag migrates to the permeate side and then extends back towards the feed side, which would be in line with the

hypothesis, or the pathways grow from the feed side until the dendrite reaches the permeate-side surface.

Furthermore, while the formation of Ag electron-conducting dendrites are the cause for the CO_2 and O_2 flux improvement shown in Fig. 4. 8, the flux is still an order of magnitude lower than other wholly Ag-supported dual-phase membranes in the literature. Another possible reasons for this gap could be due to the amount of Ag used. In this study, a fixed amount of ~17 mg was plated onto each membranes surface; however, it was unknown what the optimal amount of Ag required is. It is possible the quantity of Ag is too low and thicker and more numerous dendrites are required to achieve the optimal electron-conduction for comparable fluxes to wholly Ag-supported membranes. Alternatively, the amount of Ag could be too high and the pores may be becoming blocked. Therefore, the effect the amount of Ag added to the dual-phase membrane has on flux should be tested to identify the highest flux is achievable for the given membrane geometry.

4.4   Conclusion

This work presented in this chapter described the fabrication of a low-Ag content, electron-conducting membrane:

- The membrane was fabricated using an inert macroporous Al_2O_3 support with a thin porous Ag layer plated onto the feed-side surface.
- Permeation experiments showed that a CO_2 and O_2 chemical gradient was required to redistribute the Ag layer to form connected electron-conducting pathways across the membrane.
- The presence of these pathways produced a flux of 5.0 and 2.5×10^{-2} mL min^{-1} cm^{-2} for CO_2 and O_2 respectively, which is 500% improvement when compared to a non-Ag-plated Al_2O_3-MC membrane.
- However, this flux is an order of magnitude lower than the best Ag-supported membranes reported in the literature, thus further studies are required to understand how this flux can be improved.

The four hypothesized stages for dendritic growth were confirmed by post-experiment analysis:

- SEM-EDX analysis of the feed and permeate side of the tested Ag/Al_2O_3-MC membrane confirmed the complete dissolution of the Ag-plated layer followed by partial (~3 wt% of total Ag) migration and precipitation on the permeate side.
- The location of the remaining Ag and proof of the subsequent growth stage was confirmed by micro-CT, which unveiled numerous Ag pathways, connected from the feed to the permeate side of the membrane.
- Electron-conduction of the pathways was confirmed using two-point DC, which explains the improved gas flux.

While the four hypothesized stages have been confirmed and the dissolution and migration of the Ag layer is understood, the growth stage remains unexplained.

Chapter 5. Development of the self-forming silver membrane: structure, sealing and mechanisms

This Chapter presents results, which build upon the work conducted in Chapter 3 and 4. Here the mechanism for Ag pathway growth is discussed, and the effect of Ag loading, operation temperature and membrane geometry on the flux of the membrane is explored. Issues related to sealing of dual-phase membranes is also explored. Much of the work presented here is used in the publication accepted by *Energy & Environmental Science* titled "Dendritic Ag self-assembly in molten-carbonate membranes for efficient CO_2 capture" with the remainder in preparation for an article entitled "Influence of sealing materials on gas flux for dual-phase membranes" to be submitted to *Journal of Membrane Science*.

5.1 Introduction

Chapter 4 demonstrated how precipitation of a dopant in the molten carbonate phase of a dual-phase membrane could be used advantageously to add electron conduction to an inert support. However, while the self-forming Ag pathways increased the CO_2 and O_2 flux when compared to an non-Ag-plated Al_2O_3-MC membrane, the flux was an order of magnitude lower than other wholly Ag-supported dual-phase membranes reported in the literature. The difference in flux is likely linked to the membranes electron conductivity as a result of the amount of Ag added prior to operation.

Due to the nature of the plating process, modification of the amount of Ag plated onto the surface is technically difficult. The mass of Ag added to the surface is limited by the total volume of palladium seeds coated onto the surface during sensitisation/ activation (see section 4.2.1). However, if too many seeding, and subsequent plating cycles are used, the membrane would lose its porosity due to Ag build-up which would restrict carbonate infiltration. Therefore, a new method of Ag introduction is required to test higher (and lower) amounts of Ag addition. Since it is now known that Ag migrates due to its dissolution on the feed side during permeation, the same dendrite growth process should be achievable using Ag powder doped into the carbonate mixture before infiltration. If an Ag powder with a particle size larger than the 200 nm pores is used, a layer of Ag will be left on the surface of the feed side after infiltration due to the low solubility limit of Ag in molten carbonates. This layer would then undergo the same corrosion procedure shown with the electroless plated layer. This method of Ag introduction would remove the requirement for costly palladium and hazardous hydrochloric acid and hydrazine, which are used in the electroless plating procedure. Furthermore, the synthesis time would be significantly reduced, all important considerations for future scale-up.

While the reasons for fabricating a low-Ag content dual-phase membrane makes sense from a flux and cost perspective, there are however drawbacks for Ag-supported membranes that the Ag/Al_2O_3-MC membrane must overcome to demonstrate its worth. For example, Ag membranes have stability issues related to retaining carbonates within the porous network at temperatures exceeding 650°C [60]. This is due to poor wetting of carbonates on Ag (contact angle $63° \pm 2°$ [80]) and, sintering of porous Ag supports at high temperature resulting in a reduction of porosity and loss of carbonate. An attempt was made to decrease Ag sintering by coating the surface with a refractory ZrO_2 layer [62]. This membrane demonstrated that it was able to operate at temperatures up to 850°C. However, the longest experiment was a 40-hour test at 800°C which still saw a 20% flux decline during this period, thus the stability of the

membrane at elevated temperatures when using this surface modification method remains to be seen.

As well as leaks from carbonate retention issues, dual-phase membranes also suffer from leaks as a result of sealant breaks due to the high temperatures used. In an industrial application a compact geometry with no hot-sealing region will be used, such as hollow fibres [48], [123]. However, it is common that a pellet membrane geometry is used for initial lab-scale testing of a new support material, which requires a hot-sealing region. Therefore, it is important to select a sealant that can withstand the harsh conditions of a dual-phase membrane system. The sealant used in Chapter 4 was Au ink, which has only been used once previously [92], likely due to its high cost. Furthermore, the highest temperature investigated in that study was 450°C. Therefore, the 650°C operating temperature reported in Chapter 4 constitutes the highest operating temperature used with an Au ink sealant. Thus, it is unclear how this sealant will respond when testing the Ag/Al_2O_3-MC membranes stability beyond this temperature. One such sealant that could be used in place of Au and has been used widely in the dual-phase membrane literature is Ag ink [40], [47], [49], [54], [56], [58], [59], [62], [69], [124]. This sealant has demonstrated its ability to withstand temperatures up to 850°C for the self-forming NiO membrane and has also shown it can maintain a seal for 900 hours at 600°C when used in the aforementioned dealloyed Ag membrane system. In addition, it is important to understand the interaction between the sealant and the molten carbonate during permeation.

The CT work conducted in Chapter 4 displayed the presence of dendritic Ag pathways inside a tested Ag/Al_2O_3-MC membrane. However, the image was constructed after operation and provided no context for how the Ag pathways grow during permeation. Furthermore, the CT images were unable to discern where the Ag resides within a single pore due to the size of the pores being below the voxel dimensions of the CT. The membrane support presented in Chapter 3, which contains 150 µm diameter, 500 µm long, straight, unrestricted pores, would provide an ideal support to visualise the Ag pathways within a pore. Furthermore, this membrane geometry would help to explore the effect membrane thickness and pore tortuosity has on CO_2 and O_2 flux, something that was briefly discussed in Chapter 4.

These topics outline the steps required to gain a greater understanding of the Ag/Al_2O_3-MC membrane. In this chapter, four different dual-phase membrane system parameters were modified:

1. *Ag loading* – The amount of Ag loading into the molten carbonate was modified using a less complicated method of Ag doping and the respective fluxes of each loading was compared.

2. *Operation temperature* – The membranes ability to operate at temperatures exceeding 650°C was tested.

3. *Sealant* – The membranes stability was tested using two different membrane sealants.

4. *Geometry* – The effect modifying the geometry has on flux was explored using the support presented in Chapter 3.

In addition, a study was conducted to explain how the Ag pathways grow during permeation and where the pathways reside within a single pore using Micro-CT.

5.2   Experimental

5.2.1   Al$_2$O$_3$ support preparation

Two membrane supports were used for the study; pressed-pellet and parallel pore. The preparation procedures for each support are described in section *2.1.1*.

5.2.2   *Method of Ag introduction and molten carbonate preparation*

Ag was introduced into the Ag/Al$_2$O$_3$ membrane *via* two different methods. The first method, which was used explicitly for the pressed-pellet support, introduced Ag *via* dry impregnation. Based on the porosity of the Al$_2$O$_3$ pressed-pellet support, 0.3 mL of 1.25×10^{-5} M AgNO$_3$ solution was added dropwise into the support and dried for 12 hours at 100°C to remove the water, to leave AgNO$_3$ particles. The support was then placed in a furnace and heated in air to 600°C at a rate of 1°C min^{-1} and held for 3 hours to decompose the nitrate to form finely dispersed nanoscale metallic Ag particles throughout the internal and external surfaces of the Al$_2$O$_3$ support. The support was then cooled at 1°C min^{-1} in Ar to ensure the Ag was in its metallic form.

The second method introduced Ag into the Ag/Al$_2$O$_3$ membrane *via* directly doping the ternary eutectic carbonate powder with Ag powder (Alfa Aesar, -100 mesh (<150 µm), 99.95% metals basis). Five mixtures were made with different amounts of Ag doped into the pre-prepared ternary carbonate eutectic: 0.25, 1.5, 3, 6 and 10 mol%.

5.2.3   *Permeation measurements*

For permeation tests the parallel pore membrane reactor (Fig. 2. 3) and the pressed pellet membrane reactor (Fig. 2. 2) were used for their respective supports. One feed-side inlet gas was used in this study:

1. 50 mol% CO$_2$, 25 mol% O$_2$ in N$_2$

One permeate-side inlet gas was used in this study:

1. 100 mol% Ar

Reactor temperatures used in this study range between 650-750°C depending on the experiment. For the time-resolved mechanistic study, experiments were stopped after different lengths of operation during permeation – up to and including stable flux. The experiments were stopped by rapid cooling of the membranes under permeating conditions to quench the membrane for post-experimental analysis.

5.2.4 *Dual-phase membrane characterisation*

Observation of the Ag nano-particle distribution on the Al_2O_3 pressed-pellet support using dry impregnation was performed using SEM. Sample preparation was performed using the same procedure described in section 4.2.5 and scanning was performed using the same procedure as described in section 3.2.4.

Micro computed tomography was performed using a Zeiss Xradia 520 Versa (Carl Zeiss X-ray Microscopy, Pleasanton, USA) and a Nikon XT H 225 (Nikon Metrology UK Ltd, Tring, UK). The scanning procedure for the Nikon XT H 225 was described in section 4.2.5[8]. The scan performed on the Zeiss Xradia 520 Versa was conducted at an optical magnificent of 4x, which combined with geometrical magnification and binning 1 gave a voxel dimension of 0.897 µm, at a voltage and power of 80 kV and 7W, respectively. The exposure time used for this scan was 15 s, to give average counts above 5000 and the number of projections was 2201. This technique was used to was used to observe the Ag distribution throughout the internals of both dual-phase membrane supports used in this study at various stages of electron-conducting pathway growth.

Two-point DC technique was used to measure the electrical conductivity of membranes at various stages of electron-conducting pathway growth[9]. The same conductivity measurements described in section 4.2.5 was carried out for each membrane.

---

[8] Experiments were performed by Dr. Francesco Iacoviello from UCL, images were constructed by Dr. Josh Bailey from UCL and data was interpreted by Liam McNeil.

[9] Experiments were performed by Dr. Evangelos Papaioannou and Dr Gaurav Gupta from Newcastle University and data was interpreted by Liam McNeil.

5.3 Results & Discussion

5.3.1 Impact of the amount of Ag addition and temperature on permeation flux

To test the generality of the Ag addition approach and reduce the complexity of the synthesis procedure, Ag powder was mixed with the carbonate powder before infiltration into the porous Al_2O_3 support. The amount of Ag added was varied between 0 and 10 mol%, to determine its effect on CO_2 and O_2 flux at 650°C (Fig. 5. 1).
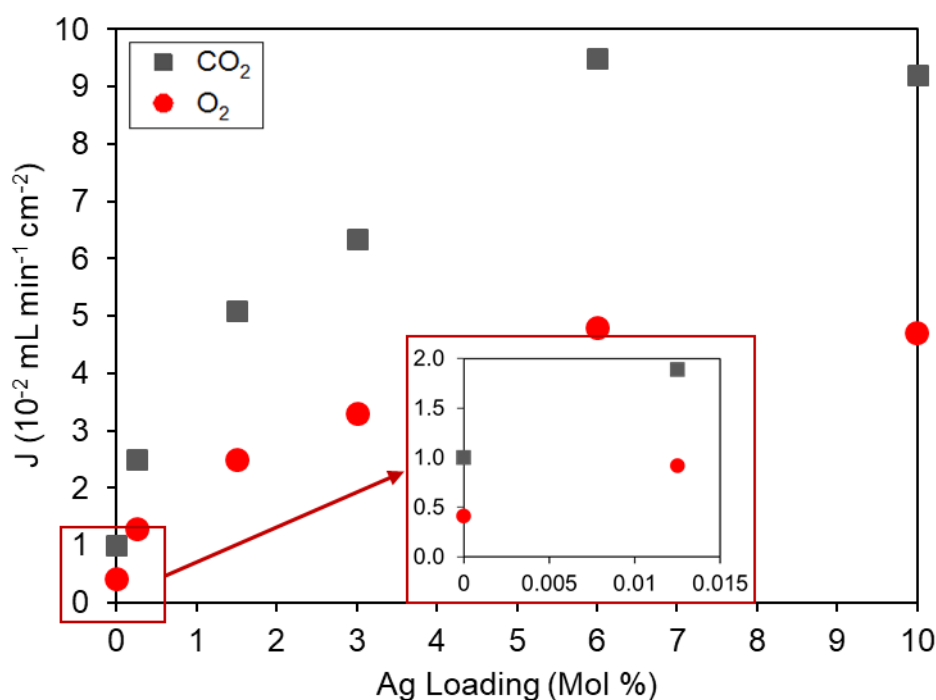
Fig. 5. 1 Stable CO_2 and O_2 flux as a function of Ag loading in the carbonate at 650°C. Feed-side inlet: 50 mol% CO_2, 25 mol% O_2 in N_2. Permeate-side inlet: Ar.

For each Ag loading experiment, it was ensured that the membranes achieved stable flux for 4 hours before stopping the experiment and quenching the membrane. The mean flux ($\bar{J}$) value over that 4-hour period was taken as the reported flux (as displayed by the data point markers in Fig. 5. 1). The flux evolutions prior to the stable region for each Ag loaded membrane are compared and discussed in detail in the next subsection (see section 5.3.2). The standard deviation (σ) of the data in the stable flux region was calculated and reported with $\bar{J}$ in Table 5. 1. The data used for the stable flux period and the calculations performed to achieve $\bar{J}$ and σ are presented in the appendix (see section A. 3). Due to the stability of the flux in the stable flux region and the minimal noise from the FT-IR and the mass spectrometer used, the σ is smaller than the data point markers in Fig. 5. 1, thus no error bars where added to the figure.

Table 5. 1 CO_2 and O_2 mean (μ) flux and standard deviation (σ) in stable flux region.

Ag loading (mol%)	$\bar{J}$ CO_2 flux (mL min^{-1} cm^{-2})	σ (mL min^{-1} cm^{-2})	$\bar{J}$ O_2 flux (mL min^{-1} cm^{-2})	σ (mL min^{-1} cm^{-2})
0	1.0×10^{-2}	6.4×10^{-5}	0.4×10^{-2}	1.3×10^{-3}
0.0125	1.9×10^{-2}	1.7×10^{-4}	0.9×10^{-2}	1.8×10^{-3}
0.25	2.4×10^{-2}	7.0×10^{-5}	1.3×10^{-2}	6.7×10^{-4}
1.5	4.6×10^{-2}	8.3×10^{-4}	2.4×10^{-2}	2.4×10^{-3}
2.5 *	5.0×10^{-2}	4.4×10^{-4}	2.5×10^{-2}	1.2×10^{-3}
3	6.3×10^{-2}	1.4×10^{-3}	3.3×10^{-2}	2.5×10^{-3}
6	9.5×10^{-2}	1.7×10^{-3}	4.8×10^{-2}	1.2×10^{-3}
10	9.0×10^{-2}	1.3×10^{-3}	4.6×10^{-2}	2.4×10^{-3}

* Electroless plated membrane from Chapter 4.

When 0.25 mol% Ag was loaded into the carbonates, a CO_2 and O_2 flux of 2.4 and 1.3×10^{-2} mL min^{-1} cm^{-2} respectively was achieved, which was more than double that displayed by the undoped ternary carbonate mixture (1.0 and 0.4×10^{-2} mL min^{-1} cm^{-2} for CO_2 and O_2 respectively). Flux increased with Ag loading, reaching a maximum of 9.5 and 4.8×10^{-2} mL min^{-1} cm^{-2} for CO_2 and O_2 respectively at 6 mol% Ag powder in the carbonate, before plateauing beyond this Ag loading. A reason for the plateau beyond this point could be a result of pores becoming blocked due to increased Ag loading, thus restricting gas transport. It is also important to note, that all Ag loaded membranes achieved a 2:1 CO_2:O_2 ratio which is in agreement with other electron-conducting membranes in the literature and the Ag-plated membrane presented in Chapter 4 using the same gas feed. The addition of Ag into the membrane is effective, not only due to the increased electrical conductivity the Ag provides, but also because the membrane requires little Ag to achieve the order of magnitude increase in flux achieved here. 6 mol% Ag equates to 1.25 vol% of the 55% porous Al_2O_3 structure. Therefore, only 3.8×10^{-3} cm^{-3} of molten carbonate is displaced by the addition of Ag, thus the presence of Ag has little effect of the volume of carbonate ions required for CO_2 transport.

Comparison of the flux for the electroless plated membrane from Chapter 4 with the powder-doped membranes showed that the plated membranes gas flux fits the same Ag loading trend. For the electroless plated membrane, a final Ag weight of 17 mg (2.5 mol%) was measured, providing a flux of 5.0 and 2.5×10^{-2} mL min^{-1} cm^{-2} for CO_2 and O_2 respectively at 650°C (see section 4.3.3). This measured flux is between the membranes doped with 1.5 and 3.0 mol% Ag using the powder doping method. This suggests that the method of Ag doping is not critical to the flux of a pressed pellet membrane used here. Therefore, this indicates that Ag powder should

be used instead of electroless plating for all future experiments as it is cheaper, quicker and less hazardous to fabricate an Ag powder-doped membrane and there is no identifiable difference in the outcome of the gas flux.

For all of the Ag loadings tested it would be reasonable to assume that Ag in the bulk of the membrane during permeation would be present as a solid, as the Ag loadings far exceeded the solubility limit of Ag in molten alkali carbonates at 650 °C (of the order of 0.01 mol% [110]). However, in all cases, a small amount of Ag would also be dissolved in the carbonates, and its effect on membrane flux could not be discriminated from that of Ag in the solid phase in the pathways. Therefore, by using dry impregnation technique 0.0125 mol% was added to the membrane, which is the same order of magnitude as the solubility limit of Ag in molten carbonate. The Ag was deposited on the feed-side surface in the form of nanoparticles as displayed in (Fig. 5. 2).
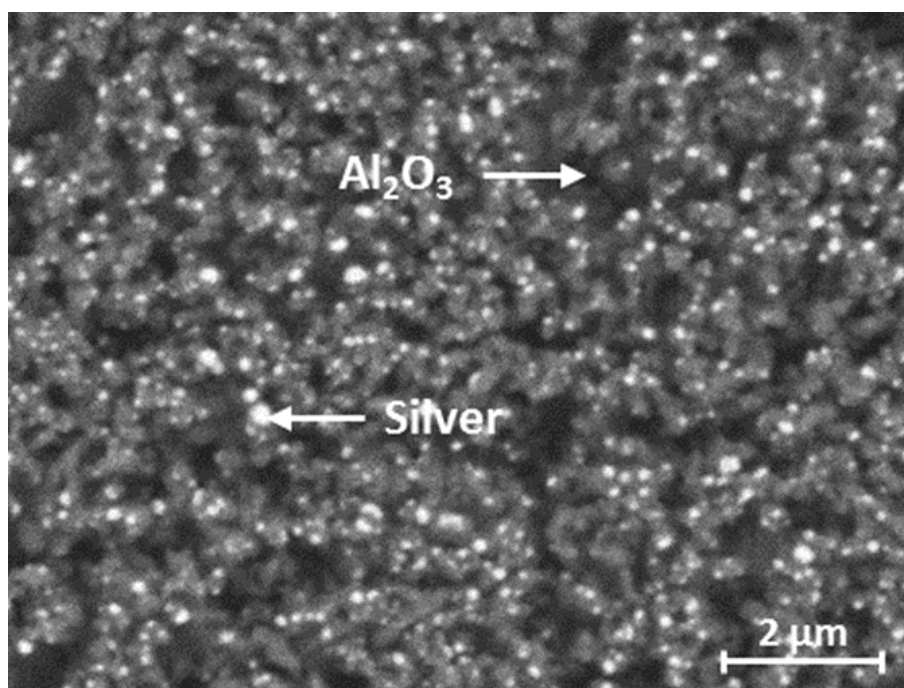
Fig. 5. 2 SEM image of the feed side of an untested Al_2O_3 support, impregnated with Ag nanoparticles.

The dry impregnated membrane showed that during permeation, dissolved Ag was still able to improve the CO_2 and O_2 flux by almost a factor of 2 when compared to an undoped Al_2O_3-MC membrane (1.90 and 0.92 × 10^{-2} mL min^{-1} cm^{-2} for CO_2 and O_2 respectively, as shown by the inset of (Fig. 5. 1)). This was a far smaller improvement in flux, but nonetheless existent, as compared to conditions under which solid Ag would be present (Fig. 5. 1), thus indicating that Ag is required as solid pathways for electron conduction to achieve appreciably higher fluxes.

5.3.2 Mechanism for dendritic Ag pathway formation

For each of the Ag loading experiments described previously, only the stable flux regions were reported. However, the transient behaviour leading up to this stable value can help to understand how the Ag pathways form. Fig. 5. 3 displays the full experimental flux data for an Al_2O_3-MC membrane with 6 mol% Ag doped into the molten carbonate (henceforth referred to as 6 mol% Ag/Al_2O_3-MC membrane), fed with 50 mol% CO_2, 25 mol% O_2 in N_2 at 650°C. Full experimental data for all other Ag-doped membranes displayed in Fig. 5. 1 can be found in the appendix (see section A. 4)
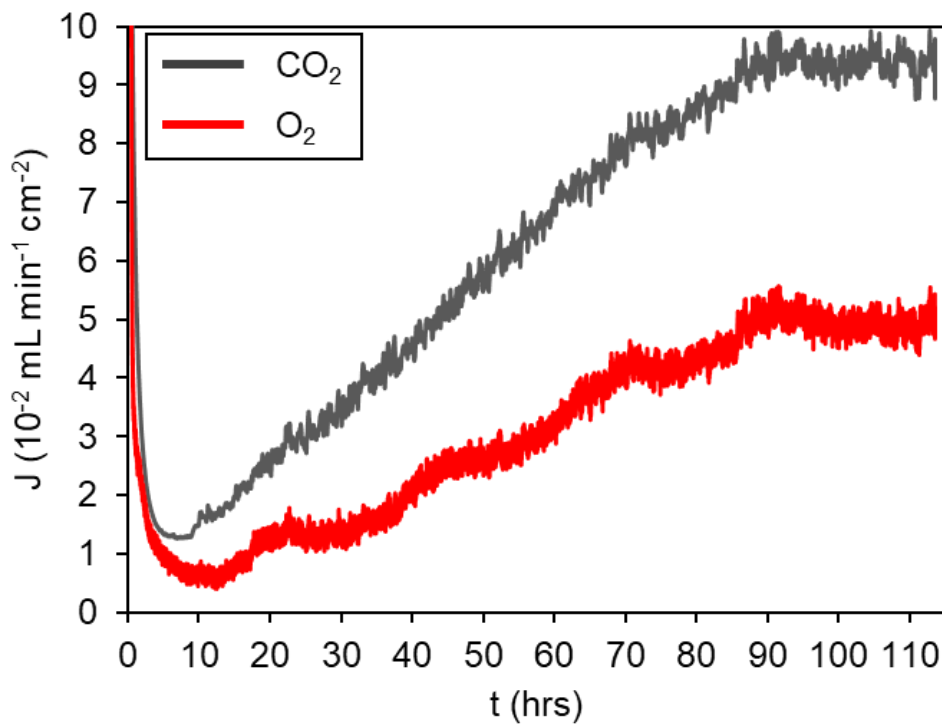
Fig. 5. 3 CO_2 and O_2 flux evolution for a 6 mol% Ag/Al_2O_3-MC membrane fed with 50 mol% CO_2, 25 mol% O_2 in N_2 at 650°C.

The transient behaviour is similar to that seen in Chapter 4 for the electroless plated membrane, where the membrane took 75 hours to stabilize after a consistent gradual increase in flux when being fed with the same gas mixture (see Fig. 4. 8). This again, highlights the similarity in performance for the powder-doped and electroless-plated membranes. In this instance, the 6 mol% Ag/Al_2O_3-MC membrane took 90 hours to achieve stability and remained stable for 24 hours before finishing the experiment and rapidly cooling the membrane. The gradual increase in CO_2 and O_2 flux up until 90 hours indicates that pathways are likely forming during this period, resulting in an increase in electron conduction and consequently, an increase in flux. Furthermore, Fig. 5. 3 shows that the CO_2 and O_2 flux maintained its 2:1 ratio throughout the experiment from 10 hours onwards, which could indicate that initial pathway growth is fast,

meaning that the start of the experiment (< 10 hours) should be targeted to understand pathway growth. However, it is possible that an external factor could also be contributing to this flux ratio which will be discussed in section 5.3.4.

To identify any trends in transient flux behaviour between different Ag-loaded membranes that could help to explain the mechanism for Ag pathway growth, five membranes, each loaded with varying amounts of Ag powder (0.0125 to 6 mol%) and fed with 50 mol% CO_2, 25 mol% O_2 in N_2 were compared (Fig. 5. 4). It can be broadly concluded that each loaded membrane experienced a similar transient behaviour before achieving their respective stable flux reported in Fig. 5. 1, *i.e.* the flux starts off low prior to 10 hours of operation and gradually increases before reaching a plateau (stable flux region).
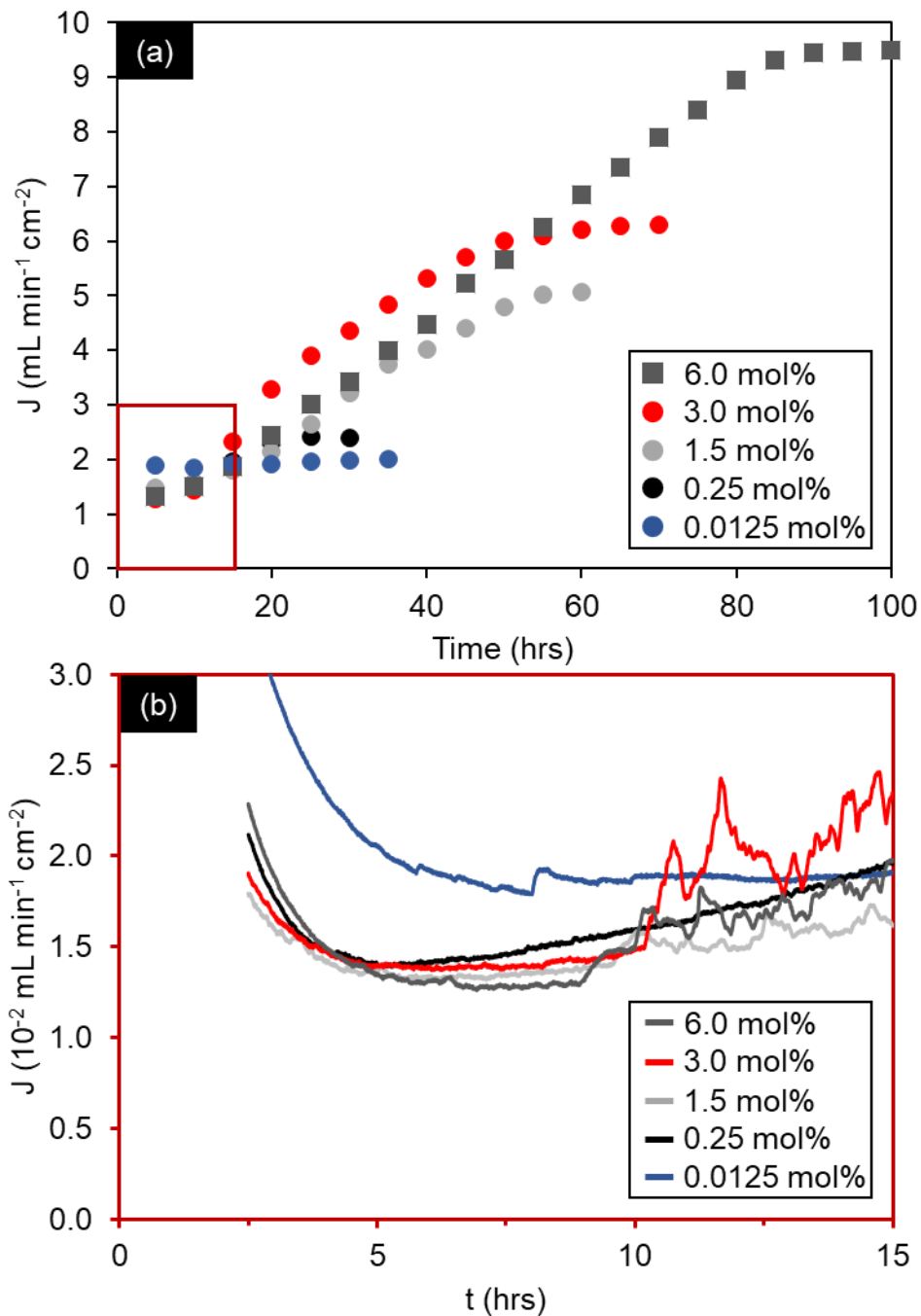
Fig. 5. 4 CO_2 flux evolution with time for each Ag loaded membrane (0.0125 – 6 mol%) at 650°C. (a) Full experiment, (b) first 15 hours. Feed-side inlet: 50 mol% CO_2, 25 mol% O_2 in N_2.

Fig. 5. 4 shows that the amount of Ag loaded into the membrane has an impact on the transient flux behaviour. More specifically, membranes loaded with more Ag took longer to achieve stable flux. The 6 mol% Ag/Al_2O_3-MC membrane took 90 hours to stabilise while the 0.25 mol% Ag/Al_2O_3-MC membrane took 25 hrs and the membrane with Ag below its solubility limit (0.0125 mol%) only took 7.5 hrs to stabilise. Furthermore, the amount of Ag loading impacts gas flux *i.e.* more Ag loading results in higher fluxes, which supports the conclusions

drawn from Fig. 5. 1, however due to the increase in Ag loading it takes longer for the membrane to achieve this higher flux. Based on the knowledge that these membranes form Ag pathways under a CO_2 and O_2 driving force (as shown in Chapter 4, Fig. 4. 14), it is reasonable to assume the difference between the flux stabilisation periods is due to the time required to redistribute the Ag. When more Ag is loaded into the membrane, the Ag takes longer to completely redistribute into Ag pathways, therefore the flux gradually increases for longer before reaching a plateau at a higher flux value. However, regardless of Ag loading, all Ag loaded membranes undergo a similar transient region prior to 10 hours of operation (see Fig. 5. 4b). In this region, all membranes experience an initial decline in flux prior to 5 hours of operation as the permeate-side chamber is cleared of 50 mol% CO_2, 25 mol% O_2 in N_2 used during heat-up (see section 2.1.3 for heat-up procedure). For the following 5 hours, the fluxes appear to be stable before increasing at ~10 hours. Following this, the membranes flux continues to increase before stabilising at a time and point dictated by the amount of Ag added. This indicates that dissolution of the Ag limits the process prior to 10 hours of operation, whereas beyond 10 hours of operation the CO_2 flux is limited by the amount of Ag loading.

Based on this transient flux behaviour routinely observed at the beginning of each permeation experiment (Fig. 5. 4b), it was postulated that Ag pathway growth occurred during this period, before high and stable permeation flux was observed. To investigate the Ag pathway growth process, five membranes, each loaded with the same Ag carbonate mixture (6 mol%), were fed with 50 mol% CO_2, 25 mol% O_2 in N_2 at 650°C. During permeation, each membrane was quenched at various time intervals up to and including stable flux (2, 6, 10, 20 and 115 hours). The quenched membranes were then analysed using micro-CT to examine pathway growth at their respective quenching points (Fig. 5. 5a-e). A CO_2 and O_2 flux evolution plot for the membrane operated for 115 hours was used as a guide to understand at which points during permeation the individual membranes were quenched (Fig. 5. 5f).
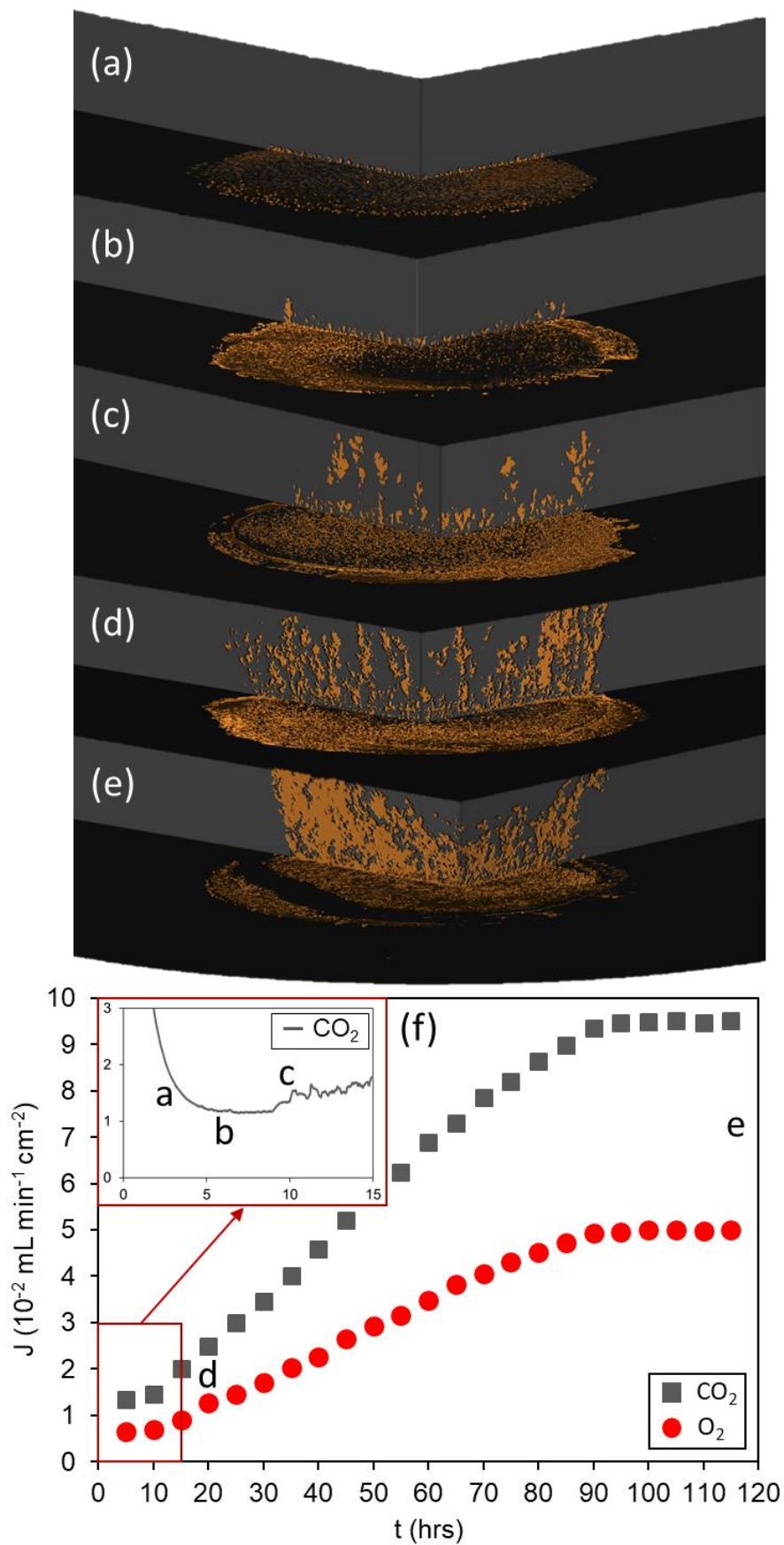
Fig. 5. 5 CT of the cross-section of five 6 mol% Ag/Al_2O_3 membranes stopped after; (a) 2 hours; (b) 6 hours; (c) 10 hours; (d) 20 hours; (e) 115 hours of operation. Their corresponding position during Ag pathway formation is marked on a representative CO_2 and O_2 flux plot (f) from the 115-hour sample at 650°C. Feed-side inlet: 50 mol% CO_2, 25 mol% O_2 in N_2.

The 6 mol% Ag/Al$_2$O$_3$-MC membranes quenched after 2, 6 and 10 hours of operation were scanned using micro-CT to investigate Ag pathway growth in the low flux period (Fig. 5. 5a-c). First, at 2 hours it can be seen that Ag has migrated to the permeate side, in agreement with SEM images (Fig. 4. 9d). After 6 hours, it can be seen that Ag pathways begin to grow back towards the feed side of the membrane, until they span the entire width of the membrane at around 10 hours. Up to this point, no electronically conductive path between feed and permeate side of the membrane has formed (as seen in Chapter 4, Fig. 4. 14 and Fig. 4. 15), restricting the flux to the low values observed during this period (see inset of Fig. 5. 5f and Fig. 5. 4b). From here, the pathways continue to grow, possibly both in thickness and in number (20 and 115 hours), offering increased electronic conductivity across the membrane and increasing the permeation of CO$_2$ and O$_2$ *via* reaction (5.5). At 90 hours of operation, all of the added Ag has now been dissolved and redistributed throughout the membrane, leading to flux stabilization beyond 90 hours. Fractal-like dendrites formed from precipitated Ag in molten salts under an electrochemical driving force have been shown to produce unique electronically-conductive composite materials with an ultra-low percolation threshold [125]–[127].

In this scenario, the dendrite is likely formed by Ag dissolution on the feed side *via* the reaction mechanism previously discussed in section 4.1, where O$_2$ reacts with the Ag to form Ag$_2$O followed by reaction with CO$_2$ to form CO$_3^{2-}$ and Ag$^+$. The anions and cations then move down their concentration gradient as a result of the CO$_2$ and O$_2$ concentration gradient applied across the membrane. Upon reaching the permeate-side surface, the CO$_3^{2-}$ releases CO$_2$ due to the low pCO$_2$ in the inert permeate-side gas. The resulting oxide ion released from the carbonate ion dissociation recombines with the Ag$^+$ to form Ag$_2$O, which subsequently releases O$_2$ due to its instability in an inert atmosphere at temperatures above 200°C [114], thus producing metallic Ag. This metallic Ag acts as a nucleation point for subsequent migrating Ag particles to deposit. This Ag deposition process occurs because Ag plating (or deposition) on an already plated (or deposited) particle is easier due to the ease of electron transfer between the Ag$^+$ and the Ag^0. Furthermore, the deposited Ag decreases the diffusional path length, which is favourable for a migrating Ag$^+$. As a result of continuous migration and deposition, the diffusional path length will continue to get shorter and thus, the Ag dendrite will start to grow back towards the feed-side surface until it spans the entire cross-section of the membrane. This is in-line with the findings, that small quantities of Ag can be used to produce a self-forming electronically conductive dendritic Ag membrane. The microstructural properties of the self-formed dendrites produced during permeation are displayed in Fig. 4. 14 and Fig. 5. 5c-e.

To understand how pathway growth affects the conductivity of the membrane and consequently the flux of the membrane, the same five permeation-tested and CT-scanned 6 mol% Ag/Al₂O₃-MC membranes were tested using two-point DC. A blank porous Al_2O_3 support was also tested and used as a reference (Fig. 5. 6).
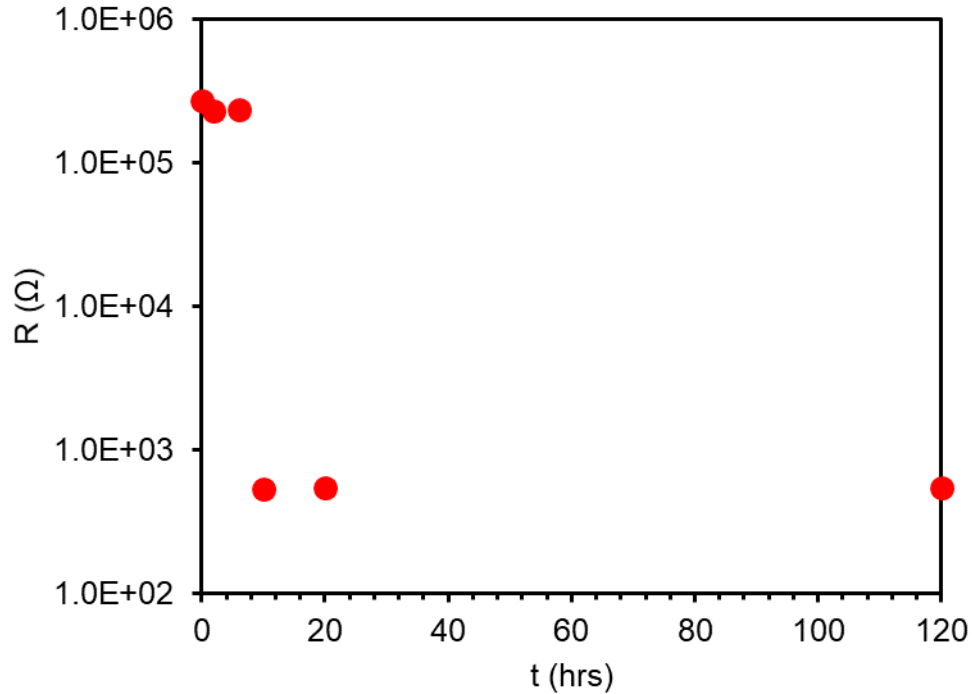
Fig. 5. 6 Resistance from two-point DC resistance measurements for the five tested Ag/Al₂O₃-MC dual-phase membranes stopped at different points during Ag pathway formation. The membranes were fed with 50 mol% CO_2 and 25 mol% O_2 at 650°C.

The membranes operated for less than 10 hours, including the blank Al_2O_3 support, had a resistance three orders of magnitude higher than the 3 membranes operated for 10 hours or longer. This indicates that the presence of the dendrites that form after 10 hours increased the conductivity of the membrane. This can also help to explain this increase in flux during this period. Using the data from Fig. 5. 6 the resistivity of the membrane can be calculated using equation (5.1):

$$\rho = R\frac{A}{l} \tag{5.1}$$

where A and l is the active permeate-side area (m²) and thickness (m) of the membrane, respectively and R is the resistance which is equal to (5.2):

$$R = \frac{V}{I} \tag{5.2}$$

where V and I are voltage (V) and current (A), respectively. The membranes operated for longer than 10 hours had a resistivity of 20 Ω m. This is 11 orders of magnitude lower than the

resistivity of Al_2O_3 (1.0×10^{12} Ω m) [128] and 9 orders of magnitude higher than the resistivity of Ag (1.6×10^{-8} Ω m) [128]. Thus, the membrane has a higher resistance compared to a dense wholly Ag sample, albeit far less than Al_2O_3. There are however limitations to this procedure that can cause these high resistivities. For instance, not all Ag pathways fully extend across the membrane as it is unclear where the molten carbonate resides within a single pore *i.e.* molten carbonate may reside beneath the surface and the Ag will only extend as far back as the molten carbonate. Therefore, contact between the Ag pathways the Ag electrode for two-point DC may be limited and inconsistent. In addition, the porous Al_2O_3 framework contained randomly packed pores, which meant the pathways formed were tortuous, thus increasing the path length for conduction. Furthermore, it is also likely that multiple conductive pathways (or one thick pathway) could converge into a singular (or thinner) pathway creating a "bottleneck" where the conduction is limited by the size of the single pathway, ignoring contact points contribution. Lastly, as explained in the proposed mechanism for *in-situ* Ag pathway growth, once the Ag pathway extends back to the feed-side surface the presence of O_2 will react with the tip of all dendrites forming Ag_2O which is not as electron conductive as pure Ag. One way this could have been averted to ensure the tips of the Ag pathways on the feed-side are metallic Ag would be to remove the O_2 from the feed gas during cooling. However, regardless of limitations in the measurements or the membrane operation, the results are indicative of conduction being present after 10 hours of operation.

The conductivity of the membranes after 10 hours of operation, which is the inverse of resistivity, was 5×10^{-4} S cm^{-1}. This is 6 orders of magnitude lower than the conduction Zhang *et al.* [56] received for their LNO membrane. However, for their study they separately fabricated a dense bar of LNO instead of using a tested membrane, thus their sample will have had much less resistance than the membranes used here, due to the porosity and tortuosity of the conductive pathway for a dual-phase membrane. Furthermore, the temperatures used for their four-point DC experiments were between 550 and 850°C, whereas the samples tested here (Fig. 5. 6) were at room temperature due to limitations of the equipment used. Furthermore, the conductivity reported here is 3 orders of magnitude lower than the ionic conductivity of molten carbonate (~0.1 S cm^{-1}) [129], [130], thus further indicating the result is likely an underestimation due to the aforementioned limitations of the DC measurements. Had the conductivity been 3 orders of magnitude lower than carbonate ion conductivity, then the addition of Ag into the membrane would not have displayed an order of magnitude improvement in gas flux, as shown in this study.

114

To understand the difference in resistance between samples tested for shorter or longer than 10 hours, Ag pathway volume calculations were performed based on the 3D reconstructed CT data. Volume calculations were conducted by counting the voxels in a given area and multiplying by the cube of the voxel dimensions (10.4 μm^3). Fig. 5. 7 (primary y-axis) shows that as time progresses the amount of Ag in the cross-section (bulk) of the membrane increases, which consequently allows more Ag pathways to connect across the cross-section of the membrane, until all the Ag has been redistributed after 115 hours. The volume calculations were completed using the following equation (5.3):

$$\% \, Ag \, in \, the \, bulk = \frac{Volume \, of \, Ag \, in \, the \, bulk}{Final \, volume \, of \, Ag \, in \, the \, bulk} \tag{5.3}$$

For these calculations it was assumed that the 'final volume of Ag in the bulk' was achieved after 115 hrs *i.e.* all Ag volumes were divided by the Ag volume after 115 hours. This assumption was made based on the fact that the flux had not changed for 25 hours which implied that the pathways had stopped forming. However, it is possible pathways may still be forming but gas transport was no longer limited by electron conduction.

However, the increased volume of Ag in the bulk with time does not reliably support the presence of connected Ag pathways. To ensure the volume of Ag in the bulk is distributed in a way that connects across the membrane, volume calculations must be completed that highlight the amount of Ag on each membrane surface. These calculations were completed by comparing the volume of Ag on the feed- and permeate-side surfaces as described by equation (5.4):

$$\% \, Ag \, on \, feed\text{-}side \, surface = \frac{Volume \, of \, Ag \, on \, feed\text{-}side \, surface}{Volume \, of \, Ag \, on \, permeate\text{-}side \, surface} \tag{5.4}$$

The calculated volumes on the feed- and permeate-side surfaces were considered to be 1 voxel thick, which translates to a cube which is 10 µm thick, corresponding with the thickness of the Ag on the permeate side shown in Fig. 4. 11. Fig. 5. 7 (secondary y-axis) shows that the membrane operated for less than 10 hours had no Ag on the feed-side surface, thus indicating that no pathways were connected across the membrane cross-section at this point, regardless of the presence of Ag in the bulk. From 10 hours onwards, the volume of Ag on the feed side increased with the volume of Ag in the bulk, until reaching 115 hours where it was assumed all Ag had been redistributed. The increased volume of Ag in the bulk with time (Fig. 5. 7 – primary y-axis), combined with the fact that Ag starts to appear on the feed-side surface with time (Fig. 5. 7 – secondary y-axis) indicates the presence of connected conductive pathways. This helps to explain why the resistance decreases after 10 hours of operation and consequently the flux starts to increase at the same time. In addition, Fig. 5. 7 (secondary y-axis) shows that the

115

volume of Ag on the feed and permeate-side surfaces never match, with much more Ag appearing on the permeate side. This is in-line with the suggestion that Ag pathways may not extend the entire cross-section (possibly due to the melt residing beneath the surface), which explains the high resistance compared to a dense Ag sample. The difference in volumes on each surface could also suggest that more pathways extend from the permeate-side surface, but the pathways either reach dead-ends or form bottlenecks where multiple pathways converge into a singular pathway.
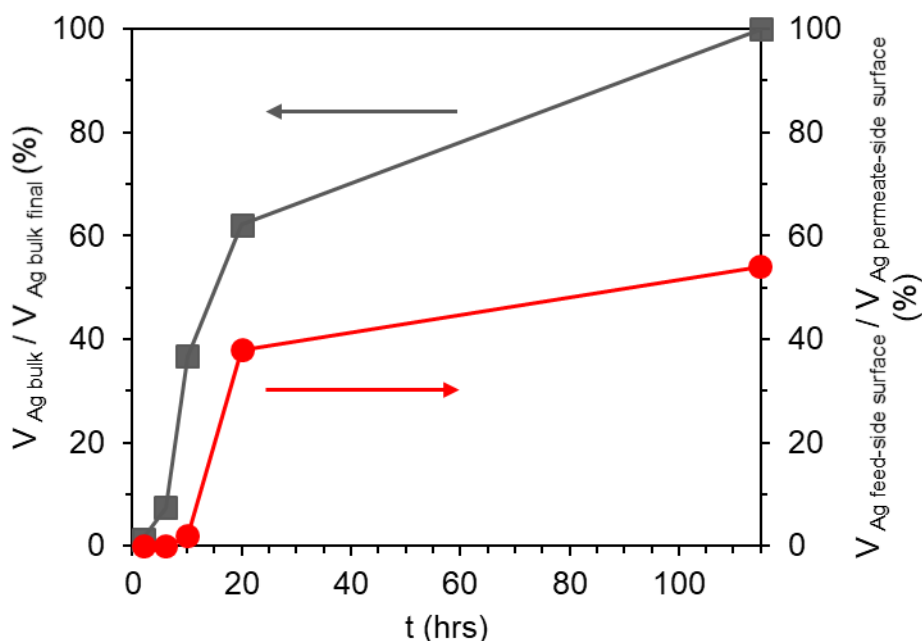
Fig. 5. 7 Quantity of Ag in the membrane cross-section as a function of time and quantity of Ag connected between feed- and permeate-side surfaces as a function of time. The membranes were fed with 50 mol% CO_2 and 25 mol% O_2 at 650°C.

5.3.3 The effect of temperature on the Ag/Al_2O_3-MC membrane

Flux enhancement as a result of the formation of Ag pathways can be considered in the context of wholly Ag-supported membranes. The development of electron-conducting Ag pathways, producing an electronically conductive support, allows enhanced CO_3^{2-} transport *via* reaction (5.5) and consequently improved CO_2 and O_2 transport across the membrane.

$$CO_2 + \frac{1}{2}O_2 + 2e^- \leftrightarrow CO_3^{2-} \qquad (5.5)$$

However, other mechanisms are possible, as discussed in section 1.1, such as reaction (5.6):

$$CO_{2\,(g)} + O_{2\,(s)}^{2-} \leftrightarrow CO_{4\,(l)}^{2-} \qquad (5.6)$$

In addition to the two-point DC experiments shown in Fig. 4. 15 and Fig. 5. 6, electron conduction was evidenced indirectly by the CO_2 and O_2 flux ratios. For all membranes with Ag

added, the CO_2:O_2 flux ratios were 2:1, in agreement with reaction (5.5) and other electron-conducting supported membranes in the literature. However, there have been studies from Ag membranes where the CO_2:O_2 ratio was closer to 1:1 or 2:3 in favour of higher O_2 flux [57], [58]. This observed ratio was due to a proposed bi-pathway transport mechanism, which comes as a result of pore coarsening from the dealloying technique employed for their support fabrication process. This pore coarsening causes molten carbonate to be pushed out of the pores and wet the permeate-side surface which results in a reduction in triple-phase boundaries to promote reaction (5.5) and instead promotes a new two-phase CO_2 and O_2 transport pathway using peroxymonocarbonate (5.7):

$$\frac{1}{2}O_2 + CO_3^{2-} \leftrightarrow CO_4^{2-} \tag{5.7}$$

Therefore, since the ratio in this study is consistently 2:1 (CO_2:O_2), it is possible that the Ag/Al_2O_3-MC membrane has sufficient wettability during permeation to avoid molten carbonate from leaving the pores and wetting the permeate-side surface and thus, maintaining the triple-phase boundaries. This is supported by the fact that the amount of carbonates added were enough to only fill the porous network.

To gain insight into the mechanism for CO_2 and O_2 transport and to demonstrate the Ag/Al_2O_3-MC membranes stability at high temperatures, an Arrhenius plot was formed from stable flux (J_{CO_2} and J_{O_2}) measurements at temperatures between 650-750°C (Fig. 5. 8). For this study, a 6 mol% Ag/Al_2O_3-MC membrane was used as it achieved the highest fluxes in the previous Ag loading experiments.
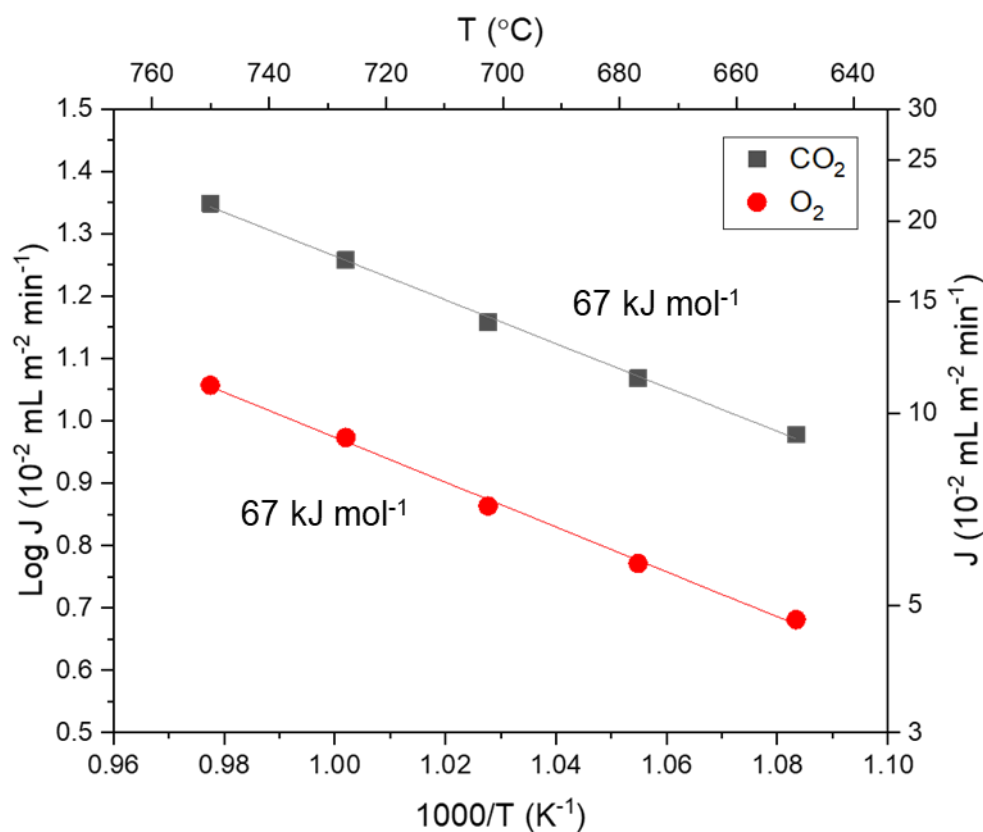
Fig. 5. 8 Arrhenius plot of stable CO_2 and O_2 fluxes with a 6 mol% Ag/Al_2O_3-MC membrane between 650 and 750°C. Feed-side inlet: 50 mol% CO_2, 25 mol% O_2 in N_2. Permeate-side inlet: Ar.

The results demonstrated that the 6 mol% Ag/Al_2O_3-MC membrane continued to perform at temperatures exceeding 650°C, whereas other wholly-Ag membranes have failed previously as a result of support sintering and wettability issues with molten carbonate [60]. The 6 mol% Ag/Al_2O_3-MC membrane was able to achieve a stable flux of 22×10^{-2} mL (NPT) min^{-1} cm^{-2} at 750°C while maintaining the same 2:1 CO_2:O_2 ratio, indicating that at temperatures exceeding 650°C the triple-phase boundaries on the permeate side are maintained.

The only Ag membrane able to operate under the same temperatures was reported by Zhang *et al.* [62]. The fluxes from the uncoated Ag membrane can be used to emphasize the improvements made by the 6 mol% Ag/Al_2O_3-MC membrane at temperatures above 650°C (Fig. 5. 8). When comparing the fluxes at 650°C, the uncoated membrane achieved a flux of 0.8 mL min^{-1} cm^{-2}, which is 8.4 times higher than the membrane presented in this study (0.095 mL min^{-1} cm^{-2}). However, when the uncoated membrane was operated at 700°C the flux decreased to 0.6 mL min^{-1} cm^{-2}, due to wettability and sintering issues previously described with uncoated Ag membranes. Due to these issues, the flux gap between the membranes was reduced to 4.2-fold, because while the uncoated membranes flux declined, the 6 mol%

Ag/Al_2O_3-MC membranes flux continued to increase. However, the flux was still lower further indicating that modification of the membrane's geometry is necessary.

The Arrhenius plot showed that both J_{CO_2} and J_{O_2} had the same effective activation energy (E_a) of 67 kJ mol^{-1}, indicating a coupled transport mechanism for CO_2 and O_2 (Fig. 5. 8) which further agrees with reaction (5.5). In this case, the effective activation energy corresponds to all processes that results in a transmembrane flux of CO_2 or O_2, *i.e.* surface reactions and bulk transport processes. The result is therefore useful for comparing our results with other membranes in the literature. E_a values were similar to other Ag membranes reported in the literature, where E_a values typically range from 60 to 80 kJ mol^{-1} for CO_2 and O_2 transport [57], [60], [62]. Furthermore, it has been reported elsewhere [57], [59] that the activation energy for CO_3^{2-} conduction in molten carbonate is approximately 30 kJ mol^{-1}. This indicates that the surface exchange reactions are rate limiting rather than CO_3^{2-} diffusion. Based on the work from Chapter 3, where it was found that the release of CO_2 from the permeate-side surface was slower than the uptake of CO_2 from the feed-side surface, it is likely that the release of CO_2 on the permeate side is the rate limiting process for this membrane.

5.3.4 *Impact of sealant on dual-phase membrane flux*

The carbonate retention issues exhibited by wholly Ag-supported membranes also effects the membranes stability over long periods of time across all temperatures. Sealant breaks are another causal factor of dual-phase membrane leaks. Therefore, to see if the Ag-doped membranes presented here suffer the same issues, the length of operation for a 6 mol% Ag/Al_2O_3-MC membrane was compared with an Al_2O_3-MC membrane (Fig. 5. 9).
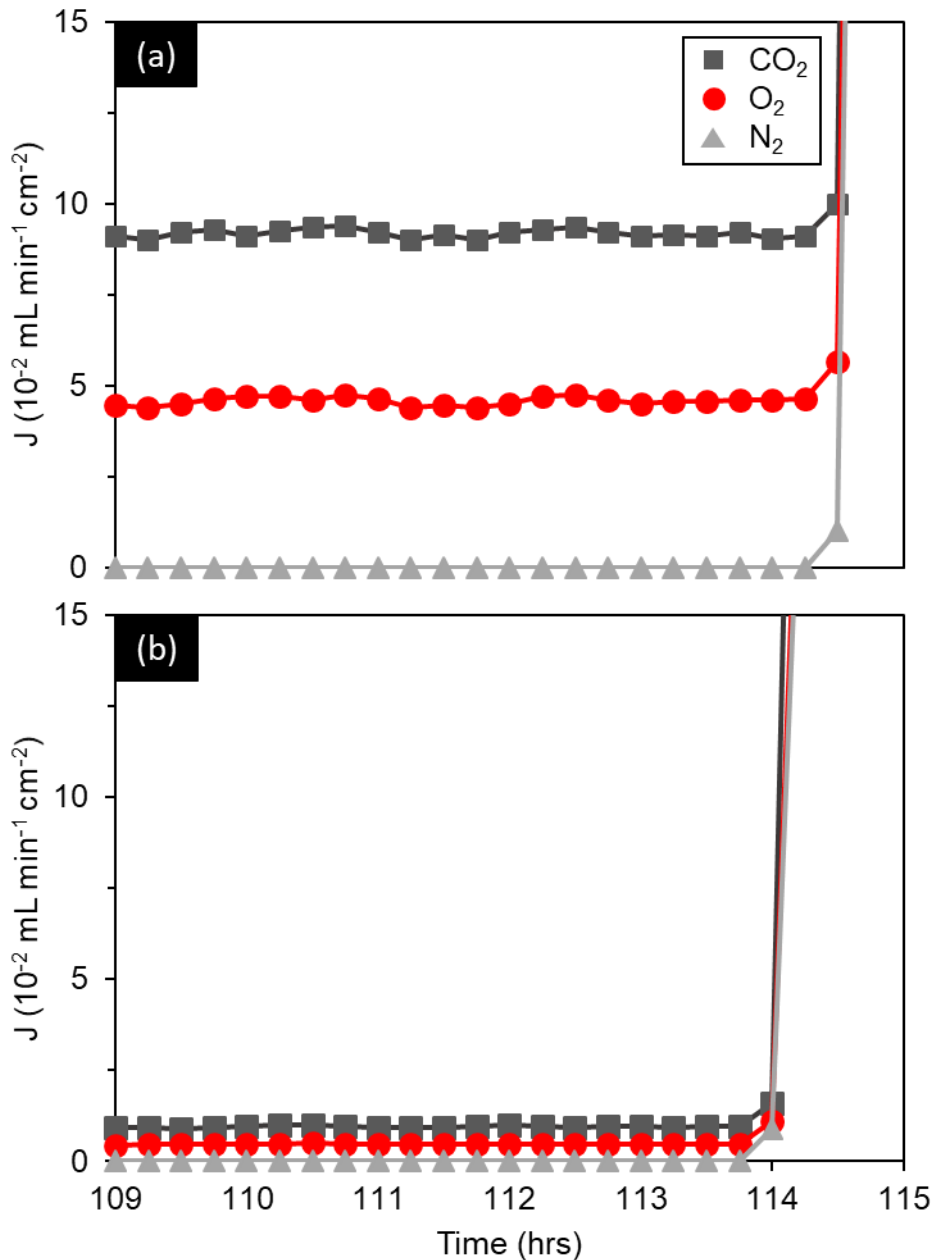
Fig. 5. 9 Transmembrane leak comparison for (a) 6 mol% Ag/Al_2O_3-MC and (b) Al_2O_3-MC membrane at 650°C.

Fig. 5. 9 illustrates the development of two transmembrane leaks for two different permeation experiments at 650°C and after approximately 115 hours of operation: Fig. 5. 9a 6 mol% Ag/Al_2O_3-MC membrane and Fig. 5. 9b Al_2O_3-MC membrane. Comparison of the two sets of data showed both the Ag-doped and undoped membranes succumbed to leaks after similar lengths of operation. If Ag's wettability with molten carbonate or sintering had been a factor in the membranes eventual leak, then the 6 mol% Ag/Al_2O_3-MC membrane would likely have leaked sooner than the Al_2O_3-MC membrane. Furthermore, if Fig. 5. 9a is compared to a long-term permeation experiment for an Ag-supported membrane, such as that shown by Zhang *et al.* [54] it is apparent that the behaviour in which the membranes here leak are different. For

their Ag-supported membrane, the CO_2 and O_2 flux begins to decline after 160 hours, as the membrane sinters and pushes molten carbonate out of the pores (wettability could also be a causal factor). As molten carbonate is pushed out, the N_2 flux (which also acts as their leak detector) increases over a 150-hour period due to pores opening up until the experiment was stopped. A similar leak pattern has been seen with the lithiated NiO membrane, albeit at 850°C. In contrast, the 6 mol% Ag/Al_2O_3-MC membrane presented in this study had a stable CO_2 flux with zero N_2 flux until the membrane catastrophically fails over a 10 to 20 second period. The magnitude of this catastrophic failure, described by the sudden change in N_2 flux, is more likely a result of a sealant leak, rather than the result of pores gradually becoming free of molten carbonates from sintering or wettability issues.

To test whether the sealant was the cause of the catastrophic leak and attempt to increase the longevity of the membrane, a permeation experiment was performed using a 6 mol% Ag/Al_2O_3-MC membrane, where a commonly used Ag ink sealant [40], [47], [49], [54], [56], [58], [59], [62], [69], [124] was used in place of the previously used Au ink sealant (Fig. 5. 10a).
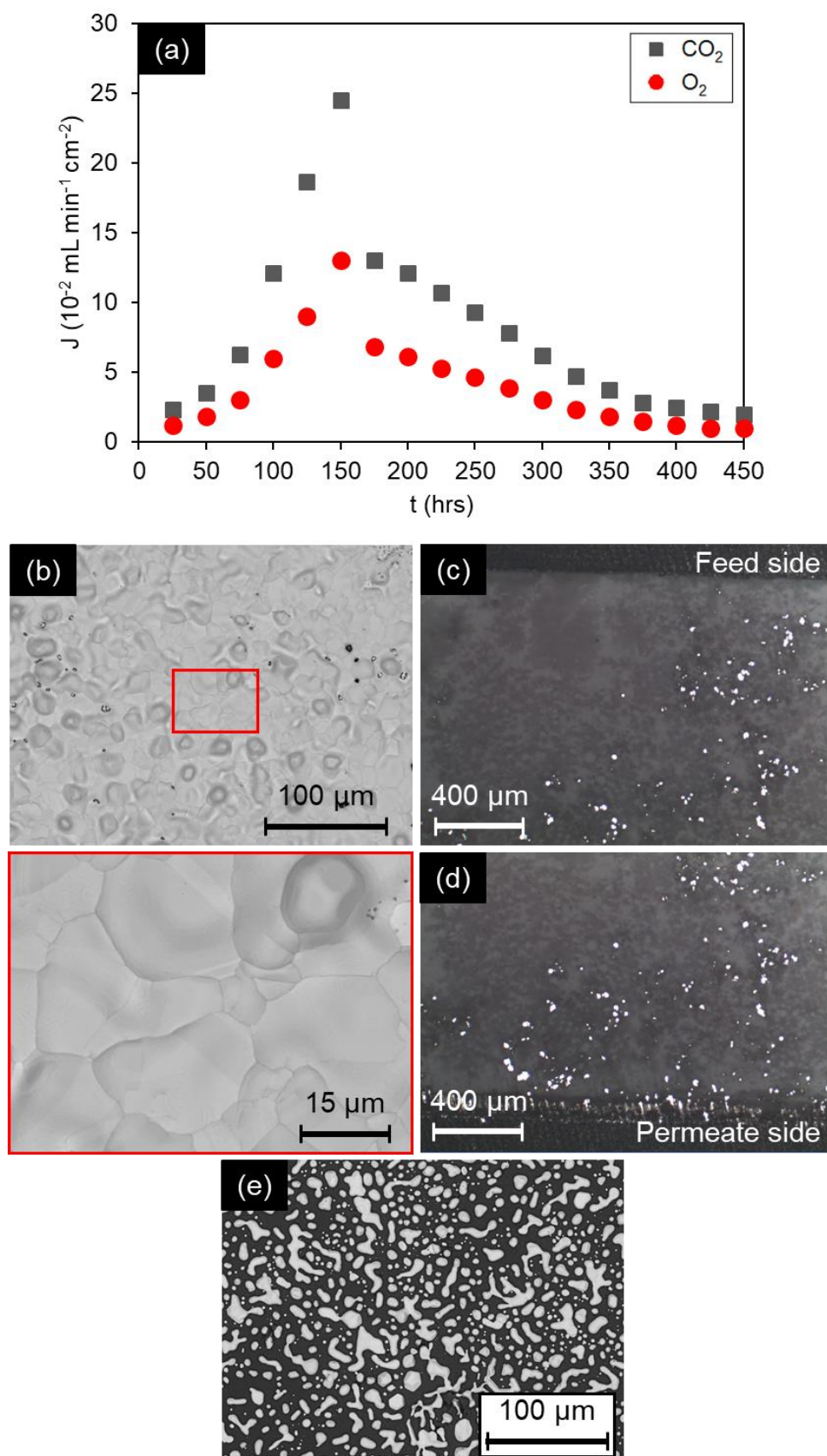
Fig. 5. 10 (a) CO_2 and O_2 flux evolution with time for a 6 mol% Ag/Al$_2$O$_3$-MC membrane with an Ag sealant at 650°C (b) SEM images of the permeate side after used (c) digital image of the feed-side cross-section after use (d) digital image of the permeate-side cross-section after use (e) SEM image of the permeate side of an Au-sealed membrane (for reference) after use. Feed-side inlet: 50 mol% CO_2, 25 mol% O_2 in N_2.

The use of the Ag sealant allowed the 6 mol% Ag/Al_2O_3-MC membrane to operate for at least 450 hours without a detectable leak. This indicated that the leaks from the Au-sealed Ag/Al_2O_3-MC membrane were linked to sealant failure and not a result of sintering or wettability issues. However, the experiment was stopped before the membrane leaked due to a flux limitation that came with this improved longevity. The membrane saw a decline beyond 150 hours, which appeared to stabilize at around 0.02 mL min^{-1} cm^{-2} after 450 hours of operation. A reason for the flux decline can be explained by analysing the permeate-side surface after operation using SEM (Fig. 5. 10b). It is clear the porous Al_2O_3 permeate-side surface has become more blocked with Ag for the Ag-sealed membrane compared to the Au-sealed membrane after use (compare Fig. 5. 10b and Fig. 5. 10e). However, the permeate side pore blocking is not due to continued migration from the Ag powder added to the carbonate as a result of the longer permeating conditions exposure. This is evidenced by the digital microscope image of the cross-section at the feed and permeate-side surfaces (Fig. 5. 10c and d, respectively and Fig. A. 15) that shows Ag pathways are still connected across the membrane. Therefore, the extra Ag on the permeate-side surface must come from another source *i.e.* the Ag sealant. It is likely, that the Ag sealant has migrated *via* a similar method to the Ag powder. The consequence of this is that the combination of both migration mechanisms (powder and sealant) has resulted in the membrane becoming blocked.

To determine if the Ag sealant contributed to the membranes blockage, an undoped Al_2O_3-MC membrane, sealed with Ag ink, was fed with 50 mol% CO_2, 25 mol% O_2 in N_2 in the feed-side inlet and pure Ar in the permeate-side inlet at 650°C (Fig. 5. 11).
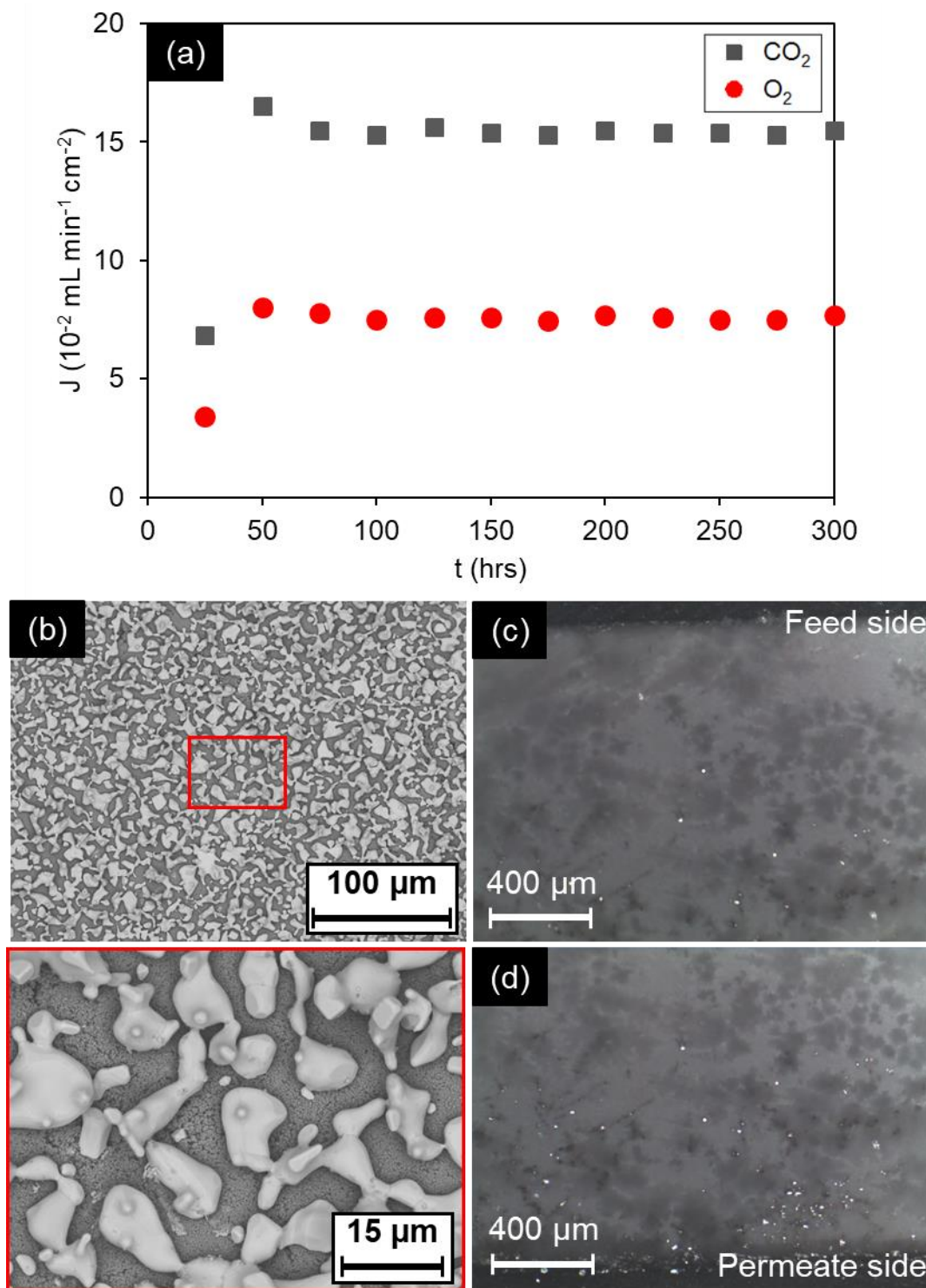
Fig. 5. 11 (a) CO_2 and O_2 flux evolution with time for a undoped Al_2O_3-MC membrane with an Ag sealant at 650°C. (b) SEM images of the permeate side after used. (c) digital image of the feed-side cross-section after use. (d) digital image of the permeate-side cross-section after use. Feed-side inlet: 50 mol% CO_2, 25 mol% O_2 in N_2.

Fig. 5. 11b shows SEM images of the permeate side after operation which prove that without Ag powder added to molten carbonate, Ag is still found on the permeate side as a result of sealant migration. This explains why the membrane became blocked with both Ag powder and an Ag sealant, resulting in a decline in flux. Furthermore, Fig. 5. 11a demonstrates that without

the competition for space on the permeate side from the two Ag migration mechanisms, the membrane operated stably for at least 300 hours, achieving a CO_2 flux of 0.15 mL min^{-1} cm^{-2} before the experiment was stopped. It is also worth noting that after analysing the cross-section using a digital microscope (Feed-side surface – Fig. 5. 11c and permeate-side surface – Fig. 5. 11d and full cross-section – Fig. A. 16) it appears that the migrated Ag sealant forms a nucleation point for the pathways to extend towards the feed-side surface of the membrane. This agrees with the time resolved micro-CT study which showed that pathways first migrate to the permeate side of the membrane before extending back towards the feed side (Fig. 5. 5). However, for this experiment the Ag did not start at the feed side which indicates that pathway formation is independent of the starting location of Ag and is only controlled by the direction of CO_3^{2-} movement across the membrane (from the feed side to the permeate side) driven by CO_2 permeation.

Interestingly, the fluxes of both Ag-sealed membranes presented in Fig. 5. 10a and Fig. 5. 11a are higher than their equivalent Au-sealed membranes. The flux of Ag-sealed 6 mol% Ag/Al$_2$O$_3$-MC membrane (Fig. 5. 10a) before the decline at 150 hours of operation reached a maximum of 0.25 mL min^{-1} cm^{-2}, which is a factor of 2.5 higher than that shown with an Au-sealed 6 mol% Ag/Al$_2$O$_3$-MC membrane. Similarly, the Ag-sealed Al$_2$O$_3$-MC membrane achieved a CO_2 flux of 0.15 mL min^{-1} cm^{-2}, which was a factor of 15 higher than the Au-sealed Al$_2$O$_3$-MC membrane. These flux differences suggest that the Ag sealant was contributing to the flux. Therefore, the flux of 0.25 mL min^{-1} cm^{-2} for the 6 mol% Ag/Al$_2$O$_3$-MC membrane can be considered to have two main contributing factors; flux from the Ag powder and flux from the Ag sealant at the points where the sealant is in contact with the permeating area of the membrane. By addition of CO_2 fluxes from the Au-sealed 6 mol% Ag/Al$_2$O$_3$-MC membrane (0.095 mL min^{-1} cm^{-2}) and the undoped Ag-sealed Al$_2$O$_3$-MC membrane (0.15 mL min^{-1} cm^{-2}) an overall flux of 0.245 mL min^{-1} cm^{-2} is achieved, which is in agreement with the Ag-sealed 6 mol% Ag/Al$_2$O$_3$-MC membrane (0.25 mL min^{-1} cm^{-2}). However, the flux of the Ag-sealed Al$_2$O$_3$-MC membranes does not decrease after 150 hours, thus further indicating that the flux decline shown in Fig. 5. 10a is likely due to blockage on the permeate side as a result of migration competition from the sealant and the added Ag powder.

An illustration for how the Ag sealant contributes to the membranes flux is described in Fig. 5. 12. The illustration shows that the Ag sealant could be acting as an electron-conducting bridge for gas transport.
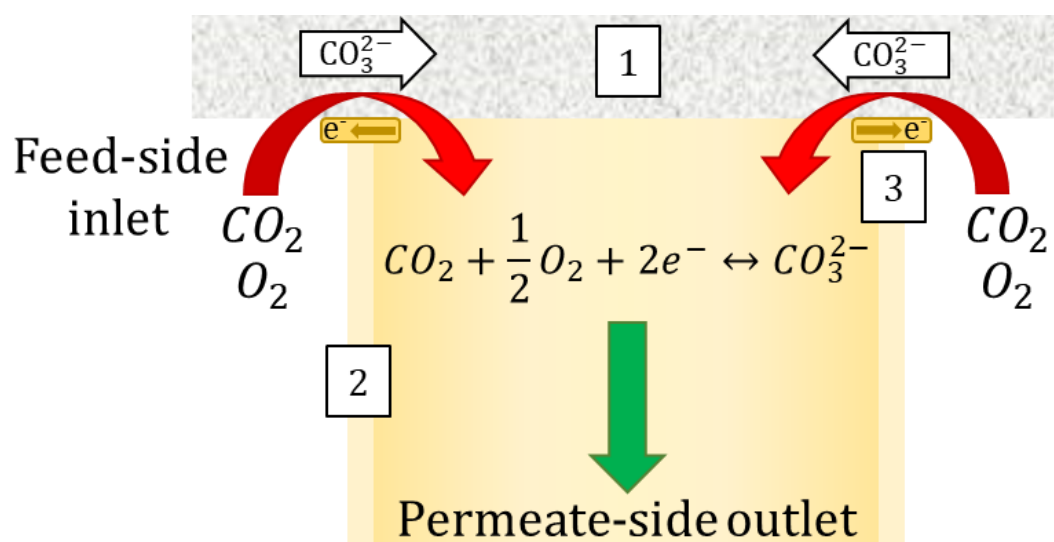
Fig. 5. 12 Schematic illustration of CO_2 and O_2 facilitated transport *via* an electronically conductive sealant. (1) Dual-phase membrane, (2) Dense inert inner tube, (3) Electron-conducting sealant.

The illustration describes a similar three-stage gas transport process used for most membranes (1) feed-side surface reaction, (2) diffusion and (3) permeate-side surface reaction:

1. Firstly, the CO_2 and O_2 from the feed gas reacts with the molten carbonate within the dual-phase membrane. This reaction normally takes place at a point that provides the fastest gas transport (the preferential route), which depending on the thickness of the membrane support is often from the top feed-side surface to the bottom permeate-side surface. However, when a non-conducting or oxide conducting supported membrane is fed with a CO_2 and O_2 containing gas, the availability of an electron-conducting bridge between the dual-phase membrane and the inner tube provides a preferential route for CO_2 and O_2 coupled transport. Therefore, the feed-side reaction takes place at the three-phase boundary that connects the dual-phase membrane to the inner tube: molten carbonate – sealant – gas. The reaction that occurs is displayed in Fig. 5. 12 and reaction (5.5) and is similar to the interaction between the feed gas and a Ag/Al_2O_3-MC membrane described previously.

2. The reaction at the three phase boundary results in the formation of a carbonate ion which moves down its concentration gradient towards the permeate-side surface.

3. Once the carbonate ion reaches the same 'molten carbonate – sealant – gas' three-phase boundary on the opposing side of the membrane, the reverse of reaction (5.5) occurs.

Based on this hypothesis, all electron-conducting sealants used in the literature could be contributing to the membrane's gas flux if a CO_2 and O_2 driving force is present across the membrane. To test this theory, an Au-sealed, undoped Al_2O_3-MC membrane was fed with two

different gas mixtures (50 mol% CO_2, 25 mol% O_2 in N_2 and 50 mol% CO_2 in N_2) and the CO_2 and O_2 flux for each mixture was compared (Fig. 5. 13).
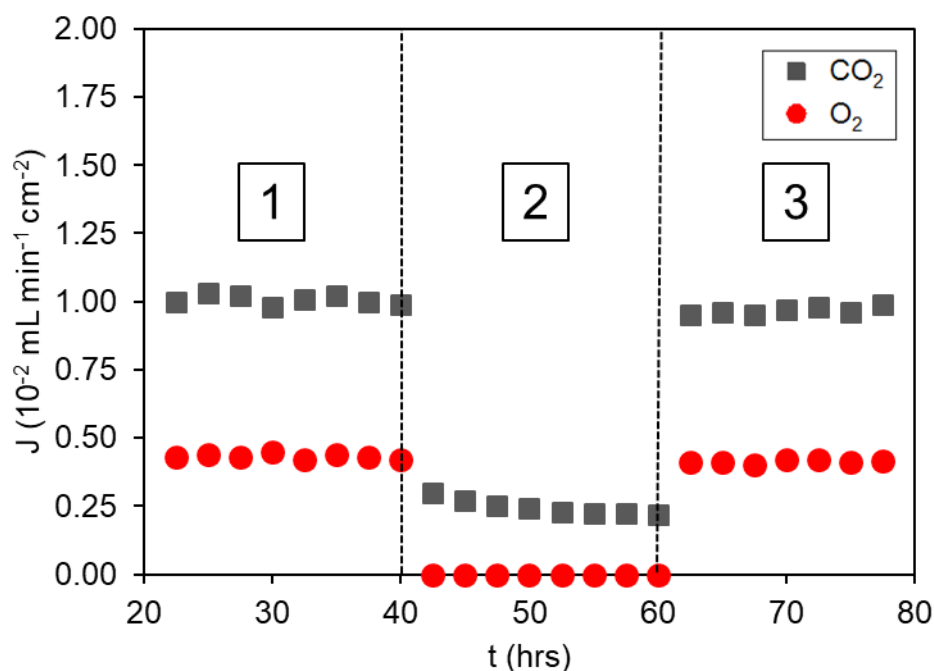
Fig. 5. 13 CO_2 and O_2 fluxes as a function of feed-side inlet gases across three feeding segments for an Au-sealed undoped Al_2O_3-MC membrane at 650°C. (1) 50 mol% CO_2, 25 mol% O_2 in N_2, (2) 50 mol% CO_2 in N_2 and (3) 50 mol% CO_2, 25 mol% O_2 in N_2.

Fig. 5. 13 demonstrates that the membrane had a higher CO_2 flux when CO_2 and O_2 were fed together compared with feeding the same concentration of CO_2 alone. This flux enhancement with the CO_2 and O_2 feed is due to the electron-conduction from the Au ink acting as an electron conducting pathway, similar to that of the Ag pathways described in this work. The sealant connects from the feed-side surface to the permeate-side surface and has direct contact with the molten carbonate throughout the entire cross-section. Therefore, at the triple phase boundary on each membrane surface the electron-conducting sealant allows the initiation of the permeation mechanism described in section 4.1. This can help to explain why a 2:1 flux ratio is seen at the start of Fig. 5. 3. Since Ag is the most electron-conducting metal, it is reasonable to see a 2.5 times flux improvement with the 6 mol% Ag/Al_2O_3-MC membrane when Ag ink is used in place of Au ink (up to 150 hours of operation). Furthermore, the relationship between the Ag sealant and the gas flux enhancement may also help to explain to why the sealant migrates (Fig. 5. 10b), since it has already been shown in Chapter 4 that Ag migration is linked to gas flux.

The results presented here demonstrate that the 6 mol% Ag/Al_2O_3-MC membrane has the ability to operate for a minimum of 450 hours without leaking, however care must be taken when

selecting a sealant for the future. Based on these results, it is possible the reason the LNO membranes [56] gas flux was able to compete with an Ag-supported membrane was due to the use of Ag ink as a sealant. Furthermore, several of the best Ag membranes also used Ag ink as a sealant which could have also contributed to their flux [54], [57]–[59]. Thus, for electron-conducting supports sealed with Ag, it is unclear how much of the flux is a result of the support or the sealant.

Ag has also been used for oxide-conducting supports [40], [47], [49]. When only CO_2 is used in the feed gas, it is likely that the impact on flux will not be as severe as with CO_2 and O_2 together, as O_2 is needed together with CO_2 to consume the electron from the Ag and activate reaction (5.5). However, as shown in Chapter 4, even without O_2 in the feed-side inlet, Ag was found to migrate to the permeate side and had a positive flux enhancement of approximately 200%, albeit with an Al_2O_3 support. Thus, the contribution an Ag sealant could have on a support such as SDC or LSCF fed with CO_2 alone remains to be seen. However, a study from Tong *et al.* [44] used an Ag-sealed SDC membrane fed with CO_2 and O_2 and found O_2 co-permeated in a ~ 5:1 CO_2:O_2 ratio. This indicated that the primary mechanism for oxide-conducting membranes displayed by reaction (5.8) is consistent:

$$CO_{2\,(g)} + O^{2-}_{(l)} \leftrightarrow CO^{2-}_{3\,(l)} \tag{5.8}$$

However, the presence of co-permeated O_2 indicates that an additional electron-conducting mechanism is likely present as described by reaction (5.5). Furthermore, when pO_2 was increased, the CO_2 flux increased with O_2 flux, indicating that the transport of O_2 was coupled with CO_2, similar to that of an electron-conducting support. This finding does not agree with a model created by Rui *et al.* [35] where they concluded that O_2 permeation through a ceramic supported membrane is independent of CO_2 flux. The authors described that the O_2 co-permeation likely came from the electron conductivity of the SDC support (as described in Section 1.2.2). However, they made no reference to their use of an Ag sealant and the results presented here indicate that the coupled CO_2 and O_2 transport could also be a result of electron donation from their Ag ink sealant.

Therefore, to eradicate any flux contribution from the sealant for a lab-scale pellet membrane reactor, an ideal scenario would be to use a membrane that has no hot-sealing region. This would prevent any sealant leaks and remove the need for a costly Au or Ag sealant and eliminate any interference with flux so that the true effect of the support material, or carbonate dopant, can be displayed.

5.3.5   Use of the parallel pore support for the Ag/Al$_2$O$_3$-MC membrane

To demonstrate the effect of removing the flux contribution from the sealant when feeding the membrane with CO_2 and O_2, the parallel pore membrane system from Chapter 3 was used which has no hot-sealing region. The same experiment used for Fig. 5. 13 was repeated. In this case, a parallel pore membrane support was used in place of the pressed alumina support. The support was infiltrated with undoped molten carbonates and was fed with two different gas mixtures (50 mol% CO_2, 25 mol% O_2 in N_2 and 50 mol% CO_2 in N_2) at 650°C and the CO_2 and O_2 flux for each mixture was compared (Fig. 5. 14).
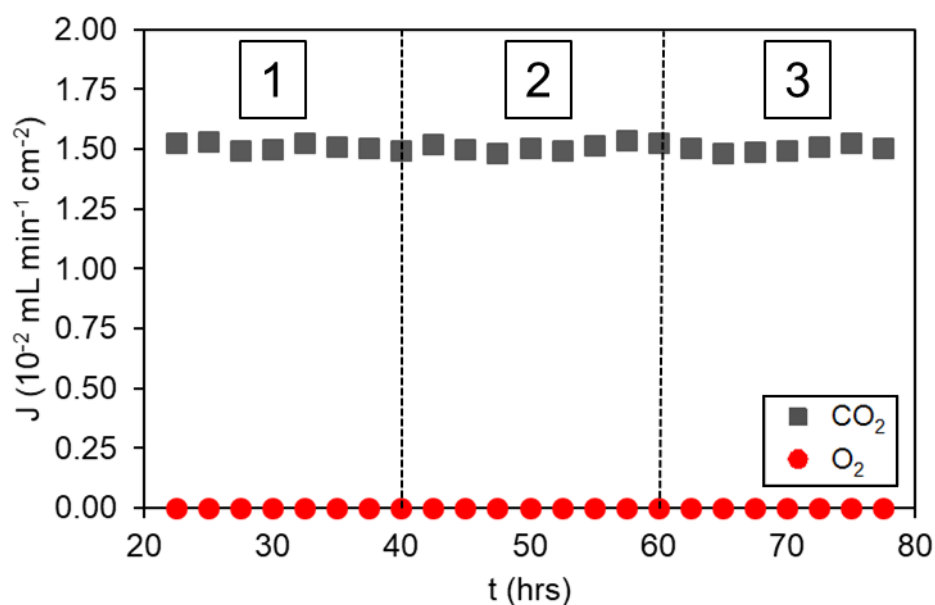
Fig. 5. 14 CO_2 and O_2 fluxes as a function of feed-side inlet gases across three feeding segments for a sealant-free undoped parallel pore Al$_2$O$_3$-MC membrane at 650°C. (1) 50 mol% CO_2, 25 mol% O_2 in N_2, (2) 50 mol% CO_2 in N_2 and (3) 50 mol% CO_2, 25 mol% O_2 in N_2.

Fig. 5. 14 shows that when an inert Al$_2$O$_3$ membrane support with no sealant is used, there is no difference between feeding CO_2 and O_2 together compared to CO_2 alone, further indicating the impact of the sealant on the flux of the membrane.

As well as offering a model system for studying the effect of sealant removal on gas flux, the large size of the pores used for this membrane system (150 µm diameter inlet and 75 µm diameter outlet) offered an opportunity to determine precisely where the Ag resided within the pores using a higher resolution Micro-CT (Versa). To achieve this, a permeation experiment was performed. The parallel pore membrane was infiltrated with 6 mol% Ag-doped carbonates (henceforth referred to as the 6 mol% Ag/Al$_2$O$_3$-MC parallel pore membrane) and was fed with 50 mol% CO_2 and 25 mol% O_2 at 650°C for 24 hours before quenching the sample for CT imaging (Fig. 5. 15).
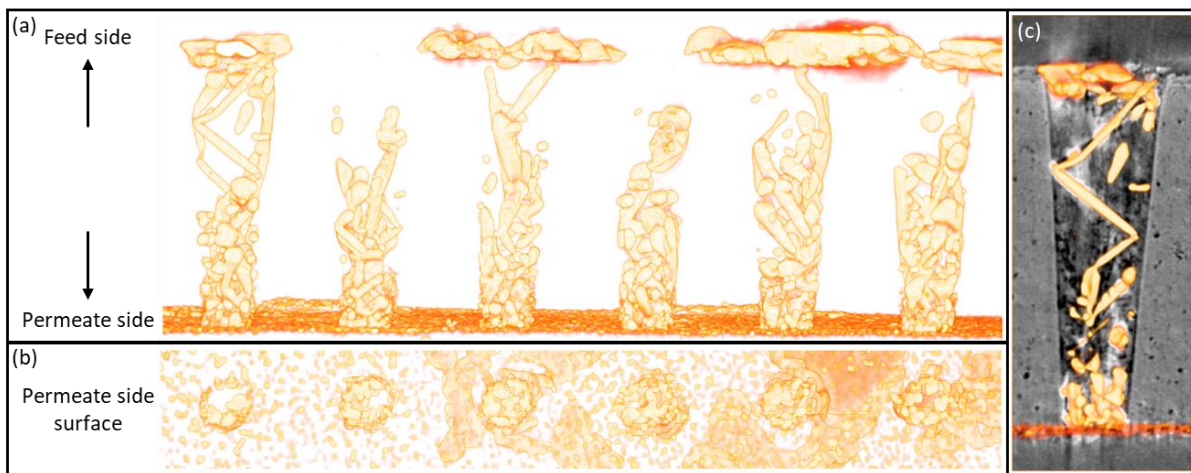
Fig. 5. 15 CT of a collection of pores in a tested 6 mol% Ag/Al_2O_3-MC parallel pore membrane system; (a) cross-section view with ceramic phase removed; (b) permeate-side surface with ceramic phase removed; (c) single parallel pore with ceramic phase. Parallel pore membrane operated with 6 mol% Ag in the carbonates and operated at 650°C. Feed-side inlet: 50 mol% CO_2, 25 mol% O_2 in N_2. Permeate-side inlet: Ar.

The CT image of the cross-section view of a selection of pores in the parallel pore membrane (Fig. 5. 15a) showed that the dissolved Ag formed thin microstructures, that only partially covered the Al_2O_3 pore walls. This could explain the membranes ability to retain carbonates and function at high temperatures (Fig. 5. 8) as compared to wholly Ag-supported membranes, as portions of the highly wettable Al_2O_3 surface remained uncovered and in contact with molten carbonate. This also helps to explain the consistent 2:1 CO_2:O_2 ratio described in section 5.3.3 because the highly wettable Al_2O_3 helps to retain the carbonates within the pores and maintain the high density of triple-phase boundaries on the permeate-side surface. This is in line with the work by Tong *et al.* [59] which showed they were able to increase the wettability between the support and molten carbonate by coating the walls of the Ag support with a nano-layer of Al_2O_3. An alternative approach by Fang *et al.* [58] showed that by decreasing the pore-size ($< 1\mu m$) they were able to improve the wettability, producing a membrane that could operate for 900 hours at 600°C.

In addition, the CT images showed that in every pore, Ag was invariably found as a deposit of the permeate-side surface, having migrated from the feed side during the 25-hour permeation experiment with Ag-loaded carbonates. As described previously, this Ag deposition on the permeate-side likely provides a nucleation point for pathways growth back towards the feed-side surface. However, the extent to which the pathways extend towards the feed side was inconsistent. In some cases, similar to those seen in Fig. 5. 5, the Ag appeared to form a connected path across the entire cross-section of the Al_2O_3 support. In other pores, the conductive pathways were discontinuous, or stopped short of spanning the entire cross-section.

Of course, connected pathways beneath the resolution limitation of the CT scanning could be present. Alternatively, it is possible that not every pore needs a connected Ag pathway to achieve the CO_2 flux shown. Instead, it is possible that a small number of connected electronically conductive pathways may be sufficient to improve permeation by providing preferential fast-transport routes, indicating that further optimisation would be possible.

Fig. 5. 15b shows a top down view looking into the pores from the permeate side. The image showed that while Ag can be found in the middle of the pores, invariably, the Ag connects to the Al_2O_3 wall at some point within the Ag structures (see also Fig. A. 13). This is also shown in Fig. 5. 15c where the Ag structures appear to follow the outline of the laser-drilled pore (see also Fig. A. 14). Therefore, it is possible that Ag initially deposits on the support wall due to the favourable surface energies of the Al_2O_3 [131]. This initial deposition of Ag then acts as a nucleation point for the Ag to grow into the dendritic structures seen in Fig. 5. 5e.

The parallel pore membranes 2000 straight, unrestricted pores, each with a path length of 500 µm provided an opportunity to study the effect of pore geometry and membrane thickness on the flux of the Ag/Al_2O_3-MC membrane. From the same permeation experiment described previously for the Ag-doped parallel pore membrane, a flux of 1.25 mL cm^{-2} min^{-1} was achieved (Fig. 5. 16). Furthermore, since Fig. 5. 14 confirmed that the parallel pore membranes flux was not preferential towards an oxidising feed gas due to their being no electron conducting sealant, the flux reported he is solely a result of Ag doped into the carbonates. In fact, the flux of the 6 mol% Ag/Al_2O_3-MC parallel pore membrane is two orders of magnitude higher than the undoped Al_2O_3-MC parallel pore membrane fed with the same CO_2 and O_2 containing gas feed shown in Fig. 5. 14.
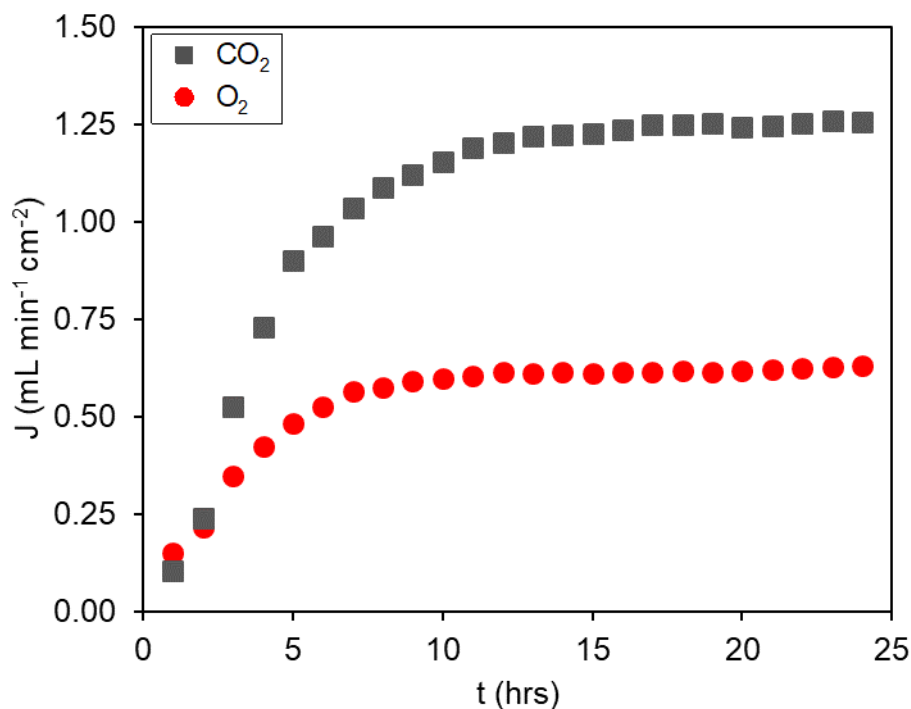
Fig. 5. 16 CO_2 and O_2 flux evolution with time in a 6 mol% Ag/Al_2O_3-MC parallel pore membrane at 650°C. Feed-side inlet: 50 mol% CO_2, 25 mol% O_2 in N_2. Permeate-side inlet: Ar.

Furthermore, this flux was a factor of 13 higher than the 6 mol% Ag/Al_2O_3-MC pressed pellet membrane (with an Au sealant) also presented in this thesis (Fig. 5. 1) and roughly 50% greater than any wholly Ag membrane reported in the literature at 650°C. The highest CO_2 flux at 650°C from an Ag-supported membrane until now was the uncoated membrane which achieved a flux of ~0.8 mL cm^{-2} min^{-1} [60]. However, more recently an Ag membrane with a ZrO_2 overcoat achieved a flux of 0.9 mL min^{-1} cm^{-2} [62], albeit at 850°C, but the parallel pore membrane surpassed this, while operating 200°C lower. The flux also surpassed the electron-conducting lithiated NiO membrane which achieved a flux of ~1.1 mL min^{-1} cm^{-2} at 850°C [56].

Furthermore, when expanding the comparison to encompass oxide-conducting membranes, the flux reported here was unrivalled at 650°C for membranes fed with CO_2 alone and only bettered by an asymmetric tubular SDC membrane operated at 850°C or above (1.45 mL min^{-1} cm^{-2}) [83]. An SDC membrane operating at 650°C and fed with 4.8 mol% H_2 and 48 mol% CO_2 achieved a flux of 1.5 mL min^{-1} cm^{-2} [51]. However, the authors reported that the membranes experience flux degradation after 10 hours of operation. Furthermore, H_2 was used in the feed gas, which acted as a buffer to lower the partial pressure of O_2 to increase oxide ion transport. A similar technique could be employed with the 6 mol% Ag/Al_2O_3-MC parallel pore membrane to increase the flux further. A study by Fang *et al.* [58] demonstrated how the flux of a wholly

Ag-supported dual-phase membrane could be increased by a factor of 2 by adding 9.41 mol% H_2 into the Ar permeate-side inlet. As well as the improved flux the H_2 addition offers, it also provides a method for removing the co-permeated O_2 *via* reaction (5.9) which is an important consideration for upscale:

$$CO_3^{2-} + H_2 \leftrightarrow CO_2 + H_2O + 2e^- \qquad (5.9)$$
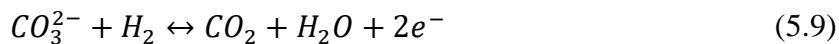
An LSCF supported membrane, which is both oxide and electron conducting, was able to achieve a flux of 4.0 mL min^{-1} cm^{-2} at 950°C with the same oxidising feed gas used here [39]. However, due to flux being exponentially dependent upon temperature for LSCF membranes, the flux dropped to 1.7 mL min^{-1} cm^{-2} at 850°C. Thus, by extrapolating the data it can be estimated that the flux would be ~0.14 mL min^{-1} cm^{-2} at 650°C.

The parallel-pore membrane displayed superior performance for at least two reasons: 1) decreased pore tortuosity and 2) reducing the membrane thickness from ~1.75 mm to ~500 μm. The difference in membrane thicknesses can be normalised between the two membrane systems and compared with the literature by reporting permeability (mol m^{-1} s^{-1} Pa^{-1} – see Table A. 1 for comparison with different permeation units for all membranes presented in the thesis at 650°C). The 6 mol% Ag/Al$_2$O$_3$-MC parallel pore membrane has a CO_2 permeability of 9.4 × 10^{-11} mol m^{-1} s^{-1} Pa^{-1} (or ~280000 Ba), while the pellet membrane in this study is of the same order of magnitude (3.6 × 10^{-11} mol m^{-1} s^{-1} Pa^{-1} or ~110000 Ba). Both membranes presented in this study achieved the permeability required for economically competitive CO_2 capture (10^{-13}-10^{-12} mol m^{-1} s^{-1} Pa^{-1}) [76], while the parallel pore membrane also achieved the permeance required for cost effective CO_2 capture from a post-combustion gas stream (1.9 × 10^{-7} mol m^{-2} s^{-1} Pa^{-1} when the target was 10^{-7} mol m^{-2} s^{-1} Pa^{-1}) [132]. The ZrO_2 coated Ag dual-phase membrane [62] out-performed the parallel pore membrane when compared using permeability, producing a permeability of 17.7 × 10^{-11} mol m^{-1} s^{-1} Pa^{-1}. The difference between the permeabilities is due to the fact that the ZrO_2 study used 15 mol% in the feed gas compared to 50 mol% used in this thesis. Permeability dictates that CO_2 transport increases linearly with pCO_2 in the feed gas. Therefore, if two identical membranes are fed with 25 mol% and 50 mol% CO_2 respectively, the flux will be two times higher for the latter, while the permeability will be the same. However, published experimental data disagrees with this model. A study by Tong *et al.* [57] used two identically prepared Ag membranes (0.82 mm thick, 40% porosity, coated with Al_2O_3) in two different experiments in the same study. One experiment used a 15 mol% CO_2, 10 mol% O_2 in 75 mol% N_2 feed gas, while the other used 42 mol% CO_2, 42 mol% O_2 in 8 mol% N_2 feed gas (each at 650°C). The CO_2 permeability for the former was ~ 6.0 × 10^{-11} mol m^{-1} s^{-1} Pa^{-1}, while the latter was ~ 1.0 × 10^{-10} mol m^{-1} s^{-1} Pa^{-1}. These differences indicate

that the relationship between flux and feed gas partial pressure is not linear. Work by Patrício *et al.* [44] also demonstrated that the relationship between flux and partial pressure in the feed side is not linear. They found that when the same GDC membrane was fed with 10 mol% CO_2 at 850°C a flux of 0.3 mL min^{-1} cm^{-2} was achieved and then when the partial pressure of CO_2 in the feed gas was increased to 40 mol% the flux increased by a factor of less than 2. These results suggest that as pCO_2 in the feed gas is increased there becomes a point when the changes begin to see diminishing returns in flux. The work conducted in Chapter 3 (Fig. 3. 3) could help to explain this phenomenon. In Chapter 3 it was concluded that the permeate-side surface reaction involving the dissociation of carbonate ions and the release of CO_2 was a slower process compared to the reverse feed-side surface association reaction. Therefore, increasing the partial pressure of CO_2 in the feed gas will receive diminishing returns. While the feed-side surface can absorb CO_2 at a faster rate, the process will be limited kinetically by the rate at which the permeate-side surface can the release CO_2. As a result, consideration should be made when comparing the permeability of membranes with low and high pCO_2 in the feed gas.

Aside from the different membrane thicknesses, surface coatings, feed gases, porosities and pore structures, another factor should be considered when comparing the fluxes of membranes presented in this thesis to other Ag membranes in the literature. In the early Ag membrane work, the carbonate mixture routinely used was a binary $(Li/K)_2CO_3$ (62 mol% Li_2CO_3 – 38 mol% K_2CO_3) [60] and in the more recent work a binary $(Li/Na)_2CO_3$ is used (52 mol% Li_2CO_3 – 48 mol% Na_2CO_3) [57]–[59], [62]. Fig. 3. 7 from Chapter 3 proved that when Li was not present in the melt the CO_2 flux decreased by 50%, indicating that higher Li loadings in the melt would likely result in increased CO_2 flux. For the work presented in this study, a ternary $(Li/Na/K)_2CO_3$ mixture was used (42.5 mol% Li_2CO_3 – 32.5 mol% Na_2CO_3 – 25 mol% K_2CO_3) which has lower Li loadings than the aforementioned membranes. Thus, using a $(Li/Na)_2CO_3$ mixture in the future may result in higher CO_2 fluxes than those already presented in this study.

Lastly, the membranes presented in this thesis demonstrate how the amount of Ag used can be reduced while still achieving high fluxes. By normalising the data for the quantity of Ag used in a given volume of membrane, it is clear that the Ag/Al_2O_3-MC membranes presented in this thesis would provide high permeability with reduced Ag content. This is shown by the 6 mol% Ag/Al_2O_3-MC parallel pore membrane having a permeability per mol of Ag one order of magnitude higher the best Ag-supported membranes in the literature (Fig. 5. 17). The 6 mol% Ag/Al_2O_3-MC pressed pellet membrane with the unmodified highly tortuous pore network was able to achieve the same permeability per mol of Ag as the best Ag-supported membranes in the literature.
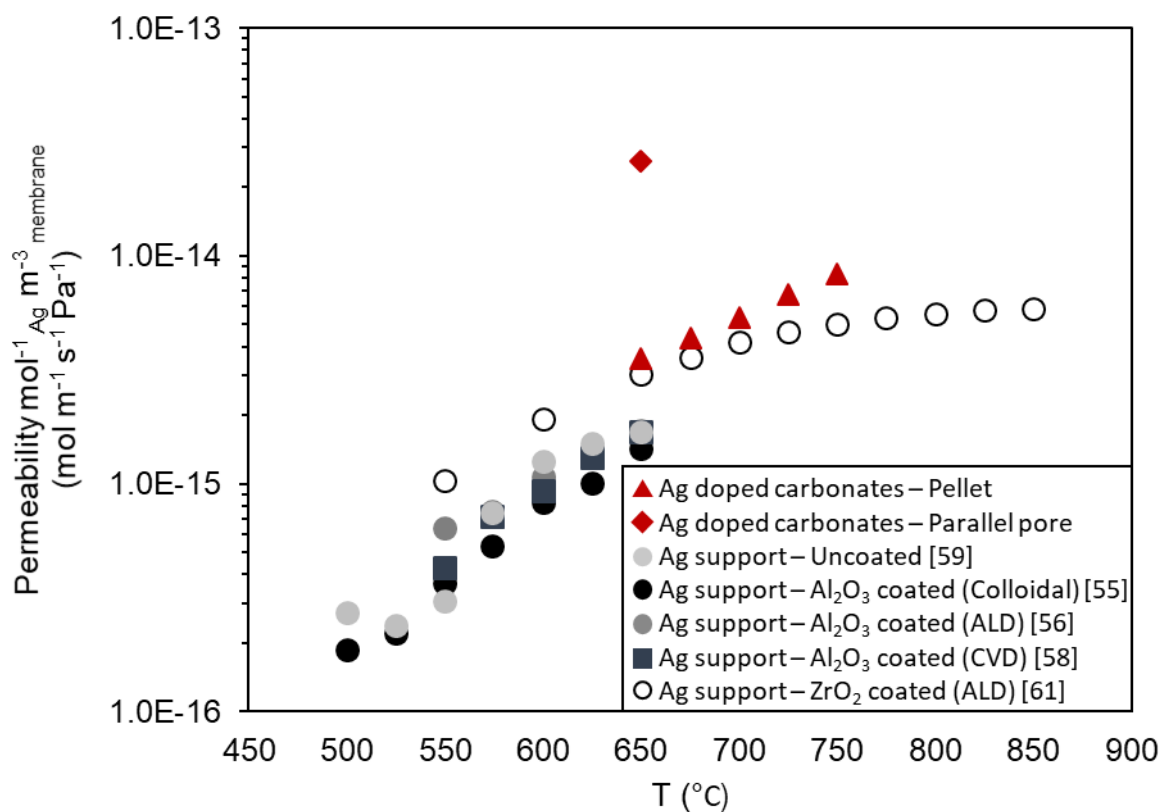
Fig. 5. 17 Comparison of CO_2 permeability per mol of Ag for the 6 mol% Ag-doped carbonate pellet and parallel pore membranes developed in this study, with wholly Ag-supported membranes available in the literature.

Clearly, to achieve the high fluxes that Ag-supported membranes are capable of, it is not necessary for the entire support to be fabricated from Ag. Instead, a low-cost support such as Al_2O_3 can be used in its place while a small quantity of Ag can be added into the carbonates, and permeation used to create a self-assembling dendritic Ag electronically conductive support. The amount of Ag used for the parallel pore membrane was 4 mg compared to ~4 g used for the uncoated Ag membrane, albeit on research scale (Fig. 5. 17).

While it is clear that the parallel pore membrane is not a viable option for scale-up due to the cost of laser drilling the pores, the principle of reducing the amount of Ag used is clear. Furthermore, the parallel pore membrane was designed with large pores to help visualise the Ag location inside a pore for the nano-CT study, therefore the capillary pressure in a single pore is lower than a pellet support, which is not ideal for long-term operation or for pressurised operation. To achieve fluxes similar to the parallel pore system whilst reducing the cost of the Al_2O_3 support, it is suggested that a well-controlled pore forming technique is used, such as those displayed by hollow fibre membranes prepared by combined phase inversion and sintering method [133].

5.4 Conclusion

The work presented in this chapter displayed advancements made in the understanding of the Ag/Al$_2$O$_3$-MC membrane:

- The method of Ag introduction was simplified. It was found that 6 mol% Ag powder loading in molten carbonate produced the highest CO$_2$ flux of 9.5×10^{-2} mL min^{-1} cm^{-2} with a 2:1 CO$_2$:O$_2$ flux ratio.

- When Ag is introduced below the solubility limit (0.0125 mol%) there is minimal flux improvement compared to membranes doped with enough Ag to form electronically conductive pathways. This indicates that the formation of the Ag electron-conducting pathways are required to achieve the highest flux improvement.

- The 6 mol% Ag/Al$_2$O$_3$-MC membrane was able to reach stable flux between 650-750°C without showing any decline in gas flux and maintaining the same 2:1 CO$_2$: O$_2$ ratio throughout.

- The Au sealant limited the membranes operation to 115 hours of use. Using an Ag sealant allowed the membrane to operate for a minimum of 450 hours without leaking. However, it was found the Ag sealant contributed to the gas flux by creating an electron-conducting bridge across the membrane resulting in Ag migrating to the permeate side and blocking off the membrane.

- The time-resolved mechanistic study identified that the Ag pathways form by the precipitation of Ag on the permeate side (also seen in Chapter 4), which creates a nucleation point for the pathways to extend back towards the feed side during permeation.

- The electron-conducting pathways were found to only partially cover the Al$_2$O$_3$ pore walls. This could explain why the membrane did not suffer leaks due carbonate retention issues because of sufficient contact between the melt and the highly wettable Al$_2$O$_3$ support.

- Two-point DC confirmed that membranes operated for less than 10 hours were not conductive which supports the CT results which depict that connected pathways are only present after 10 hours of operation.

- After modifying the membranes pore geometry and thickness using the parallel pore membrane, a CO$_2$ flux of 1.25 mL min^{-1} cm^{-2} at 650°C was achieved. This flux is higher than any electron-conducting membrane reported in the literature regardless of temperature, while using 3 orders of magnitude less Ag.

Chapter Six – Conclusion and Future Work

This Chapter summarises the results and discussion from the three results chapters presented in this thesis and provides details of recommendations for future work to be conducted in this field of study.

6.1   Conclusion

The research presented in this thesis focussed on the fabrication of a low-cost, high-flux dual-phase membrane by using a cheap, inert support infiltrated with a modified molten carbonate. This work presents a novel contribution to the dual-phase membrane literature as the first study to provide functionality to an otherwise inert support by doping the molten carbonate melt with a foreign material, resulting in an increase in gas flux. Specifically, a cheap, inert Al_2O_3 support infiltrated with a molten carbonate doped with Ag was found to achieve fluxes greater than any Ag-supported dual-phase membrane reported in the literature, at 650°C. Conversely, molten carbonate doped with La_2O_3 had no observable effect on gas flux. Similarly, the addition of oxide species into the melt *via* the introduction of O_2 into the permeate-side inlet had limited effect on flux improvement.

The first objective of this thesis was to determine which process was slower between the uptake and release of CO_2 on each side of the dual-phase membrane. Using a non-conducting Al_2O_3 support the release of CO_2 from the permeate-side surface of the membrane was found to be slower. Using this finding, two different approaches were made to increase the rate of this process. Since it has been previously reported that oxide conductivity in the melt can limit gas transport, particularly when an inert support is used, the two methods explored here aimed to manipulate the oxide concentration within the melt in order to increase carbonate ion transport and subsequently increase CO_2 flux. The first approach introduced a dopant, or foreign cation, into the melt that had a lower stability in its carbonate form than the alkali cations already present, *i.e.* the release of CO_2 and oxide ions (or decomposition) was more thermodynamically favourable for the dopant. Therefore, the less stable cation, in this case La, would more readily release CO_2 and oxide ions on the permeate side, thus improving the gaseous flux across the membrane. However, due to the low solubility of La_2O_3 in molten carbonate, only 0.5 mol% could be added under high pCO_2 and an order of magnitude less for low pCO_2. Therefore, when 0.5 mol% La_2O_3 was added to the molten carbonate, the La cations migrated down their concentration gradient to the permeate side during permeation, causing exposure to pure Ar, *i.e.* low pCO_2, which resulted in precipitation of the La, thus removing any effect on flux. The precipitation caused a blockage on the permeate-side surface, which resulted in a decline in CO_2 flux. The second method attempted to replace the conventional carbonate decomposition reaction on the permeate-side surface with a reaction that introduces oxide ions into the melt. This was achieved by introducing O_2 into the permeate-side inlet gas with Ar. By manipulating the permeate-side gas feed *via* the introduction of O_2, a ~50% increase in flux was produced when compared to using pure Ar in the permeate-side inlet, however this flux remained over an

138

order of magnitude lower the best dual-phase membranes in the literature. Similar to the La_2O_3 work, the reason for the limited flux improvement is due to the low solubility of O_2 in molten carbonate. Therefore, to achieve high fluxes by doping the molten carbonate, the dopant should likely still offer performance enhancement if it precipitates out of solution *i.e.* the precipitated dopant must be conductive.

As an alternative method for molten carbonate modification to enhance gas flux, the molten carbonate was used as a carrier to redistribute Ag to form electron-conducting pathways. Conversely to Chapter 3, it was essential for this dopant to have low solubility in molten carbonate. However, unlike the precipitated $La_2O_2CO_3$ from Chapter 3, which acted as an insulator, the precipitated Ag reverts to its metallic, electron-conducting form. Therefore, the Ag could be manipulated to pose an effect on the membrane after it precipitates. Thus, based on the non-equilibrium conditions in dual-phase membranes, Ag was used to form electronically conductive dendrites, resulting in a low-Ag content, high-flux, electron-conducting dual-phase membrane, namely an Ag/Al_2O_3-MC membrane.

In Chapter 4, the first dendritic Ag/Al_2O_3-MC membrane was fabricated. To achieve this, Ag was introduced into the membrane *via* electroless-plating and molten carbonate carried the Ag throughout the membrane *in-situ* during gas permeation. The redistribution of Ag to create connected Ag dendrites across the membrane occurred *via* four hypothesised stages: Ag dissolution on the feed side, migration to the permeate side, precipitation on the permeate side and growth back to the feed side. The *in-situ* formation of the Ag/Al_2O_3-MC membrane was tested under different gaseous driving forces and it was found that CO_2 and O_2 needed to be present together in the feed gas for all four of the hypothesised stages to occur. Micro-CT and two-point DC were used on tested Ag-plated membranes to confirm the presence and conduction of the Ag dendrites, respectively. However, these techniques were unable to ascertain the order in which the hypothesized stages occurred. Furthermore, while the electroless-plated membrane offered a 500% flux improvement when compared to a reference undoped membrane of the same support material and geometry, the flux was still an order of magnitude lower than the best wholly Ag-supported membranes.

Chapter 5 built upon the work presented in presented in Chapter 4. This was approached from two angles: understanding the mechanism for dendrite growth and further testing for improvement of the Ag/Al_2O_3-MC membrane. For the former, a time-resolved mechanistic study was performed. This study confirmed the order in which the four hypothesised stages for the formation of the dendrites occur. Using micro-CT complemented by flux data, it was found that the Ag dendrites formed by Ag^+ migrating down their electrochemical gradient to the

permeate side and precipitating to reform Ag. This creates a nucleation point for subsequent Ag precipitation, which causes Ag to extend back towards the feed-side surface. This process occurred during the first 10 hours of operation while the flux was at its lowest, with all membranes prior to this point showing no connected dendrites across the membrane. After 10 hours, the membrane exhibited an increase in gas flux, which can be explained by the newly formed electron-conducting dendrites, which occur at the same time. This is supported by two-point DC which shows that the membranes had a greater resistance before 10 hours of operation *i.e.* since connected electron-conductive pathways had not yet been formed across the membrane, no conductivity was measured, which explains the low flux in this region.

To understand the Ag/Al$_2$O$_3$-MC membranes flux capabilities, further permeation experiments were conducted. Firstly, the method of Ag introduction into the membrane was simplified by adding Ag powder directly into the molten carbonate. This lowered the membranes fabrication time and cost and removed hazards associated with electroless-plating. A study of the effect Ag loading in the molten carbonate has on flux was carried out. It was found that 6 mol% loading achieved the highest CO$_2$ flux of 9.5×10^{-2} mL (NPT) min^{-1} cm^{-2}.

Using the optimal Ag loading in the molten carbonate, the membranes ability to operate at temperatures exceeding 650°C was tested. This study showed that the 6 mol% Ag/Al$_2$O$_3$-MC membrane was able to achieve stable flux at temperatures reaching up to 750°C without showing any sign of flux degradation. The CO$_2$ flux at 750°C was 22×10^{-2} mL (NPT) min^{-1} cm^{-2} and maintained the same 2:1 CO$_2$:O$_2$ flux ratio. This indicates that the membrane was able to sufficiently retain molten carbonate within its pores at high temperatures, which prevented a shift in the CO$_2$:O$_2$ ratio in favour of O$_2$, which has been seen with some Ag-supported membranes in the literature. This was supported by a high-resolution CT scan of a used Ag/Al$_2$O$_3$-MC membrane, which showed that Ag does not coat the entire wall of the support, allowing sufficient contact with the highly wettable Al$_2$O$_3$ support. However, the 6 mol% Ag/Al$_2$O$_3$-MC membrane succumbed to leaks beyond 750°C due to breaks in the sealant. Furthermore, at 650°C the membrane was unable to operate beyond 115 hours before leaking due to the same reason. Therefore, attempts were made to improve the membranes stability by replacing the Au ink sealant with a more commonly used Ag ink sealant. This study found that, the new sealant allowed the membrane to operate for a minimum of 450 hours without any leaks. However, the sealant interfered with the membranes flux by acting as an electron-conducting bridge, allowing a peak flux 2.5 times higher than the same membrane with an Au sealant. This interaction with gas transport caused the sealant to migrate to the permeate-side active area in competition with the Ag powder from the feed side. This resulted in the membrane

permeate-side surface becoming blocked due to Ag build-up, which caused a decline in flux beyond 150 hours. This result showed us that the Ag/Al_2O_3-MC membranes have potential to operate for hundreds of hours and likely do not suffer the same wettability issues as other wholly Ag-supported membranes. However, it is recommended that when trying to fairly assess the flux capabilities of a new support material, especially an electronically conductive material, that Ag is not used as the sealant. Au should also not be used, while the corrosion is negligible in molten carbonates, the sealant does still offer an electron-conducting bridge for increased CO_2 and O_2 flux, albeit to a much lower degree than Ag.

By decreasing the Ag/Al_2O_3-MC membranes thickness and pore tortuosity by using a novel parallel pore membrane support, a CO_2 flux of 1.25 mL min^{-1} cm^{-2} at 650°C was achieved, which is a factor of 13 higher than the pressed-pellet membrane. This reported flux is unparalleled by any electron-conducting support in the literature at 650°C. Furthermore, the amount of Ag used for this membrane was three orders of magnitude lower than an Ag-supported membrane, albeit on a research scale. It should also be noted that the parallel pore membrane had no hot sealing region, thus it can be confidently deduced that the route of gas transport was not affected by any factors aside from the addition of Ag into the carbonate melt. The only dual-phase membrane fed with CO_2 alone or CO_2 and O_2 together to out-perform this membrane in terms of flux was an asymmetric tubular SDC membrane operating at 850°C or above. The 6 mol% Ag/Al_2O_3-MC parallel pore membrane reached a permeance and permeability in the range reported as required for economically competitive carbon capture (1.9 × 10^{-7} mol m^{-2} s^{-1} Pa^{-1} where the target is 10^{-7} mol m^{-2} s^{-1} Pa^{-1} and 9.4 × 10^{-11} mol m^{-2} s^{-1} Pa^{-1} where the target is 10^{-13}-10^{-12} mol m^{-1} s^{-1} Pa^{-1}).

6.2   Future Work

The results presented in this thesis explore the initial findings of a new high-flux dual-phase membrane for CO_2 separation. However, more work can be done improve the membrane further. Below is a non-exhaustive list of recommendations for how this work can be progressed further in the future:

- *Test different CO_2 and O_2 ratios* – The membranes presented in this study were subjected to 2:1 $CO_2:O_2$ gas feed ratios. Due to the stoichiometry of the reaction mechanisms suggested in the literature and in this work, the gas flux was the same 2:1 ratio. While no leak was detected across the membrane, thus supporting the proposed mechanisms, it would be useful to understand how the flux ratio behaves with variation of the feed gas composition.

- *In-situ conductivity tests* – Post-experiment electron conductivity tests presented in this study provided evidence of electron conducting pathways, supported by CT and SEM analysis. While the time resolved mechanistic study gave an indication of the time region in which these pathways form, an *in-situ* electron conductivity experiment would provide a more precise measurement, which can be correlated in real-time with the increase in flux witnessed during the same time region. Furthermore, *in-situ* oxide ion conductivity measurements would be useful in parallel with electron conductivity measurements to understand how the oxide conductivity changes as the Ag pathways form (and thicken) resulting in a decrease in support porosity. As mentioned by other authors in the literature, a balance must be made between the conductivity of the support and the porosity of the membrane. By performing *in-situ* mixed conductivity tests this relationship can be explored.

- *Improve sealant for long term operation* – In this study, the use of a Ag sealant displayed the membranes ability to operate for a minimum of 450 hrs without succumbing to transmembrane leaks. However, due to the electron conductivity of the Ag sealant and its interaction with the molten salt and the feed gas, the sealant migrated to the permeate-side surface resulting in an initial increase in gas flux followed by a subsequent decrease due to blockage of the permeate-side surface. To improve the longevity of the dual-phase membrane, while restricting the interaction with the molten salt and gas phase, an inert sealant should be used in the future.

- *In-situ Ag migration visualisation* – The time resolved mechanistic study revealed that the Ag pathways initially migrate to the permeate-side surface before extending back towards the feed-side surface. A reason for this is due to the migrated Ag forming a

nucleation point which decreases the diffusional path length for the migrating Ag. While values for Ag solubility in molten carbonate reported in the literature suggest that the pathways are solid during permeation it would be useful to see how the pathways grow to help confirm the nucleation hypothesis suggested in this thesis. A possible methodology for this study would be to use an Al_2O_3 single crystal porous support with one surface plated with Ag and infiltrated with molten carbonate. Then using a microscope and the application of a gaseous driving force the Ag migration and pathway growth process could be visualised in real-time. Alternatively, if the membrane cell is unable to create a gaseous driving force due to the availability of only one gaseous feed, then a blanked pore filled with molten carbonate could be used and an inert bubble can be created inside the molten carbonate filled blank pore, which simulates the same gaseous driving force environment as a dual-phase membrane.

- *Co-permeated O_2 removal* – In this thesis, Ar was used as the permeate-side inlet gas to simulate the conditions for gas separation using a dual-phase membrane. However, this set-up is unlikely to be used for future scale-up as the permeate-side outlet is a mixture of CO_2, O_2 and Ar, thus the Ar needs to be removed, as well as the co-permeated O_2. To test whether this is possible using membrane presented here, it is suggested that the membrane system described by Fang *et al.* [58] is explored. Using this membrane set-up, the co-permeated O_2 can be removed by adding H_2 into the permeate-side inlet to produce steam which can be condensed to create a pure CO_2 product.

- *Geometry optimisation* – Two membrane geometries were explored in this thesis. The first pressed pellet geometry provided a thick support which was ideal to understand how the pathways grow during permeation. However, the random pore network combined with the comparatively large membrane thickness meant the flux suffered. Alternatively, the parallel pore membrane provided thin, well-defined, controlled and straight pores which resulted in an order of magnitude increase in gas flux compared to the pressed pellet membrane. Furthermore, the parallel pore membrane allowed a reliable assessment of the membranes capabilities due to the removal of flux contribution from a sealant. However, while this geometry displayed the importance of straight pores, the pores were fabricated used a laser which is expensive, and the flat disk-like geometry is not ideal for effective upscale membrane packing. Therefore, it is suggested that the membrane is fabricated in a hollow fibre geometry.

References

[1] F. Joos and R. Spahni, "Rates of change in natural and anthropogenic radiative forcing over the past 20,000 years," *Proc. Natl. Acad. Sci.*, vol. 105, no. 5, pp. 1425–1430, 2008.

[2] NOAA Research, "Trends in Atmospheric Carbon Dioxide," 2019. [Online]. Available: https://www.esrl.noaa.gov/gmd/ccgg/trends/global.html.

[3] C. Le Quéré *et al.*, "Global Carbon Budget 2017," *Earth Syst. Sci. Data Discuss.*, vol. pre print, no. November, pp. 1–79, 2017.

[4] GCCSI, "Global status of CCS. Special report: Introduction to industrial carbon capture and storage," 2016.

[5] IEA and UNIDO, "Technology roadmap: Carbon capture and storage in industrial applications," 2011.

[6] N. MacDowell *et al.*, "An overview of CO_2 capture technologies," *Energy Environ. Sci.*, vol. 3, no. 11, pp. 1645–1669, 2010.

[7] M. Bui *et al.*, "Carbon capture and storage (CCS): The way forward," *Energy Environ. Sci.*, vol. 11, no. 5, pp. 1062–1176, 2018.

[8] M. E. Boot-Handford *et al.*, "Carbon capture and storage update," *Energy Environ. Sci.*, vol. 7, no. 1, pp. 130–189, 2014.

[9] R. Anantharaman, T. Peters, W. Xing, M. L. Fontaine, and R. Bredesen, "Dual phase high-temperature membranes for CO_2 separation-performance assessment in post- and pre-combustion processes," *Faraday Discuss.*, vol. 192, pp. 251–269, 2016.

[10] G. T. Rochelle, "Amine Scrubbing for CO_2 Capture," *Science (80-.).*, vol. 325, no. 5948, pp. 1652–1654, 2009.

[11] Global CCS Institute, "CO_2 Capture Technologies - Post Combustion Carbon Capture (PCC)," 2012.

[12] S. Wang *et al.*, "Advances in high permeability polymer-based membrane materials for CO_2 separations," *Energy Environ. Sci.*, vol. 9, no. 6, pp. 1863–1890, 2016.

[13] C. G. Bezzu *et al.*, "A spirobifluorene-based polymer of intrinsic microporosity with improved performance for gas separation," *Adv. Mater.*, vol. 24, no. 44, pp. 5930–5933, 2012.

[14] M. Carta *et al.*, "Triptycene induced enhancement of membrane gas selectivity for microporous Tröger's base polymers," *Adv. Mater.*, vol. 26, no. 21, pp. 3526–3531, 2014.

[15] S. Kasahara, E. Kamio, T. Ishigami, and H. Matsuyama, "Effect of water in ionic liquids on CO_2 permeability in amino acid ionic liquid-based facilitated transport membranes," *J. Memb. Sci.*, vol. 415–416, pp. 168–175, 2012.

[16] S. Kasahara, E. Kamio, and H. Matsuyama, "Improvements in the CO_2 permeation selectivities of amino acid ionic liquid-based facilitated transport membranes by controlling their gas absorption properties," *J. Memb. Sci.*, vol. 454, pp. 155–162, 2014.

[17] S. Kasahara, E. Kamio, A. Yoshizumi, and H. Matsuyama, "Polymeric ion-gels containing an amino acid ionic liquid for facilitated CO_2 transport media," *Chem. Commun.*, vol. 50, no. 23, pp. 2996–2999, 2014.

[18] M. M. Khan *et al.*, "Enhanced gas permeability by fabricating mixed matrix membranes of functionalized multiwalled carbon nanotubes and polymers of intrinsic microporosity (PIM)," *J. Memb. Sci.*, vol. 436, pp. 109–120, 2013.

[19] J. Liao *et al.*, "Fabrication of high-performance facilitated transport membranes for CO_2 separation," *Chem. Sci.*, vol. 5, no. 7, pp. 2843–2849, 2014.

[20] A. S. Kovvali, H. Chen, and K. K. Sirkar, "Dendrimer membranes: A CO_2-selective molecular gate [2]," *J. Am. Chem. Soc.*, vol. 122, no. 31, pp. 7594–7595, 2000.

[21] H. P. Hsieh, *Inorganic Membranes for Separation and Reaction*, 3rd ed. Elsevier Science, 1996.

[22] Y. S. Lin, "Microporous and dense inorganic membranes: Current status and prospective," *Sep. Purif. Technol.*, vol. 25, no. 1–3, pp. 39–55, 2001.

[23] M. Anderson, H. Wang, and Y. S. Lin, "Inorganic membranes for carbon dioxide and nitrogen separation," *Rev. Chem. Eng.*, vol. 28, no. 2–3, pp. 101–121, 2012.

[24] Y. Hasegawa, T. Tanaka, K. Watanabe, K. Byeong-Heon, Jeong Kusakabe, and S. Morooka, "Separation of CO_2-CH_4 and CO_2-N_2 systems using ion-exchanged FAU-type zeolite membranes with different Si/Al ratios," *Korean J. Chem. Eng.*, vol. 19, no. 2, pp. 309–313, 2002.

[25] X. Gu, J. Dong, and T. M. Nenoff, "Synthesis of defect-free FAU-type zeolite

membranes and separation for dry and moist CO_2/N_2 mixtures," *Ind. Eng. Chem. Res.*, vol. 44, no. 4, pp. 937–944, 2005.

[26] K. Kusakabe, T. Kuroda, and S. Morooka, "Separation of carbon dioxide from nitrogen using ion-exchanged faujasite-type zeolite membranes formed on porous support tubes," *J. Memb. Sci.*, vol. 148, no. 1, pp. 13–23, 1998.

[27] L. M. Robeson, "Correlation of separation factor versus permeability for polymeric membranes," *J. Memb. Sci.*, vol. 62, pp. 165–185, 1991.

[28] L. M. Robeson, "The upper bound revisited," *J. Memb. Sci.*, vol. 320, no. 1–2, pp. 390–400, 2008.

[29] B. Cales and J. F. Baumard, "Oxygen semipermeability and electronic conductivity in calcia-stabilized zirconia," *J. Mater. Sci.*, vol. 17, no. 11, pp. 3243–3248, 1982.

[30] B. Cales and J. F. Baumard, "Mixed Conduction and Defect Structure of ZrO_2-CeO_2-Y_2O_3 Solid-Solutions," *J. Electrochem. Soc.*, vol. 131, no. 10, pp. 2407–2413, 1984.

[31] J. Sunsaro, S. Baumann, J. M. Serra, W. A. Meulenberg, S. Liu, and Y. S. Lin, "Mixed ionic-electronic conducting (MIEC) ceramic-based membranes for oxygen separation," *J. Memb. Sci.*, vol. 320, no. 1–2, pp. 13–41, 2008.

[32] S. Yun and S. Ted Oyama, "Correlations in palladium membranes for hydrogen separation: A review," *J. Memb. Sci.*, vol. 375, no. 1–2, pp. 28–45, 2011.

[33] N. W. Ockwig and T. M. Nenoff, "Membranes for Hydrogen Separation," *Chem. Rev.*, vol. 10, no. 107, pp. 4078–4110, 2007.

[34] J. Kniep and Y. S. Lin, "Effect of zirconium doping on hydrogen permeation through strontium cerate membranes," *Ind. Eng. Chem. Res.*, vol. 49, no. 6, pp. 2768–2774, 2010.

[35] Z. Rui, M. Anderson, Y. S. Lin, and Y. Li, "Modeling and analysis of carbon dioxide permeation through ceramic-carbonate dual-phase membranes," *J. Memb. Sci.*, vol. 345, no. 1–2, pp. 110–118, 2009.

[36] J. L. Wade, K. S. Lackner, and A. C. West, "Transport model for a high temperature, mixed conducting CO2 separation membrane," *Solid State Ionics*, vol. 178, no. 27–28, pp. 1530–1540, 2007.

[37] T. Yamaguchi, T. Niitsuma, B. N. Nair, and K. Nakagawa, "Lithium silicate based membranes for high temperature CO2 separation," *J. Memb. Sci.*, vol. 294, no. 1–2, pp.

16–21, 2007.

[38]   X. Dong, J. Ortiz Landeros, and Y. S. Lin, "An asymmetric tubular ceramic-carbonate dual phase membrane for high temperature CO2separation," *Chem. Commun.*, vol. 49, no. 83, pp. 9654–9656, 2013.

[39]   Y. S. L. T. T. Norton, J. O. Landeros, "Stability of La − Sr − Co − Fe Oxide − Carbonate Dual-Phase Membranes for Carbon Dioxide Separation at High Temperatures," *Ind. Eng. Chem. Res*, vol. 69, no. 13, pp. 1005–1020, 2014.

[40]   T. T. Norton and Y. S. Lin, "Ceramic-carbonate dual-phase membrane with improved chemical stability for carbon dioxide separation at high temperature," *Solid State Ionics*, vol. 263, pp. 172–179, 2014.

[41]   M. Anderson and Y. S. Lin, "Carbonate-ceramic dual-phase membrane for carbon dioxide separation," *J. Memb. Sci.*, vol. 357, no. 1–2, pp. 122–129, 2010.

[42]   H. Ahn *et al.*, "YSZ-carbonate dual-phase membranes for high temperature carbon dioxide separation," *J. Ind. Eng. Chem.*, vol. 20, no. 5, pp. 3703–3708, 2014.

[43]   O. Ovalle-Encinia, H. Pfeiffer, and J. Ortiz-Landeros, "$Ce_{0.85}Sm_{0.15}O_2$-$Sm_{0.6}Sr_{0.4}Al_{0.3}Fe_{0.7}O_3$ composite for the preparation of dense ceramic-carbonate membranes for CO2 separation," *J. Memb. Sci.*, vol. 547, no. October 2017, pp. 11–18, Feb. 2018.

[44]   S. G. Patrício, E. Papaioannou, G. Zhang, I. S. Metcalfe, and F. M. B. Marques, "High performance composite CO2 separation membranes," *J. Memb. Sci.*, vol. 471, pp. 211–218, 2014.

[45]   E. I. Papaioannou, H. Qi, and I. S. Metcalfe, "'Uphill' permeation of carbon dioxide across a composite molten salt-ceramic membrane," *J. Memb. Sci.*, vol. 485, pp. 87–93, 2015.

[46]   Z. Rui, M. Anderson, Y. Li, and Y. S. Lin, "Ionic conducting ceramic and carbonate dual phase membranes for carbon dioxide separation," *J. Memb. Sci.*, vol. 417–418, pp. 174–182, 2012.

[47]   T. T. Norton, B. Lu, and Y. S. Lin, "Carbon dioxide permeation properties and stability of samarium-doped-ceria carbonate dual-phase membranes," *J. Memb. Sci.*, vol. 467, pp. 244–252, 2014.

[48] M. Zuo, S. Zhuang, X. Tan, B. Meng, N. Yang, and S. Liu, "Ionic conducting ceramic-carbonate dual phase hollow fibre membranes for high temperature carbon dioxide separation," *J. Memb. Sci.*, vol. 458, pp. 58–65, 2014.

[49] J. Tong, L. Zhang, M. Han, and K. Huang, "Electrochemical separation of CO_2 from a simulated flue gas with high-temperature ceramic-carbonate membrane: New observations," *J. Memb. Sci.*, vol. 477, pp. 1–6, 2015.

[50] J. Tong, L. Zhang, J. Fang, M. Han, and K. Huang, "Electrochemical Capture of CO_2 from Natural Gas Using a High-Temperature Ceramic-Carbonate Membrane," *J. Electrochem. Soc.*, vol. 162, no. 4, pp. E43–E46, 2015.

[51] L. Zhang *et al.*, "High CO2 permeation flux enabled by highly interconnected three-dimensional ionic channels in selective CO2 separation membranes," *Energy Environ. Sci.*, vol. 5, no. 8, pp. 8310–8317, 2012.

[52] L. Zhang, X. Li, S. Wang, K. G. Romito, and K. Huang, "High conductivity mixed oxide-ion and carbonate-ion conductors supported by a prefabricated porous solid-oxide matrix," *Electrochem. commun.*, vol. 13, no. 6, pp. 554–557, 2011.

[53] J. L. Wade, C. Lee, A. C. West, and K. S. Lackner, "Composite electrolyte membranes for high temperature CO_2 separation," *J. Memb. Sci.*, vol. 369, no. 1–2, pp. 20–29, 2011.

[54] L. Zhang, Y. Gong, K. S. Brinkman, T. Wei, S. Wang, and K. Huang, "Flux of silver-carbonate membranes for post-combustion CO_2 capture: The effects of membrane thickness, gas concentration and time," *J. Memb. Sci.*, vol. 455, pp. 162–167, 2014.

[55] L. Zhang, Y. Gong, J. Yaggie, S. Wang, K. Romito, and K. Huang, "Surface modified silver-carbonate mixed conducting membranes for high flux CO_2 separation with enhanced stability," *J. Memb. Sci.*, vol. 453, pp. 36–41, 2014.

[56] P. Zhang, J. Tong, and K. Huang, "A self-forming dual-phase membrane for high-temperature electrochemical CO_2 capture," *J. Mater. Chem. A*, vol. 5, no. 25, pp. 12769–12773, 2017.

[57] J. Tong, X. Lei, J. Fang, M. Han, and K. Huang, "Remarkable O_2 permeation through a mixed conducting carbon capture membrane functionalized by atomic layer deposition," *J. Mater. Chem. A*, vol. 4, no. 5, pp. 1828–1837, 2016.

[58] J. Fang, J. Tong, and K. Huang, "A superior mixed electron and carbonate-ion conducting metal-carbonate composite membrane for advanced flue-gas carbon

capture," *J. Memb. Sci.*, vol. 505, pp. 225–230, 2016.

[59] J. Tong, F. Si, L. Zhang, J. Fang, M. Han, and K. Huang, "Stabilizing electrochemical carbon capture membrane with Al_2O_3 thin-film overcoating synthesized by chemical vapor deposition," *Chem. Commun.*, vol. 51, no. 14, pp. 2936–2938, 2015.

[60] N. Xu, X. Li, M. A. Franks, H. Zhao, and K. Huang, "Silver-molten carbonate composite as a new high-flux membrane for electrochemical separation of CO_2 from flue gas," *J. Memb. Sci.*, vol. 401–402, pp. 190–194, 2012.

[61] S. J. Chung, J. H. Park, D. Li, J. I. Ida, I. Kumakiri, and J. Y. S. Lin, "Dual-phase metal-carbonate membrane for high-temperature carbon dioxide separation," *Ind. Eng. Chem. Res.*, vol. 44, no. 21, pp. 7999–8006, 2005.

[62] P. Zhang, J. Tong, Y. Jee, and K. Huang, "Stabilizing a high-temperature electrochemical silver-carbonate CO_2 capture membrane by atomic layer deposition of a ZrO_2 overcoat," *Chem. Commun.*, vol. 52, no. 63, pp. 9817–9820, 2016.

[63] L. Zhang, J. Tong, Y. Gong, M. Han, S. Wang, and K. Huang, "Fast electrochemical CO_2 transport through a dense metal-carbonate membrane: A new mechanistic insight," *J. Memb. Sci.*, vol. 468, pp. 373–379, 2014.

[64] J. Fang, N. Xu, T. Yang, P. Zhang, J. Tong, and K. Huang, "CO_2 capture performance of silver-carbonate membrane with electrochemically dealloyed porous silver matrix," *J. Memb. Sci.*, vol. 523, no. July 2016, pp. 439–445, 2017.

[65] N. T. Veziroglu, S. A. Sherif, and F. Barbir, *Hydrogen energy solutions*. Elsevier Inc., 2005.

[66] A. L. Dicks, "Molten carbonate fuel cells," *Curr. Opin. Solid State Mater. Sci.*, vol. 8, no. 5, pp. 379–383, 2004.

[67] S. Scaccia, S. Frangini, and S. Dellepiane, "Enhanced O_2 solubility by RE2O3 (RE = La, Gd) additions in molten carbonate electrolytes for MCFC," *J. Mol. Liq.*, vol. 138, no. 1–3, pp. 107–112, 2008.

[68] O. Ovalle-Encinia, H. Pfeiffer, and J. Ortiz-Landeros, "CO_2 Separation Improvement Produced on a Ceramic–Carbonate Dense Membrane Superficially Modified with Au–Pd," *Ind. Eng. Chem. Res.*, vol. 57, no. 28, pp. 9261–9268, 2018.

[69] P. Zhang, J. Tong, and K. Huang, "Self-Formed, Mixed-Conducting, Triple-Phase

Membrane for Efficient CO_2 /O_2 Capture from Flue Gas and in Situ Dry-Oxy Methane Reforming," *ACS Sustain. Chem. Eng.*, vol. 6, no. 11, pp. 14162–14169, 2018.

[70] Z. Rui, H. Ji, and Y. S. Lin, "Modeling and analysis of ceramic-carbonate dual-phase membrane reactor for carbon dioxide reforming with methane," *Int. J. Hydrogen Energy*, vol. 36, no. 14, pp. 8292–8300, 2011.

[71] P. Zhang, J. Tong, and K. Huang, "Combining Electrochemical CO_2 Capture with Catalytic Dry Methane Reforming in a Single Reactor for Low-Cost Syngas Production," *ACS Sustain. Chem. Eng.*, vol. 4, no. 12, pp. 7056–7065, 2016.

[72] M. Anderson and Y. S. Lin, "Carbon Dioxide Separation and Dry Reforming of Methane for Synthesis of Syngas by a Dual-phase Membrane Reactor," *AIChE J.*, vol. 59, no. 6, pp. 2207–2218, 2013.

[73] X. Dong and Y. S. Lin, "Catalyst-free ceramic-carbonate dual phase membrane reactor for hydrogen production from gasifier syngas," *J. Memb. Sci.*, vol. 520, pp. 907–913, 2016.

[74] X. Dong and W. Jin, "Mixed conducting ceramic membranes for high efficiency power generation with CO2 capture," *Curr. Opin. Chem. Eng.*, vol. 1, no. 2, pp. 163–170, 2012.

[75] U. Ali *et al.*, "Process simulation and thermodynamic analysis of a micro turbine with post-combustion CO_2 capture and exhaust gas recirculation," *Energy Procedia*, vol. 63, no. 44, pp. 986–996, 2014.

[76] N. Bryan *et al.*, "Development of mixed matrix membranes containing zeolites for post-combustion carbon capture," *Energy Procedia*, vol. 63, pp. 160–166, 2014.

[77] A. Brune, M. Lajavardi, D. Fisler, and J. . Wagner Jr., "The electrical conductivity of yttria-stabilized zirconia prepared by precipitation from inorganic aqueous solutions," *Solid State Ionics*, vol. 106, no. 1–2, pp. 89–101, 2002.

[78] L. C. Wen *et al.*, "Electrical properties of Sm-doped ceria (SDC) and SDC carbonate composite," *J. Chinese Chem. Soc.*, vol. 60, no. 11, pp. 1359–1364, 2013.

[79] I. Bloom, M. T. Lanagan, M. Krumpelt, and J. L. Smith, "The Development of $LiFeO_2$ - $LiCoO_2$ -NiO Cathodes for Molten Carbonate Fuel Cells," *Cell*, vol. 146, no. 4, pp. 1336–1340, 1999.

[80] J. M. Fisher and P. S. Bennett, "Corrosion and wetting behaviour of metals and steels

with molten alkali carbonates," *J. Mater. Sci.*, vol. 26, no. 3, pp. 749–755, 1991.

[81] J. Ortiz-Landeros, T. Norton, and Y. S. Lin, "Effects of support pore structure on carbon dioxide permeation of ceramic-carbonate dual-phase membranes," *Chem. Eng. Sci.*, vol. 104, pp. 891–898, 2013.

[82] B. Lu and Y. S. Lin, "Asymmetric thin samarium doped cerium oxide-carbonate dual-phase membrane for carbon dioxide separation," *Ind. Eng. Chem. Res.*, vol. 53, no. 34, pp. 13459–13466, 2014.

[83] X. Dong, H. C. Wu, and Y. S. Lin, "CO_2 permeation through asymmetric thin tubular ceramic-carbonate dual-phase membranes," *J. Memb. Sci.*, vol. 564, no. July, pp. 73–81, 2018.

[84] B. Lu and Y. S. Lin, "Synthesis and characterization of thin ceramic-carbonate dual-phase membranes for carbon dioxide separation," *J. Memb. Sci.*, vol. 444, pp. 402–411, 2013.

[85] Y. Kanazawa and M. Kamitani, "Rare earth minerals and resources in the world," *J. Alloys Compd.*, vol. 408–412, pp. 1339–1343, 2006.

[86] H. Onoda and Y. Kurioka, "Selective removal and recovery of samarium from mixed transition metal solution using phosphoric acid," *J. Environ. Chem. Eng.*, vol. 4, no. 4, pp. 4536–4539, 2016.

[87] K. C. Sole, J. Parker, P. M. Cole, and M. B. Mooiman, "Flowsheet options for cobalt recovery in African copper–cobalt hydrometallurgy circuits," *Miner. Process. Extr. Metall. Rev.*, vol. 40, no. 3, pp. 1–13, 2018.

[88] W. Xing *et al.*, "Improved CO_2 flux by dissolution of oxide ions into the molten carbonate phase of dual-phase CO2 separation membranes," *Sep. Purif. Technol.*, vol. 212, no. September 2018, pp. 723–727, 2019.

[89] T. Chen, B. Yu, Y. Zhao, Y. Li, and Y. S. Lin, "Carbon dioxide permeation through ceramic-carbonate dual-phase membrane-effects of sulfur dioxide," *J. Memb. Sci.*, vol. 540, no. February, pp. 477–484, 2017.

[90] T. Chen, H. C. Wu, Y. Li, and Y. S. Lin, "Poisoning Effect of H_2S on CO_2 Permeation of Samarium-Doped-Ceria/Carbonate Dual-Phase Membrane," *Ind. Eng. Chem. Res.*, vol. 56, no. 49, pp. 14662–14669, 2017.

[91] H. Devianto, S. P. Yoon, S. W. Nam, J. Han, and T. H. Lim, "The effect of a ceria coating on the H_2S tolerance of a molten carbonate fuel cell," *J. Power Sources*, vol. 159, no. 2, pp. 1147–1152, 2006.

[92] G. Zhang, E. I. Papaioannou, and I. S. Metcalfe, "Selective, high-temperature permeation of nitrogen oxides using a supported molten salt membrane," *Energy Environ. Sci.*, vol. 8, no. 4, pp. 1220–1223, 2015.

[93] J. Johnson and J. Winnick, "Electrochemical membrane separation of chlorine from gaseous hydrogen chloride waste," *Sep. Purif. Technol.*, vol. 15, no. 3, pp. 223–229, 1999.

[94] D. Townley and J. Winnick, "Flue Gas Desulfurization Using an Electrochemical Sulfur Oxide Concentrator," *Ind. Eng. Chem. Process Des. Dev.*, vol. 20, no. 3, pp. 435–440, 1981.

[95] M. Franke and J. Winnick, "Membrane Separation of Sulfur Oxides from Hot Gas," *Ind. Eng. Chem. Res.*, vol. 28, no. 9, pp. 1352–1357, 1989.

[96] W. Xing *et al.*, "Steam-promoted CO_2 flux in dual-phase CO_2 separation membranes," *J. Memb. Sci.*, vol. 482, pp. 115–119, 2015.

[97] S. Frangini and A. Masi, "Molten carbonates for advanced and sustainable energy applications: Part I. Revisiting molten carbonate properties from a sustainable viewpoint," *Int. J. Hydrogen Energy*, vol. 41, no. 41, pp. 18739–18746, 2016.

[98] J. Ren, J. Lau, M. Lefler, and S. Licht, "The Minimum Electrolytic Energy Needed to Convert Carbon Dioxide to Carbon by Electrolysis in Carbonate Melts," *J. Phys. Chem. C*, vol. 119, no. 41, pp. 23342–23349, 2015.

[99] S. Licht and H. Wu, "STEP iron, a chemistry of iron formation without CO_2 emission: Molten carbonate solubility and electrochemistry of iron ore impurities," *J. Phys. Chem. C*, vol. 115, no. 50, pp. 25138–25147, 2011.

[100] W. R. Carper, P. G. Wahlbeck, and T. R. Griffiths, "DFT models of molecular species in carbonate molten salts," *J. Phys. Chem. B*, vol. 116, no. 18, pp. 5559–5567, 2012.

[101] A. N. Shirsat, M. Ali, K. N. G. Kaimal, S. R. Bharadwaj, and D. Das, "Thermochemistry of $La_2O_2CO_3$ decomposition," *Thermochim. Acta*, vol. 399, no. 1–2, pp. 167–170, 2003.

[102] I. Barin, *Thermochemical Data of Pure Substances*, Third. VHC, 1995.

[103] S. Frangini and S. Scaccia, "The role of foreign cations in enhancing the oxygen solubility properties of alkali molten carbonate systems: Brief survey of existing data and new research results," *Int. J. Hydrogen Energy*, vol. 39, no. 23, pp. 12266–12272, 2014.

[104] S. Frangini and S. Scaccia, "The Dissolution of Oxygen in La_2O_3-Added 52⁄48 mol % Li⁄Na Molten Carbonate Determined by Gas Solubility Measurements," *J. Electrochem. Soc.*, vol. 152, no. 11, p. A2155, 2006.

[105] D. Peeters, D. Moyaux, and P. Claes, "Solubility and Solvation of Carbon Dioxide in the Molten II . Theoretical Part," *Eur. J. Inorg. Chem.*, vol. 3, no. 4, pp. 589–592, 1999.

[106] L. J. Chen, C. J. Lin, J. Zuo, L. C. Song, and C. M. Huang, "First spectroscopic observation of peroxocarbonate/ peroxodicarbonate in molten carbonate," *J. Phys. Chem. B*, vol. 108, no. 23, pp. 7553–7556, 2004.

[107] H. Nafe, "Conductivity of alkali carbonates, carbonate-based composite electrolytes and IT-SOFC," *ECS J. Solid State Sci. Technol.*, vol. 3, no. 2, pp. 7–14, 2014.

[108] O. Hirsch, K. O. Kvashnina, L. Luo, M. J. Süess, P. Glatzel, and D. Koziej, " High-energy resolution X-ray absorption and emission spectroscopy reveals insight into unique selectivity of La-based nanoparticles for CO_2 ," *Proc. Natl. Acad. Sci.*, vol. 112, no. 52, pp. 15803–15808, 2015.

[109] K. Matsuzawa, T. Mizusaki, S. Mitsushima, N. Kamiya, and K. I. Ota, "The effect of La oxide additive on the solubility of NiO in molten carbonates," *J. Power Sources*, vol. 140, no. 2, pp. 258–263, 2005.

[110] G. J. Janz, A. Conte, and E. Neuenschwander, "Corrosion of Platinum Gold Silver and Refractories in Molten Carbonates," *Natl. Assoc. Corros. Eng.*, vol. 19, pp. 292–294, 1963.

[111] London Metal Exchange, "LME Silver," 2019. [Online]. Available: https://www.lme.com/Metals/Precious-metals/LME-Silver#tabIndex=0.

[112] London Metal Exchange, "LME Nickel," 2019. [Online]. Available: https://www.lme.com/Metals/Non-ferrous/Nickel#tabIndex=0.

[113] W. M. Haynes, *CRC Handbook of Chemistry and Physics*, 91st ed. CRC Press, 2010.

[114] G. I. N. Waterhouse, G. A. Bowmaker, and J. B. Metson, "The thermal decomposition

of silver (I, III) oxide: A combined XRD, FT-IR and Raman spectroscopic study," *Phys. Chem. Chem. Phys.*, vol. 3, no. 17, pp. 3838–3845, 2001.

[115] G. J. Janz, E. Neuenschwander, and A. Conte, "Corrosion of silver in molten alkali carbonates," *Corros. Sci.*, vol. 3, no. March, pp. 177–180, 1963.

[116] S. N. Paglieri and J. D. Way, "Innovations in palladium membrane research," *Sep. Purif. Methods*, vol. 31, no. 1, pp. 1–169, 2002.

[117] P. P. Mardilovich, Y. She, Y. H. Ma, and M. H. Rei, "Defect-Free Palladium Membranes on Porous Stainless-Steel Support," *AIChE J.*, vol. 44, no. 2, pp. 310–322, 1998.

[118] S. Lamouri *et al.*, "Control of the γ-alumina to α-alumina phase transformation for an optimized alumina densification," *Bol. la Soc. Esp. Ceram. y Vidr.*, vol. 56, no. 2, pp. 47–54, 2017.

[119] A. R. Olszyna, P. Marchlewski, and K. J. Kurzydłowski, "Sintering of high-density, high-purity alumina ceramics," *Ceram. Int.*, vol. 23, no. 4, pp. 323–328, 1997.

[120] L. Zhang, Z. Mao, J. D. Thomason, S. Wang, and K. Huang, "Synthesis of a homogeneously porous solid oxide matrix with tunable porosity and pore size," *J. Am. Ceram. Soc.*, vol. 95, no. 6, pp. 1832–1837, 2012.

[121] L. C. Witjens, J. H. Bitter, A. J. Van Dillen, W. M. Arnoldbik, F. H. P. M. Habraken, and K. P. De Jong, "Improving the control of the electroless plating synthesis of Pd/Ag membranes for hydrogen separation using Rutherford backscattering," *J. Memb. Sci.*, vol. 254, no. 1–2, pp. 241–248, 2005.

[122] B. D. Ratner, *Surface Properties and Surface Characterization of Biomaterials*, Third Edit., no. 2002. Elsevier, 2013.

[123] S. Zhuang *et al.*, "Dense composite electrolyte hollow fibre membranes for high temperature CO2 separation," *Sep. Purif. Technol.*, vol. 132, pp. 712–718, 2014.

[124] X. Jiang, J. Zhu, Z. Liu, S. Guo, and W. Jin, "CO_2-Tolerant $SrFe_{0.8}Nb_{0.2}O_{3-\delta}$-Carbonate Dual-Phase Multichannel Hollow Fiber Membrane for CO2 Capture," *Ind. Eng. Chem. Res.*, vol. 55, no. 12, pp. 3300–3307, 2016.

[125] A. M. S. El Din and G. Wranglén, "Dendrite formation and electrocrystallization of silver from molten salts," *Electrochim. Acta*, vol. 7, no. 1, pp. 79–90, 1962.

[126] T. B. Reddy, B. T. Laboratories, and M. Hill, "Surface Diffusion Processes and Dendritic

Growth in the Electrodeposition of Silver from Molten Halides," pp. 117–123.

[127] C. Yang *et al.*, "Fractal dendrite-based electrically conductive composites for laser-scribed flexible circuits," *Nat. Commun.*, vol. 6, pp. 1–10, 2015.

[128] J. F. Shackelford and W. Alexander, *CRC Materials Science and Engineering Handbook*, Third. 2001.

[129] P. L. Spedding, "Electrical Conductance of Molten Alkali Carbonate Binary Mixtures.," *J. Electrochem. Soc.*, vol. 120, no. 8, pp. 1049–1052, 1973.

[130] T. Kojima, Y. Miyazaki, K. Nomura, and K. Tanimoto, "Electrical conductivity of molten Li_2CO_3-X_2CO_3 (X: Na, K, Rb, and Cs) and Na_2CO_3 - Z_2CO_3 (Z: K, Rb, and Cs)," *J. Electrochem. Soc.*, vol. 154, no. 12, pp. 222–230, 2007.

[131] Z. Zuo, Y. Wen, and S. Zhang, "Interface-induced nucleation and growth: a new route for fabricating ordered silver nanohole arrays," *Nanoscale*, vol. 10, no. 29, pp. 14039–14046, 2018.

[132] T. C. Merkel, H. Lin, X. Wei, and R. Baker, "Power plant post-combustion carbon dioxide capture: An opportunity for membranes," *J. Memb. Sci.*, vol. 359, no. 1–2, pp. 126–139, 2010.

[133] S. Liu, K. Lin, and R. Hughes, "Preparation of porous aluminium oxide (Al_2O_3) hollow fibre membranes by a combined phase-inversion and sintering method," *Ceram. Int.*, vol. 29, no. 7, pp. 875–877, 2003.
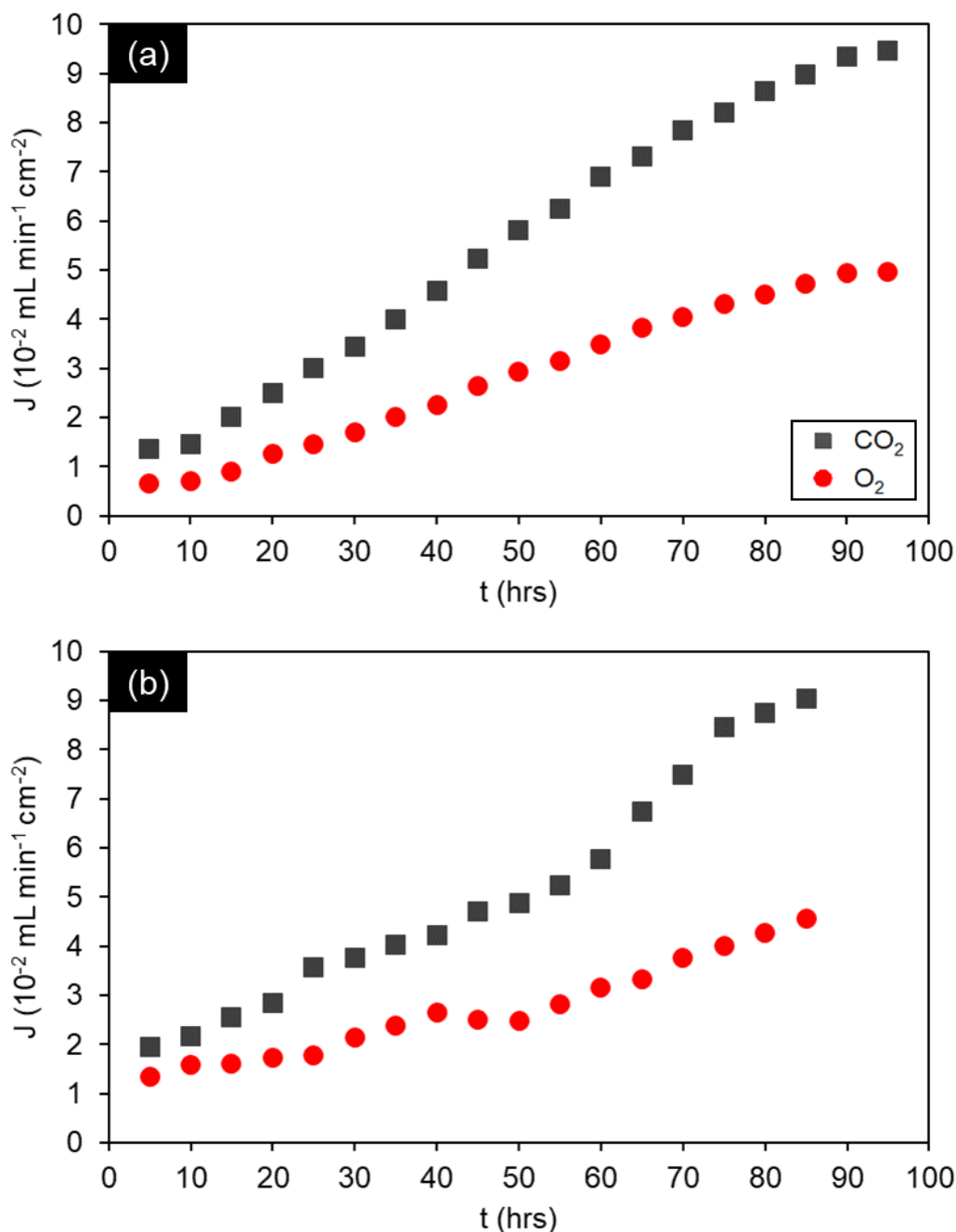
Appendix

A. 1 Experiment repeatability

Fig. A. 1 Comparison of the CO_2 and O_2 flux evolution of two identically prepared 6 mol% Ag/Al_2O_3-MC membranes. Both membranes were operated at 650°C and had the following gas feed regime: Feed-side inlet: 50 mol% CO_2, 25 mol% O_2 in N_2 and permeate-side inlet: Ar.

The stable flux region between the two experiments showed a 5% difference in flux, combined with a 10% difference in the time taken to achieve the stable flux region. This indicates good repeatability of the data presented in these studies. Fig. A. 1b showed a less linear increase in

flux compared to Fig. A. 1a. Since there was no detectable leak for either experiment, this variation in the transient behaviour is likely due to differences in the random pore network, which can affect the growth of the Ag pathways.

A. 2   Ion current conversion

Conversion of ion current into mol fraction for O_2 used the following equation (A.1):

$$y_i = \left[\frac{\alpha_i - \alpha_{i_{LB}}}{\alpha_{i_{UB}} - \alpha_i} \right] \times UB \tag{A.1}$$

Where the ion current is (α) and the mol fraction is (y) and i is the gas component (O_2 for (A.1) and N_2 for (A.2)). The upper- and lower-boundary calibration cylinders are represented by LB and UB.

To account for air leaks into the permeate-side chamber the following subtraction is made to equation (A.1):

$$y_i = \frac{\left[\frac{\alpha_i - \alpha_{i_{LB}}}{\alpha_{i_{UB}} - \alpha_i} \right] \times UB \times 0.89}{4} \tag{A.2}$$

A. 3 Stable flux region data and calculations

The error for the stable flux data points were calculated from the standard deviation (σ) of the data collected during the 4-hour stable flux period. σ is the square root of variance (σ^2) which is calculated using the following equation (A.3):

$$\sigma^2 = \frac{\Sigma(J - \bar{J})^2}{N} \tag{A.3}$$

Where J is the flux at a single data point from within the 4-hours stable flux period and N is the number of data points. A sample stable flux period plot for CO_2 and O_2 is displayed in Fig. A. 2 for a 6 mol% Ag/Al_2O_3-MC membrane. Data for each Ag-doped membranes' (0.0125-10 mol%) stable flux period are also presented in the appendix (Fig. A. 3 – Fig. A. 7).
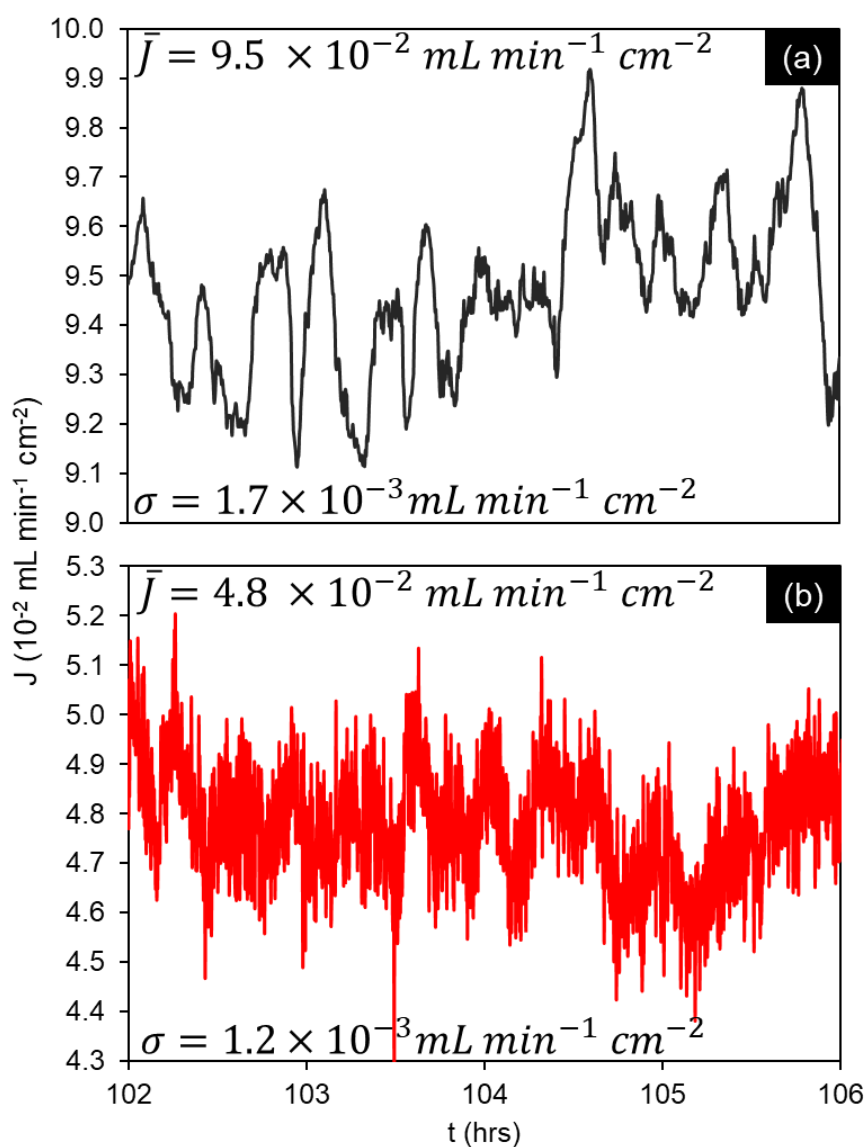
Fig. A. 2 Stable flux region for (a) CO_2 and (b) O_2 in a 6 mol% Ag/Al_2O_3-MC membrane. Feed-side inlet: 50 mol% CO_2, 25 mol% O_2 in N_2.

Fig. A. 2 shows the entire stable flux region data used to calculate $\bar{J}CO_2$ and O_2 for the 6 mol% Ag/Al$_2$O$_3$-MC membrane. While the data shows fluctuations, the individual data points do not stretch far from the mean (μ) value which is displayed by the small σ (1.7 and 1.2×10^{-3} mL min^{-1} cm^{-2} for CO_2 and O_2 respectively). This is why no error bars were added to Fig. 5. 1 as the error was small than the data point markers.
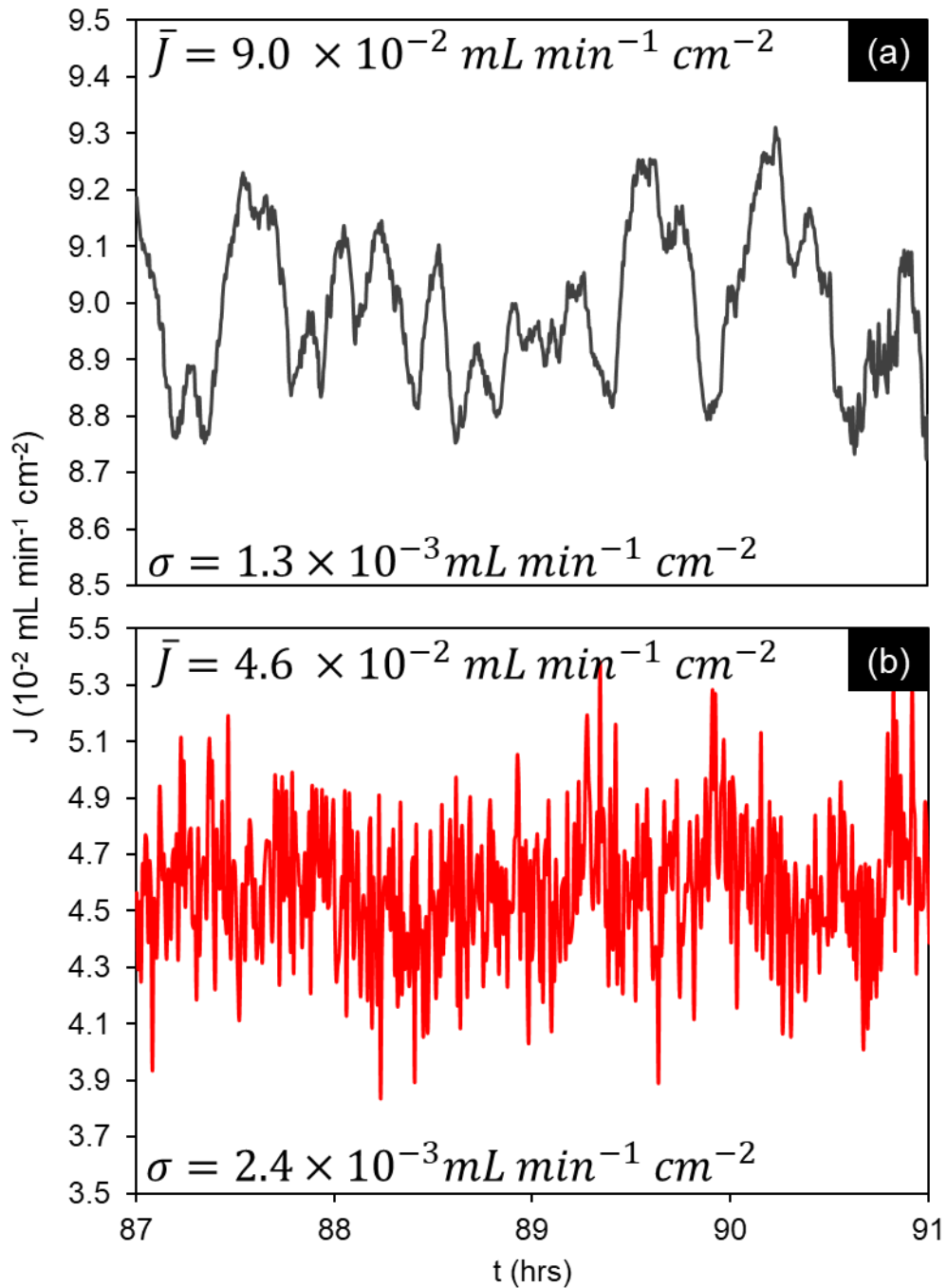

Fig. A. 3 Stable flux region for (a) CO_2 and (b) O_2 in a 10 mol% Ag/Al$_2$O$_3$-MC membrane. Feed-side inlet: 50 mol% CO_2, 25 mol% O_2 in N_2.
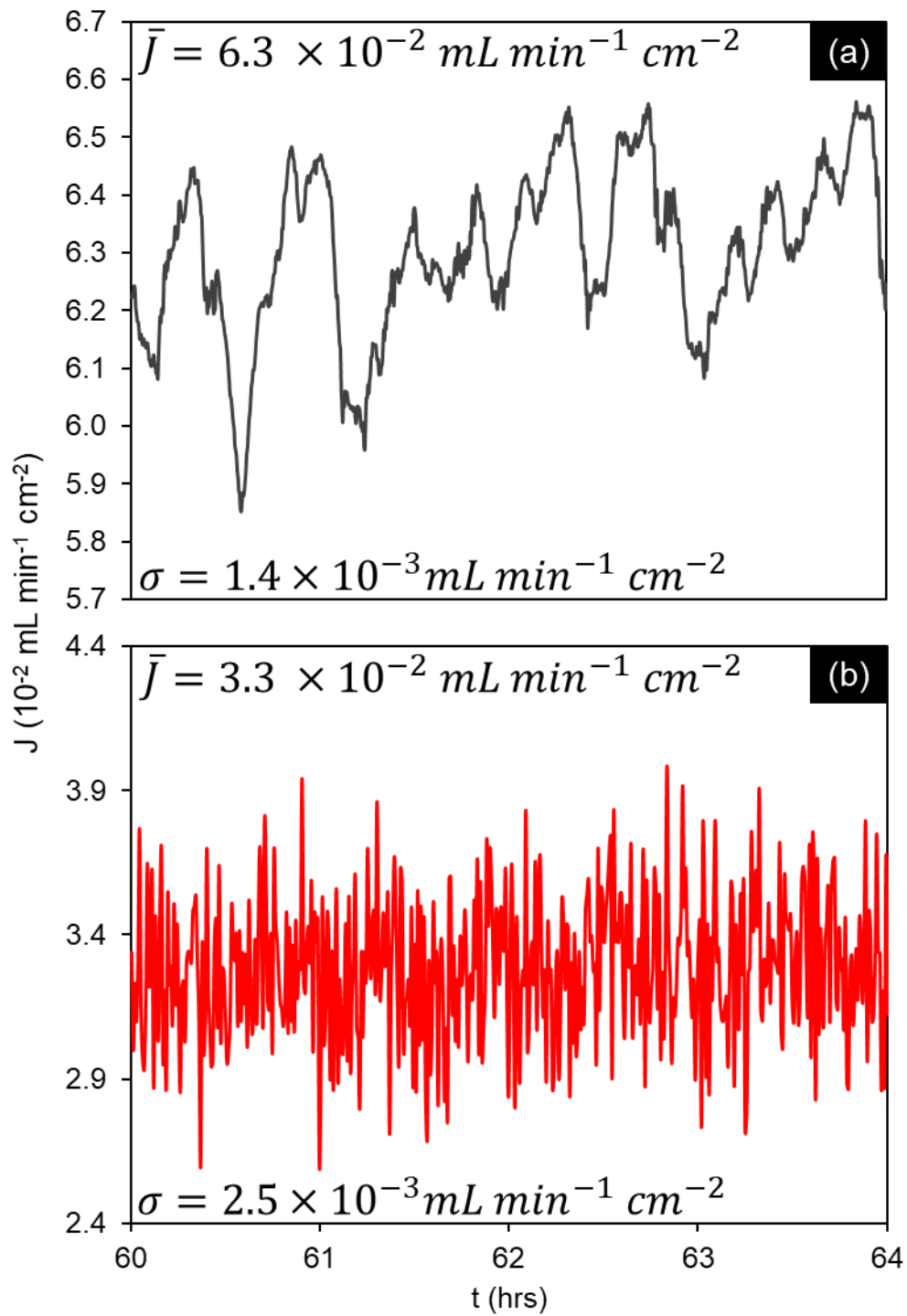
Fig. A. 4 Stable flux region for (a) CO_2 and (b) O_2 in a 3 mol% Ag/Al_2O_3-MC membrane. Feed-side inlet: 50 mol% CO_2, 25 mol% O_2 in N_2.
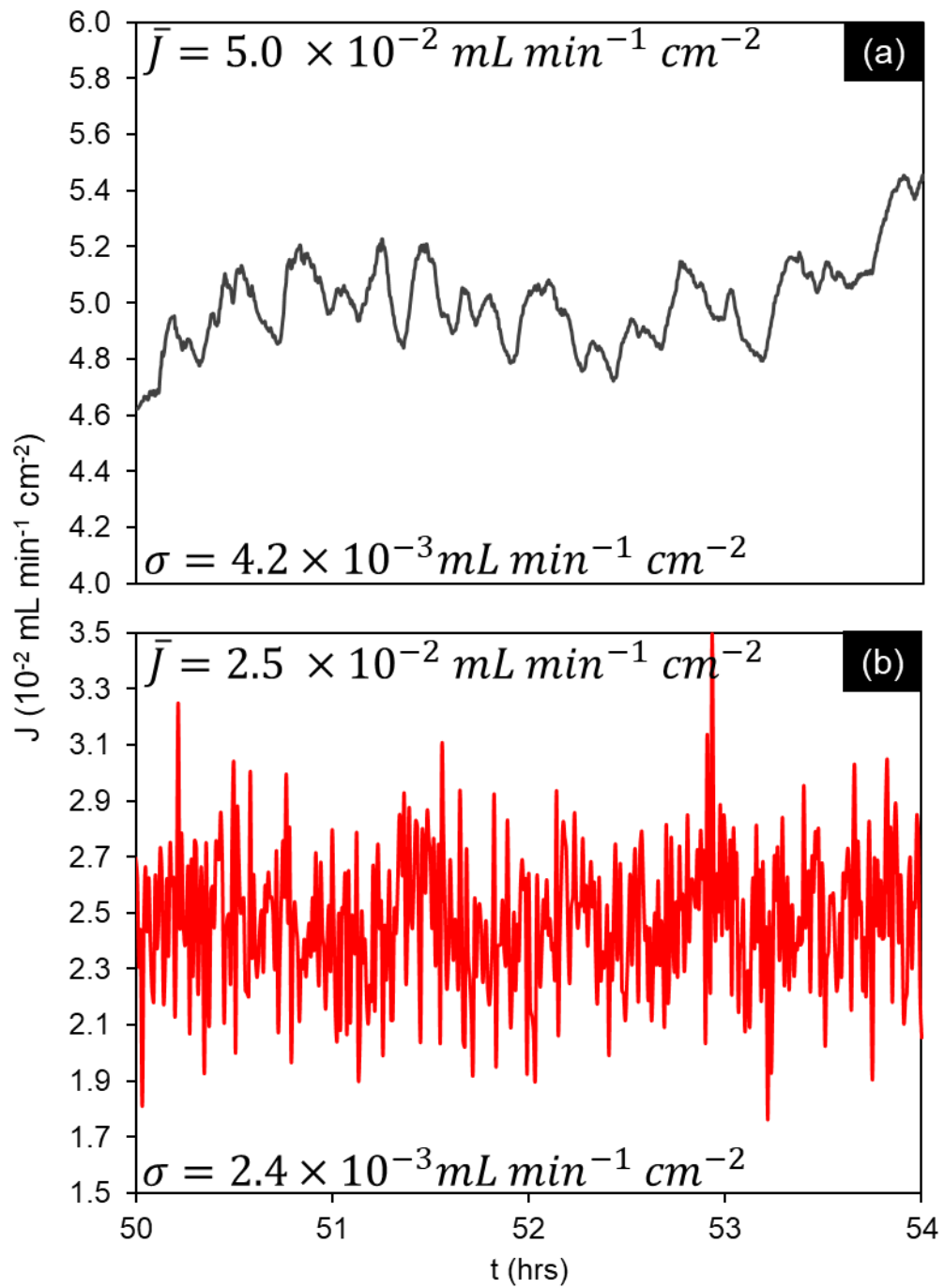
Fig. A. 5 Stable flux region for (a) CO_2 and (b) O_2 in a 1.5 mol% Ag/Al_2O_3-MC membrane. Feed-side inlet: 50 mol% CO_2, 25 mol% O_2 in N_2.
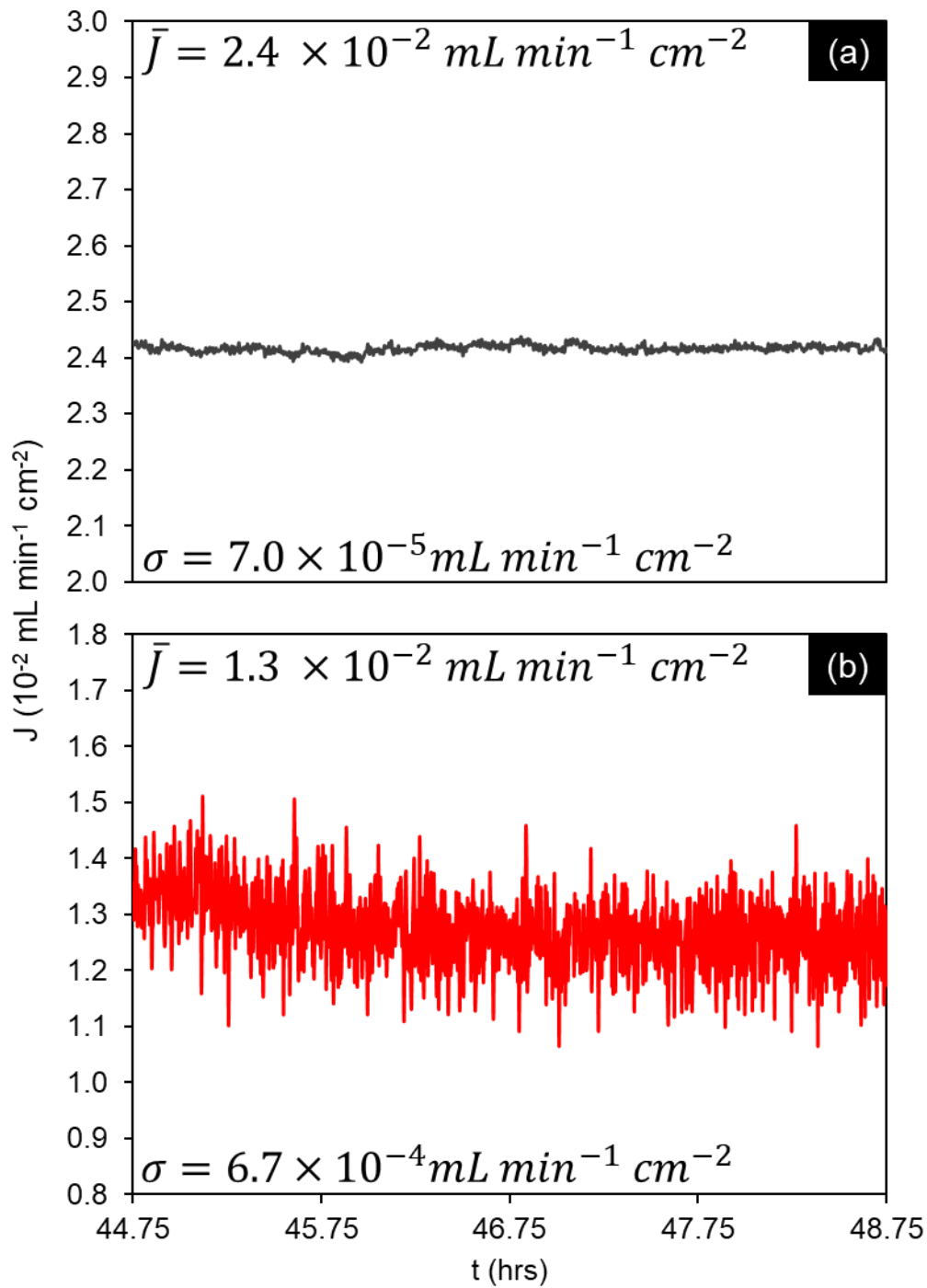
Fig. A. 6 Stable flux region for (a) CO_2 and (b) O_2 in a 0.25 mol% Ag/Al_2O_3-MC membrane. Feed-side inlet: 50 mol% CO_2, 25 mol% O_2 in N_2.
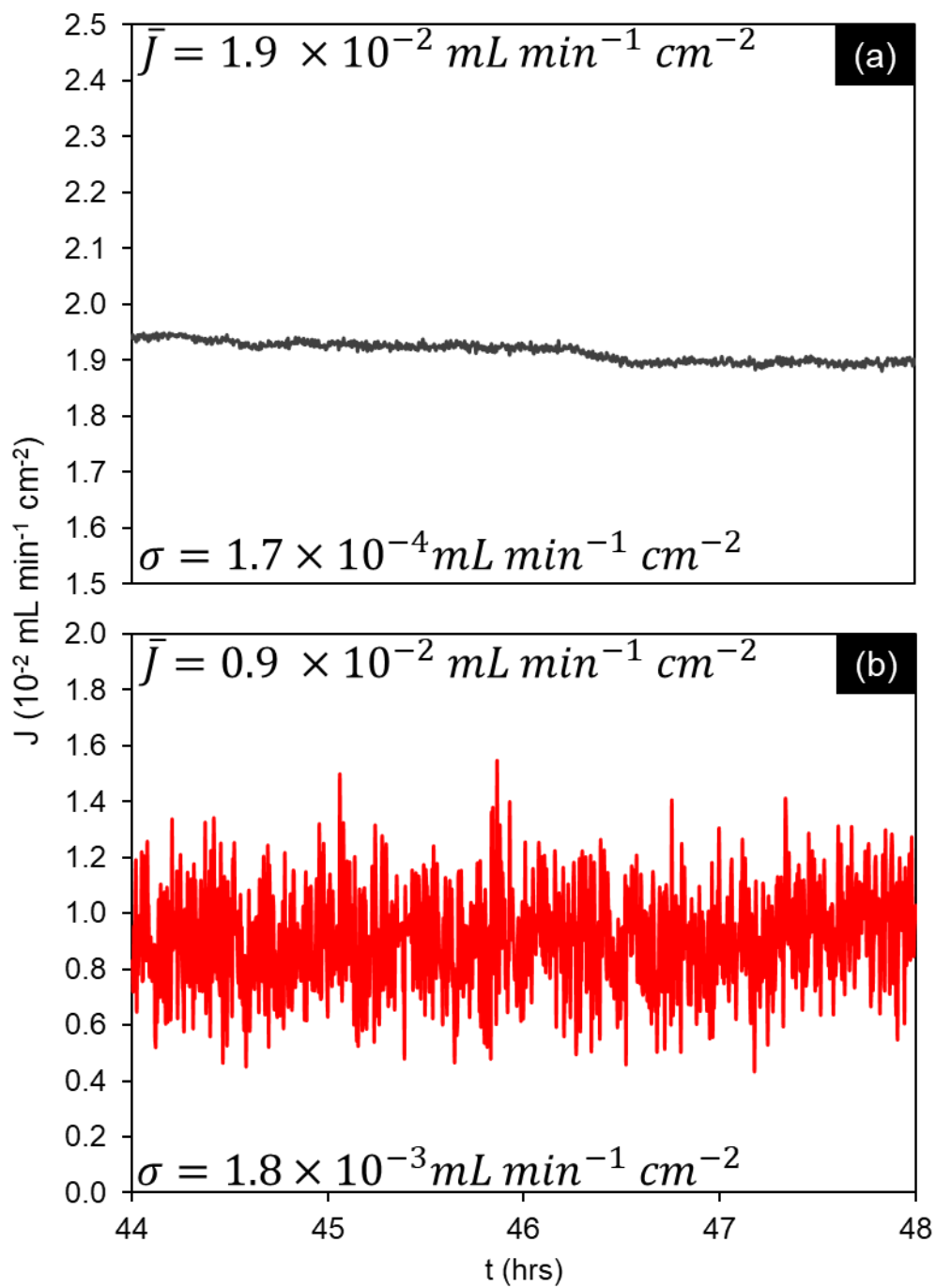
Fig. A. 7 Stable flux region for (a) CO_2 and (b) O_2 in a 0.0125 mol% Ag/Al_2O_3-MC membrane. Feed-side inlet: 50 mol% CO_2, 25 mol% O_2 in N_2.

A. 4 Flux evolution plots for powder-doped Ag/Al$_2$O$_3$-MC pellet membranes

Full un-cut CO$_2$ and O$_2$ flux experimental data for powder-doped Ag/Al$_2$O$_3$-MC can be found in this appendix subsection.
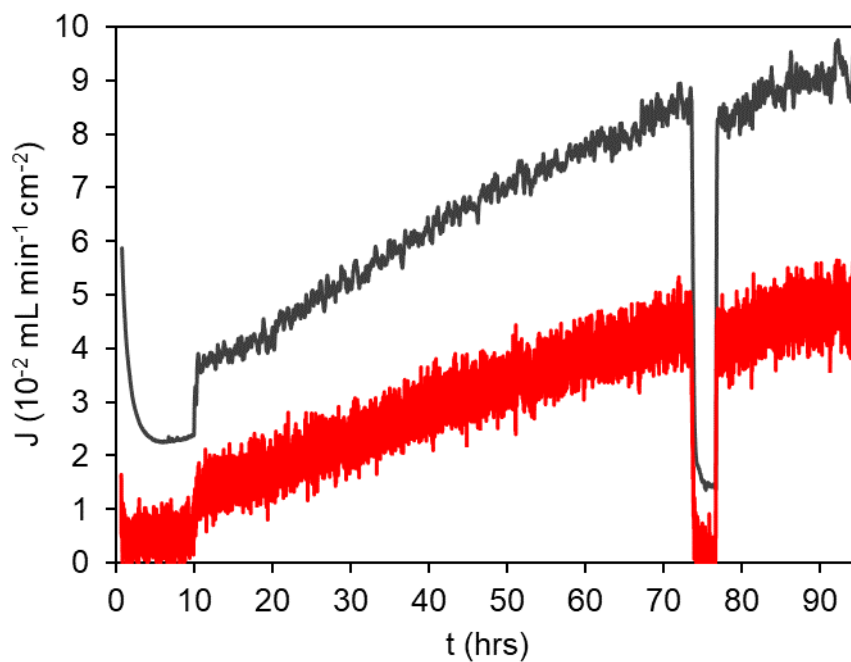

Fig. A. 8 CO$_2$ and O$_2$ flux evolution for a 10 mol% Ag/Al$_2$O$_3$-MC membrane fed with 50 mol% CO$_2$, 25 mol% O$_2$ in N$_2$ at 650°C. Decrease in CO$_2$ and O$_2$ flux between 73 and 77 hours is due to a leak test where the feed gas was temporarily switched to 50 mol% CO$_2$ in N$_2$.
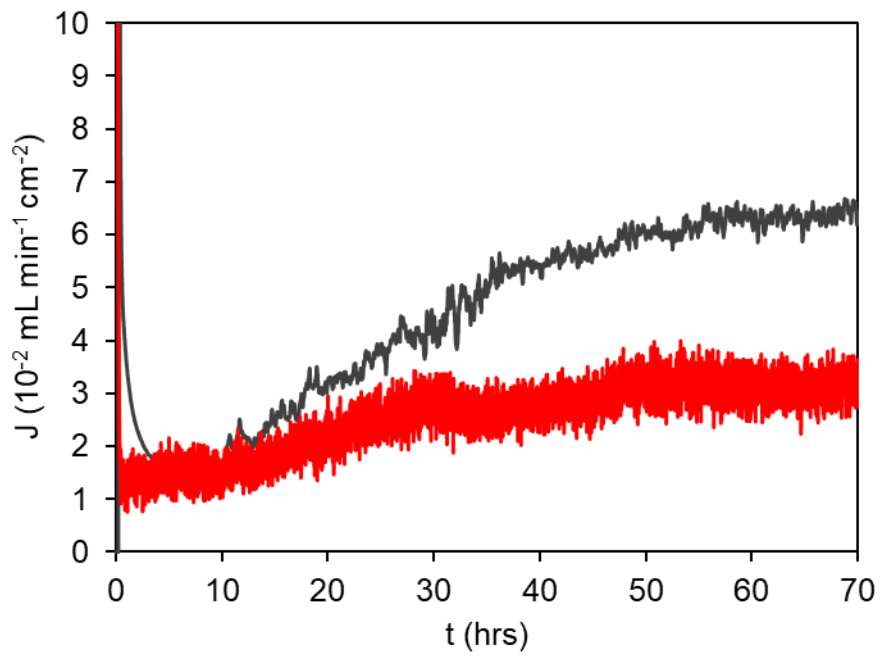
Fig. A. 9 CO_2 and O_2 flux evolution for a 3 mol% Ag/Al_2O_3-MC membrane fed with 50 mol% CO_2, 25 mol% O_2 in N_2 at 650°C.
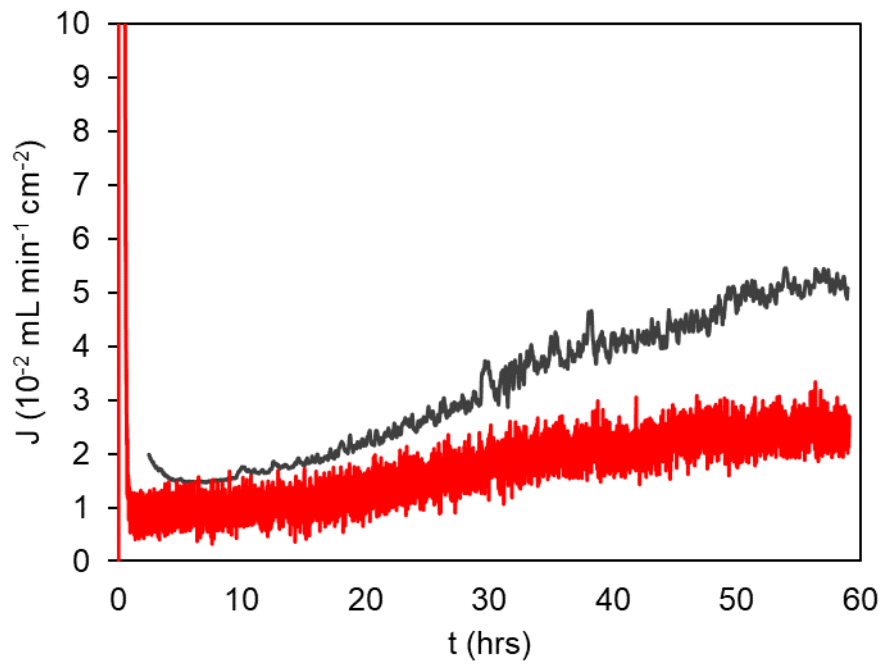
Fig. A. 10 CO_2 and O_2 flux evolution for a 1.5 mol% Ag/Al_2O_3-MC membrane fed with 50 mol% CO_2, 25 mol% O_2 in N_2 at 650°C.
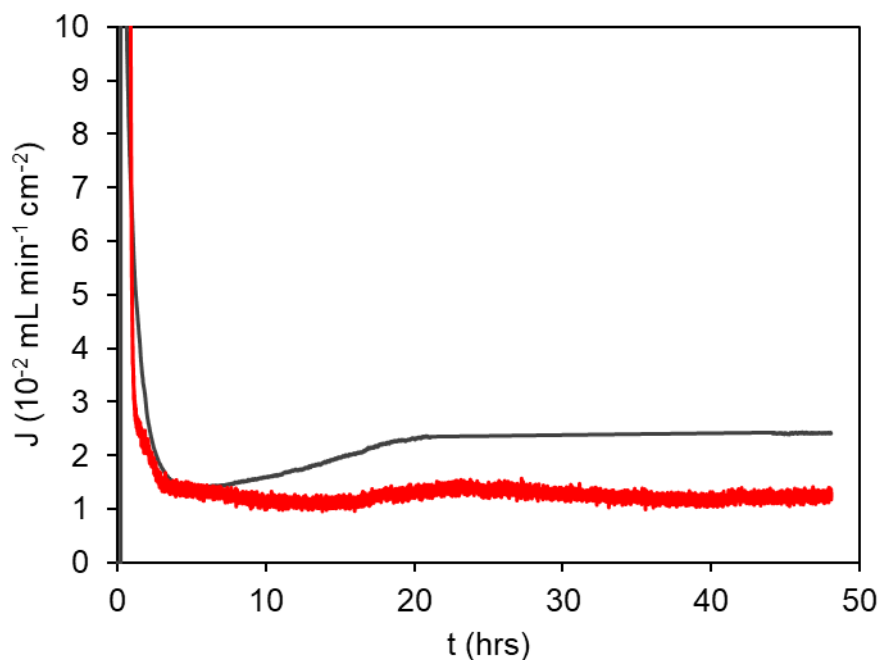
Fig. A. 11 CO_2 and O_2 flux evolution for a 0.25 mol% Ag/Al_2O_3-MC membrane fed with 50 mol% CO_2, 25 mol% O_2 in N_2 at 650°C. Gap in CO_2 flux data between 21 and 44 hours is due to the FT-IR running out of liquid N_2 causing the detector to shut-down.
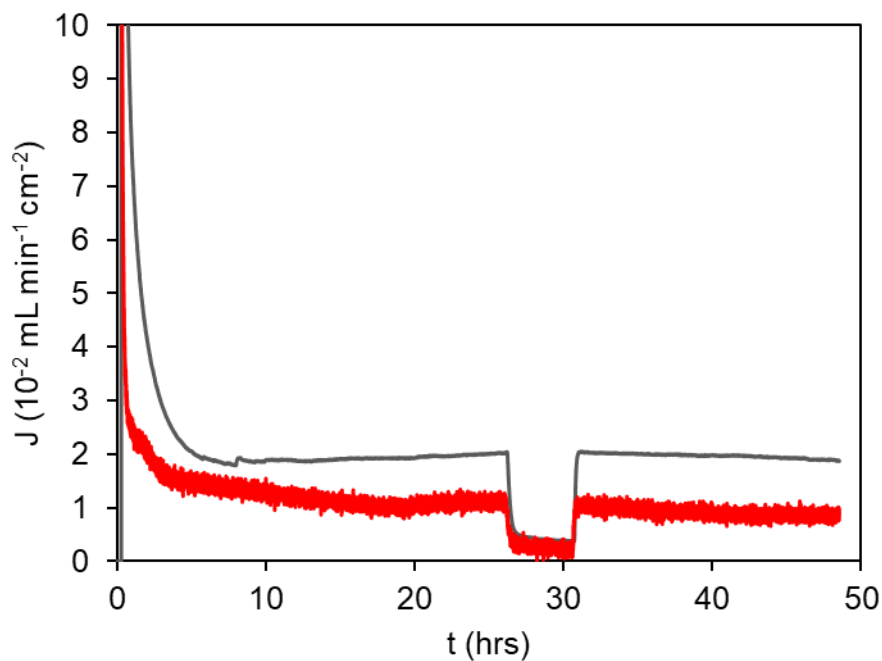

Fig. A. 12 CO_2 and O_2 flux evolution for a 0.0125 mol% Ag/Al_2O_3-MC membrane fed with 50 mol% CO_2, 25 mol% O_2 in N_2 at 650°C. Decrease in CO_2 and O_2 flux between 36 and 31 hours is due to a leak test where the feed gas was temporarily switched to 50 mol% CO_2 in N_2.

A. 5 Flux, permeance and permeability comparison

Table A. 1 Comparison CO_2 flux, permeance and permeability as a function of feed-side inlet gas for all membranes presented in Chapter 4 and 5 at 650°C.

Feed-side inlet gas	CO_2 Flux (mL min^{-1} cm^{-2})	CO_2 Permeance (mol m^{-2} s^{-1} Pa^{-1})	CO_2 Permeability (mol m^{-1} s^{-1} Pa^{-1})
Al_2O_3-MC pellet membrane			
50 mol% CO_2 in N_2	0.0015	2.2×10^{-10}	3.9×10^{-13}
25 mol% O_2 in N_2	< 0.0015*	N/A	N/A
50 mol% CO_2, 25 mol% O_2 in N_2	0.010	1.3×10^{-9}	3.8×10^{-12}
6 mol% Ag/Al_2O_3-MC pellet membrane			
50 mol% CO_2 in N_2	0.0025	3.7×10^{-10}	4.2×10^{-13}
25 mol% O_2 in N_2	< 0.0015*	N/A	N/A
50 mol% CO_2, 25 mol% O_2 in N_2	0.10	1.3×10^{-8}	3.6×10^{-11}
Al_2O_3-MC parallel pore membrane			
50 mol% CO_2 in N_2	0.015	2.2×10^{-9}	4.0×10^{-12}
25 mol% O_2 in N_2	< 0.0015*	N/A	N/A
50 mol% CO_2, 25 mol% O_2 in N_2	0.015	2.2×10^{-9}	4.0×10^{-12}
6 mol% Ag/Al_2O_3-MC parallel pore membrane			
50 mol% CO_2 in N_2	0.03	4.4×10^{-9}	3.0×10^{-12}
25 mol% O_2 in N_2	< 0.0015*	N/A	N/A
50 mol% CO_2, 25 mol% O_2 in N_2	1.25	1.9×10^{-7}	9.4×10^{-11}

* Does not reach stable flux due to constant decomposition of CO_2

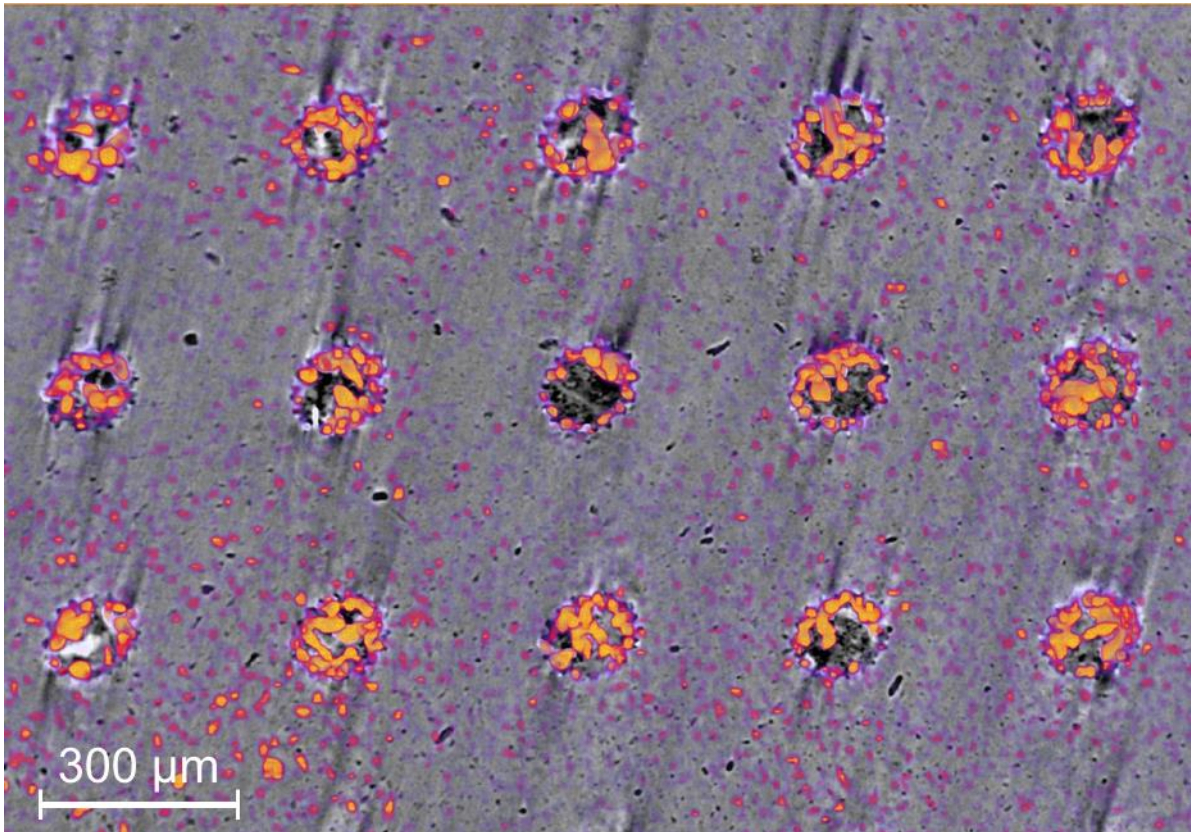A. 6   Extra CT images of the tested 6 mol% Ag/Al$_2$O$_3$-MC parallel pore membrane

Fig. A. 13 Ag (orange) can be observed attached to the pore walls of the parallel pore Al$_2$O$_3$ support. Clustering of Ag towards the middle of the pore is a result of the conical pore shape (150 μm Ø at the near surface, 75 μm Ø at the far surface). The 6 mol% Ag/Al$_2$O$_3$-MC parallel pore membrane was operated at 650°C. Feed-side inlet: 50 mol% CO$_2$, 25 mol% O$_2$ in N$_2$. Permeate-side inlet: Ar.
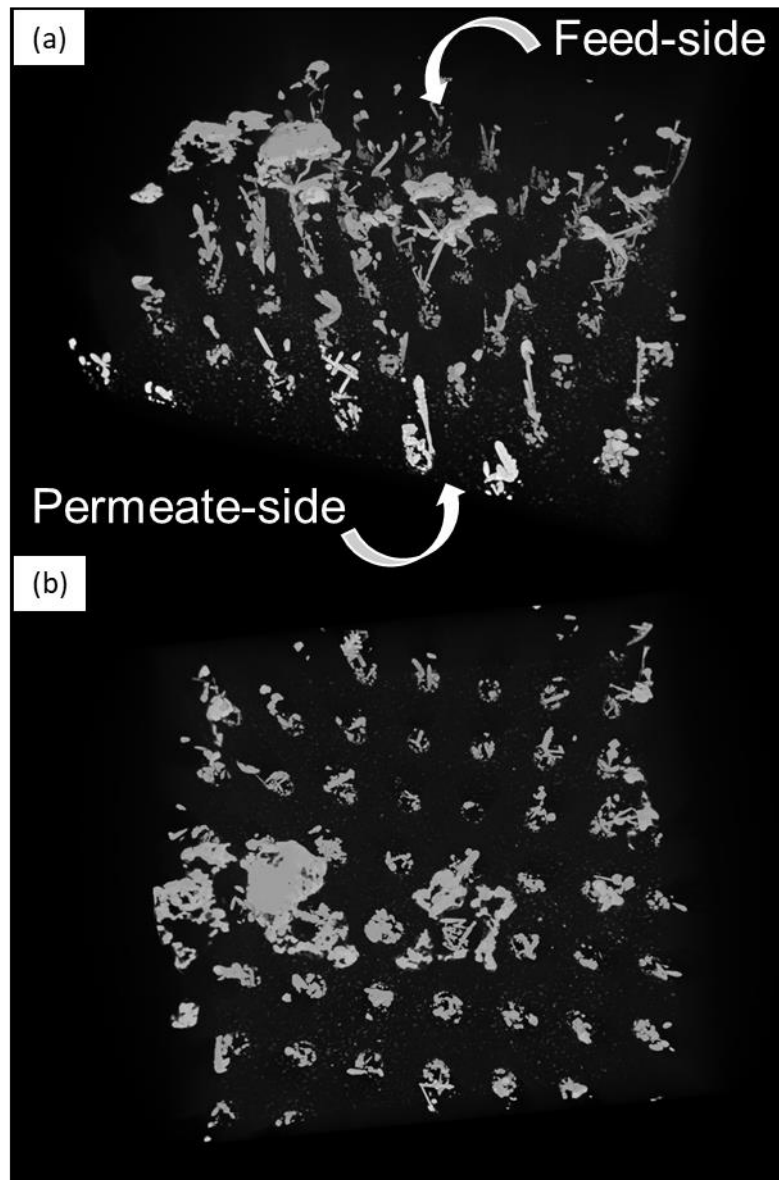
Fig. A. 14 CT of a collection of pores in a tested 6 mol% Ag/Al_2O_3-MC parallel pore membrane system with the ceramic support phase removed; (a) side view; (b) top view. The 6 mol% Ag/Al_2O_3-MC parallel pore membrane was operated at 650°C. Feed-side inlet: 50 mol% CO_2, 25 mol% O_2 in N_2. Permeate-side inlet: Ar.

Fig. A. 15 Digital image of the cross-section of an Ag-sealed Ag/Al_2O_3-MC membrane after use. Feed-side inlet: 50 mol% CO_2, 25 mol% O_2 in N_2.

Fig. A. 16 Digital image of the cross-section of an Ag-sealed Al_2O_3-MC membrane after use. Feed-side inlet: 50 mol% CO_2, 25 mol% O_2 in N_2.